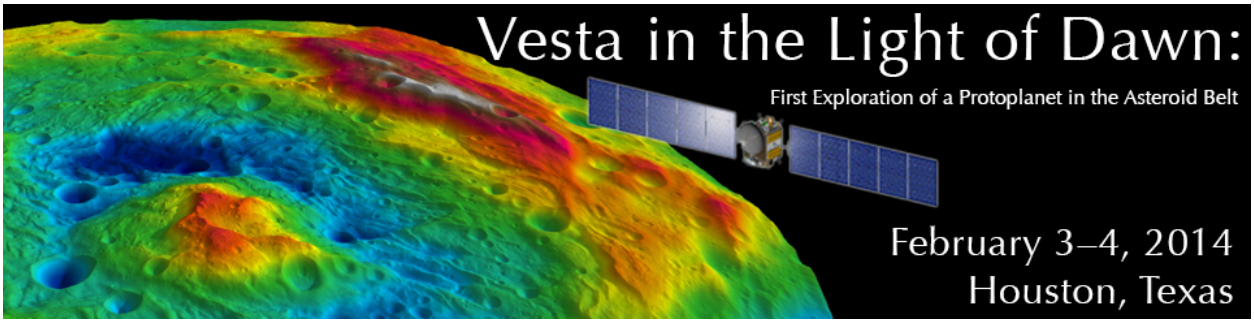

Program and Abstract Volume

LPI Contribution No. 1773

LUNAR AND PLANETARY INSTITUTE

USRA

Vesta in the Light Dawn:
First Exploration of a Protoplanet in the Asteroid Belt

February 3–4, 2014 • Houston, Texas

Institutional Support

Universities Space Research Association

Conveners

Paul Schenk
Lunar and Planetary Institute

Richard P. Binzel
Massachusetts Institute of Technology

Scientific Organizing Committee

Paul Schenk, *Lunar and Planetary Institute*

Richard P. Binzel, *Massachusetts Institute of Technology*

Maria Cristina De Sanctis, Istituto di Astrofisica e Planetologia Spaziale, INAF*, Italy*

Jian-Yang Li, *Planetary Science Institute*

Harry McSween, *University of Tennessee*

Thomas Prettyman, *Planetary Science Institute*

Vishnu Reddy, *Planetary Science Institute*

Carol Raymond, *Jet Propulsion Laboratory*

Andrew Rivkin, *Applied Physics Laboratory, Johns Hopkins University*

David A. Williams, A*rizona State University*

Lunar and Planetary Institute 3600 Bay Area Boulevard Houston TX 77058-1113

LPI Contribution No. 1773

Compiled in 2014 by

Meeting and Publication Services
Lunar and Planetary Institute
USRA Houston
3600 Bay Area Boulevard, Houston TX 77058-1113

This material is based upon work supported by NASA under Award No. NNX08AC28A. Any opinions, findings, and conclusions or recommendations expressed in this volume are those of the author(s) and do not necessarily reflect the views of the National Aeronautics and Space Administration.

The Lunar and Planetary Institute is operated by the Universities Space Research Association under a cooperative agreement with the Science Mission Directorate of the National Aeronautics and Space Administration.

Abstracts in this volume may be cited as

Author A. B. (2014) Title of abstract. In *Vesta in the Light of Dawn: First Exploration of a Protoplanet in the Asteroid Belt,* p. XX. LPI Contribution No. 1773, Lunar and Planetary Institute, Houston.

ISSN No. 0161-5297

Preface

This volume contains abstracts that have been accepted for presentation at the Vesta in the Light of Dawn: First Exploration of a Protoplanet in the Asteroid Belt, February 3–4, 2014, Houston, Texas.

Administration and publications support for this meeting were provided by the staff of the Meeting and Publication Services Department at the Lunar and Planetary Institute.

Technical Guide to Sessions

Monday, February 3, 2014

8:40 a.m.	Lecture Hall	Vesta in the Solar System
1:15 p.m.	Lecture Hall	Vesta: Geology of a Small Planet
3:30 p.m.	Lecture Hall	Vesta: Impacts Large and Small
6:00 p.m.	Great Room	Poster Session: Vesta at Large

Tuesday, February 4, 2014

9:00 a.m.	Lecture Hall	Vesta on the Outside: Surface Composition
1:30 p.m.	Lecture Hall	Vesta on the Inside: Core and Mantle

Contents

Program

Monday, February 3, 2014
VESTA IN THE SOLAR SYSTEM
8:40 a.m. Lecture Hall

Chairs: **Richard Binzel**
Faith Vilas

8:40 a.m. Binzel R. P. *
Discovery and Earth-Based Reconnaissance of Vesta **[#2045]**
For decades Earth-based astronomers built the case for Vesta as a large basalt covered asteroid possibly linked to HED meteorites. The success of Dawn's confirming findings and new results offers ongoing lessons for planetary exploration.

9:00 a.m. Russell C. T. *
A Journey in Space and Time: First Stop Vesta **[#2053]**
The Dawn mission is a voyage in space and time to interview the oldest intact survivor of the evolved solar system.

9:20 a.m. Vilas F. * Hendrix A. R. Li J.-Y. Cochran A. L.
Vesta in the Ultraviolet/Blue: What We Knew Before Dawn's Arrival, and How does it Augment What We Learned from Dawn? **[#2050]**
Earth-based telescopic data on asteroid 4 Vesta prior to Dawn's arrival are discussed in the context of predictions before the mission and results after the mission.

9:35 a.m. Bottke W. F. *
On the Origin and Evolution of Vesta and the V-Type Asteroids **[#2024]**
We explore whether Vesta and some V-type asteroids were originally denizens of the terrestrial planet region. We also examine whether some V-types are fragments from Vesta-like objects that were dynamically removed from the primordial main belt.

9:55 a.m. DISCUSSION

10:05 a.m. BREAK

10:20 a.m. Lazzaro D. *
Vesta and its Family: Composition Versus Evolution

10:40 a.m. Buratti B. J. * Dalba P. A. Hicks M. D.
Vestoids, Vesta, and HEDs: What Explains Their Color Differences? **[#2015]**
The color differences among the vestoids, Vesta, and the HEDs can be explained by particle sizes and by the addition of spectrally neutral carbonaceous material. The effects of phase reddening are slight and do not explain the differences.

10:55 a.m. Longobardo A. * Capaccioni F. Palomba E. De Sanctis M. C. Tosi F. Schroeder S. E. Li J.-Y. Capria M. T. Ammannito E. Raymond C. A. Russell C. T.
Retrieval of Disk-Resolved Phase Functions of Vesta and Comparison with Other Asteroids **[#2028]**
In this work we obtain visible/infrared phase functions of Vesta dark and bright regions. We try to find an equivalent photometric of these regions, by comparing their phase functions with those found in other asteroids of different spectral type.

11:10 a.m. Li J.-Y. * Buratti B. J. De Sanctis M. C. Denevi B. W. Hoffmann M. Longobardo A. Mottola S. Nathues A. Reddy V. Russell C. T. Schröder S. E.
The Photometric Properties of Vesta and the Implications **[#2032]**
We summarize the globally averaged photometric properties of Vesta and the comparisons with other rocky bodies in the solar system, and discuss the implications in both photometric properties and photometric modeling.

11:25 a.m. O'Brien D. P. * Marchi S. Morbidelli A. Bottke W. F. Schenk P. Russell C. T. Raymond C. A.
The Impact History of Vesta **[#2049]**
We have developed a crater chronology for Vesta based on dynamical models of the evolution of the asteroid belt.

11:45 a.m. DISCUSSION

Monday, February 3, 2014
VESTA: GEOLOGY OF A SMALL PLANET
1:15 p.m. Lecture Hall

Chairs: **Andrew Rivkin**
Brett Denevi

1:15 p.m. Jaumann R. * Russell C. T. Raymond C. A. Pieters C. M. Yingst R. A. Williams D. A. Buczkowski D. L. Schenk P. De Sanctis M. C.
Vesta's Geological Features **[#2011]**
Vesta's diverse geology exhibits impact basins and craters of all sizes and unusual shapes, ejecta blankets, large troughs, impact basins, enigmatic dark material, and considerable evidence for mass wasting and surface alteration processes.

1:35 p.m. Williams D. A. * Yingst R. A. Garry W. B.
Strategies for the Geologic Mapping of Small Airless Bodies: The Vesta Example **[#2014]**
This presentation will discuss the geologic mapping campaign of the asteroid Vesta that was part of the Dawn Nominal mission, including goals and methods of the mapping program, the challenges of mapping on small airless bodies, and lessons learned.

1:50 p.m. Scully J. E. C. * Russell C. T. Yin A. Jaumann R. Carey E. McSween H. Y. Raymond C. A. Reddy V. Le Corre L. Castillo-Rogez J.
Vestan Gullies and Their Formation Mechanisms **[#2001]**
Gullies are classified, based on morphology, into two types: linear and curvilinear. We propose that curvilinear gullies are morphological evidence for localized water on Vesta, which is in keeping with recent meteorite and remote sensing evidence.

2:05 p.m. Capria M. T. * Tosi F. De Sanctis M. C. Ammannito E. Capaccioni F. Fonte S. Frigeri A. Longobardo A. Palomba E. Zambon F. Schroeder S. Denevi B. Williams D. A. Titus T. Blewett D. Russell C. T. Raymond C. A.
Thermophysical Analysis of Pitted Terrains on Vesta **[#2005]**
Pitted terrains have been found on Vesta, where they are seen as regions with high thermal inertia. We present a detailed analysis of the thermophysical characteristics of this kind of terrains.

2:20 p.m. Tosi F. * Zambon F. Capria M. T. De Sanctis M. C. Capaccioni F. Ammannito E. Titus T. N. Palomba E. Russell C. T. Raymond C. A. Dawn Science Team
Global Resolved Temperature Maps of Vesta **[#2026]**
We present, for the first time, global resolved temperature maps of Vesta as derived by the Visible and Infrared Mapping Spectrometer (VIR) onboard Dawn.

2:35 p.m. Denevi B. W. * Blewett D. T. Buczkowski D. L. Capria M. T. De Sanctis M. C. Le Corre L. Li J.-Y. Marchi S. Nathues A. O'Brien D. P. Petro N. E. Prettyman T. H. Preusker F. Reddy V. Russell C. T. Scully J. E. C. Sunshine J. M. Tosi F. Williams D. A.
The Preservation and Geologic Effects of Exogenic and Hydrated Materials on Vesta **[#2029]**
We review the geologic consequences of the presence of hydrated minerals on an otherwise volatile-poor body, with an examination of how Vesta can inform our understanding of the effects of exogenic materials on other bodies.

2:50 p.m. Prettyman T. H. * Beck A. W. Feldman W. C. Lawrence D. J. McCoy T. J. McSween H. Y. Mittlefehldt D. W. Peplowski P. N. Raymond C. A. Reedy R. C. Russell C. T. Titus T. N. Toplis M. J. Yamashita N.
Vesta's Elemental Composition **[#2043]**
Elemental mapping by Dawn's gamma ray and neutron detector reveals the colorful chemistry of Vesta's howarditic regolith.

3:10 p.m. DISCUSSION

Monday, February 3, 2014
VESTA: IMPACTS LARGE AND SMALL
3:30 p.m. Lecture Hall

Chairs: **David O'Brien**
Debra Buczkowski

3:30 p.m. Schenk P. * O'Brien D. McSween H. Buczkowski D. Gaskell R. Otto K. Preusker F. Marchi S. Yingst A. Mest S. Raymond C. Russell C.
Megascale Impacts in Vesta's South Pole: The Morphologic Constraints **[#2039]**
The 505-km-wide impact basin, Rheasilvia, on Vesta is the largest with respect to planet diameter observed to date. Here we present an overview of Dawn mission findings for large impacts and the constraints they place on impact models and HED's.

3:50 p.m. Jutzi M. * Ivanov B.
Modelling the Rheasilvia Impact **[#2008]**
We present an overview of recent 2D and 3D modeling of the formation of the giant Rheasilvia basin. The various model approaches will be discussed in the context of the observations of Vesta by Dawn.

4:10 p.m. Otto K. A. * Jaumann R. Krohn K. Matz K.-D. Preusker F. Roatsch T. Schenk P. Scholten F. Stephan K. Raymond C. A. Russell C. T.
Mass-Wasting Features in Vesta's South Polar Region **[#2010]**
We analysed mass-wasting features correlated with the Rheasilvia and Veneneia basins including intra-crater mass wasting, flow-like and creep-like features, slumping blocks, landslides, and curved ridges.

4:25 p.m. Mittlefehldt D. W. * Nathues A. Beck A. W. Hoffmann M. Schaefer M. Williams D. A.
Geological Structures in the Walls of Vestan Craters **[#2041]**
We are examining geological structures in the walls of vestan craters using Dawn Framing Camera imagery. All appear to represent structures in the megaregolith. We have yet to find unequivocal evidence for primary crustal structures on Vesta.

4:40 p.m. Carsenty U. * Wagner R. Jaumann R. Schröder S. E. Raymond C. A. Russell C. T.
Boulders on the Surface of Vesta — The Southern Hemisphere **[#2036]**
We conducted an exhaustive search for boulders and their corresponding craters in the southern hemisphere of Vesta. We identified 4644 boulders, associated with 72 craters. The craters vary in size between 1 and 37km.

4:55 p.m. Buczkowski D. L. * Wyrick D. Y. Kahn E. Barnouin O. Nathues A. Gaskell R. W. Roatsch T. Preusker F. Russell C. T.
The Tectonics of Vesta **[#2037]**
Framing Camera images revealed the presence of multiple structural features at a variety of scales on Vesta. Analysis of these structures was performed to better understand their genesis and implications for the asteroid.

5:10 p.m. Bowling T. J. * Johnson B. C. Melosh H. J.
Formation of Equatorial Graben on 4 Vesta Following the Rheasilvia Basin Forming Impact **[#2018]**
The equatorial graben on 4 Vesta were opened by a stress wave within 500 seconds of the Rheasilvia basin forming impact. The amount of extension expected is dependent on porosity, core strength, and damage to the body from previous impacts.

5:25 p.m. Stickle A. M. * Schultz P. H. Buczkowski D. L. Iyer K. A.
The Effects of Giant Impact into a Differentiated Vesta: Implications for Large-Scale Trough Formation **[#2025]**
Dawn observed two sets of approximately linear faults on the surface of the asteroid 4 Vesta. Our experimental and numerical results show that this is a natural consequence of large, oblique impacts into a spherical, differentiated target.

5:40 p.m. DISCUSSION

Monday, February 3, 2014
POSTER SESSION: VESTA AT LARGE
6:00 p.m. Great Room

Roatsch Th. Kersten E. Matz K.-D. Preusker F. Scholten F. Jaumann R. Raymond C. A. Russell C. T.
The Atlases of Vesta **[#2007]**
One of the major goals of the mission is a global mapping of Vesta. Atlases from Survey, HAMO, and LAMO mission phases were calculated. Nomenclature for geological features was propsed to IAU and applied to the atlases.

Roatsch Th. Schröder S. E. Mottola S. Matz K.-D. Kersten E. Jaumann R. Raymond C. A. Russell C. T.
The Colors of Vesta **[#2006]**
One of the goals of the Dawn mission was a global color mapping of Vesta. True color was achieved by scaling images acquired through the red, green, and blue filters to RGB values calculated from the CIE color matching functions and a Vesta spectrum.

Preusker F. Scholten F. Matz K.-D. Roatsch T. Jaumann R. Raymond C. A. Russell C. T.
Global Shape of (4) Vesta from Dawn FC Stereo Images **[#2027]**
After about one year in orbit of (4) Vesta, the Dawn Framing Camera (Dawn FC) acquired several thousand clear filter images. We have used these images to derive a global shape of (4) Vesta represented by a digital terrain model (DTM).

Scully J. E. C. Yin A. Russell C. T. Buczkowski D. L. Williams D. A. Blewett D. T. Ruesch O. Hiesinger H. Le Corre L. Mercer C. Yingst R. A. Garry W. B. Jaumann R. Roatsch T. Preusker F. Gaskell R. W. Schröder S. E. Ammannito E. Pieters C. M. Raymond C. A.
Geomorphology and Structural Geology of Saturnalia Fossae and Adjacent Structures in the Northern Hemisphere of Vesta **[#2002]**
This work examines the link between impact cratering processes and structural and geologic features in Vesta's northern hemisphere through a mapping study of the Saturnalia Fossae, adjacent structural features and geologic units.

Stephan K. Jaumann R. De Sanctis M. C. Tosi F. Ammannito E. Krohn K. Zambon F. Marchi S.
Vesta — Compositional Fingerprint of Small Fresh Impact Craters **[#2004]**
We investigated the spectral properties of small fresh impact craters with respect to their geo- and geomorphological context in order to further understand the composition of the upper as well as lower parts of Vesta's crust.

McFadden L. A. Skillman D. R. Memarsadeghi N. Li J.-Y. Mutchler M. McLean B. Carsenty U. Mottola S. Hellmich S. Sykes M. V. Tricarico P. Palmer E. Russell C. T. Raymond C. A.
Experiment to Determine the Upper Limits and Completeness of Dawn's Search for Satellites at Vesta **[#2009]**
Dawn's satellite working group planned and executed a satellite search upon approach to Vesta. We report efforts to determine our upper limits of detection and completion. No satellites were found with 50% completeness to apparent visual magnitude 20.54.

Le Corre L. Reddy V. Schmedemann N. Becker K. J. O'Brien D. P. Yamashita N. Peplowski P. N. Prettyman T. H. Li J.-Y. Cloutis E. A. Denevi B. W. Kneissl T. Palmer E. Gaskell R. W. Nathues A. Gaffey M. J. Mittlefehldt D. W. Gary W. B. Sierks H. Russell C. T. Raymond C. A.
Nature of the "Orange" Material on Vesta from Dawn **[#2048]**
The Dawn mission revealed distinct units on Vesta with red spectral slope. Oppia ejecta is identified as "Leslie unit" postulated by Gaffey (1997). Orange material composition is unlikely to be metal or olivine. Its nature is most likely impact melt.

Zambon F. De Sanctis M. C. Schröder S. Tosi F. Li J.-Y. Longobardo A. Ammannito E. Blewett D. T. Palomba E. Capaccioni F. Frigeri A. Capria M. T. Fonte S. Mittlefehldt D. W. Nathues A. Pieters C. Russell C. T. Raymond C. A.
Global View of the Bright Material on Vesta **[#2023]**
In this work we will give a global view of the bright material on Vesta. We studied the mineralogy of the bright material units through the spectral parameters analysis.

Reedy R. C. Prettyman T. H. Yamashita N.
Peaks in Dawn Gamma-Ray Spectra at and Near Vesta **[#2047]**
The peaks in gamma-ray spectra at various distances from Vesta are presented and summarized. Spectra from Vesta for low- and high-neutron leakage fluxes are also presented.

Szurgot M.
Mean Composition of Feldspar in HED Meteorites and in Protoplanet Vesta **[#2052]**
Mean composition of feldspar in 28 HED meteorites has been determined and compared with the mean composition of feldspar in HED meteorites parent body. Vesta mean feldspar predicted by various models is very close to eucrites and howardites feldspar.

Voropaev S. A.
Some Petrological Constrains on the Vesta Mantle from the Study of Gravitational Potential by the Dawn Mission **[#2021]**
In order to explore the implications of the gravity and shape for the interior structure of Vesta, simple two-layer mass-balance model was explored with an assumed core as two axial oblate ellipsoid.

Slyuta E. N.
Gravitational Deformation and Thermal History of Vesta **[#2012]**
Significant difference between the magnitude of the stress deviator on Vesta and the yield strength of stony meteorites confirms that Vesta in the early stages of its existence has subjected to strong heating, and, perhaps, even to complete melting.

Schenk P. Vincent J.-B. Bray V. Kramer G.
Cratering on a Small Planet: Morphologies of Fresh Craters and the Simple-Complex Transition on Vesta **[#2042]**
We examine simple crater formation processes and the simple-complex crater transition on Vesta, the largest non-lunar asteroidal/dwarf planet visited to date.

Kochemasov G. G.
From Vesta to Ceres: Predicting Spectacular Dichotomous Convexo-Concave Shape for the Largest Mini-Planet in the Main Asteroid Belt **[#2003]**
Predicting spectacular dichotomous convexo-concave shape of Ceres is based on available poor quality images but mainly on comparative wave planetology showing that all celestial bodies in non-circular keplerian orbits are warped and wave1 bends them.

Tuesday, February 4, 2014
VESTA ON THE OUTSIDE: SURFACE COMPOSITION
9:00 a.m. Lecture Hall

Chairs: **Lucille Le Corre**
Vishnu Reddy

9:00 a.m. Reddy V. * Le Corre L. Nathues A. Li J.-Y. McCord T. B. Gaffey M. J. Russell C. T. Raymond C. A.
Vesta Surface Colors and Mineralogy **[#2035]**
We present summary of color observations of Vesta from Dawn Framing Cameras. Comparison of ground based and HST observations of Vesta with those from Dawn is also presented. Nature of color units and their mineralogy is summarized.

9:20 a.m. De Sanctis M. C. * Ammannito E. Combe J. P. Jaumann R. McCord T. B. McFadden L. A. McSween H. Y. Pieters C. A. Raymond C. A. Russell C. T.
Vesta Mineralogy in the Light of Dawn **[#2020]**
The data from Dawn VIR characterized and mapped the mineral distribution on Vesta, strengthened the
Vesta–HED linkage, discovered hydrated materials, found olivine in an unexpected location, providing new insights into Vesta's formation and evolution.

9:40 a.m. Clenet H. * Jutzi M. Barrat J.-A. Gillet Ph.
Adapted Modified Gaussian Model: No Detection of Olivine in Regions Predicted to be Mantle-Rich from Models of Planet-Scale Collisions **[#2013]**
We use an adapted version of the Modified Gaussian Model on VIR images. Despite focusing on two regions in the southern hemisphere where mantle-rich rocks are expected, we found no olivine. We also look at pyroxenes composition at a local scale.

9:55 a.m. Ruesch O. * Hiesinger H. DeSanctis M. C. Ammannito E. Palomba E. Longobardo A. Capria M. T. Capaccioni F. Frigeri A. Tosi F. Zambon F. Fonte S. Magni G. Raymond C. A. Russell C. T.
Some more Locations of Possible Exposed Olivine on Vesta Using VIR/Dawn Data **[#2030]**
We developed and calibrated specific parameters to isolate the olivine signature within the near-IR data acquired by VIR/Dawn. We found that potential olivine occurs as local exposures mainly within the eastern hemisphere of Vesta.

10:10 a.m. BREAK

10:25 a.m. Palomba E. * Longobardo A. De Sanctis M. C. Marchi S. Zambon F. Tosi F. Ammannito E. Capaccioni F. Capria M. T. Russell C. T. Raymond C. A.
Nature of Dark Material Units on Vesta: Implications for Regolith Formation and Carbonaceous Material Delivery **[#2031]**
A catalogue of dark material units on the Vesta surface is listed. A spectral analysis revealed the carbonaceous chondrites (CC) as main darkening agents and a fine-grained regolith. Implications for regolith formation and CC delivery are discussed.

10:40 a.m. Rivkin A. S. *
Exogenic OH on Vesta: Implications from and for Other Asteroids **[#2040]**
Evidence suggests infall from carbonaceous chondrites, a process that may be widespread, is responsible for the presence of hydrated material on Vesta. I will discuss the implications of this process, both problems it solves and creates.

10:55 a.m. McSween H. Y. * Mittlefehldt D. W. Dawn Science Team
Vesta in the Light of Dawn, but Without HEDs? **[#2016]**
Dawn's exploration of Vesta has depended critically on HEDs. As a way of describing HEDs, we explore what petrologic and geochemical predictions could have been made without these meteorites.

11:15 a.m. DISCUSSION

Tuesday, February 4, 2014
VESTA ON THE INSIDE: CORE AND MANTLE
1:30 p.m. Lecture Hall

Chairs: **Walter Kiefer**
Harry McSween

1:30 p.m. Raymond C. A. * Park R. S. Asmar S. W. Konopliv A. S. De Sanctis M. C. Jaumann R. McSween H. Y. Prettyman T. H. Russell C. T. Smith D. E. Toplis M. Zuber M. T.
Constraints on Vesta's Interior Evolution from Dawn Geophysical Data **[#2051]**
Dawn gravity, topography and spectral data provide constraints on Vesta's origin and evolution. Surface heterogeneity supports evidence from the gravity field for intracrustal compositional variations consistent with discrete magmatic systems.

1:50 p.m. Ermakov A. I. * Zuber M. T. Smith D. E. Raymond C. A. Fu R. R.
Modeling Vesta's Internal Structure with Dawn Gravity and Shape Models **[#2019]**
We use Vesta gravity and topography in connection with the geochemically derived constraints to study Vesta's internal structure, rotational history and compensation state.

2:05 p.m. Marchi S. * De Sanctis M. C. Ammannito E. McSween H. Y. McFadden L. A. Raymond C. A. Elkins-Tanton L. T. Bottke W. F. Russell C. T.
New Insights on the Differentiation of Asteroid Vesta **[#2044]**
The detection of olivine on the surface of Vesta will be discussed in relation to the inferred collisional and geological evolution of the asteroid.

2:20 p.m. Kiefer W. S. * Mittlefehldt D. W.
Core Formation and Evolution of Asteroid 4 Vesta **[#2038]**
HED meteorite siderophiles require separation of metal and silicates prior to eucrite solidification. Core formation most likely occurred as a metallic rain in a magma ocean. Dynamo models are sensitive to the distribution of heat producing elements.

2:35 p.m. Toplis M. J. * Mizzon H. Forni O. Prettyman T. H. McSween H. Y. McCoy T. J. Mittlefehldt D. W. DeSanctis M. C. Raymond C. A. Russell C. T.
Bulk Composition of Vesta as Constrained by the Dawn Mission and the HED Meteorites **[#2033]**
Mass-balance and thermodynamics are used to constrain core size/density and mantle mineralogy of chondritic bodies with eucrite crust. Comparison with HED's and data from Dawn is most consistent with a Na-poor H-chondrite bulk composition for Vesta.

2:50 p.m. BREAK

3:05 p.m. Formisano M. * De Sanctis M. C. Federico C. Turrini D.
Thermal and Geophysical History of Vesta **[#2017]**
We analyze the thermal and geophysical history of Vesta by using a 1D conductive-convective-radiative model, investigating the link between the evolution of the internal structure and thermal heating due to short and long-lived radionuclides.

3:20 p.m. Tkalcec B. J. * Brenker F. E.
Early Dynamic Mantle Movements in the Young, Semi-Crystallized Vesta **[#2022]**
Structural studies of olivine-rich diogenites indicate that the solidification of the HED parent body was not a static progression, but involved large-scale dynamic mantle movements, not unlike those experienced by the early Earth.

3:35 p.m. Hoff C. Jones J. H. * Le L.
Experimental Constraints on a Vesta Magma Ocean **[#2046]**
Thermodynamic models of a Vesta magma ocean (MELTS) are inconsistent with experiments and with chemical analyses of natural eucrites. Therefore, there is currently no experimental evidence for a relationship between eucrites and diogenites.

3:50 p.m. Elkins-Tanton L. T. * Mandler B. E. Fu R. R.
Placing Vesta in the Range of Planetesimal Differentiation Models **[#2034]**
The HED meteorites are best modeled by melt extraction from a mush into shallow magma chambers, a model consistent with inefficient crystal settling in an interior magma ocean.

4:10 p.m. DISCUSSION AND PANEL

DISCOVERY AND EARTH-BASED RECONNAISSANCE OF VESTA. R. P. Binzel, Department of Earth, Atmospheric, and Planetary Sciences, Massachusetts Institute of Technology, Cambridge, MA 02139 USA

Summary: In many ways Vesta epitomizes the advancement of planetary science, where objects begin as astronomical targets (known for decades or centuries) and are transformed into geological worlds by *in situ* exploration. This talk will review the circumstances of Vesta's discovery in 1807 and earliest reported physical measurements. Vesta was then at the center of the advent of asteroid physical studies in the 1970's with the recognition of its basaltic-like surface spectrum and resemblance to HED meteorites [1] and the arguments for its likelihood as "the" HED meteorite parent body [2]. Astronomical and dynamical discovery of the pathway for that link [3,4] predicted and subsequently revealed [5] major impact excavation at the south pole of Vesta. Rotational mapping, via time-resolved spectroscopy [6] and direct imaging [7] revealed a hemispheric dichotomy for Vesta. All of these Earth-based deductions, implying Vesta was akin to being "the fifth terrestrial planet" [8] with a thermal history pre-dating the Moon, made Vesta a tempting prime target for a Discovery-class mission. NASA agreed and Dawn emerged from the competition. The extent to which Earth-based observations correctly predicted in advance Vesta's detailed nature, and the areas that missed the mark, offer lessons for the ongoing endeavor of planetary exploration.

[1]T. B. McCord, J.B., Adams, T.V. Johnson, Asteroid Vesta: Spectral reflectivity and compositional cmplications. Science **168**, 1445-1447 (1970). [2] G. J. Consolmagno, M.J., Drake, Composition and evolution of the eucrite parent body: evidence from rare earth elements. Geochimica et Cosmochimica Acta **41**, 1271-1282 (1977). [3] R. P. Binzel, S. Xu, Chips off of asteroid 4 Vesta: Evidence for the parent body of basaltic achondrite meteorites. Science **260**, 186-191 (1993). [4] J. Wisdom, Meteorites may follow a chaotic route to Earth. *Nature* **315**, 731-733 (1985). [5] P. H. Thomas, R. P. Binzel, M. J. Gaffey, A. D. Storrs, E. N. Wells, B. H. Zellner, Impact excavation on asteroid 4 Vesta: Hubble space telescope results. *Science* **277**, 1492-1495 (1997). [6] M.J. Gaffey, Surface lithologic heterogeneity of Asteroid 4 Vesta. Icarus **127**, 130–157 (1997). [7] R. P. Binzel, M. J. Gaffey, P. C. Thomas, B. H. Zellner, A. Storrs, E. Wells, Geologic mapping of Vesta from 1994 Hubble space telescope images. *Icarus* **128**, 95-103 (1997). [8] K. Keil, Geologic history of asteroid 4 Vesta: The smallest terrestrial planet. In *Asteroids III*, W. Bottke, A. Cellino, P. Paolicchi, R. P. Binzel, Eds. (Univ. Arizona Press, Tucson), 573-584 (2002).

ON THE ORIGIN AND EVOLUTION OF VESTA AND THE V-TYPE ASTEROIDS. W.F. Bottke[1], [1]Southwest Research Institute, Boulder, CO, USA (bottke@boulder.swri.edu)

Introduction. Vesta is one of the most fascinating and best studied asteroids in the asteroid belt. Our insights not only come from DAWN data, but also from decades of in-depth studies of both the HED meteorites, almost certainly from Vesta, and Vesta asteroid family members. Together, they provide powerful constraints describing how Vesta reached its current state. The problem facing collisional and dynamical modelers is to assemble a self-consistent story from these clues that can plausibly match what we know of the origin and evolution of the asteroid belt, meteorites, and the surfaces of inner solar system bodies.

Here we explore several intriguing issues regarding the origin of Vesta, same-sized differentiated bodies, and smaller V-type asteroids (bodies with spectra like Vesta). To address this work, we need the look at many questions, such as: (i) how, where, and how fast did differentiated planetesimals like Vesta grow? (ii) how were they affected by collisional evolution within a primordial disk that also contains protoplanets? (iii) how did the differentiated fragments of these collisions survive to the present? The constraints available to solve these problems are diverse but cryptic; they include meteorite samples (e.g., irons, HEDs), remote observations of unusual asteroids like (16) Psyche, which may be an exposed core of a Vesta-like asteroid, in situ studies of (4) Vesta, and so on.

What We Think We Know. A possible starting point for this discussion concerns the iron meteorites, many which may have come from the cores of differentiated asteroids like Vesta [e.g., 1, 2]. Core formation for some of these bodies appears to be ancient and may be nearly contemporaneous with the origin of the CAIs [3,4]. Iron meteorites may also represent two-thirds of the 100-150 unique asteroid parent bodies sampled among all meteorites [2]. Taken at face value, these factors suggest that differentiated parent bodies and their fragments should be common today in the main asteroid belt. If so, one might argue the main belt was once teeming with several tens or more of Vesta-like bodies, many which were disrupted.

Evidence supporting this scenario, however, is surprisingly meager. Spectroscopic observations of many tens of asteroid families show few signs that their parent bodies once had distinct iron cores nor mantles/crusts derived from melted rock [5]. Instead, we see the opposite: most asteroid families investigated to date are made up of members with remarkably similar spectroscopic signatures and albedos. There is also an apparent paucity of asteroids that might come from the exposed mantles of disrupted differentiated bodies.

For the V-type asteroids, almost all of them are D < 10 km, consistent with fragments from cratering events on very large asteroids [6]. Most in the inner main belt have similar inclinations to Vesta, and are most easily explained as Vesta family members dispersed in semi-major axis by (i) high ejection velocities and (ii) a billion years or more of Yarkovsky evolution. More puzzling are the smattering of V-types in the central/outer main belt; they are scattered over a wide range of eccentricities and inclinations, and have no obvious dynamical association with Vesta. Recent spectra work also suggests they are unrelated to Vesta.

Taken together, we have a conundrum. Somehow, we need to make lots of differentiated bodies, extract material from their deep interiors, yet hide or eliminate most of the expected traces that would come from extraction. How can this be done?

Pathway to a Solution. As a possible solution, consider that planetesimals are predominantly heated, overall, by the decay of short-lived radionuclides like ^{26}Al [7]. This means that only the fastest and/or largest growing bodies have a chance to melt globally [8]. According to planetesimal formation models, faster-growing bodies are those that form closer to the Sun. This may suggest that many iron meteorite parent bodies formed in the terrestrial planet region [1]. These differentiated planetesimals may have also evolved side-by-side with larger and similar-sized protoplanets. Collisions between these bodies were inevitable, and their accretion was inefficient [9]. Hit and run collisions were presumably common, with the fragments often forming core-enriched bodies. Repeated hit and run collisions could leave naked molten cores or core fragments buried by remnant mantle and crustal silicates [10]. Collisional evolution in the terrestrial region was also intense [1], and only the largest, strongest, or most fortunate bodies survived for very long.

Capturing Objects in the Main Belt. In this view, only a modest number of fully and partially differentiated bodies were likely to be indigenous to the main belt. The rest may be hit and run byproducts from the terrestrial planet region that were captured in the main belt region by early dynamical processes. This could explain why the asteroid belt has a number of sizable but isolated fragments that look like they came from differentiated protoplanets. We hypothesize that central/outer main belt V-types are potentially small fragments from "Vesta's sisters" that were scattered into the main belt from the terrestrial planet region. There is some evidence for this, with a few eucrites having different oxygen isotopes than standard eucrites [11].

There are many dynamical scenarios that could move terrestrial planet region material (TPM) onto stable orbits within the main belt region. One involves gravitational scattering among planetary embryos [1].

Another involves scattering/capture opportunities within the Grand Tack model when Jupiter migrates across the primordial asteroid belt [12]. In Fig. 1 we evaluate

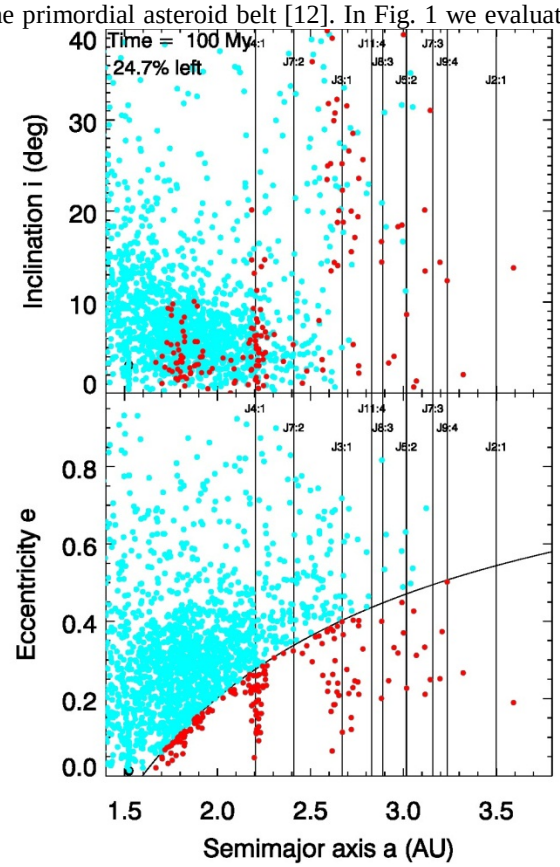

Fig. 1. Objects scattering off of Mars (blue dots) enter into non-Mars-crossing orbits (red dots) through primordial mean motion resonances of giant planets. Giant planets orbits defined by [23]. Most red objects have inclinations < 20°. Many are on stable orbits within the main belt region after 300 My, the end of the simulation.

TPM capture within the Nice model, with the giant planets residing for hundreds of My on nearly-circular, co-planar orbits in a much more compact configuration than they have today (all between 5-12 AU) [13]. We simulated how planetary perturbations affected test bodies started outside the primordial main belt region. We found that many bodies scattering off of Mars were able to enter into the primordial main belt via "fossil" mean motion resonances, where they stayed for 100s of My. These bodies were permanently captured when the host resonances moved via late giant planet migration, possibly at ~4.1-4.2 Ga.

Indigenous Vestas in the Primordial Main Belt?. These results also suggest a second possible scenario to explain fragments of differentiated bodies in the main belt. Let us suppose that Vesta once had "sister" objects in the main belt. This idea would be consistent with dynamical models predicting the asteroid belt had considerably more mass long ago that was eventually eliminated by a dynamical depletion process (e.g., sweeping resonances caused by planetary migration [13,14], ejection by planetary embryos [1] or Jupiter interacting with the asteroid belt [10]).

To investigate these issue, we used *Boulder*, a collisional code capable of simulating the dynamical depletion and collisional fragmentation of multiple planetesimal populations using a statistical particle-in-the box approach [15]. We input into *Boulder* an estimate of the primordial main belt size distribution stretched across many semimajor axis zones as well as a number of Vesta-like objects. We tracked these populations and their fragments for hundreds of My until the time of the late giant planet migration ~4 Ga. We then assumed the populations dynamically lost sufficient mass that collisional grinding over the next 4 Gy could produce the current main belt population.

Our preliminary results suggest the history of Vesta and her putative sisters can be used to constrain main belt history. We find that an excited primordial main belt with more than 3-4 Vestas after the first few My produces too many V-type fragments; collisions/dynamics cannot get rid of all of the evidence. Thus, only a very few Vestas ever existed in the main belt region. Collisions on these bodies prior to their dynamical removal might be responsible for the V-types seen in the central/outer main belt. These results would also be consistent with dynamical work indicating that the primordial asteroid belt only lost a factor of 3-4 of its mass during late giant planet migration [16].

Vesta's Family. We find that Vesta's observed family of $D < 10$ km objects has such a steep size distribution that it has an 80% probability of being < 1 Gy old. If true, Vesta's largest basin Rheasilvia, the presumed source of much of the Vesta family, is similarly young, as suggested by superposed crater counts [17]. This result fits with growing evidence that most of the prominent meteorite classes were produced by young asteroid families.

References: [1] Bottke, W. F. et al. (2006) Nature 439, 821. [2] Burbine, T.H. et al. (2002) Asteroids III (U. Arizona Press), 657; [3] Halliday, A.N. & Kleine, T. (2006) MESS II (U. Arizona Press), 775. [4] Baker, J., et al. (2005) Nature 436, 1127. [5] Cellino, A. et al. (2002) Asteroids III (U. Arizona), 632; [6] Durda et al. (2007) Icarus 186, 498. [7] Srinivasan, G. et al. (1999) Science 284, 1348. [8] Grimm, R.E. & McSween, H.Y. (1993) Science 259, 653. [9] Asphaug, E. et al. (2006) Nature 439, 155. [10] Asphaug, E., et al. (2011) Earth Planet. Sci. Lett. 308, 369. [11] Srinivasan, G. et al. (1999) Science 284, 1348.[12] Walsh, K. et al. (2011) Nature 475, 206. [13] Tsiganis, K. et al. (2005) Nature 435, 7041. [14] Gomes et al. 2005. Nature 435, 466. [15] Morbidelli, A. et al. (2010) Astron. J 140, 1391. [16] Nesvorny & Morbidelli (2012) arXiv:1208.2957. [17] Marchi et al. (2012) Science 336, 690.

FORMATION OF EQUATORIAL GRABEN FOLLOWING THE RHEASILVIA IMPACT ON ASTEROID 4 VESTA. T. J. Bowling[1], B. C. Johnson[2], and H. J. Melosh[1,2], [1]Department of Earth, Atmospheric, and Planetary Sciences, Purdue University, 550 Stadium Mall Drive, West Lafayette, IN, 47907 (tbowling@purdue.edu); [2]Department of Physics, Purdue University, 525 Northwestern Avenue, West Lafayette, IN, 47907.

Introduction: The geologically recent (~1 Gya) Rheasilvia impact basin on asteroid 4 Vesta is nearly equal in size to the diameter of the asteroid [1, 2] and is the largest known impact basin in the asteroid belt. The stress wave produced by an impact of this size is capable of deforming the surface of a body at considerable distance from the basin itself. The Dawn spacecraft has observed a set of troughs thought to be related to the Rheasilvia impact. These troughs lie ~60-100 degrees from, and lie orthogonal to, the basin center [1]. The spatial relationship between crater and troughs suggests that they are related, with the troughs being a distal effect of the impact itself. Furthermore, a second, older set of troughs were observed in the northern hemisphere of Vesta, and have a similar spatial relationship to the older, slightly smaller Venenia impact basin [1]. Further analysis of the faults that bound these troughs suggest that they are in fact graben systems and accommodate several kilometers of extension [3].

While the spatial relationship between the graben systems and the large impact basins suggest strongly that they are related, it is unclear exactly what mechanism is responsible for their formation. One possibility is that they are the result of long term deformation related to the collapse of the Rheasilvia basin. On the other hand, they could have opened as a result of localized impact induced stresses (as has been suggested for the origin of Ithaca Chasma on Tethys [4]), opening concurrently with the transient crater and before the arrival of impact ejecta. If this is the case, we must be able to explain why the Rheasilvia impact created a fresh est of graben instead of re-activating the pre-existing system formed by the earlier Venenia impact. In other words, we must understand what kind of strains are induced by the passage of the impact stress wave as well as how these strains were concentrated only in one region of the body, where the graben system is found. To better understand this issue, we perform numerical modeling of the Rheasilvia impact event. We directly calculate the strains induced by the impact stress wave to gain insight into where strains are localized and what mode of deformation should be expected.

Digital Formats: The Rheasilvia impact was simulated using the iSALE shock physics code [5-7]. Our simulations are run in two dimensions with cylindrical symmetry on an Eulerian (fixed cell) computational mesh with 400 meter resolution, sufficient to resolve the deformation in the near surface of the target. The impactor is treated as a 37 kilometer diameter dunite body striking at 5.5 km s^{-1}. Impact parameters were determined by fitting the observed topography of the Rheasilvia basin to impact model [8]. The target is treated as a spherical body with a basalt crust, a dunite mantle, and a ductile iron core. The thermodynamics of each material are addressed using the ANEOS equation of state. Massless tracer particles are distributed throughout the mesh and follow material flow. By treating each tracer as the node of a quadrilateral element we can calculate individual strain tensor components as a function of time. This provides insight into what types of deformation should be expected in different regions of the target.

Heading Styles: The dominant mode of strain in the target's crust following the passage of the impact stress wave is shear, or (in spherical coordinates) change in radius with respect to latitude. Shear strains on the order of 5% are found throughout much of the target's crust. This is likely a result of spallation in the near surface and basing shearing at the crust mantle boundary. Shearing of this magnitude is capable of deforming the surface on its own, perhaps producing half graben systems. However, the presence of strong shear throughout much of the crust cannot explain why Rheasilvia related graben are found only near the equator of Vesta. Strains along equal lines of longitude, however, show a strong localization of extension in the region where graben are observed. Strains within this locus are on the order of ~1-2%, consistent with strains of ~1-5% based on observation, and are of the correct mode to produce graben of the observed orientation. This suggests that the formation of the equatorial graben on Vesta opened immediately following the Rheasilvia impact, before the arrival of any ejecta from the basin.

Three important parameters controlling the magnitude and localization of extensional stresses in the target body are porosity, core strength, and damage from previous impacts. As the impact stress wave passes through the target's mantle and crust, pore space is crushed out. This saps energy from the wave and greatly reduces the amount of deformation. If the mantle porosity is set at 5%, similar to estimates based on radiometric tracking of the Dawn spacecraft [1], the amount of extensional strain in the region where gra-

ben are found is insufficient to match observation. However, this result may be an effect of the strength of the porous material used (the strength above which pore space begins to be crushed out), and warrants further investigation.

The presence of a ductile core seems to be responsible for localizing the extensional strains in the region where graben are observed. While the strength of Vesta's core is currently unknown, the strength of meteoritic iron has been shown to be dependent on the amount of nickel and carbon in the alloy [9]. In addition, the strength of metals is dependent on accumulated strain [10], and it is possible that previous impacts, such as the one that formed the Venenia basin, could have served to harden Vesta's core. When a 'strong' core rheology is implemented, one in which much of the core deforms elastically as the impact stress wave passes, strains are no longer localized. The dependence of strain localization on core strength and strain magnitude on mantle porosity, coupled with two sets of independently produced graben, can perhaps provide a window into the chemical composition of Vesta's core, the material properties of its mantle, and the asteroid's impact history.

Impacts that occurred on 4 Vesta before the Rheasilvia basin forming event were capable of significantly damaging much of the body. By damage, we are referring to the fragmentation of rock by shock induced strain. When damage occurs, both the angle of internal friction and cohesion of the material are reduced. In otherwords, the strength of the rock is significantly lowered. Damaged material can be induced into non-elastic deformation at lower shock pressures than un-damaged material. We simulate the Rheasilvia forming impact into a target that is already completely damaged through previous impacts. By including previous damage the equatorial model strains can be increased to ~3%, which is close to the value needed to match the observed graben systems. These results suggest that Vesta is likely fractured and damaged throughout its crust and mantle, and in some ways represents the asteroids belt's largest 'rubble pile'.

References: [1] Jaumann R. et al. (2012) *Science, 336,* 687. [2] Schenck P. et al. (2012) *Science*, *336*, 694. [3] Buczkowski D. L. et al. (2012) *GRL,* 39, L18205. [4] Moore J. M. et al. 2004. *Icarus* 171:421. [5] Wünnemann K. et al. 2006. *Icarus, 180,* 514. [6] Amsden A. et al. 1980. *Los Alamos National Laboratory Report, LA-8095*. [7] Ivanov B. A. et al. 1997. *International Journal of Impact Engineering* 20:411. [8] Ivanov B. A. and Melosh H. J. 2012. *43rd Lunar and Planetary Science Conference* #2148. [9] Petrovic J. J. (2001) *J. Material Sci., 36,* 1579. [10] Johnson G. R. and Cook W. H. (1983) *7th Int. Symposium on Ballistics*, Hague

Acknowledgements: We gratefully acknowledge the developers of iSALE, including Gareth Collins, Kai Wünnemann, Boris Ivanov, Jay Melosh, and Dirk Elbeshausen. We would also like to thank the Dawn science team for feedback and advice on this project.

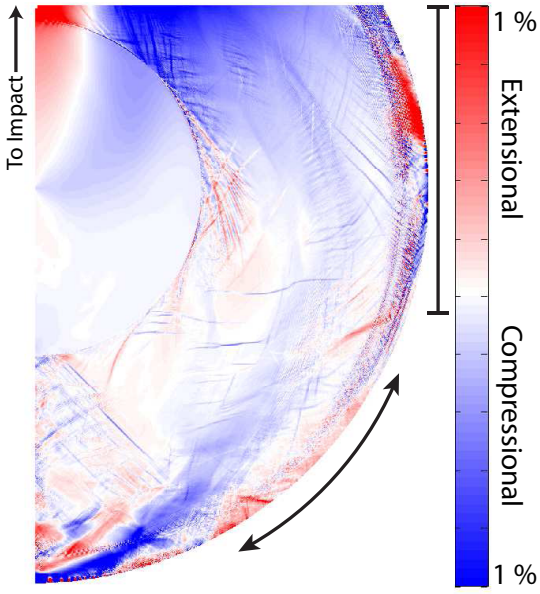

Figure 1: Strains in a completely damaged Vesta-like target body 500 seconds after impact. The image shows a cross section of Vesta from 60 degrees away from the impact point (upper right) to the antipode (bottom). This simulation was run with a mantle porosity of 2% and a crust porosity of 5%. The initial compressive strength of the core was 170 MPa. The strains displayed are change in latitude with relation to latitude, or strains along equal lines of longitude. The black arrow in the bottom of the figure gives a sense of the direction of strains. The black bar gives a sense of the region in which Rheasilvia related graben are found. Within this region there is a locus of strong extensional strain.

THE TECTONICS OF VESTA. D.L. Buczkowski[1], D.Y. Wyrick[2]., E. Kahn[1], O. Barnouin[1], A. Nathues[3], R.W. Gaskell[4], T. Roatsch[5], F. Preusker[5], C.T. Russell[6]. [1]JHU-APL, Laurel, MD; [2]SwRI®, San Antonio, TX; [3]Max Planck Institute, Katlenburg-Lindau, Germany; [4]PSI, Tucson, AZ; [5]DLR, Berlin, Germany; [6]UCLA, Los Angeles, CA.

Introduction: Framing Camera (FC) images from NASA's Dawn spacecraft revealed the presence of multiple structural features at a variety of scales on Vesta. Analysis of these structures was performed to better understand their genesis.

Models of Asteroid Tectonics: Numerical calculations have indicated that impacts into asteroids could be responsible for the formation of fractures. Axisymmetric calculations a Stickney-sized impact in a Phobos-like ellipsoid predicts sizes of spall that compare favorably with the spacing of grooves and fractures seen on Phobos [1], supporting the idea that these feature were in fact the result of the Stickney impact [2]. Simulations also indicate that impacts into the flat portion of an elongated ellipsoid generate circumferential fractures perpendicular to the impact normal, while impacts on the curved ends of the asteroid result in fracturing mainly at the antipode [3]. This model is consistent with observations of Ida [3,4] and Eros [5].

Lineated small bodies could alternately be fragments of larger parent bodies on which the structures actually formed. For example, a pre-existing structure throughout most of Eros was found to be consistent with a fabric inherited from a parent body [6]. These putative parent bodies are larger and maybe even differentiated, meaning that their surface structures could possibly be the result of internal processes such as rifting or uplift. Vesta, being large and differentiated [7], is our first opportunity to search for such planetary style tectonism on an asteroid.

Impact-Related Structures: Features observed on Vesta include an equatorial set of wide flat-floor troughs bound by steep scarps, named Divalia Fossae. These 86 linear structures encircle the asteroid for ~240º longitude. Lengths vary from 19 - 380 km and widths are up to 15 km; vertical displacements along the underlying faults range from ~2 up to 5 km.

A second set of large-scale features, the Saturnalia Fossae, extend to the NW at an angle from Divalia. The primary structure is ~390 km long, 39.2 km wide and accommodates up to 4 km of vertical displacement [8]. Shallower walls, rounded edges, infilling and heavy cratering suggest it is an older feature than the Divalia structures. Seven Saturnalia grooves range from 31-212 km long [8].

The orientation of both fossae is consistent with models of giant impact into a differentiated asteroid [e.g. 8-12]. The poles of the two fracture plane sets cluster roughly at the coordinates of the centers of the Rheasilvia and Veneneia basins (Fig. 1). The older Saturnalia features have poles that cluster at 60º ± 10º latitude and 160º longitude, roughly the center of the older Veneneia basin. The Divalia poles cluster at 78º ± 10º latitude [8,13]; the pole longitudes vary, but all poles are on Rheasilvia's central mound. Clustered poles indicate that the fracture planes are similarly oriented and likely share a common formation mechanism [5,6]. Therefore, despite the large scale of these structures, it seems that they are the result of impact.

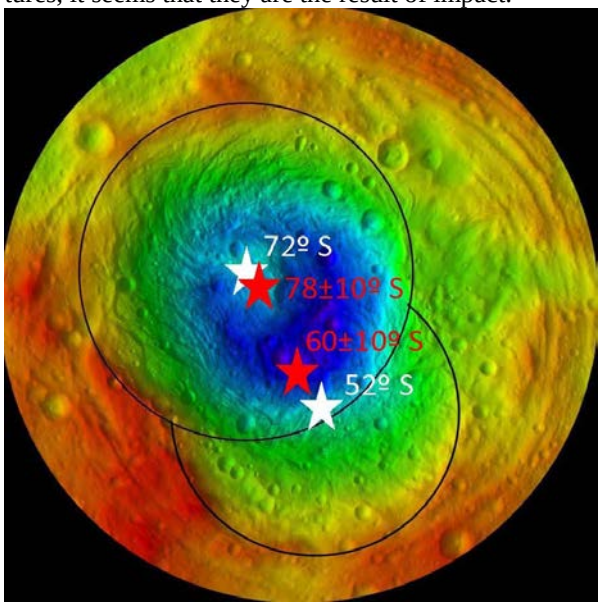

Figure 1. Topographic image of south pole of Vesta. White stars and numbers show latitudes of the centers of Rheasilvia (upper) and Veneneia (lower). Red stars and numbers show the poles of the two sets of fossae.

Possible Non-Impact Structures: The equatorial troughs do not cut the Vestalia Terra plateau (VT), but there are three long pit crater chains (PCCs) observed on its surface [8,14]. PCCs are hypothesized to form when dilational motion on buried normal faults cause overlying material to collapse into the opening portions of the buried fault [15]. The merged pits of the VT PCCs show signs of collapse but distinct fault faces can also be observed [14], suggesting that they are indeed representative of subsurface faulting of the plateau [8].

As the PCC Albalonga Catena progresses westward it phases from being a topographically low feature of merged pits into being the topographically high Brumalia Tholus (Fig. 2a,b). Westward of the hill, merged pits are again visible in the slope data (Fig. 2c). Brumalia Tholus may have formed as a magmatic intrusion utilized the Albalonga fault as a conduit to the surface and deformed the overlying rock [16].

Teia crater impacts the northern face of Brumalia Tholus (Fig. 2) and thus its ejecta is likely sampling Brumalia's core material. These ejecta have a distinct smeared and flow-like texture and a distinct false color in the FC color data. VIR shows that while the background VT material is howarditic [17], the Teia ejecta are more diogenitic [18]. VIR also identified diogenite inside small craters on the top of Brumalia Tholus. These identifications of plutonic diogenite are consistent with the hill representing a magmatic intrusion.

Discussion: Brumalia Tholus as a magmatic intrusion requires that Albalonga faulting occurred before volcanism on Vesta ceased >4.4Ga [e.g. 19,20], long before the Rheasilvia impact (1 Ga [21] or 3.6 Ga [22]). While Albalonga faulting could be the result of an earlier impact, it is also possible that it formed by internal magmatic processes.

Dike injection has been shown to sometimes result in overlying graben formation on Earth, Mars and Venus [e.g. 24,25] and so it is possible that the VT faults formed due to diogenitic intrusion into the crust [26]. However, while the orientation of the VT faults suggests they have a common formation mechanism, only Albalonga Catena shows any evidence of magmatic intrusion. This strongly implies that the faults pre-date the Brumalia intrusion, rather than being caused by it.

Instead, the VT faults may have formed due to extension during the upwelling of the plateau, as VT has been theorized to be a fossil magma plume [23]. Then, due to speculated differences in fault depth, only Albalonga was intruded by the deep molten material.

Regardless, either model invokes internal magmatic processes (not impact) in the formation of the observed structures. Thus the VT PCCS may be the first observation of internally-driven faulting on an asteroid.

References: [1] Asphaug & Melosh (1993) *Icarus* **101**, 144-164 [2] Thomas & Veverka (1979) *Icarus* **40**, 394-405 [3] Asphaug et al (1996) *Icarus* **120**, 158-184 [4] Veverka et al (1994) *Icarus* **107**, 399-411 [5] Buczkowski et al (2008) *Icarus* **193**, 39-52 [6] Thomas et al (2002) *GRL* **29**(10), doi:10.1029/2001GL014599 [7] Russell et al (2012) *Science* **336**, 684-686, *doi:*10.1126/science.1219381 [8] Buczkowski et al (2012) *GRL* doi:10.1029/2012GL052959 [9] Buczkowski et al (2012) *GSA*, Abs. 152-4 [10] Ivanov & Melosh (2012) *43rd LPSC*, Abs. 2148 [11] Stickle et al (2013) *44th LPSC* Abs. 2417 [12] Bowling et al (2013) *44th LPSC* Abs. 1673 [13] Jaumann et al (2012) *Science* **336** doi: 10.1126/science.1219122 [14] Buczkowski et al. (2011) LPSC abs. 2263 [15] Wyrick et al. (2004) *JGR* doi:10.1029/2004JE002240 [16] Buczkowski et al (2013) *44th LSPC*, Abs. 1996 [17] DeSanctis *et al*. (2012) *Science* doi:10.1126/science.1219270 [18] DeSanctis et al (2013) *EPSC* Abs. 173 [19] Schiller et al (2010) *73rd Ann. Meteor. Soc. Mtg.*, Abs. 5042 [20] McSween et al (2011) *Space Sci. Rev*. **163**, 141-174, doi:10.1007/s11214-010-9637-z [21] O'Brien et al (2012) *43rd LPSC*, Abs. 2688 [22] Schmedemann et al. (in revision) *Planet. Space Sci* [23] Raymond et al. (2013) *44th LPSC*, Abs. 2882 [24] Ernst et al (2001) *Ann. Rev. Earth Planet. Sci.* **29**, 489-534 [25] Wilson & Head (2002) *JGR* **107**(E8), 1-24, doi: 10.1029/2001JE001593 [26] Barrat et al (2010) *Geochim. Cosmochim. Acta* **74,** 6218-6231.

Acknowledgements: This work was funded by the Dawn at Vesta Participating Science Program.

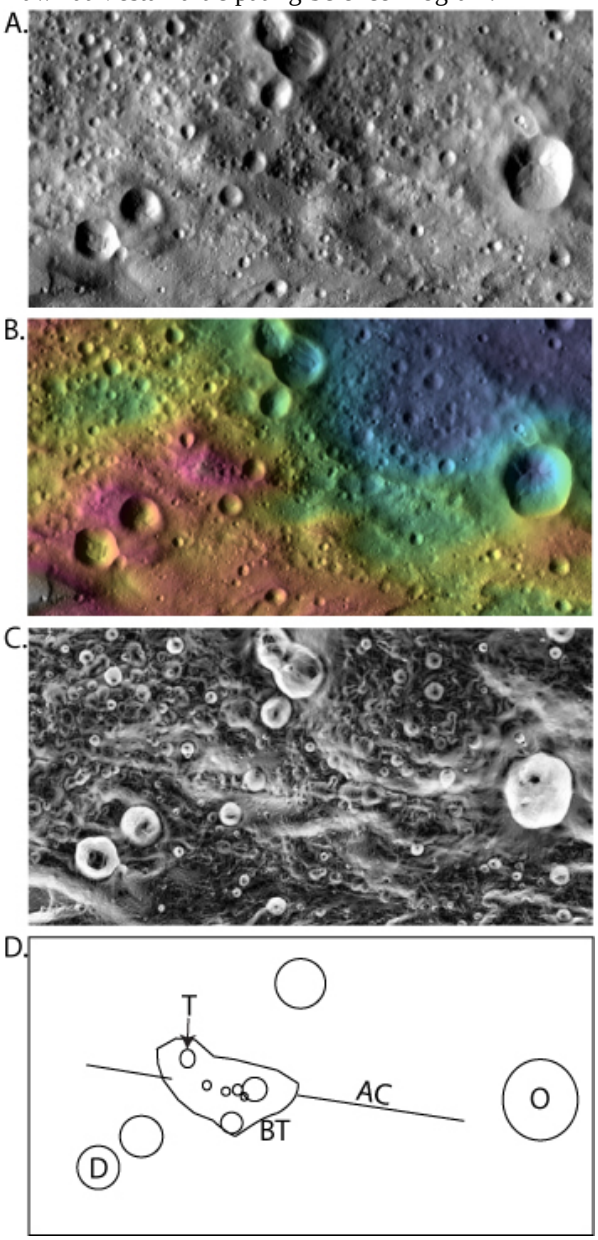

Figure 2. Eastern Vestalia Terra. A) FC mosaic. B) Topography. C) Slope data. D) Sketch map. BT= Brumalia Tholus; AC=Albalonga Catena; T=Teia; O=Oppia; D=Drusilla. Unnamed craters also drawn.

Vestoids, Vesta, and HEDs: What explains their color differences? B. J. Buratti[1], P. A. Dalba[2], and Michael D. Hicks[1] [1]Jet Propulsion Laboratory California Inst. of Technology (4800 Oak Grove Dr., Pasadena, CA 91109; bonnie.buratti@jpl.nasa.gov)

Introduction: One of the most common classes of terrestrial meteorites, the Howardite-Eucrite-Diogenite (HED) assemblage, presents a similar - although diverse mineralogy - to that of Vesta (as inferred from reflection spectra), and it is believed to originate on the asteroid [1]. The link between the HED meteorites and Vesta are provided by the V-type, or vestoid, class of asteroids that appear to be dynamically related to Vesta [2] and that present similar reflection spectra [1,3,4]. Although this picture presents a fairly consistent story – for example, the spectral properties of vestoids as a group are not consistent with any Main Belt asteroid other than Vesta, many details remain to be worked out and several inconsistencies need to be resolved. It has been known for years that the vestoids and HEDs present generally stronger band strengths and redder visible spectral slopes than Vesta [5,6]. The *Dawn* mission also showed the seeming absence or minor role of lunar-type space weathering on Vesta [7] and possibly vestoids. Possible reasons for the differences among Vesta, vestoids, and the HEDs include different compositions, phase reddening, different particle sizes, or space weathering.

Observations: Three types of observations were used in this analysis: ground-based data which includes high resolution spectra of Near Earth vestoids (the reservoir of the HED meteorites) and archived observations [3], spectra from the RELAB archive of HED spectra at Brown University [8], and observations from the *Dawn* Framing Camera (FC) [9].

Results: Both the ground-based and *Dawn* observations had phase reddening parameters applied [9,10] such that they were at the same effective geometry as the RELAB measurements (see Figure 1). Since these corrections are slight and do not significantly bring into alignment the three data sets, phase reddening cannot explain the differences among the three data sets.

For S-type asteroids and the lunar surface, the effects of space weathering tend to redden the spectrum in the visible and mute the absorption bands (11). For Vesta, no such situation exists; in fact, higher albedo regions tend to be redder. Based on *Dawn* results, another mechanism of space weathering is caused by micron-sized opaque particles reducing the spectral contrast and generally darkening the surface [7]. In the lower impact velocity regime of Vesta, brecciation is more important than impact volatization: this form of space weathering is essentially mechanical rather than chemical ("space weathering" may even be a misnomer). In this scenario, the HEDs are in the correct place in Figure 1 for a "fresher", less weathered surface. The redder color of the vestoids is also explained by space weathering: their surfaces are "fresher" than that of Vesta.

in

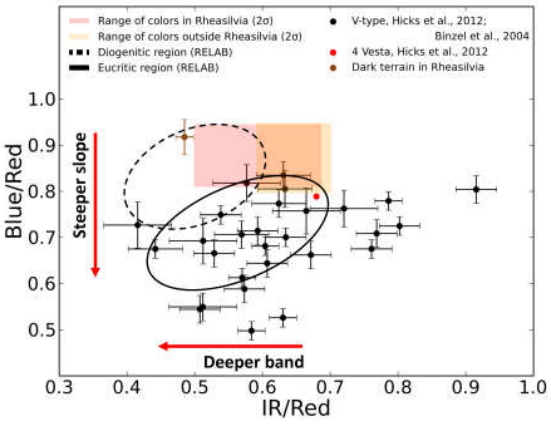

Figure 1. A color-color plot showing the visible slopes (y-axis) and the band depth (x-axis) of vestoids (black dots), Vesta off the Rheasilvia Basin (pastel orange), and on the Rheasilvia Basin (pink). These measurements are from published data from the *Dawn* Framing Camera (FC) [9]. The dotted oval is the position of the diogenite meteorites from the RELAB archive, and the solid oval represents the eucrite samples. (The howardite class of meteorites dwells intermediate between the diogenites and eucrite endmembers.) For comparison, other stony asteroids are shown, illustrating that only the vestoids are near the spectral properties of Vesta. The "dark terrain" on Rheasilvia is the material with the smallest visible slope and deepest pyroxene band: it is represented primarily by the ejecta material surrounding the Oppia crater. It is outside of the 2σ range of the basin's colors. Corrections for phase reddening have been made.

A related alteration mechanism is the addition of spectrally neutral, low-albedo hydrated carbonaceous material to Vesta's surface. [12, 13, 14]. This material should be less prevalent on vestoids, as they possess smaller gravitational wells and thus cannot attract and retain as much exogenous infall. Because the material is spectrally neutral, the vestoids would be redder than Vesta.

Another important factor for explaining the spectral differences may be the particle size of grains in the regolith of Vesta. Pieters et al. [15] showed that the spectrum of Vesta between 0.3 and 2.6 μm fits a typi-

cal howardite meteorite if the particle sizes are less than 25 μm. The band depth in both diogenites and eucrites (especially) is less for samples composed of smaller particles; for the eucrites, the band depth is about 20% less for the fine particles [9]. This is about the size of the discrepancy between the meteorites and the FC data for Vesta in Figure 1. Other lines of evidence point to the existence of small particles on the surface of Vesta. The V-type asteroids are very rough at RADAR wavelengths [16]), but at visible wavelengths Vesta appears to be smoother than the typical asteroid [17]. This condition is explained by the infilling of facets and asperities on the surface by fine particles, similar to the "ponding" seen on Itakawa and Eros, but on a smaller scale. With the larger gravity field of Vesta, small particles would be more likely to be retained than on the smaller vestoids. The high albedo of Vesta [18] also suggests an abundance of fine particles.

Conclusions: The two major factors that explain the discrepancies in optical properties between Vesta, the HEDs, and the vestoids are differing particle sizes and the addition of low-albedo spectrally neutral carbon-rich material to Vesta. With its stronger gravity well, Vesta retains small particles that result from collisional processes: these particles render the surface brighter and bluer. Compounding the effect is the additional of spectrally neutral carbonaceous material. The effects of phase reddening are only slight.

References: [1] McCord, T. et al. (1970). *Science* **168**, 1445-1447. [2] Zappala, V. et al. (1990). *Astron. J.* **100**, 2030-2046. [3] Binzel, R., and S. Xu (1993). . *Science* **260**, 186-191. [4] Moskovitz, N. A. et al. (2010). *Icarus* **208**, 773-788. [5] Burbine, T. H. et al. (2001). Meteoritics and Planetary Science 36, 761-78. [6] Pieters et al., (2006). Asteroids, Comets, Meteors Proc. IAU Sym 229, 1-17. [7] Pieters, C. et al., (2012). *Nature* **491**, 79-82. [8] http://www. planetary.brown.edu/relab [9] Buratti, B. J. et al. (2013). Accepted for publication in *JGR Planets.* [10] Hicks, M. D. et al. (2013). Accepted for publication in *Icarus.* [11] Binzel, R. P. et al., (2004). *Icarus* **170**, 259-294. [12] McCord, T. B. et al. (2012). *Nature* **491**, 83-86. [13] DeSanctis, M. C. et al. (2013). *Science* **336**, 697-700. [14] Prettyman, T. H. et al., (2012). *Science* **338**, 242-246. [15] Pieters, C. et al. (2011). *Space Science Reviews* **163**, 117-139. [16] Benner, L. et al. (2008). *Icarus* **198**, 294-304. [17] Buratti, B. J. et al. (2012). *LPSC* **43**, #1527. [18] Reddy, V. et al. (2012). *Science* **336**, 700-704.

Acknowledgements: This research was carried out at the Jet Propulsion Laboratory, California Institute of Technology under contract to the National Aeronautics and Space Administration. We acknowledge support from the *Dawn* Participating Scientist program. This research utilizes spectra acquired by the NASA RELAB facility at Brown University.

THERMOPHYSICAL ANALYSIS OF PITTED TERRAINS ON VESTA. M. T. Capria[1], F. Tosi[1], M. C. De Sanctis[1], E. Ammannito[1], F. Capaccioni[1], S. Fonte[1] , A. Frigeri[1], A. Longobardo[1], E. Palomba[1] , F. Zambon[1], S. Schroëder[2] , B. Denevi[3], D. A. Williams[4], T. A. Titus[5], D. Blewett[6], C. T. Russell[7] and C. A. Raymond[8].

[1] INAF-IAPS Istituto di Astrofisica e Planetologia Spaziali, Via del Fosso del Cavaliere, 100, 00133 Rome, Italy; [2] Institute of Planetary Research, German Aerospace Center (DLR), Rutherfordstrasse 2, D-12489 Berlin, Germany; [3] The Johns Hopkins University Applied Physics Laboratory, Laurel, MD 20723; [4] School of Eart and Space Exploration, Arizona State University, Tempe, Arizona 85287-1404; [5] U.S. Geological Survey, Flagstaff, AZ, USA; [6] The Johns Hopkins University Applied Physics Laboratory, Laurel, MD, USA; [7] Institute of Geophysics and Planetary Physics, University of California at Los Angeles, 3845 Slichter Hall, 603 Charles E. Young Drive, East, Los Angeles, CA 90095-1567, USA; [8] NASA/Jet Propulsion Laboratory and California Institute of Technology, 4800 Oak Grove Drive, Pasadena, CA 91109, USA.

Introduction: Pitted terrains are known on Mars [1, 2] and have recently been discovered on Vesta [3] by the Dawn spacecraft during its year-long orbital mission [4]. These terrains, always associated with impact craters, occur as thin, heavily pitted deposits. The formation of such terrain on Mars is attributed to the rapid degassing of volatiles in the target material as a consequence of an impact. For this reason, the origin of pitted terrain has interesting implications for the volatile content of the target and the impactor. On Vesta, a similar formation mechanism, involving devolatilization of hydrated minerals has been proposed [3], but the details of the process and the implications for the structural characteristics of the surface are still uncertain.

Pitted terrains on Vesta: Pitted terrains have been found on the floors of Vesta's Marcia and Calpurnia craters [0°-20°N, 180°E-220°E (in the Claudia system)], and within Cornelia crater [10°S-0°, 220°E-230°E (in the Claudia system)]. These regions are all characterized by the presence of a hydroxyl (OH) absorption, mainly in the ejecta [5, 6]. From the initial analysis of Approach data [7] (pixel resolution 1.3 km), it appears that these areas are characterized by a thermal inertia higher than Vesta's average of 30 ± 10 Jm^{-2} $s^{-0.5}$ K^{-1}. In particular, part of Marcia crater exhibits the highest thermal inertia value yet found on Vesta, 50 ± 5 Jm^{-2} $s^{-0.5}$ K^{-1}. These higher than average values can be attributed to structural properties of the surface layer, related to a higher degree of compactness or a higher proportion of exposed bare rock.

Results on high resolution data: We are in the process of refining the analysis of the pitted terrain areas by using the higher-resolution data acquired during the Survey and HAMO phases of the Dawn mission. The technique is similar to the one used to analyze the Approach data. A thermophysical model, giving as a result thermal inertia as a function of thermal conductivity, is used. The initial results from the analysis of Survey and HAMO observations confirm and extend the earlier findings obtained with lower resolution data. Higher than average thermal inertia prevails on and around areas in which pitted terrain have been found; in addition, a few more small regions with a thermal inertia of 50 ± 5 Jm^{-2} $s^{-0.5}$ K^{-1} have also been identified (see fig. 1).

Future work and conclusion: Our thermophysical model strives to provide the best possible simulation of the characteristics of the materials that may be present on the surface of Vesta. We are in the process of improving the expressions for thermal conductivity and density used in the code, and are updating the simulations to better model the structural effects that rapid devolatilization could have on surface material. To this end, we are planning to adapt results on the effect of similar phenomena on Earth and Mars, taking into account the lack of atmosphere and the lower gravity of Vesta.

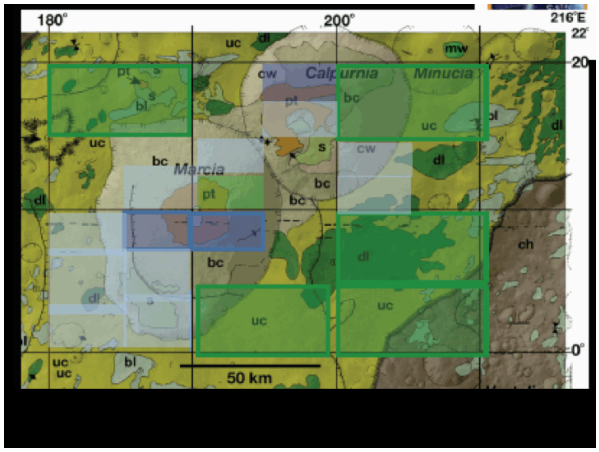

Figure 1: Thermal inertia map of the Marcia and Calpurnia craters superimposed on a geological map (in the Claudia system) [8]. Color code is the following: green, thermal inertia of 30± 10 Jm^{-2} $s^{-0.5}$ K^{-1} + average sub-pixel roughness; light blue, thermal inertia of 40± 10 Jm^{-2} $s^{-0.5}$ K^{-1} + low sub-pixel roughness; blue, thermal inertia of 50± 5 Jm^{-2} $s^{-0.5}$ K^{-1} + low sub-pixel roughness.

Acknowledgements: This work was supported by the Italian Space Agency (ASI), ASI-INAF Contract. The authors would like to thank the Dawn Science, Operation and Instrument. The VIR instrument was developed under the leadership of INAF, Italy's National Institute for Astrophysics, Rome. The instrument was built by SELEX-Galileo, Florence, Italy

References: [1] L. L. Tornabene et al. (2012) *Icarus*, 220, 348-368. [2] J. M. Boyce et al. (2012) *Icarus*, 221, 262-275. [3] B. Denevi et al. (2012) *Science,* 338, 246. [4] De Sanctis, M. C., et al. (2012) *Science*. [5] T. Prettyman et al. (2012) *Science*, 338 [5] M. C. De Sanctis et al. (2012) *Astrophys. J. Lett.*, 758. [7] M.T. Capria et al. 82013) *EPSC 2013*. [8] D. A. Williams et al., *EGU 2012*, 5686.

BOULDERS ON THE SURFACE OF VESTA – The Southern Hemisphere. U. Carsenty[1], R. Wagner[1], R. Jaumann[1], S.E. Schröder [1], C.A. Raymond[2], C.T. Russell[3]. [1]DLR, Berlin Germany (uri.carsenty@dlr.de), [2]JPL, California Institute of Technology, [3]UCLA, Institute of Geophysics.

Introduction: Images from the Dawn mission Low Altitude Mapping Orbit (LAMO) [1,2,3,4] enable us to study the surface of Vesta at a spatial resolution of 20m per pixel. We are using the imaging data to identify surface features down to the 30m size range, and also measure their sizes when above - 80m.

Boulders Studies:

Boulders are the product of impacts on planetary bodies. The rims of craters formed in hard bedrocks are littered with blocks of rocks [5]. The blocks are usually largest on the rim because the ejection velocity is lowest there. The block size should be affected by variables such as rock strength, preexisting cracks, and perhaps impact velocity. The boulders ascend along the crater inner wall from some distance below the original surface, in consonance with the inverted stratigraphy of the rim region. "These shattered fragments of the original subsurface rock layers are further reduced in size as they participate in the strongly sheared excavation flow and are thrown to their final resting places on the rim" [5]. Rocky boulders are frequently observed on the surfaces of planetary bodies and their residence times on the surface can reveal the nature and rates of small scale erosion and weathering processes. The destruction of lunar surface boulders [6] is largely accomplished by collisional disruption due to a small number of relatively energetic impact events that deliver the critical rupture energy. A few hundred boulders were identified on Lutetia [7]. Most are concentrated around the central crater in Baetica regio with a few more apparently associated with Patavium crater**.** The size range of boulders visible to the camera is about 60-300 m. The authors evaluated various destruction mechanisms for ejecta blocks and concluded that using current estimates of the number of small asteroids in the main belt, destruction by impacts of small (several meters diameter) projectiles limits the lifetime of the boulders to 300 million years. This might also apply to Vesta.

The Vesta Data Set: We conducted an exhaustive search for boulders and their corresponding craters in the southern hemisphere of Vesta. We identified 4644 boulders, associated with 72 craters. Some 1400 of these boulders are larger than 80m in diameter and we can derive their size distribution. For the smaller boulders we can only mark their position to study the spatial distribution. In a few cases the craters are in a double or even triple arrangement, so that we have only 62 distinct crater units associated with the boulders. The craters vary in size between 1 and 37km, with a higher abundance of craters with diameters around 8 and 22km. There are small craters surrounded by large number of boulders and large craters associated with only few boulders. The largest number of boulders, (803) surround the crater Cornelia (225.59E, 9.32S. 15km diameter) – see Fig. 1.

Discussion

Formation of boulders requires the presence of a *consolidated subsurface bedrock layer*. The *size* and *depth* of the crater is directly defined by the *impact energy*. The projectile penetrates the regolith and *shatters the bedrock, excavating* the crater cavity. The boulders are ejected in ballistic trajectories and their spatial distribution can be correlated to the geometry of the impact and the structure of the bedrock layer where they formed. The retention of boulders is a function of the gravity field, while their destruction is accomplished by collisions with small meteorite (flux of small meteorite at the main asteroid belt) and other small secondary projectiles from nearby impact craters (regolith gardening).

The Case of Vesta - various scenarios

All the parameter presented above - crater size, subsurface layers and relative age - and the interplay between them are essential in order to understand and explain the observations. We observe a large crater without boulders next to a small crater with boulders. Is the layer of competent material not globally present ? The thickness of the non-consolidated regolith must be included in this analysis. The erosion of boulders is a function of time. Is the presence of boulders a criteria for young age? and does it correlate with other methods to determine geological ages. It might be that all craters (above a threshold size) had boulders in the past, those that do not have them now might be significantly older. This study will add to the general understanding of the structure of the southern basins.

References:

[1] Mest et al. (2013) JGR in Review.
[2] Russell, C.T.& Raymond, C.A. (2011) Space Sci. Rev. 163, 3-23.
[3] Jaumann, R. et al. (2012) Science 336, 687-690.
[4] Russell et al. (2012) Science 336, 684-686.
[5] Melosh H.J. (1988) Impact Cratering.
[6] Basilevsky A.T. et al. (2013) PSS3576.
[7] Kueppers M. et al. (2012) PSS 66, 71-78.

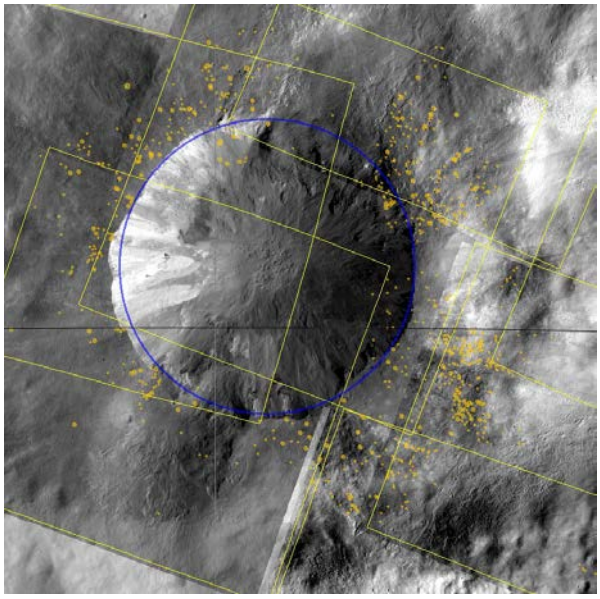

Fig 1a – Cornelia crater – 15km diameter.
The 803 boulders are marked in yellow.

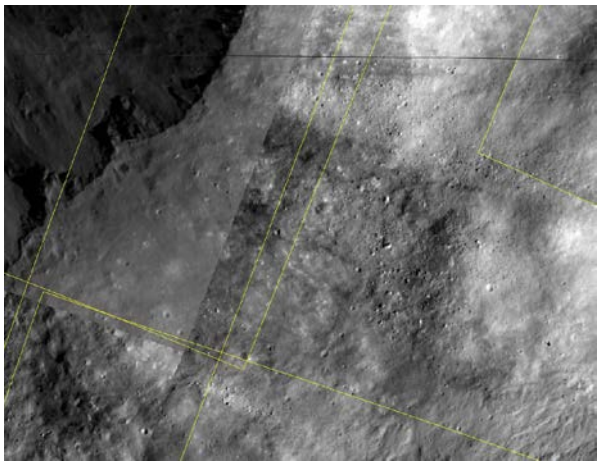

Fig. 1b - The SE corner of Cornelia crater with its extended boulder field. The distance between the 2 largest boulders (above each other near the center) is 900m.

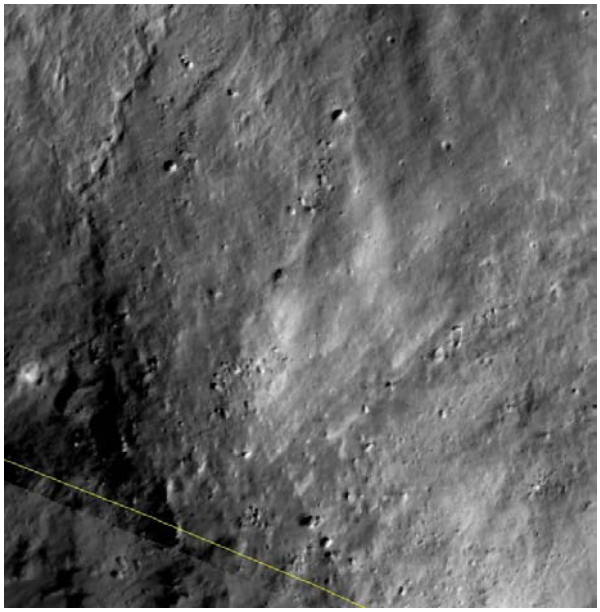

Fig. 1c - The NE corner of Cornelia crater with its extended field of boulders. The distance between the 2 large boulders (almost EW oriented) is 2km.
The size of large boulders is 200m.

ADAPTED MODIFIED GAUSSIAN MODEL: NO DETECTION OF OLIVINE IN REGIONS PREDICTED TO BE MANTLE-RICH FROM MODELS OF PLANET-SCALE COLLISIONS. H. Clenet[1], M. Jutzi[2], J.-A. Barrat[3] and Ph. Gillet[1], [1]Institute of Condensed Matter Physics, Ecole Polytechnique Fédérale de Lausanne (EPFL), Switzerland (harold.clenet@epfl.ch), [2]Physics Institute, University of Bern, Switzerland, [3]Université de Bretagne Occidentale, Institut Universitaire Européen de la Mer, France.

Introduction: Despite many studies on the Howardite-Eucrite-Diogenite (HED) meteorite suite, the internal structure of asteroid 4-Vesta is still debated. Some studies favor the hypothesis of a global magma ocean, leading to a layered structure and a relatively thin crust [e.g. 1]. Other petrological and geochemical evidences tend to favor a more complex structure, involving intrusions, which also implies a thicker crust [e.g. 2]. Recent data from the Dawn mission now shed a new light on this question.

Dawn's global mapping have revealed that the south polar depression is actually composed of two overlapping basins, Veneneia and Rheasilvia [3]. While only one impact cannot excavate rocks from deep, the most recent numerical simulations taking into account both events show that rocks exposed in the Rheasilvia region could come from a depth of much more than 40 km [4,5]. In the case of a thin crust, a succession of two impacts would have then surely digged into the mantle, producing large outcrops of olivine-rich rocks.

The Dawn spectrometer (VIR) is perfectly designed to detect mafic minerals [6]. However, no trace of olivine has been found up to now in the southern hemisphere [7,8]. It is nevertheless true that detecting olivine on the surface of Vesta is challenging [9].

An adapted version of the Modified Gaussian Model (MGM, [10]) has been recently developed to take into account the olivine-pyroxene(s) mixtures [11]. This procedure has been successfully applied to Mars

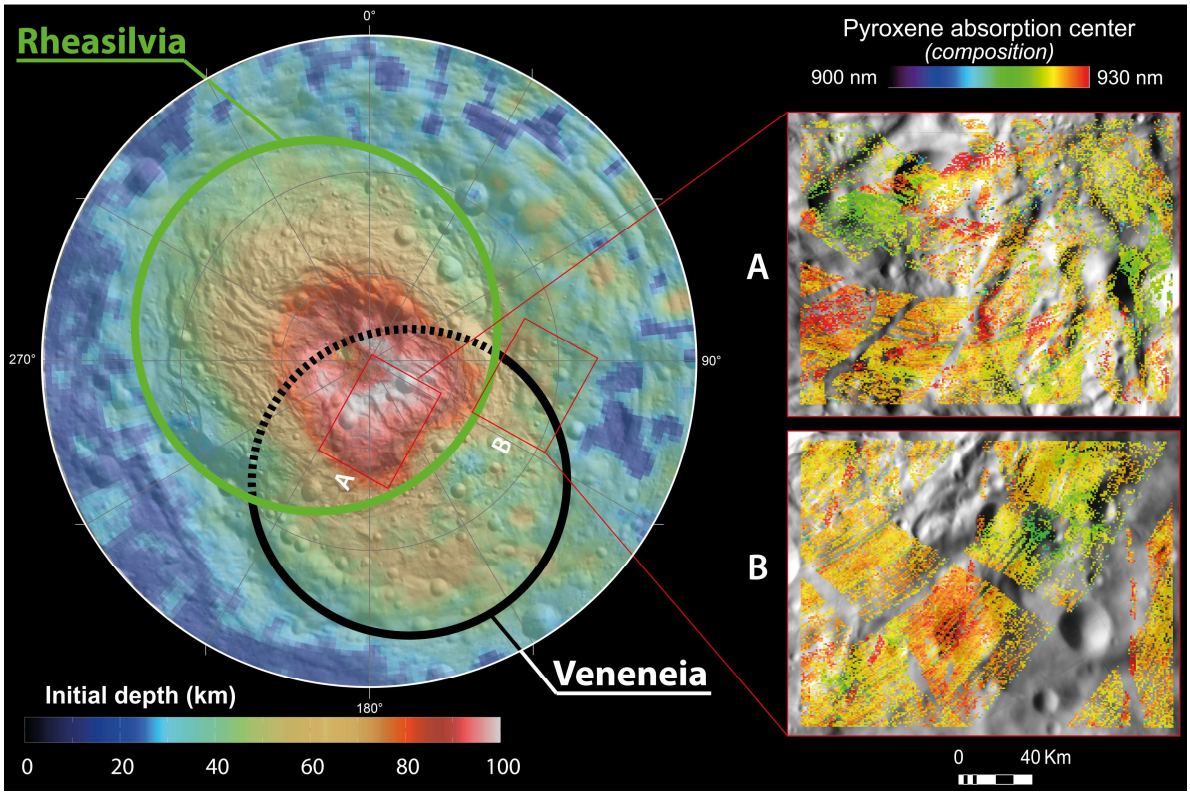

Fig. 1: Pyroxenes composition in the two areas tested. Left: Localization of the two zones relatively to Rheasilvia and Veneneia basins and to the initial depth of the rocks before impacts (determined from numerical simulations [4]); Right: Results of the adapted MGM procedure for the pyroxene absorption center at 1 µm. Region A corresponds to rocks supposed to come from the deepest while region B refers to a spot enriched in diogenite-like lithology [8]. In both areas, no olivine has been found.

[12] and the Moon [13]. Here we test this approach on VIR images in the Rheasilvia region to search for olivine and characterize pyroxenes compositions.

Data selection and processing: The VIR images were first processed through the classical ISIS pipeline. We include a photometric correction using parameters from [14,15,16]. Bad pixels were also filtered using the associated quality cubes. The combination of VIR visible and near-infrared was done after shifting the visible part to correct any geographical misalignment between the two detectors. Conversion to I/F was done using Kurucz solar irradiance spectrum resampled at VIR-IR sampling and resolution. Finally all the VIR images have been projected and assembled in a mosaic covering all the southern hemisphere of Vesta.

Due to the waiting period before the public release of the VIR dataset and the computing time required to run the MGM, we choose to focus on two particular areas (Figure 1). The first one, labelled A, corresponds to the place where we expect to find the rocks that come from the deepest, up to more than 80 km, according to [4]. The second place, labelled B, refers to a spot enriched in diogenite-like lithology according to [8]. Both areas are places where outcrops of rocks containing olivine could occur.

We then applied there our MGM procedure. MGM is designed to deconvolve absorption bands in reflectance spectra using a series of Gaussian functions and a spectral continuum modeled by a polynomial shape. An automated procedure involving different numbers of Gaussians, depending on the potential complexity of the mixture, has been implemented (all the details can be found in [11]). The resulting band parameters (center, strength, width) are finally used to interpret the spectrum in terms of modal abundances and chemical compositions.

Results: Before applying our MGM procedure blindly on the VIR dataset, we tested its capabilities on few HED spectra described in [17]. MGM results show that we were successfully able to predict the presence of olivine in two harzburigtic diogenites (NWA4223 and NWA5380).

We then applied our MGM procedure on the two selected areas. The first result is that we were unable to find any trace of olivine in accordance with observations made by the Dawn team.

Pyroxenes absorption centers, deducted from Gaussians parameters, fall within the HED fields as defined in [7,8]. Most of our detections corresponds to diogenite or howardite. We plot in Figure 1 the two maps of the absorption centers at 1 µm. In both areas, variations are observed at a local scale and on almost the same range of values. Those local variations seem to be mainly related to the distribution of small impact craters excavating the shallow subsurface. At first order, there is no evidence that a relationship between the very local surface composition observed today and the initial depth of rocks exists, or it has been masked by the late impact gardening. This relationship is only observed at the asteroid scale, as seen on the maps in [8].

Conclusion: The lack of olivine detection in the Veneneia/Rheasilvia region implies that olivine, if present, do not represent a large fraction of the whole rocks. This argue against the idea that mantle is excavated in this region. Considering the depth of excavation predicted in the case of two impacts, our results would favor the hypothesis of a thick crust with a crustal thickness of more than 80 km.

We now plan to extend the MGM processing to the rest of the mosaic. This will improve the statistics on pyroxenes compositions. In the same time, we will look at the olivine-rich region found very recently by [18] in the northern hemisphere. We will try to characterize their chemical composition to check how those detections relate to olivines in HED.

References: [1] Mandler B. E. and Elkins-Tanton L. T (2013) *Meteoritics & Planet. Sci.*, 10.1111/maps.12135. [2] Yamaguchi A. et al. (2011) *JGR*, 10.1029/2010JE003753. [3] Schenk P. et al. (2011) *Science*, 10.1126/science.1223272. [4] Jutzi M. et al. (2013) *Nature*, 10.1038/nature11892. [5] Ivanov B. A. and Melosh H. J. (2013) *JGR*, 10.1002/jgre.20108. [6] De Sanctis M. C. et al. (2011) *Space Sci. Rev.*, 10.1007/s11214-010-9668-5. [7] McSween H. Y. et al. (2013) *JGR*, 10.1002/jgre.20057. [8] Ammannito E. et al. (2013) *Meteoritics & Planet. Sci.*, 10.1111/maps.12192. [9] Beck A. W. et al. (2013) *Meteoritics & Planet. Sci.*, 10.1111/maps.12160. [10] Sunshine J. M. et al. (1990) *JGR*, 95, 6955-6966. [11] Clenet H. et al. (2011) *Icarus*, 10.1016/j.icarus.2011.03.002. [12] Clenet H. et al. (2013) *JGR*, 10.1002/jgre.20112. [13] Clenet H. et al. (2013) *44th LPSC*, Abstract 1494. [14] Reddy V. et al. (2012) *Science*, 10.1126/science.1219088. [15] De Sanctis M. C. et al. (2013) *Meteoritics & Planet. Sci.*, 10.1111/maps.12138. [16] Li J.-Y. et al. (2012) *Asteroids, Comets, Meteors*, Abstract 6387. [17] Beck P. et al. (2011) *Icarus*, 10.1016/j.icarus.2011.09.015. [18] Ammannito E. et al. (2013) *Nature*, 10.1038/nature12665.

THE PRESERVATION AND GEOLOGIC EFFECTS OF EXOGENIC AND HYDRATED MATERIALS ON VESTA. Brett W. Denevi[1], David T. Blewett[1], Debra L. Buczkowski[1], Maria Teresa Capria[2], Maria Cristina De Sanctis[2], Lucille Le Corre[3], Jian-Yang Li[3], Simone Marchi[4], Andreas Nathues[5], David P. O'Brien[3], Noah E. Petro[6], Thomas H. Prettyman[3], Frank Preusker[7], Vishnu Reddy[3], Christopher T. Russell[8], Jennifer E. C. Scully[8], Jessica M. Sunshine[9], Federico Tosi[2], David A. Williams[10]. [1]The Johns Hopkins University Applied Physics Laboratory, Laurel, MD USA, [2]INAF, Istituto di Astrofisica e Planetologia Spaziali, Rome, Italy, [3]Planetary Science Institute, Tucson, AZ, USA, [4]NASA Lunar Science Institute, Boulder, CO, USA, [5]Max Planck Institute for Solar System Research, Katlenburg-Lindau, Germany, [6]NASA Goddard Space Flight Center, Greenbelt, MD, USA, [7]Deutsches Zentrum fur Luft- und Raumfahrt (DLR), Institute of Planetary Research, Berlin, Germany, [8]University of California, Los Angeles, CA, USA, [9]University of Maryland, College Park, MD, USA, [10]Arizona State University, Tempe, AZ, USA.

Introduction: In most respects Vesta resembles a typical airless body, where impact cratering, regolith mixing and downslope movement dominate its geology [e.g., 1,2]. However, Vesta appears to be unique among asteroids observed by spacecraft to date in the degree to which its geology has been influenced by exogenic materials. With the highest geometric albedo of any large rocky body (0.38) [3], Vesta is also striking because of the presence of heterogeneous deposits of dark material with geometric albedos as low as ~0.1 [4]. The majority of this low-reflectance material has been interpreted as exogenic in origin, the result of mixing with carbonaceous impactors [5–8]. Here we review the geologic consequences of the presence of hydrated minerals on an otherwise volatile-poor body, with an examination of how Vesta can inform our understanding of the effects of exogenic materials on other bodies.

Vesta's Pitted Terrain: From Dawn's highest resolution images of Vesta (pixel scales <20 m), clusters of closely spaced, irregular rimless pits (Fig. 1) were identified on several crater floors (Marcia, Cornelia, Licinia, and possibly Numisia) and, in one case, within crater ejecta (Marcia) [9]. The morphology of these pits is consistent with formation due to the rapid release of volatiles, triggered by heating from an impact event. Volatile escape is thought to erode the surface during escape, leaving coalescing pits that have a "soap-bubble"-like geometry [10]. The most prominent examples of the pitted terrain are associated with the 70-km impact crater, Marcia. Marcia formed within a broad region of low-albedo, high hydrogen [5] (Fig. 1), high OH- [8] and thick regolith [11]. It is the largest young impact crater on Vesta, with an estimated age of ~40-120 million years [9,12,13]. The pitted terrain at Marcia occurs within regions that show evidence for impact melt, suggesting substantial heating from an impact event that may have occurred at higher than average velocity [9,13]. Cornelia, which appears to be of comparable or younger age, shows similarly distinct pitted terrain within its floor, whereas such features at Licinia and Numisia are more degraded.

The pitted terrain may be closely tied to Vesta's dark material. Spectra of low-reflectance deposits indicate the presence of OH- and possibly H_2O [8], and Gamma Ray and Neutron Detector (GRaND) data find regions with over 400 μg/g H that correspond to areas of low albedo [5]. With low albedo and an average of 9 wt% H_2O bound within crystal lattices, carbonaceous chondrite meteorites are a likely source of this dark material [e.g., 14,15]. Heating from later impacts into carbonaceous-bearing regolith would result in devolatilization and the production of H_2O vapor. For H concentrations consistent with the GRaND results, calculations of the gas pressure of water vapor within regolith pore space show that it would be thousands of times higher than the overburden pressure of overlying soil; escaping water vapor would easily erode the soil to form the observed pits. Such devolatilization is consistent with the observation that while Marcia crater is located within a region of elevated hydrogen, its immediate surroundings are low in H [5] (Fig. 1).

Similar pitted terrain has been observed within numerous relatively young impact craters on Mars, and a conceptual model for its formation via degassing of a volatile-rich target surface [10,16] applies equally to Vesta. While ground ice was considered as a volatile source on Mars, the results for Vesta suggest that only hydrated minerals are required [9]. The observation that few craters contain pitted terrain at ice-rich high latitudes on Mars [16] may support a mineralogic origin for the volatiles responsible for the formation of pitted terrain on Mars as well.

Discussion: With abundant deposits of carbonaceous debris and the influence of these materials in creating impact-related landforms, Vesta's geology has been affected by exogenic materials to a degree not observed on other airless bodies studied to date. Given the long collisional history of the Solar System, the influence of exogenic materials on Vesta would seem to be a natural consequence; perhaps the real question is why are such effects not more commonly observed on other airless bodies? On the Moon and Mercury, hydrogen is thought to be largely in the form of water

ice segregated within permanently shadowed regions near the poles or solar-wind implanted hydrogen whose main effect may be on the chemical space weathering of the surface. Exogenic materials are observed at low abundances within the lunar regolith (<2% in Apollo regolith samples [17]), but do not contribute to regional (or localized) variations in albedo or geology. Neither are such large effects of exogenic materials seen on other asteroids visited by spacecraft to date. This begs the question, has Vesta undergone some unique collisional history that resulted in unusually large exogenic effects on its surface? While this is possible, we instead suggest that a combination of factors resulted in a higher degree of preservation of exogenic materials on Vesta's surface.

The first of these factors is impact velocity, which plays a large role in the degree of preservation of impactors. The high average impact velocities for the Moon (19 km/s) and even higher velocities for Mercury (43 km/s) [18] result in efficient vaporization of the impactor such that little original material is preserved and any volatiles are lost. In contrast, impact velocities on Vesta are closer to 5 km/s on average, and hydrated clasts observed within HED meteorites confirm that impacts at main-belt velocities do not always lead to devolatilization of the impactor [e.g., 19]. Moreover, the structures of the carbonaceous chondrites clasts in howardites are consistent with a "gentle deposition" on the Vesta surface.

But why do asteroids like Eros, Lutetia, Itokawa, and Steins show little evidence for the influence of exogenic materials? One factor may be the high albedo of Vesta, and models and samples that show it has a dearth of endogenic volatiles, both of which allow for the easier detection and identification of carbonaceous material as exogenic. Another important factor may be the size and structure of the body, which could enhance or inhibit preservation of exogenic materials. Whereas a large, differentiated asteroid like Vesta can preserve a heterogeneous regolith, smaller bodies with no core are more likely to be disrupted or homogenized by seismic shaking, and the ejecta of a single impact can affect the entire surface [20]. These asteroids may also be fragments of larger bodies and thus not preserve the early regolith, whereas the degree of exogenic material on Vesta's surface could indicate that it records the ancient delivery and mixing of exogenic material that was common throughout the Solar System [5,8] (e.g., the "late veneer").

We conclude that the largest coherent rocky bodies within the asteroid belt should show the effects of such exogenic material. Further, on asteroids with abundant hydrated minerals, whether exogenic or native, pitted terrain will also form at locations of high-velocity impacts, and will be preserved at the most recent of these sites. Impact cratering can thus result in not only devolatilization of impactors and target materials at high velocity, but the delivery, exposure, and redistribution of hydrated materials at lower degrees of shock.

Acknowledgements: This work was supported by grant NNX11AC28G from NASA's Dawn at Vesta Participating Scientist program. The authors gratefully acknowledge the support of the Dawn Instrument, Operations, and Science Teams. This work was also supported by an Italian Space Agency (ASI) grant.

References: [1] Jaumann R. et al., *Science* 336, 687–690 (2012). [2] Williams D. A. et al., *Planet. Space Sci.* (2013), doi:10.1016/j.pss.2013.06.017. [3] Li J.-Y. et al., *Icarus* 226, 1252–1274 (2013). [4] Reddy V. et al., *Science* 336, 700–704 (2012). [5] Prettyman T. H. et al., *Science* 338, 242–246 (2012). [6] Reddy V. et al., *Icarus* 221, 544–559 (2012). [7] McCord T. B. et al., *Nature* 491, 83–86 (2012). [8] De Sanctis M. C. et al., *ApJ* 758, L36 (2012). [9] Denevi B. W. et al., *Science* 338, 246–249 (2012). [10] Boyce, J. M. et al., *Icarus* 221, 262–275 (2012). [11] Denevi B. W. et al., *EPSC*, EPSC2012–813 (2012). [12] Marchi S. et al., *Planet. Space Sci.*, in press (2013). [13] Williams D. A. et al., *Icarus*, submitted (2013). [14] Rubin, A. E. et al., *Geochem. Cosmochim. Acta* 71, 2361–2382 (2007). [15] Cloutis, E. A. et al., *Icarus* 216, 309–346 (2011). [16] Tornabene L. L. et al., *Icarus* 220, 348–368 (2012). [17] McKay D. S. et al., in *Lunar Sourcebook*, Heiken, Vaniman, French, Eds. (Cambridge Univ. Press, Cambridge, 1991), 285–356. [18] Le Feuvre, M., M. A. Wieczorek, *Icarus* 197, 291–306 (2008). [19] Zolensky, M. E. et al., *Met. Planet. Sci.* 31, 518–537 (1996). [20] Thomas, P. C. et al., *Nature* 413, 394–396 (2001).

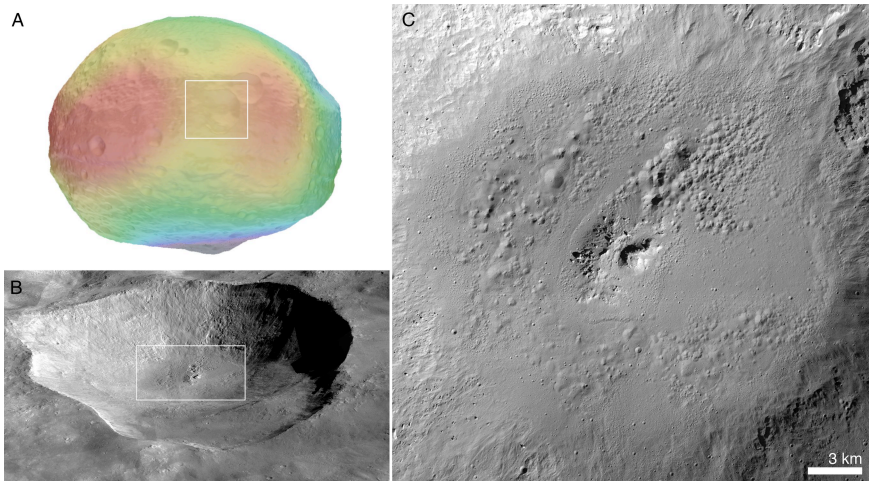

Fig. 1. A) Shape model of Vesta showing the location of Marcia crater (box). Colors shows H content [5] scaled from 0–400 μg/g. B) Synthetic perspective view of Marcia crater, location of C) shown in white box. C) Type example of pitted terrain on the floor of Marcia crater.

VESTA MINERALOGY IN THE LIGHT OF DAWN.

M.C. De Sanctis[1], E. Ammannito[1], J-Ph. Combe[2], R. Jaumann[3,] T.B. McCord[2], L.A. McFadden[4], H. Y. McSween[5], C.M. Pieters[6], C.A. Raymond[7], C.T. Russell[8] and the Dawn team.
[1]INAF, Istituto di Astrofisica e Planetologia Spaziale, Roma, Italy, mariacristina.desanctis@iaps inaf.it, [2] Bear Fight Institute, Winthrop, WA, USA, [3]DLR, Planetary Research Berlin, Germany, [4]NASA, GSFC, Greenbelt, MD, USA; [5]Dep. of Earth and Planetary Sciences, University of Tennessee, Knoxville, TN, USA; [6]Dep. of Geological Sci., Brown University, Providence, RI,USA, [7]JPL, Pasadena, CA, USA, [8]Institute of Geophysics and Planetary Physics, UCLA, Los Angeles, CA, USA.

Introduction: VIR-Visible InfraRed mapping Spectrometer- aboard Dawn, is the primary instrument for mapping the surface mineralogy of Vesta [1]. Vesta's spectrum has strong absorption features centered near 0.9 and 1.9 μm, indicative of Fe-bearing pyroxenes. The spectra of HED (howardite, eucrite and diogenite) meteorites have similar features. This led to the hypothesis that Vesta was the parent body of the HED clan [2,3].The data from the Dawn VIR instrument [4,5,6] characterized and mapped the mineral distribution on Vesta, strengthened the Vesta – HED linkage, discovered hydrated materials and their association with the low albedo materials, discovered olivine in an unexpected location, providing new insights into Vesta's formation and evolution.

VIR data: VIR acquired data during all the Dawn mission phases, providing very good coverage of the surface. Data of high quality, from 0.2 to 5 microns, have been acquired for a total of about 20 million spectra in 864 spectral channels. The VIR nominal pixel resolution ranges from 1.3 km (Approach phase) to 0.18-0.15 km (HAMO). The coverage obtained, allows a near global study of Vesta's surface mineralogy.

Results: Vesta spectra are dominated by pyroxene bands, but the global spectral observations of Vesta revealed several unexpected features and large variation in the pyroxenes mineralogy.

Vesta presents complex geology/topography and the mineral distribution is often correlated with geological and topographical structures. Ejecta from large craters have distinct spectral behaviors, and materials exposed in the craters show distinct spectra on floors and rims. Maps of spectral parameters show surface and subsurface unit compositions in their stratigraphic context. VIR reveals the mineralogical variation of Vesta's crustal stratigraphy on local and global scales.

The surface composition is imprinted by the huge impact that formed Rheasilvia basin. This impact excavated a large amount of material and redistributed it on Vesta's surface. Within the basin, the mineralogical composition is different, with primarily diogenites and howardites. Orthopyroxene-rich materials are present in the deepest parts of the basin and within its walls (fig. 1).

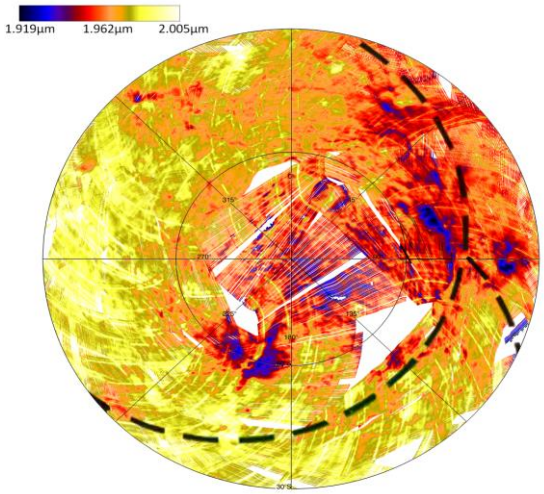

Fig.1: BII center distribution in the south polar region. The dash line represents Rheasilvia and Venenia boundaries.

Most of the VIR spectra are consistent with a surface covered by a howardite-like regolith containing varying proportions of eucrite and diogenite at different locations[5,6]. The observed distribution is suggestive of significant gardening of surface materials, consistent with a background of breccias composed of eucrite and diogenite.

Large eucrite-rich regions occur at equatorial/mid latitudes, hinting at remnants of Vesta's old crust. Diogenitic lithology, other than that within the Rheasilvia basin, is exposed in an extensive ejecta blanket produced by the Rheasilvia-forming impact. The ejecta covers a broad portion of Vesta's surface, spreading from Rheasilvia's rim far to the North.

Significant amount s of olivine are predicted by the petrogenic models and its occurrence is demonstrated

by some diogenites meteorites that are rich in olivine[ref]. Nevertheless, olivine has not been firmly detected in the Rheasilvia basin. It must be recalled that spectral detection of olivine when associated with orthopyroxene is difficult.

However, olivine has been discovered in the Northern hemisphere far from the deeply excavated southern basins [7], (fig. 2).

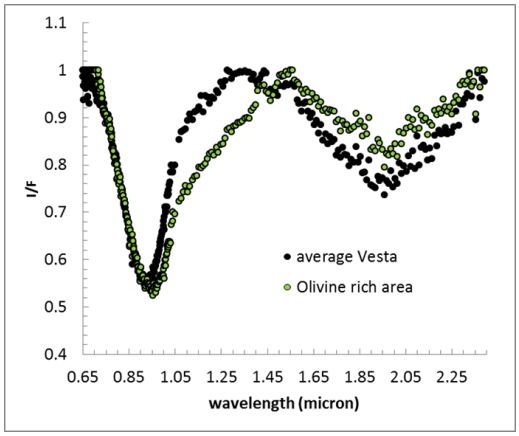

Fig. 2 Spectrum of olivine rich area in comparison with an average spectrum of Vesta.

Olivine distribution is another key detection that can help in distinguishing between competing hypothesis. The classical models foresee widespread crystallization of olivine and diogenite (magma ocean models) while other models invoke olivine and diogenite rich lithologies formed via fractionation in multiple crustal plutons. The distribution of these lithologies on Vesta can provide constraints on the formation models and on the processes that were active in the primordial solar system.

The global albedo map of Vesta [8] reveals the presence of different types of terrains: bright material (BM) and dark material (DM). The mid-southern Vestan hemisphere contains most of the bright areas, while the northern hemisphere is poor in of bright regions [9,10]. The analysis of the spectral parameters of BM shows a dependence between albedo and band depths with stronger bands corresponding to high albedo units, while no large differences in the BM mineralogy has been observed [11]. The spectral characteristics led to the interpretation that the bright areas represent fresh material excavated by recent impacts, representative of younger Vesta surface [11,12].

Dark materials are distributed unevenly, with a concentration in some regions of the equatorial belt [10]. The spectral differences among them, when present, are only subtle and suggest a composition similar to the Vestan average "material", with a small amount of a moderately darkening agent. The spectra often present a signature at about 2.8 micron[14, 15]. The low albedo and the presence of the hydration band point to CC as one of the possible darkening agent.

The 2.8-μm OH absorption is distributed across Vesta's surface and shows areas enriched and depleted in hydrated materials[14]. The uneven distribution of hydrated mineral phases indicates ancient processes that differ from those believed to be responsible for OH on other airless bodies, like the Moon. The origin of Vestan OH, mainly linked with the presence of carbonaceous materials, provides new insight on the delivery of hydrous materials in the main belt, and may offer new scenarios on the delivery of hydrous minerals in the inner solar system.

Vesta mineralogy is surprisingly rich of signs of its "ancient and recent" past, from the primordial formation and evolution to the more recent collisional evolution, spanning the history of the solar system.

Acknowledgements: The authors gratefully acknowledge the support of the Dawn Instrument, Operations, and Science Teams. This work is supported by an Italian Space Agency (ASI) grant and by NASA through the Dawn project.

References: [1] De Sanctis et al., (2011) *SSR*, 163. [2] McCord et al., (1970), *Science* 168, 1445-1447; [3] Binzel, R.P., et al., (1997) *Icarus, 128*, 95-103; [4] De Sanctis et al., 2012, *Science*, 336, 697-700; [5] De Sanctis et al., (2013), MAPS, doi:10.111/maps12138;[6] Ammannito et al., (2013), MAPS, doi: 10.111/maps12192;[7] Ammannito et al., Nature, doi: 10.1038/nature12665;[8] Schroder, S. et al., 2013, PSS. [9] Mittlefeldht, D. W., et al., (2013), Icarus, under review, [10] Jaumann et al., (2013), Icarus, under review; [11] Zambon et al., (2103), Icarus, under review; [12] Pieters et al. (2012), Nature,doi:10.1038/nature11534; [13] Palomba et al., (2013), Icarus, under review; [14] De Sanctis et al., (2012), ApJLett, doi: 10.1088/2041-8205/758/2/L36 [15] McCord et al., (2012), Nature, doi:10.1038/nature11561

PLACING VESTA IN THE RANGE OF PLANETESIMAL DIFFERENTIATION MODELS. Linda T. Elkins-Tanton[1], Ben E. Mandler[2], and Roger R. Fu[2], [1]DTM, Carnegie Institution, 5241 Broad Branch Road NW, Washington, DC 20015 (ltelkins@ciw.edu), [2]MIT, Dept. Earth, Atmospheric, and Planetary Science, 77 Massachusetts Ave., Cambridge, MA 02139, bmandler@mit.edu, rogerfu@mit.edu.

Introduction: Differentiated planetesimals are thought to have accreted from primitive material within about two million years after formation of the first solids in the solar system (e.g., [1-9]). In this scenario, sufficient ^{26}Al was present to melt the interior of planetesimals larger than ~7 km radius and allow a metallic core to differentiate from a silicate mantle (early-forming planetesimals are thought range in size to as large as Vesta or larger). The planetesimal might be capped with a lid of either primitive unmelted material, or magmatic eruptions from the interior (Fig. 1), or it may melt all the way to its surface.

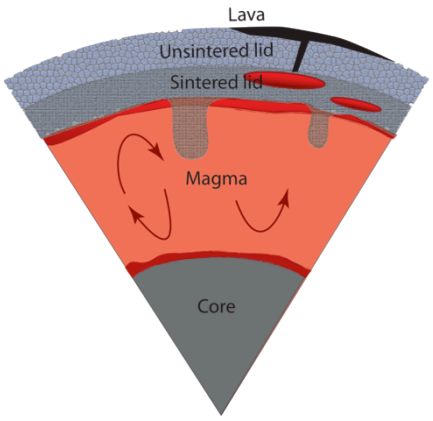

Fig. 1. Schematic cross-section of a molten planetesimal. Melting might also extent to the surface, or be limited to a partial melt retained at depth.

Questions remain about the circumstances under which a body would melt entirely, or only partially; how complex fractionation and rise of melt into and through the crust might be, including formation of secondary magma chambers; and when melts might erupt.

Hydrous fluid mobilization occurs before silicate melting: As temperature rises in a young planetesimal interior, the silicates will pass through the stability zones for several possible hydrated silicate minerals, but then a free hydrous fluid will be released (this hydrous fluid may also interact with iron metal before core formation begins – a possibility that merits further inquiry). The free hydrous fluid will be positively buoyant and will rise away from the planetesimal interior before silicate melting begins. Thus, silicate melts are likely to form from a relatively dry source and not be volatile-saturated. The buoyant fluid itself may freeze in any conductive lid, after metasomatizing some regions, or it may be lost to space [5].

Silicate melting from ^{26}Al may not be complete: If accretion is rapid and aluminum remains in the matrix, then the planetesimal is rapidly and completely melted (*e.g.*,[10]). Accretion could begin before ~1.7 Ma after CAIs, when ^{26}Al can produce some internal melting, and could then continue and permit an internally molten body to retain and add to an undifferentiated crust [8, 9, 11]. Wilson & Keil [12] predict fire-fountaining lava eruptions on Vesta driven by volatiles in magmas. Ghosh & McSween [3] describe an end-member model for Vesta in which all melt from the interior erupts onto the surface and another end-member model in which no melt extrudes; their efforts demonstrate the difficulty of arguing completely for one or another eruptive scenario.

If the silicate portion of the planetesimal has been dried by heating before melting, then magma density (and not volatile content) may dictate whether or not magmas erupt. If melt is positively buoyant with respect to its surrounds [13-16], it would also carry much of the aluminum budget with it while it rises, and prevent further internal melting, resulting in only a layer of melt at shallow depths.

Fu and Elkins-Tanton [16] find that some chondritic bulk compositions have buoyant melts, while for other bulk compositions melt is not buoyant and is therefore unlikely to erupt. For example, an unsintered crust of CV carbonaceous chondrite composition may have a density between ~2,600 and 2,900 kg m^{-3}, whereas the density of molten CV chondrite over a range of temperatures and pressures is between ~2,800 and 2,900 kg m^{-3} [16].

First minerals crystallizing from a cooling planetesimal magma ocean: At the low pressures in planetesimals, almost all the candidates for bulk chondritic silicate compositions would begin solidification by cystallizing olivine alone (Fig. 2).

Why is the first crytallizing mineral of interest? It is the mineral most likely to settle to the core-mantle boundary. Settling requires low crystal fractions and sufficient time [17]. Thus, the first-crystallizing mineral, olivine, is the mineral most likely to be in iron meteorites such as pallasites, if they represent samples of the core-mantle boundary.

Continued solidification of the planetesimal magma ocean: Over the ~0.5 kbar mantle pressure range of a planetesimal ~200 km in radius, the solidus will change by only about 10°C, and the adiabat by only ~2°C. As it cools, therefore, the entire depth of the magma ocean will contain some crystal fraction.

The magma ocean will have a high effective viscosity, perhaps in the range of hundreds to thousands of Pa s. Combined with the high heat flux of a small body cooling without an atmosphere, mineral grains would have to be large, perhaps several to 10 cm, to settle from the magma ocean.

Thus, only the earliest-forming crystals will settle, in the time before crystallinity rises. The rest of the planetesimal's mantle will solidify in bulk and *never produce an olivine cumulate*. This may be why we have no such samples in our collections.

Application to Vesta: Fractional crystallization cannot have been a dominant early process in the Vestan magma ocean because it leads to excessive Fe-enrichment in the melt [18], reinforcing the non-fractional processes predicted by the simple physical models above. Models that are dominated by equilibrium crystallization cannot produce orthopyroxene cumulates (diogenites). The best models of [18] invoke 60– 70% equilibrium crystallization of a magma ocean followed by continuous extraction of the residual melt into shallow magma chambers.

Fractional crystallization in these magma chambers combined with continuous or periodic addition of more melt from the slowly compacting crystal mush (magmatic recharge) can produce all of the igneous HED lithologies (noncumulate and cumulate eucrites, diogenites, dunites, harzburgites, and olivine diogenites). Magmatic recharge can also explain the narrow range in eucrite compositions and the variability of incompatible trace element concentrations in diogenites.

Conclusions: The simplicity of the mineral assemblages in pallasites and other iron meteorites strongly supports successful crystal settling of olivine alone at the beginning of magma ocean solidification on an internally differentiated planetesimal.

Later solidification would occur in bulk, and thus planetesimal magma oceans will not produce olivine + pyroxene cumulate, such as are predicted for the Moon, but would produce melt extraction from mushes consistent with observations from Vesta.

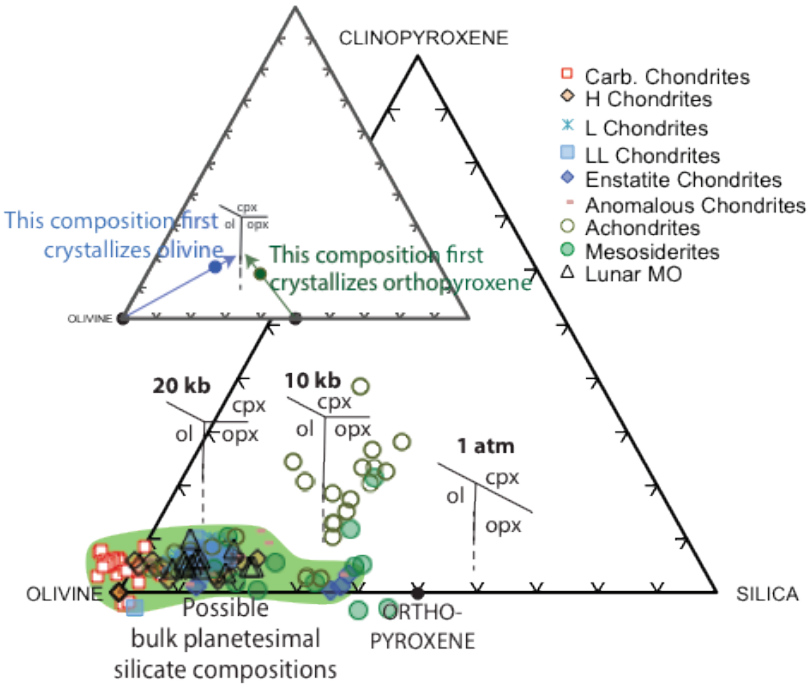

Fig 2. The silicate portions of bulk chondritic compositions [19] plotted in a ternary diagram, and described with a green field. Possible bulk compositions for a lunar magma ocean (compiled in [20] plot in the same green region. Phase boundaries for solidification of a magma ocean of peridotitic composition as an approximation of how these chondritic magma oceans would solidify, from [21]. Given the low pressure of planetesimal interiors, virtually all bulk compositions would begin to solidify by crystallizing only olivine.

References: [1] Miyamoto, M. et al. (1981) *Proc. Lunar Planet. Sci. Conf.*, 12, 1145. [2] LaTourrette, T. and G. J. Wasserburg (1998) *EPSL*, 158, 91. [3] Ghosh, A. and H. Y. McSween Jr. (1998) *Icarus*, 134, 187. [4] Young, E. et al. (1999) *Science*, 286, 1331. [5] Young, E. et al. (2003) *EPSL*, 213, 249. [6] Merk, R. et al. (2002) *Icarus*, 159, 183. [7] Ghosh, A. et al. (2003) *MAPS*, 38, 711. [8] Sahijpal, S. et al. (2007) *MAPS*, 42, 1529. [9] Elkins Tanton, L. T. et al. (2011) *EPSL*, 305, 1. [10] Hevey, P. and I. Sanders (2006) *MAPS*, 41, 95. [11] Šrámek, O. et al. (2012) *Icarus*, 217, 339. [12] Wilson, L. and K. Keil (1997) *MAPS*, 32, 813. [13] Wilson, L. and K. Keil (2012) *Chemie der Erde*, 72, 289. [14] Moskovitz, N. and E. Gaidos (2011) *MAPS*, 46, 903. [15] Neumann, W. et al. (2012) *Astron. Astrophys.*, 543. [16] Fu, R. R. and L. T. Elkins-Tanton (2013) *EPSL,* submitted . [17] Suckale, J., et al. (2012) *JGR*, 117, E08005. [18] Mandler, B. E. and L. T. Elkins-Tanton (2013) *MAPS* . [19] Jarosewich, E. (1990) *Meteoritics*, 25, 323. [20] Elkins-Tanton, L. T. et al. (2011) *EPSL*, 304, 326. [21] Stolper, E. M. (1980) *Contrib. Min. Pet.*, 74, 13.

Modeling Vesta's internal structure with Dawn gravity and shape models. Anton I. Ermakov[1], Maria T. Zuber[1], David E. Smith[1,2], Carol A. Raymond[3], Roger R. Fu[1]. [1]Department of Earth, Atmospheric and Planetary Sciences, Massachusetts Institute of Technology, Cambridge, MA 02139, USA (eai@mit.edu); [2]NASA/Goddard Space Flight Center, Greenbelt, MD, 20771, USA; [3] Jet Propulsion Laboratory, California Institute of Technology, Pasadena, CA, USA.

Introduction:

Vesta is a differentiated asteroid as confirmed by the Dawn gravity measurements [1,2]. The Rheasilvia and Veneneia impact basins in the southern hemisphere have a substantial effect on the global shape and gravity field of the asteroid. Rheasilvia makes the apparent shape of Vesta more oblate. The basins are surrounded by a belt of thicker crust [3], that can be alternatively interpreted as lower density material [4]. Hydrocode modeling of the formation of the impact basins showed that regions north of the crustal belt are not significantly affected by the impact [5] and, therefore, represent the pre-impact shape of Vesta [3,6]. We use Vesta gravity and topography in connection with the geochemically derived constraints to study Vesta's internal structure, rotational history and compensation state.

Hydrostatic equilibrium:

Vesta was likely near hydrostatic equilibrium immediately after its formation and before the giant impact basins formed [6]. Therefore, it is possible to use the northern terrains of Vesta to determine its preimpact shape and rotation state. We fit a triaxial ellipsoid with 9 degrees of freedom (three axes, three orientation angles and three coordinates of the origin) to the northern terrains unaffected by the late giant impacts [5]. The flattening and orientation of the northern ellipsoid are used to constrain the pre-impact rotation rate and rotation axis orientation. The rotation period that corresponds to the northern ellipsoid flattening is 4.95 hours, which is 7% lower than the present 5.32 hours. The polar axis of the northern ellipsoid is 3.0 ± 0.14 deg off from the current rotation axis [6]. These values are robust with respect to the definition of the region unaffected by the giant impact and constitute evidence for possible reorientation and despinning.

Geochemical constraints:

We compare internal structure models derived from gravity and topography with the results of geochemical modeling [7]. We use the estimated pre-impact rotation rate to compute hydrostatic equilibrium figures of the core and the outer shape for different bulk chondritic compositions. This allows us to eliminate the trade off between the core shape and the mantle shape. The gravity/topography internal structure constraints are consistent with geochemical models for the H-chondrite and mixed 3/4H+1/4CM bulk compositions to 1.7% and 2.4% in crust and mantle mass fractions, respectively. However, the geochemical difference in density can be masked by porosity variations. A bulk porosity of order of 10% results in a density contrast comparable or even higher than pure geochemical density contrast. Such a structure would pose a major challenge in interpretation of gravity anomalies.

Crustal inversion:

Given only gravity and topography data, an absolute mean crustal thickness cannot be computed. However, to study relative crustal thickness variations we can choose densities based on the geochemistry of HEDs [7] to invert for the crust-mantle interface. Using this approach the thinnest crust is observed in the floors of the Rheasilvia and Veneneia basins, which correspond to diogenite-rich region as inferred from the Dawn VIR [8]. Areas of thickest crust are associated with the rims of the impact basins and could be at least partially associated with impact ejecta. We explore the range of possible of crustal, mantle and core densities. The mean crustal thickness as a function of the three densities is shown in Fig. 1.

Compensation state and admittance analysis:

We use the approach of [9] to determine the global compensation state of Vesta. We find that Vesta is likely to be globally uncompensated for all wavelengths. Therefore, we can use gravity/topography admittance to directly constrain the effective density of the crust. We use spectro-spatial localization technique to study lateral effective density variations [10]. A local effective density high is observed at the intersection of the two giants basins – the region of the highest excavation depth due to impacts [5]. Another broad effective density high is located approximately in the antipodal region to the Rheasilvia center. By fitting a line to the effective density as a function of degree we can constrain the rate of density increase with depth. We observe a weak negative correlation between the effective density and the rate of density increase with depth.

References:

[1] Russell, C. T. et al. (2012) *Science*, 336, 6082, 684-686. [2] Konopliv, A. S. et al. (2013) *Icarus*, in press. [3] Ermakov, A. I. et al. (submitted to *Icarus*). [4] Park, R. S. et al., (submitted to *Icarus*). [5] Ivanov, B. A. and Melosh, H. J. (2013) *JGR*, 118, 1545-1557. [6] Fu, R. R. et al. (submitted to *Icarus*). [7] Toplis, M. J. et al. (2013) *Meteorit. & Planet. Sci.* doi:10.1111/maps.12195. [8] McSween, H. Y. et al. (2013) *JGR*, 118, 335-346. [9] Turcotte, D. L. et al. (1981) *JGR*, 96, 3951-3959. [10] Simons, F. J. et al. (2006) *SIAM Review* 48, 3, 504-536.

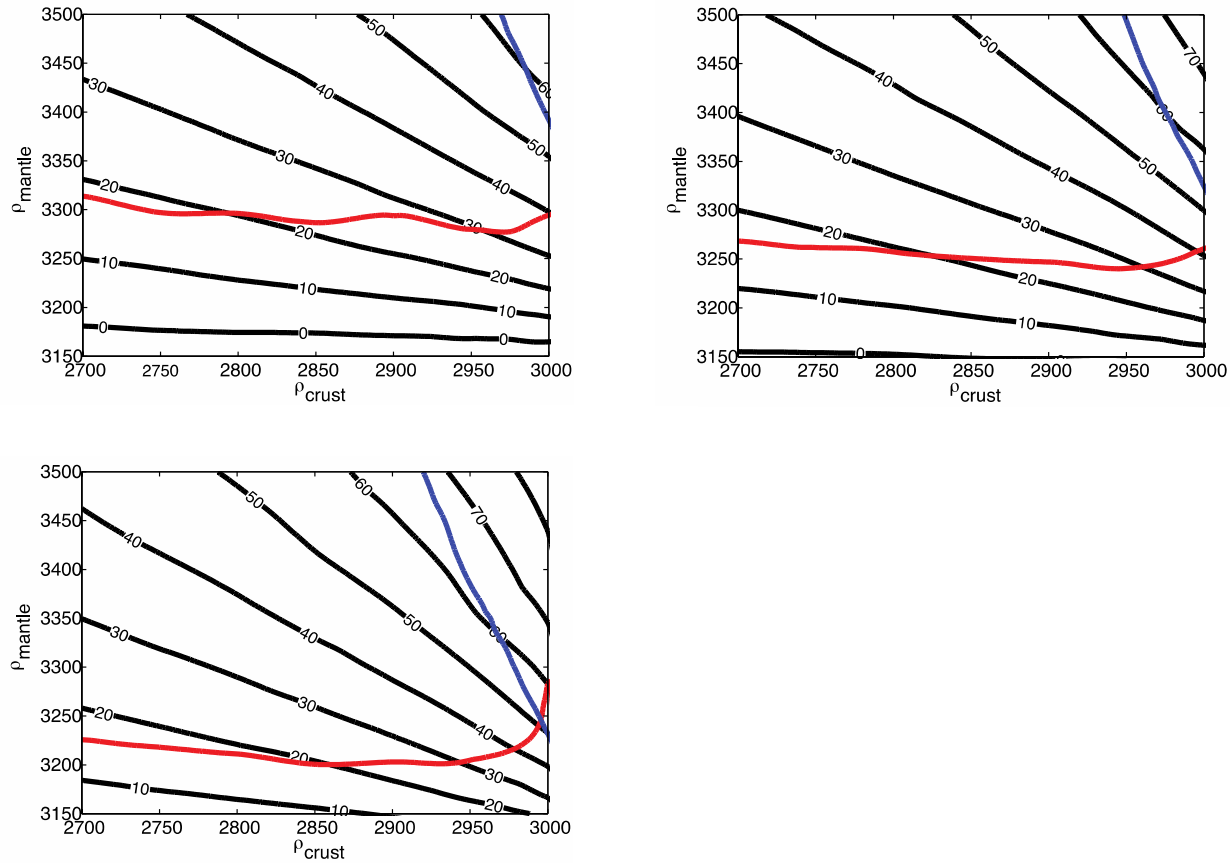

Figure 1. Mean crustal thickness as a function of mantle and crustal densities. Following [1], the mean radius of the core is 110 km. Results are shown assuming core densities of 7800 kg m^{-3} (bottom), 7400 kg m^{-3} (top right), 7100 kg m^{-3} (top left). For the densities below the red line, the minimum crustal thickness is less than zero and therefore those solutions are unphysical. For the densities right of the blue line, the maximum crustal thickness is greater than 100 km.

Thermal and Geophysical History of Vesta. M. F. Formisano[1,*], M.C. De Sanctis[1], C.Federico[1,2] and D.Turrini[1]
[1] INAF-IAPS, Via del Fosso del Cavaliere 100, 00133 Rome (Italy)
[2] Dept. of Earth Science, University of Perugia, 06123 Perugia (Italy)
[*] Corresponding author: michelangelo.formisano@iaps.inaf.it

Introduction:

4 Vesta is one of the large asteroid of Main Belt and probably it is the parent body of the HED meteorites [1]: as a consequence we know it was one of the first bodies to have formed and differentiated in the Solar System.

It represents the key to understand the first stages of the evolution of the terrestrial planets and of the Solar System in general.

We analyze the thermal and geophysical history of Vesta by using an improved version of our 1D model developed to study the heating history of asteroids (4) Vesta and (21) Lutetia ([2],[3]).

The Model:

We developed a 1D model ([2],[3]) for the contemporary solution of the heat equation with radiogenic heat source and the advection equation, which controls the percolation of the metals inside the asteroid. A parametrized convection is introduced in order to reconstruct the heating and cooling history of (4) Vesta in a timespan of 100 Ma starting from the condensation of CAIs.

We investigate the link between the evolution of the internal structure and thermal heating due to short and long-lived radionuclides, taking into account the chemical differentiation of the body and the affinity of ^{26}Al with silicates.

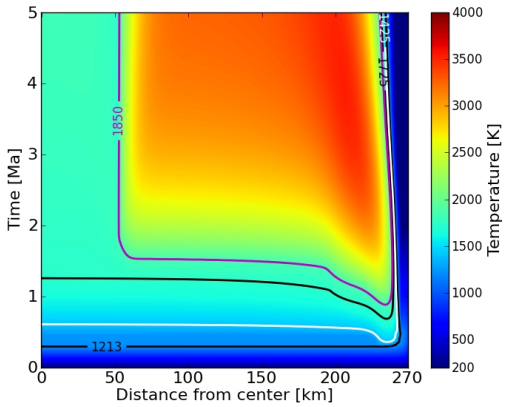

Figure 1: An example of geophysical history in case of instantaneous accretion.

We considered Vesta as a spherical body with a fixed radius (270 km) and an initial homogeneous composition similar to H-chondrites. We explored several scenarios differing in the available strength of energy due to the radiogenic heating.

Results:

We depicted several geophysical scenarios and we constrained the accretion and differentiation time of (4) Vesta as well as the size and the formation time of the core, by comparing our results to Dawn's estimate and to the constrains provided by the HED's. The cooling time and the chondritic crust evolution are also evaluated. In Fig.1 it is shown an example of geophysical history map of (4) Vesta. Our results show that Dfferentiation takes place in all scenarios in which Vesta completes its accretion in <1.4 Ma after the injection of ^{26}Al into the solar nebula. In all those scenarios where Vesta completes its formation in <1 Ma from the injection of ^{26}Al, the degree of silicate melting reaches 100 vol% throughout the whole asteroid. If Vesta completed its formation between 1 and 1.4 Ma after ^{26}Al injection, the degree of silicate melting exceeds 50 vol% over the whole asteroid, but reaches 100 vol% only in the hottest, outermost part of the mantle in all scenarios where the porosity is lower than 5 vol%. If the formation of Vesta occurred later than 1.5 Ma after the injection of ^{26} Al, the degree of silicate melting is always lower than 50 vol% and is limited only to a small region of the asteroid. The radiation at the surface dominates the evolution of the crust, which ranges in thickness from 8 to about 30 km after 5 Ma: a layer about 3–20 km thick is composed of primitive unmelted chondritic material, while a layer of about 5–10 km is eucritic.

References:

[1] De Sanctis M.C., et al. (2012), Science, 336,697; [2] Formisano M. et al. (2013), Meteoritics & Planetary Sci., 1-17,doi:10.1111/maps.12134; [3] Formisano M. et al.(2013), ApJ, 770, 50

EXPERIMENTAL CONSTRAINTS ON A VESTA MAGMA OCEAN. C. Hoff[1], J.H. Jones[2], and L. Le[3] [1]University of Massachusetts, Amherst, Department of Geology. Amherst, MA , [2]KR, NASA Johnson Space Center, Houston, TX, 77058 (john.h.jones@nasa.gov). [3]Jacobs ETS, Houston, TX, 77058

Introduction: A magma ocean model [1] was devised to relate eucrites (basalts) and diogenites (orthopyroxenites), which are found mixed together as clasts in a suite of polymict breccias known as howardites. The intimate association of eucritic and diogenitic clasts in howardites argues strongly that these three classes of achondritic meteorites all originated from the same planetoid. Reflectance spectral evidence (including that from the DAWN mission) has long suggested that Vesta is indeed the Eucrite Parent Body [e.g., 2].

Specifically, the magma ocean model was generated as follows: (i) the bulk Vesta composition was taken to be 0.3 CV chondrite + 0.7 L chondrite but using only 10% of the Na_2O from this mixture; (ii) this composition is allowed to crystallize at 500 bar until ~80% of the system is solid olivine + low-Ca pyroxene; (iii) the remaining 20% liquid crystallizes at one bar from 1250°C to 1110°C, a temperature slightly above the eucrite solidus. All crystallization calculations were performed using MELTS [1].

In this model, diogenites are produced by crystallization of olivine and pyroxene in the >1250°C temperature regime, with Main Group eucrite liquids being generated in the 1300-1250°C temperature interval. Low-Ca pyroxene reappears at 1210°C in the one-bar calculations and fractionates the residual liquid to produce evolved eucrite compositions (Stannern Trend).

We have attempted to experimentally reproduce the <1250°C portion of the MELTS Vesta magma ocean. In the MELTS calculation, the change from 500 bar to one bar results in a shift of the olivine:low-Ca pyroxene boundary so that the 1250°C liquid is now in the olivine field [e.g., 3] and, consequently, olivine should be the first-crystallizing phase, followed by low-Ca pyroxene at 1210°C, and plagioclase at 1170°C. Because at one bar the olivine:low-Ca pyroxene boundary is a peritectic, fractional crystallization of the 1210°C liquid proceeds with only pyroxene crystallization until plagioclase appears. Thus, the predictions of the MELTS calculation are clear and straightforward.

Experimental/Analytical: A starting composition was produced by quenching a synthetic liquid whose composition closely approximates that of the Righter-Drake 1250°C melt [1]. Experiments were run in 1-bar, gas-mixing Deltech furnaces, initially for short duration (SD) runs (5-7 hrs), and then long duration (LD) runs (24-180 hrs). These experiments were performed at 1250-1170°C, at oxygen fugacities near the iron-wüstite (IW) oxygen buffer, and a pressure of one bar. The lowest temperature, 1170°C, is below Stolper's original eucrite liquidus of ~1180°C [4] and is the temperature where MELTS predicts the appearance of plagioclase. The temperature is controlled via a platinum-rhodium (Type B) thermocouple system. The oxygen fugacity is controlled by flowing CO_2/CO gas and measured using a remote zirconia oxygen-fugacity electrochemical cell.

Table 1. Experimental Summary

Temp (°C)	MgO	CaO	% Melt	Duration (hrs)	Phases Present
1250 LD	9.7	9.4	100.0	23	Melt
1250 SD	8.2	10.0	93.6	5	Melt, Olivine
1225 LD	8.1	9.9	94.9	120	Melt, Olivine
1225 SD	7.5	10.4	90.1	5	Melt, Olivine, pyroxene
1210 LD	7.7	10.0	93.3	173	Melt, Olivine
1200 SD	7.6	10.2	91.8	8	Melt, Olivine
1195 LD	7.5	10.2	92.1	94	Melt, Olivine
1180 LD	6.6	10.5	89.0	49	Melt, Olivine
1170 LD	6.4	10.6	88.4	116	Melt, Olivine

The charges were suspended on rhenium loops to prevent iron loss, and the rhenium loop was in turn suspended from drop-quench, thin platinum wires. The charges were then sealed in the furnace and later drop-quenched into water.

The experiments were analyzed using a Cameca SX-100 electron microprobe for the 9 elements in the starting composition (Si, Ti, Al, Cr, Fe, Mn, Mg, Ca, Na). For phase identification and visual orientation, a scanning electron microscope (JEOL 5910LV) was used.

The initial experiments were three SD 1250°C, 1225°C, and 1200°C experiments. However, while the SD experiments gave a general sense of phase assemblages, K_D values [K_D = D(Fe)/D(Mg)] and the large amount of zoning (>5%) in the olivines indicated that longer-duration experiments were required in order to reach equilibrium. Experimental temperatures, durations, and abbreviated results are given in Table 1; CaO and MgO concentrations are for the quenched liquid.

Results: When only LD experiments are considered, olivines and melt were typically homogeneous and there was good agreement from crystal to crystal within an individual experiment. Our K_D partitioning results are also broadly consistent with Jones [5] and Filiberto et al. [6] who demonstrated a linear relation-

ship between D(Fe) and D(Mg) for olivine-melt. In addition, there is a smooth variation in the CaO and MgO contents of the quenched liquids with temperature. These observations give us confidence in our approach to equilibrium.

Nonetheless, our experimental results do not agree with the predictions of MELTS. In the temperature range of our experiments, both low-Ca pyroxene and plagioclase were predicted to appear, but only olivine is present in our experiments.

Figure 1. CaO vs. MgO for Experimental Liquids

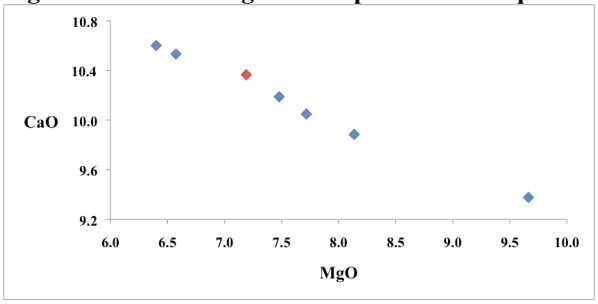

Figure 1. Blue diamonds are experimental glasses showing the liquid line of descent from the 1250°C starting composition (LD only). Red diamond is a composite of the Juvinas and Sioux County eucrites. The experimental trend matches the natural eucrite composition at a significantly higher temperature (~1190°C) than the Stolper experimental liquidus (~1180°C) [4].

This disagreement gives us serious concerns about the applicability of the MELTS calculations described above.

Discussion: As predicted by MELTS, the 1250°C composition first has olivine as the liquidus phase. However, even after experimental durations as long as ~5 days, pyroxene fails to appear. Although not as great a concern as the non-appearance of low-Ca pyroxene, plagioclase also did not appear in this same ~5-day experiment — although it was predicted to.

Several experimental observations raise questions about the utility of MELTS to model the differentiation of Vesta and to understand the origins of eucrites and diogenites: (i) The formation of diogenites at >1250°C is modeled as cotectic crystallization of olivine and orthopyroxene, but the presence of olivine in diogenites is limited, to non-existent (typically 0-5%), and the occurrence of olivine and orthopyroxene in igneous contact is rare [7]; (ii) The 1250°C liquid, which is modeled to have post-dated the production of the Main Group eucrites [1], lies within the olivine field of the OL-SI-PL pseudo-ternary, whereas natural eucrites cluster about the OL-PX-PL pseudo-invariant point, which is a more evolved composition; and (iii) previous 1-bar partial melting experiments on the Murchison chondrite at 1180°C produce eucritic liquids, leaving pnly small amounts of low-Ca pyroxene in the residuum (~5%), casting doubt as to the relationship between eucrites and diogenites (i.e., no pyroxene remains at 1200°C in the Murchison experiments) [8]. Chemically, the 1180°C pigeonites in the Murchison experiments (Mg# 73) could be consistent with the more ferroan diogenites, but not with those that are more mafic.

Therefore, concerns about how to relate eucrites and diogenites remain [8].

One possibility recently raised by [9] is that Vesta was never homogenized. Possibly eucrites are produced by partial melting of a CM/CO-like mantle, which is poor in pyroxene components, whereas diogenites are cumulates from partial melts of an L/LL-like source. This possibility would render almost any magma ocean scenario either highly improbable or impossible. But such an interpretation would be consistent with the experimental results to date.

References: [1] Righter, K. & Drake M. J. (1997) *Meteoritics & Planetary Science* **32**, 929-944. [2] Consolmagno G. and Drake M.J. (1977) *Geochim. Cosmochim. Acta* **41**, 1271-1282. [3] Bartles K.S. and Grove T.L. (1991) *Proc Lunar Planet Sci. Conf. 21st,* 351–365. [4] Stolper E. (1977) *Geochim. Cosmochim. Acta* **41**, 587-611. [5] Jones J. H. (1984) *Contrib. Min. and Pet.* **88**, 126-132. [6] Filiberto J. et al. (2009) *Am. Min.* **94**, 256-261. [7] Mittlefehldt D.W. et al. (1998) Non-chondritic Meteorites from Asteroidal Bodies, Chapter 4. In *Planetary Materials*, Reviews in Mineralogy vol. 36 (J.J. Papike, ed.), pp. 104-112; [8] Jurewicz A.J. et al. (1993) *Geochim. Cosmochim. Acta* **57**, 2123-2139; [9] Ammannito E. et al. (2013) *Nature* doi: 10.1038/nature12665.

.

Vesta's Geological Features. R. Jaumann (1,2), C.T. Russell (3), C.A. Raymond (4), C.M. Pieters (5), R.A. Yingst (6), D.A. Williams (7), D.L. Buczkowski (8), P. Schenk (9), M.C. De Sanctis (10) and the Dawn Team

(1) DLR, Planetary Research Berlin, Germany, Ralf.Jaumann@dlr.de; (2) Freie Universität Berlin, Germany; (3) UCLA, Institute of Geophysics, Los Angeles, CA, USA; (4) Jet Propulsion Laboratory, California Institute of Technology, Pasadena, CA, USA; (5) Brown University, Providence, RI, USA; (6) Planetary Science Institute, Tucson, AZ, USA; (7) Arizona State University, Tempe, AZ, USA; (8) Johns Hopkins University Applied Physics Laboratory, Laurel, MD, USA; (9) Lunar and Planetary Institute, Houston, Texas, USA;INAF, (10) Istituto di Astrofisica e Planetologia Spaziale, Area di Ricerca di Tor Vergata, Roma, Italy.

Abstract

The Dawn spacecraft collected over 28,000 images and a wealth of spectral data of Vesta's surface. These data enable analysis of Vesta's diverse geology including impact craters of all sizes and unusual shapes, a variety of ejecta blankets, large troughs, impact basins, enigmatic dark material, and considerable evidence for mass wasting and surface alteration processes [1,2,3]. Two large impact basins, Veneneia underlying the larger Rheasilvia basin dominate the south polar region [1,4]. The depression surrounding Vesta's south pole was formed by two giant impacts about one billion and two billion years ago [4,5]. Vesta's global tectonic patterns (two distinct sets of large troughs orthogonal to the axes of the impacts) strongly correlate with the locations of the two south polar impact basins, and were likely created by their formation [1,6]. Numerous unusual asymmetric impact craters and ejecta indicate the strong influence of topographic slope in cratering on Vesta [1]. One type of gully in crater walls is interpreted to form by dry granular flow, but another type is consistent with transient water flow [7]. Very steep topographic slopes near to the angle of repose are common; slope failures make resurfacing due to impacts and their associated gravitational slumping and seismic effects an important geologic process on Vesta [1]. Clusters of pits in combination with impact melt [8] suggest the presence of volatile materials underlying that melt in some crater floors. Relatively dark material of uncertain origin is intermixed in the regolith layers and partially excavated by younger impacts yielding dark outcrops, rays and ejecta [1,9]. Vesta's surface is reworked by intense impacts and thus much younger than the formation of its crust [2,5].

Major Geologic Features

1. Vesta's surface is characterized by impact craters of all sizes, a variety of ejecta blankets, large troughs extending around the equatorial region, enigmatic dark material, and considerable evidence for mass wasting (Fig. 1, 2)[1-12].

2. Dawn confirms the large impact basin covering Vesta's south pole (Rheasilvia), inferred from the Hubble Space Telescope images, and reveals evidence for an earlier, underlying large basin [1,4,5].

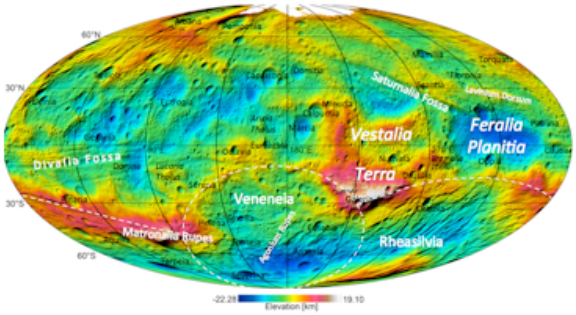

Fig 1: Geologic surface features on Vesta

3. Vesta's global tectonic patterns (two distinct sets of large troughs) strongly correlate with the locations of the two south polar impact basins, and were likely created by the formation of the basins [1,6].

4. Impact craters on Vesta range from fresh to highly degraded, comparable to the Moon, indicating an intensive cratering history over the age of the solar system [1,4].

5. Impact craters on Vesta have characteristics similar to those on smaller asteroids as well as those on the Moon and Mars, making Vesta a transitional body between asteroids and planets [1,2].

6. The primary crust is covered by a thick (100 meters to a few kilometers), multilayered, sheet of debris (regolith) formed by the accumulation of ejecta from the numerous impacts that have resurfaced Vesta over time [1].

7. Vesta exhibits rugged topography ranging from -22 km to 19 km relative to a best-fit ellipsoidal shape. Vesta's topography has a much greater

range in elevation relative to its radius (15%) than the Moon and Mars (1%) or the Earth (0.3%), but less than highly battered smaller asteroids like Lutetia (40%). This also identifies Vesta as a transitional body between asteroids and planets [1].

8. The surface of Vesta exhibits very steep topographic slopes that are near to the angle of repose. Impacts onto these steep surfaces, followed by slope failure, makes resurfacing due to impacts and their associated gravitational forces and seismic activity an important geologic process on Vesta that significantly alters the morphology of geologic features and adds to the complexity of its geologic history (Fig. 2) [1,4,10]. Linear gullies are interpreted to form by flow of dry granular material and curvilinear gullies are possibly form by transient flow of water [7].

9. Deposits of dark material is intermixed into the regolith and partially excavated by younger impacts exposed as blocks or layers out-cropping in crater walls and rims. The mixing of dark material with impact ejecta indicates that this material is processed together with the ejected material. Small craters possess continuous dark ejecta similar to lunar dark-halo impact craters, indicating that the impact excavated the material from beneath the surface. Asymmetric distribution of dark material in impact craters and ejecta suggests non-continuous distribution in the local subsurface. The composition of the dark material resembles that of the Vesta regolith. Dark material is distributed unevenly across Vesta's surface. The wide variety of the surface exposures of dark material and their different geological correlations with surface features as well as their uneven distribution indicate a globally inhomogeneous distribution in the subsurface. However on a global scale the dark material seems to be correlated with the rim and ejecta of the older Veneneia south polar basin structure. The origin of the dark material is still debated and it is tentatively suggested that dark material is exogenic, from carbon-rich low velocity impactors. However an endogenic origin, from freshly exposed mafic material or impact melt, created or exposed by impacts cannot be excluded. The broad correlation between dark material and OH hydration band, suggest the presence of carbonaceous chondrites as darkening agent. [1,9,12,13, 14, 15]

10. In contrast to models and expectations from the mineralogy of the HEDs, direct surface evidence for volcanic activity is lacking so far. This may be due to a dearth of large-scale volcanic features on Vesta and/or to the volcanism ending early in Vesta's evolution so that the evidence has been destroyed and covered up by extensive subsequent cratering, regolith formation, and resurfacing [1]. However subsurface intrusive volcanic material cannot be excluded.

11. In general, Vesta's geology is controlled by strong topography variations and regolith properties and thus differs from that of the moon and rocky planets as well as other asteroids. [1,2].

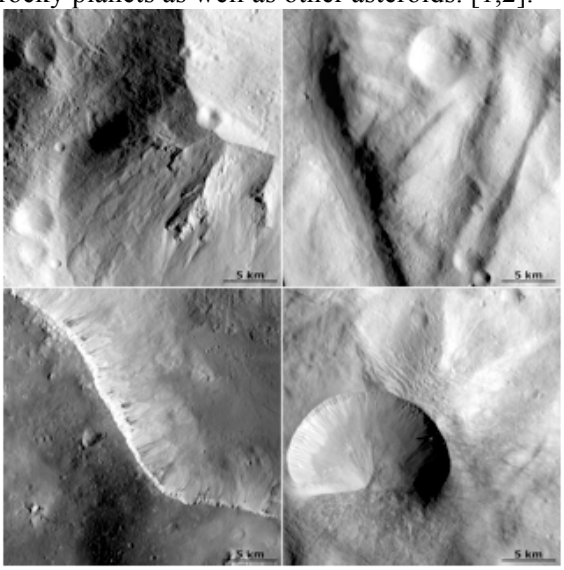

Fig 2: Surface processes on Vesta: (left) mass wasting and talus formation from scarps that also include bright and dark material (bottom); (right) surface mantling and slumping of fine material (top) and slumping of material within a crater located on a slope either due to ballistic ejecta deposit or rim failure (bottom).

References:

[1] Jaumann, R., et al., 2012, Science 336, 687-690; [2] Russell, C.T., et al., 2013, Meteoritics & Planetary Science 1–14 (2013); [3] Pieters et al., 2012, Nature, 491,79-82; [4] Schenk, P, et al., 2012, Science 336, 694-698 [5] Marchi, S., et al., 2012, Science 336, 690-694; [6] Buczkowski, D., et al., 2012, GRL, 39, L18205; [7] Scully, J. E. C., et al., 2013, EPSC; [8] Denevi, B., et al., 2012, Science 338, 246-249; [9] McCord,T.B. et al., 2013, Nature 491, 83-86; [10] Krohn, K., et al., 2013, Icarus, under revision; [11] Otto, K., et al., 2013, Icarus, submitted; [12] Reddy V., et al., Icarus 2012, 544-559; [13]Stephan, K., et al., 2013,JGR, in press; [14] De Sanctis et al, 2012, Ap.J.L., 758: L36; [15] Jaumann et al., 2013, Icarus, in review.

Modelling the Rheasilvia impact. M. Jutzi[1] and B.A. Ivanov[2], [1]Space Research and Planetary Sciences, Physics Institute, University of Bern, Switzerland, martin.jutzi@space.unibe.ch, [2]Institute for Dynamics of Geospheres, Russian Academy of Sciences, Moscow, Russia.

Introduction: Detailed views of Asteroid Vesta by NASA's Dawn mission reveal an interesting and unexpected geology [1]. The south polar depression is deeper and larger than estimated from previous Hubble Space Telescope [2] observations, consisting of two overlapping giant craters [3]. The partial overlap of the two basins (the ~500 km Rheasilvia basin on the ~400 km Veneneia basin) provide a prime example of the interaction of an younger and an older giant crater. Ejecta from collisions forming such craters are massive and globally distributed, with exhumed and deposited materials dominating the surface mineralogy. Moreover, escaped ejecta from these crater forming events are at the origin of the Vestoid asteroid family. Understanding the formation of these craters and the provenance and specific distribution of ejecta is key to understanding the observed properties of Vesta, such as the topography and the surface mineralogy, and it also allows to constrain models of the internal structure.

Impact modeling: A number of recent numerical impact modeling studies investigated the formation of the largest impact structures [4-7], possible effects on the antipodal terrain |8], and the formation of the surface troughs on Vesta [9]. Here we present an overview of recent 2D ([4],[5]), and 3D ([6],[7]) modeling of the formation of the giant Rheasilvia basin. In these studies, the effect of the presence of the underlying Veneneia basin is investigated as well.

2D modeling: Two-dimensional axisymmetric (2-D) numerical modeling of the formation of Vesta's basins was performed in [5]. The model target is presented as 3-layer sphere without rotation [5] or as a 3-layer ellipsoid rotated as a solid body [11]. The equilibrium shape and structure of the rotating target is determined by special pre-impact modeling of a liquid 3-layer sphere relaxation with self-gravity. The average for Main Belt asteroid-to-asteroid impact velocity of 5.5 kms-1 was assumed for the undifferentiated projectile with the Vesta crust density. The acoustic fluidization model was fitted to reproduce the Rheasilvia profile by diameter. Crust thickness of about 20 or 40 km seems has a weak effect on the final crater shape (Figure 1). The secondary nature of the Rheasilvia impact (over the assumed Veneneia older crater) was tested in 2D geometry with the axisymmetric impact in the central mound of the first crater.

3D modeling: The successive formation of the Veneneia and Rheasilvia basins was studied by [7], using a 3D Smooth Particle Hydrodynamics (SPH) impact code. In this modeling, the first impact in a spherical, monolithic, differentiated nonrotating asteroid leads to a basin of roughly 400 km diameter (comparable to Veneneia) and a small central peak. This result is then used as initial condition to study the formation of the second basin, Rheasilvia, which partly overlaps Veneneia. In this modeling, a spin along Veneneia's axis is used. Including pre-impact rotation and taking into account the presence of the underlying Veneneia basin distinguishes these simulations from 2D axisymmetric modeling approaches.

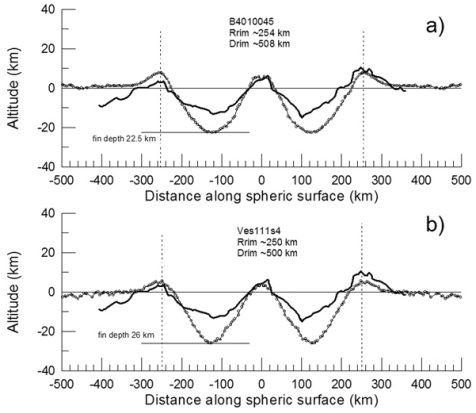

Figure 1: "Best" fit crater profiles [5]. The thick black curve is the published Rheasilvia cross section [2]. (a) – 40 km crust. (b) -20 km crust.

The outcome of the modeling of the two successive major scale collisions, Veneneia followed by Rheasilvia (Figure 2) is in reasonable agreement with the shape of Vesta as observed by Dawn. The diameter of the modeled Rheasilvia basin, though difficult to map (in the model as on Vesta), is consistent to ~ 10 % with the observations. Underlying the second structure is the Veneneia basin from the first simulation; the older basin is partly covered by ejecta from Rheasilvia but is still partly visible in Figure 1. Successive ejection of the same terrain digs deeper into Vesta. According to this modeling, rocks exposed in the Rheasilvia area come from ~60-100 km, digging beneath the crust, according to standard interior structure models. Most of the ejecta emplaced in the northern hemisphere come from ~20 km deep.

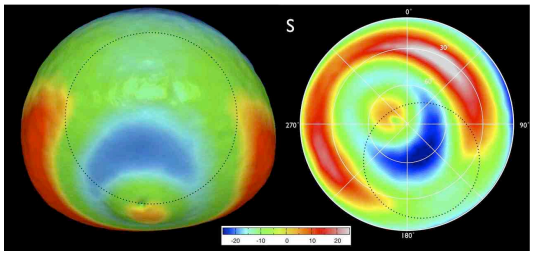

Figure 2: SPH simulation of the formation of the two giant impact features in Vesta's southern hemisphere.

Discussion In the 2D modeling by [4,5], projectile sizes ranging from ~ 30 km to 90 km were investigated. The best fit model uses 37 to 44 km projectile (providing the impact velocity of 5.5 kms^{-1}) and is able to reproduce quite well the observed crater profile. Using the impact angle efficiency for targets with dry friction [10] the equivalent projectile size for an oblique impact at 45° is estimated from the 2D model in the range of 43 to 51 km. Results of the 3D direct modeling in [7], using a 60 km projectile and more complex (non-axis symmetric) impact conditions, are also in reasonable agreement with the observed large basins and the global topography of Vesta.

Due to the different impact conditions, the models predict different degrees of damage resulting from the large impacts, varying from a fully damaged Vesta in the modeling by [7] to a only partially damaged antipodal hemisphere in the "best fit" model by [5].

Some of the uncertainties regarding the projectile sizes which form the large basins on Vesta arise from the large crater diameter to target diameter (Dc/Dt) ratio, the unknown pre-impact shape, the impact angles, the rotation axis of the target, the determination of the crater radius, etc. Furthermore, differences in numerical and material model approaches can also lead to different outcomes for a given impact geometry.

Despite these differences, the two modeling approaches also lead to results which are similar in both cases. For instance, whenever the existence of the underlying Veneneia basin is taken into account in the modeling of the Rheasilvia impact, both models predict a significant amount of material from initial depths > 50 km exposed on the surface of Vesta after the two overlapping collisions [5,7]. This finding provides important constraints regarding the internal structure of Vesta (e.g. [7]).

Despite the reasonably well simulated post-impact shape of Vesta, the numerical modeling outlined many unresolved questions.

1. An essential result of the numerical modeling is the central mound in Rheasilvia formed by the structural uplift of deep-seated material. The structural uplift should deliver target layers that were initially located deeper than 50 to 70 km to or close to the surface. If the standard geochemical models of a differentiated Vesta, which predict a crustal thickness of 20 to 40 km, are correct, it means that mantle material should be excavated by smaller impacts at the Rheasilvia central mound and should be present on Vesta's surface in the Rheasilvia area. The prediction is not confirmed by spectral imaging. Recent studies suggest that olivine is present locally on Vesta's surface but it has not been found within the south-pole basins [12].

Moreover, the first detailed geophysical modeling of observed gravity anomalies indicates that there is only a small density contrast between upper layers ("crust") and lower ("mantle") layers [13]. This is in contradiction with internal structure models of Vesta with distinct crustal layers and a sensible density contrast between crust and mantle minerals.

2. What is the origin of "mantle" Vestoids [14]? A thick upper layer with a small density contrast, if it exists, could make the ejection of dense "mantle" material difficult, even with a double impact.

3. The slow 5.5 kms^{-1} impact produces a relatively small amount of impact melt, while some DAWN observation may be interpreted as the impact melt at the surface. Hence the modeling should be extended to larger possible impact velocities and/or to include possible initial porosity into the target properties.

The differences and similarities between the various model approaches will be discussed in the context of the observations of Vesta by Dawn. Some new results regarding the provenance (within Vesta) of the escaped ejecta will be presented as well.

References: [1] Jaumann, R. *et al.* (2012) *Science* 336, 687-690. [2] Schenk, P., *et al.* (2012), *Science* 336**,** 694-697. [3] Thomas, P. C., *et al.* (1997) *Science* 277, 1492-1495. [4] Ivanov, B. A., H. J. Melosh, and E. Pierazzo (2011) *Lunar Planet. Inst. Sci. Conf. Abstracts*, #1717, Houston, Tex. [5] Ivanov, B.A. and H.J. Melosh (2013), *JGRE* 118, 1545-1557. [6] Jutzi, M., Asphaug, E. (2011) *GRL* 38. L01102. [7] Jutzi, M., E. Asphaug, P. Gillet, J.-A. Barrat, and W. Benz (2013), *Nature* 494, 207-210. [8], Bowling T.J. et al. (2013) JGR Planets, Vol. 118, 1821–1834. [9] Stickle, A.M., P.H. Schultz, and D.A Crawford (2013). *Lunar Planet. Inst. Sci. Conf. Abstracts*, #2417, Houston, Tex. [10] Elbeshausen D., *et al.* (2009) *Icarus* 204, 716-731. [11] Ivanov B. and D. Kamyshenkov(2012) *AGU Fall Meeting* abs. #P43E-04, SF CA 3-7 Dec. [12] Ammannito, E. *et al.*, (2013), *Nature* doi:10.1038/nature12665. [13] Ermakov A., Zuber M. *et al.* (2012) *AGU Fall Meeting* abs. # P41B-1889, SF CA 3-7 Dec. [14] Reddy V., et al. (2011) *Icarus* 212, 175–179.

CORE FORMATION AND EVOLUTION OF ASTEROID 4 VESTA

Walter S. Kiefer[1] and David W. Mittlefehldt[2], [1]Lunar and Planetary Institute, 3600 Bay Area Blvd., Houston TX 77058, kiefer@lpi.usra.edu, [2]Astromaterials Research Office, NASA/Johnson Space Center, Houston TX 77058, david.w.mittlefehldt@nasa.gov.

Introduction

The howardites, eucrites, and diogenites (HEDs) are a suite of related meteorite types that formed by igneous and impact processes on the same parent body [1]. Multiple lines of evidence, including infrared spectroscopy of the asteroid belt and the petrology and geochemistry of the HEDs, suggest that the asteroid 4 Vesta is the parent body for the HEDs [e.g., 2, 3]. Observations by NASA's *Dawn* spacecraft mission strongly support the conclusion that the HEDs are from Vesta [e.g., 4, 5].

The abundances of the moderately siderophile elements Ni, Co, Mo, W, and P in eucrites require that most or all of the metallic phase in Vesta segregated to form a core prior to eucrite solidification [6-8]. These observations place important constraints on the mode and timescale of core formation on Vesta. Possible core formation mechanisms include porous flow, which potentially could occur prior to initiation of silicate melting, and metallic rain in a largely molten silicate magma ocean. Once the core forms, convection within the core could possible sustain a magnetic dynamo for a period of time. We consider each process in turn.

Core Formation: Porous Flow

Melting in the Fe-FeS system begins at the eutectic temperature of 988 °C at 30 weight % S. Inclusion of a small amount of Ni will lower the eutectic temperature slightly and shift it towards lower S [9]. Existing models of the thermal evolution of Vesta all assume an Fe-Ni-S solidus of 940 °C and a near-eutectic liquidus of 960 °C [10-12] and thus require a relatively large amount of S in Vesta's core.

Assuming Vesta has sufficient S to have near-eutectic melting of the metal phase, the metal would be completely molten prior to the onset of silicate melting. At low melt fractions, liquid iron in solid silicates has a high dihedral angle and forms isolated pockets of melt [13]. The dihedral angle is a function of oxygen fugacity, with high values of fO_2 permitting connected sheets of liquid Fe [14], but Vesta likely formed under low oxygen fugacity conditions (at or below the iron-wustite buffer, [e.g., 7]). Even with a high dihedral angle, once the melt fraction of metal exceeds a few percent, connected melt channels are possible [15, 16]. Because of the low viscosity of liquid iron metal and its high density relative to silicates, Darcy flow in such connected melt channels will be efficient, allowing geologically rapid separation of the liquid metal from the solid silicate. However, this separation is likely to be imperfect: once most of the metal has drained from the silicate and the melt fraction drops below the critical level for maintaining connected channels, the channels may pinch off, trapping the last few percent of metal in the solid.

Core Formation: Magma Ocean Metallic Rain

A significant problem with the near-eutectic melting porous flow model outlined above is that the eutectic composition requires a large amount of sulfur (~30 weight %, [9]). In contrast, a recent study synthesized a broad range of constraints on Vesta's composition and favored a model composed of 75% H chondrite and 25% CM chondrite [17]. This corresponds to a core of 16 % S, 73.7 % Fe, and 10.3 % Ni, which is far removed from the Fe-FeS eutectic composition. For this low S abundance, melting of metal still begins at the eutectic temperature but does not conclude until about 1350 °C [9]. Because the HEDs are relatively depleted in volatile elements, it is possible that the S abundance will be even lower than this, which would shift the Fe-FeS liquidus to an even higher temperature. The solidus for the primitive silicate H+CM mantle is likely in the range 1100-1150 °C [18, 19]. Thus, metal and silicate melting are likely to overlap in time during the formation and differentiation of Vesta. It is worth noting that all published Vesta-specific thermal models assume that metallic melting is complete well before the onset of silicate melting [10-12]. Although the overall picture derived in those models is probably generally correct, some of the details of the inferred thermal evolution and differentiation history in those models must be incorrect. For example, in order to use Hf-W radiometric ages for metal-silicate separation [20] as a constraint on the thermal models, the metal liquidus used in the thermal model must be correct.

The viscosity of a suspension of silicate crystals in a silicate melt decreases by many orders of magnitude when the liquid fraction increases from 40% to 60% [21]. When full melting of the Fe-Ni-S metal phase is achieved at 1350-1400 °C, the silicates will be near 50% melt fraction. Assuming that Vesta formed in the first 2-3 half-lives of ^{26}Al after formation of CAIs in the solar nebula and incorporating the insulating effects of a low conductivity megaregolith layer [22], radioactive decay of ^{26}Al can easily heat Vesta to > 1400 °C, including the effects of latent heat for both the silicate and metal phases. At this stage of evolution, Vesta would effectively be a magma ocean.

Given the low viscosity of the silicate melt and the high density contrast between the metal and the silicate, metal blobs will fall to the center of Vesta by Stokes flow in a sort of metallic rain [23, 24]. Based on the various chemical and physical constraints outlined here, we favor a magma ocean and iron metal rain as the most likely method of forming a core on Vesta. Solidification of a magma ocean can also explain the compositional characteristics of the eucrites and diogenites [25].

Core Convection and a Magnetic Dynamo

Definitive observations of an intrinsic magnetic field on Vesta would constrain the structure and rate of cooling of the core and thus would provide important constraints on Vesta's thermal evolution. Unfortunately, *Dawn* did not include a magnetometer as part of its science payload. However, a remnanent magnetic field of at least 2 microtesla has been measured in the eucrite Allan Hills 81001 [26], which in turn implies that Vesta at some point in its history had a convecting liquid metal core.

The short-lived radioactive isotope ^{26}Al is a potent source of radioactive heating in the first few million years of Vesta's history and is concentrated in the silicate portion of Vesta. Thermal evolution models show that ^{26}Al heating of Vesta's mantle initially acts as a thermal blanket and strongly suppresses heat flux out of the core. Cooling of Vesta after ^{26}Al becomes extinct eventually allows the core to briefly convect, but in that model core convection ends before the crust cools below the Curie temperature, such that evidence for a magnetic dynamo would not be preserved [27].

However, several factors may modify this conclusion. First, melt migration in the silicate magma ocean transfers latent heat of melting from the interior to the near surface. Second, magmatism also transports aluminum in plagioclase from the mantle to the crust [28]. Both effects act to cool the mantle relative to models that do not include magmatism and thus reduce the thermal blanketing of the core. Third, ^{60}Fe is a possible radioactive heat source with a half-life that is several times longer than ^{26}Al. The abundance of ^{60}Fe in the solar nebula is controversial and was possibly spatially heterogeneous [29, 30], but ^{60}Ni anomalies in the eucrites Bouvante and Juvinas [31] point to the presence of ^{60}Fe in Vesta. Prior thermal evolution studies have often either neglected ^{60}Fe altogether [27] or assumed that it is 100% partitioned into the core [10, 11, 32]. It is likely that roughly equal amounts of Fe will be in the metal and the silicate portions of Vesta [17], but the much greater concentration of Fe in the core will contribute to driving core convection. We are currently assessing the effects of these factors using a modification of our model for the thermal evolution and dynamo activity on Mars [33]. This model accounts for the thermal evolution of both the core and mantle, including magmatic heat transport, and calculates transport of heat producing elements from the mantle to the crust using appropriate partition coefficients. Compositional convection in the core may also play a role in driving a geodynamo [34], although top-down solidification of the core could create a stably stratified core without a dynamo [35].

References [1] McSween et al., *Space Sci. Rev.* 163, 141-174, 2011. [2] Drake, *Meteoritics Planet. Sci.* 36, 501-513, 2000. [3] Keil, pp. 573-584 in *Asteroids III*, eds. Bottke et al., Univ. Arizona Press, 2002. [4] Russell et al., *Meteoritics Planet. Sci.*, in press, 2013. [5] McSween et al., *J. Geophys. Res.: Planets* 118, 335-346, jgre.20057, 2013. [6] Hewins and Newsom, pp. 73-101 in *Meteorites in the Early Solar System*, eds. Kerridge and Matthews, Univ. Arizona Press, 1988. [7] Righter and Drake, *Meteoritics Planet. Sci.* 32, 929-944, 1997. [8] Holzheid and Palme, *Meteoritics Planet. Sci.* 42, 1817-1829, 2007. [9] Fleet, *Rev. Mineral. Geochem.* 61, 365-419, 2006. [10] Ghosh and McSween, *Icarus* 134, 187-206, 1998. [11] Gupta and Sahijpal, *J. Geophys. Res.* 115, 2009JE003525, 2010. [12] Formisano et al., *Meteoritics Planet. Sci.*, in press, 2013. [13] Shannon and Agee, *Geophys. Res. Lett.* 23, 2717-2720, 1996. [14] Terasaki et al., *Earth Planet. Sci. Lett.* 232, 379-392, 2005. [15] Yoshino et al., Earth Planet. Sci. Lett. 222, 625-643, 2004. [16] Roberts et al., *Geophys. Res. Lett.* 34, 2007GL030497, 2007. [17] Toplis et al., *Meteoritics Planet. Sci.*, in press, 2013. [18] Jurewicz et al., *Geochim. Cosmochim. Acta* 57, 2123-2139, 1993. [19] Jurewicz et al., *Geochim. Cosmochim. Acta* 59, 391-408, 1995. [20] Kleine et al., Geochim. Cosmochim. Acta 68, 2935-2946, 2004. [21] Cashman and Sparks, *Geol. Soc. Am. Bull.* 125, 664-690, 2013. [22] Haack et al., *J. Geophys. Res.* 95, 5111-5124, 1990. [23] Höink et al., *Geochem. Geophys. Geosys*. 7, 2006GC001268, 2006. [24] Ichikawa et al., *J. Geophys. Res.* 115, 2009JB006427, 2010. [25] Mandler and Elkins-Tanton, *Meteoritics Planet Sci*., in press, 2013. [26] Fu et al., *Science* 338, 238-241, 2012. [27] Roberts et al., *Workshop on Planetesimal Formation and Differentiation*, abstract 8033, 2013. [28] Moskovitz and Gaidos, *Meteoritics Planet. Sci.* 46, 903-918, 2011. [29] Quitté et al., *Astrophys. J.* 720, 1215-1224, 2010. [30] Moynier et al., *Astrophys. J.* 741, 71, 2011. [31] Quitté et al., *Geochim. Cosmochim. Acta* 75, 7698-7706, 2011. [32] Neumann et al., *Astron. Astrophys.* 543, A141, 2012. [33] Sandu and Kiefer, *Geophys. Res. Lett*. 39, 2011GL050225, 2012. [34] Nimmo, *Geophys. Res. Lett.* 36, 2009GL037997, 2009. [35] Williams, *Earth Planet. Sci. Lett.* 284, 564-569, 2009.

FROM VESTA TO CERES: PREDICTING SPECTACULAR DICHOTOMOUS CONVEXO- CONCAVE SHAPE FOR THE LARGEST MINI-PLANET IN THE MAIN ASTEROID BELT; Kochemasov G.G., IGEM of the Russian Academy of Sciences, 35 Staromonetny, 119017 Moscow, kochem.36@mail.ru.

In compliance with the first theorem of the wave planetology –"Celestial bodies are dichotomous" [1-4 & others] – three largest asteroids of the main asteroid belt show striking tectonic similarity. Though not sharply imaged by the HST, and having differing sizes and compositions, they all show somewhat different hemispheres (Fig. 1, 2, 4,5). A flattening one side (up to development of a depression) is accompanied by a bulging of the opposite one. This dichotomous shape feature is a fundamental tectonic character of celestial bodies caused by their movements in non-circular keplerian orbits with alternating accelerations: speeding + and braking -. Arising inertia-gravity forces warp any moving and rotating (but all bodies move and rotate!) bodies in four ortho- and diagonal directions. An interference of these directions brings about uprising (+), subsiding (-) and neutral (0) regularly disposed tectonic blocks (Fig. 3). They have a stationary character (move up and down with certain periods), the same as giving them rise inertia-gravity waves are stationary waves (endless movements in non-circular orbits make them standing). Sizes of the tectonic blocks depend on lengths of the warping waves. The most pronounced tectonic wave produced feature is the tectonic dichotomy caused by the longest in any body fundamental wave 1 (long $2\pi R$, where R is a body radius). To think that this ubiquitous dichotomy is a result of a random giant impact hitting any body in a special place is completely unacceptable.

The theorem 3 of the comparative wave planetology [1-4] states: "Celestial bodies are granular". Sizes of these tectonic granules are inversely proportional to orbital frequencies: higher frequency – smaller granule, lower frequency – larger granule. There is the following row of granule sizes (a half of a wavelength): Mercury $\pi R/16$, Venus $\pi R/6$, Earth $\pi R/4$, Mars $\pi R/2$, asteroids $\pi R/1$. It follows that in the asteroid belt there is a remarkable resonance 1:1 between the fundamental wave and an individual wave also long $2\pi R$. This causes an enormous scattering of planet building material from the main asteroid belt, impossibility of gathering a planet (no Phaethon is possible!) and severe flattening of asteroids of all sizes including the largest ones (all asteroids have a well known oblong shape). Normally, along with an oblong one observes a convexo-concave shape (the best studied example is the approaching Earth asteroid Eros) [5].

This severe resonance enhanced treatment causes visible distortion of not only relatively small bodies (less than 300-400 km across), that is widespread among celestial bodies of various classes [6 , 7], but also the largest of them, more than about 500 km across. Thus, an oblong body of (1) Ceres has major/minor axes 898/788 km [8] or 970/930 km, according to J. Parker & Stern, and has a prominent dusky dark spot (Piazzi) from one side (Fig. 4). It occupies a significant part of the asteroid (a dwarf planet) – about 250 km, more than a quarter the size of Ceres and probably might be assigned to a depression (Fig. 4). Tectonically one may compare this depression with the Pacific basin hollow on Earth [9]. A NASA HST color image of Ceres PIA10235 (Fig. 5) shows spectrally different regions: relatively red and blue, hinting on different types of material and compositional dichotomy.

(2) Pallas has the radii of 291 x 278 x 250 km [10] and also represents a dichotomous shape with one bulging hemisphere and the other antipodean one more flat and dark. (4) Vesta, about 525 km across, has a deep dark depression from one side opposed to a bulging shining hemisphere [11] (Fig. 1, 2). So, in all three cases of the largest asteroids there is one tectonic peculiarity clearly showing their dichotomous nature. Inferred impacts have nothing to do with this inherent to all heavenly bodies wave induced structurization. The dichotomy is caused by an interference of fundamental waves 1(Fig. 3) weaving a structural tetrahedron. The first overtone wave 2 makes a structural octahedron (a diamond shape). So, a new planetologic thinking is strongly required. The pronounced dichotomy predicted for Ceres will strengthened this conviction.

References: [1] Kochemasov G.G. (1999) Geophys. Res. Abstracts, v. 1, # 3, 700. **[2]** Kochemasov G. G. (1994) 20th Russian-American microsymposium on planetology. Abstr., Moscow, Vernadsky Inst., 46-47. **[3]** Kochemasov G. G. (1998) Proceedings of international symposium on new concepts in global tectonics ('98 TSUKUBA), Tsukuba, Japan, Nov. 1998, 144-147. **[4]** Kochemasov G. G. (2004) In Workshop on "Hemispheres apart: the origin and modification of the martian crustal dichotomy", LPI Contribution # 1203, Lunar and Planetary Institute, Houston, p. 37. **[5]** Kochemasov G.G. (1999) On convexo-concave shape of small celestial bodies //Conference "Asteroids, comets, meteors", Cornell Univ.,USA, July 26-30, 1999, Abstract #24.22. **[6]** Kochemasov G.G. (2001) Geophysical Research Abstracts, vol. 3, CD-ROM. **[7]** Kochemasov G.G. (2000) 33rd COSPAR Scientific Assembly, 16-23 July 2000, Warsaw, Poland, Abstracts, CD-ROM. **[8]** McCarthy D.W., Jr., Freeman J.D., Drummond J.D. (1994) Icarus, v. 108, #2, pt.1, 285-297. **[9]** Kochemasov G.G. (2002) Geophysical Research Abstracts, Vol. 4, CD-ROM. **[10]** Schmidt B.E. et al. (2008) 39th LPSC, Abstract 2502 pdf. **[11]** Jian-Yang Li et al. (2008) 39th LPSC, Abstract 2253 pdf.

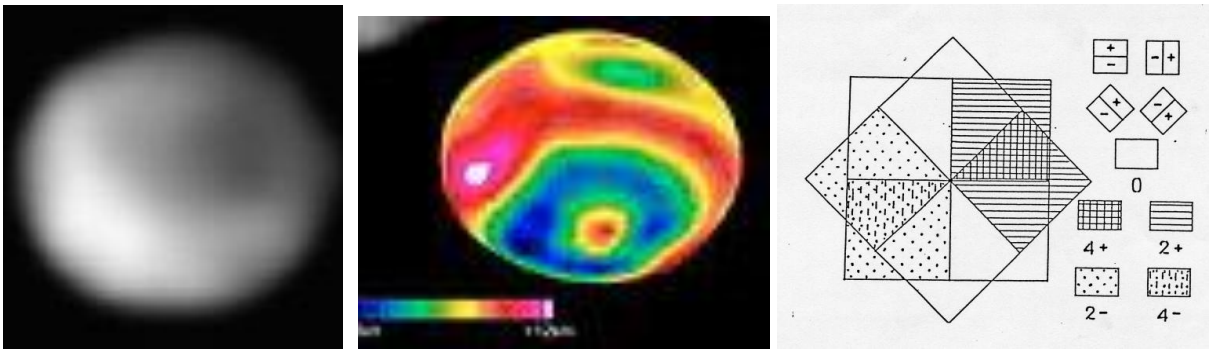

Fig. 1.-left. (4)Vesta. A dichotomous celestial body. Press release #: STScl – PR95-20. Asteroid or mini-planet? A portion of HST.WFPC2, B. Zellner, NASA, April 19, 1995. **Fig. 2.**-centre. Large depression on Vesta (Asteroid-vesta-three-views-bg.jpg).**Fig. 3**-right. Graphical presentation of sectors and dichotomy formation by interference of quantum-mechanical waves (+ or -) of 4 directions.

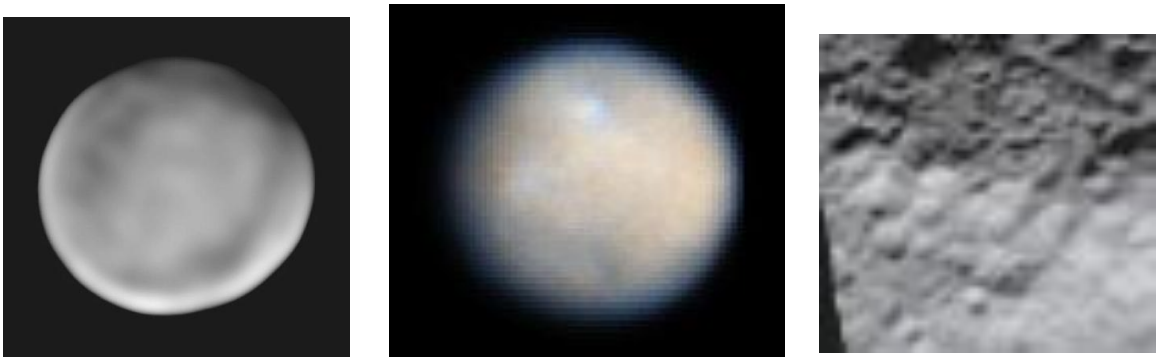

Fig. 4-left. (1)Ceres. Piazzi basin – the huge darker oval. Credit: Keck Observatory by C. Dumas (NASA-JPL). **Fig. 5**-centre. (1)Ceres. Dwarf planet. PIA10235. Credit: NASA/ESA/J. Parker, P. Thomas, L. McFadden, and M. Mutchler and Z. Levay. **Fig. 6.** Vesta, a portion of IOTD-104-page.jpg. A grid of non-impact craters long ~ 20 km.

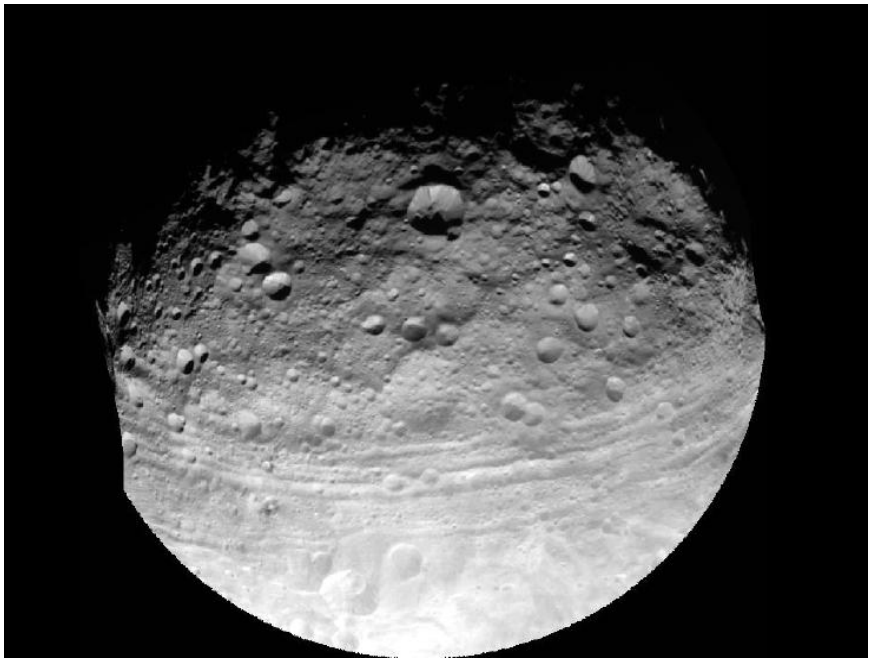

Fig. 7. Vesta, 595403main_pia14894-43_946-710.jpg

Many vestan craters considered as impact features have the wave interference nature. This is especially true for chains and regular grids of subdued ring structures often observed on vestan surface (Fig. 6). Partially imaged the northern hemisphere shows clear signs of chess-board structure developed due to intersecting waves (Fig. 7). Bordering checks intersecting lines sometimes are marked by crater chains obviously related to degassing (compare with the comet Hartley2 core).

NATURE OF THE "ORANGE" MATERIAL ON VESTA FROM DAWN. L. Le Corre[1], V. Reddy[1], N. Schmedemann[2], K. J. Becker[3], D. P. O'Brien[1], N. Yamashita[1], P. N. Peplowski[4], T. H. Prettyman[1], J.-Y. Li[1], E. A. Cloutis[5], B. W. Denevi[4], T. Kneissl[2], E. Palmer[1], R. W. Gaskell[1], A. Nathues[6], M. J. Gaffey[7], D. W. Mittlefehldt[8], W. B. Gary[9], H. Sierks[6], C. T. Russell[10], C. A. Raymond[11]. [1]Planetary Science Institute, Tucson, AZ (lecorre@psi.edu), [2]Freie Universitaet Berlin, Germany, [3]USGS, Flagstaff, AZ, [4]Johns Hopkins University, Laurel, MD, [5]University of Winnipeg, Canada, [6]MPS, Germany, [7]UND, USA, [8]NASA Johnson Space Center, Houston, TX, [9]NASA Goddard Spaceflight Center, Greenbelt, MD, [10]UCLA, CA, [11]JPL, Pasadena, CA.

Introduction: From ground-based observations of Vesta, it is well-known that the vestan surface has a large variation in albedo [1]. Analysis of images acquired by the Hubble Space Telescope allowed production of the first color maps of Vesta and showed a diverse surface in terms of reflectance [2]. Thanks to images collected by the Dawn spacecraft at Vesta, it became obvious that these specific units observed previously can be linked to geological features [3]. The presence of the darkest material mostly around impact craters and scattered in the Western hemisphere has been associated with carbonaceous chondrite contamination [4]; whereas the brightest materials are believed to result from exposure of unaltered material from the subsurface of Vesta [4] (in fresh looking impact crater rims and in Rheasilvia's ejecta and rim remants).

Here we focus on a distinct material characterized by a steep slope in the near-IR relative to all other kinds of materials found on Vesta. It was first detected when combining Dawn Framing Camera (FC) color images in Clementine false-color composites [5] during the Approach phase of the mission (100000 to 5200 km from Vesta). We investigate the mineralogical and elemental composition of this material and its relationship with the HEDs (Howardite-Eucrite-Diogenite group of meteorites).

Dawn data: For this study, we analyzed data from all instruments onboard the Dawn spacecraft. Morphology, composition and topography was derived from clear and color (7 filters in the near-IR) images from the FC [6]. VIR (Visible and IR spectrometer) spectra [7] from the Survey phase were used to derive approximate mineralogy using band parameters. From GRaND (Gamma Ray and Neutron Detector), we used maps of corrected Fe counting rate and neutron absorption.[8,9], and the composition parameter C_p [10].

Morphology of the units: Several types of orange material can be identified in the FC images, classified as follows:

Orange diffuse ejecta. We found two craters showing clearly this type of deposit, Oppia and Octavia craters (Fig. 1). In this case, the orange material seemed to be deposited as an ejecta blanket around the crater. Oppia corresponds to the "Leslie" feature observed by [11] and proposed to be olivine.

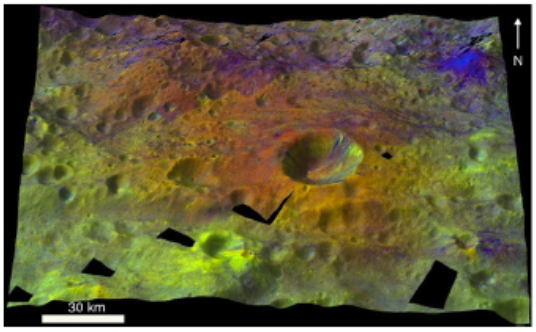

Figure 1: *Octavia crater and its orange ejecta at 60 m/pixel with "Clementine" color ratio composite (R=0.75/0.45 μm, B=0.75/0.92 μm, G=0.45/0.75 μm).*

Orange patches. These deposits have a characteristic lobate shape and possess sharp boundaries with the surrounding terrains (Fig. 2). They are smaller than the diffuse deposits.

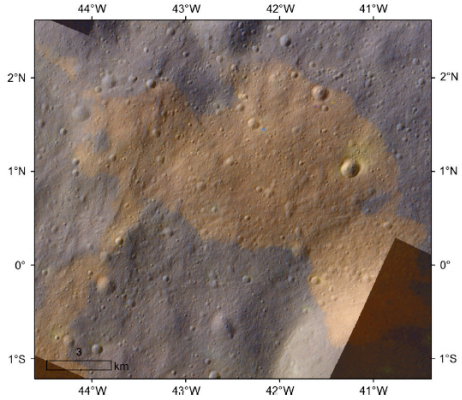

Figure 2: *Close-up view of part of an orange patch in Clementine color ratios overlaid on top of 16 m/pixel clear filter image. No difference in texture with nearby terrains is observed and no obvious topographic feature is associated with the orange material.*

Orange crater rays. Ejecta rays of orange material distributed radially around fresh-looking impact craters such as Cornelia or Rubria (Fig. 3).

Distribution across Vesta: We carried out a complete mapping of the orange material on Vesta based on 60 m/pixel FC maps (up to 50°N). The material is distributed across almost all longitudes in the equatorial region (30°S-30°N) but excluded from the Rheasilvia basin floor.

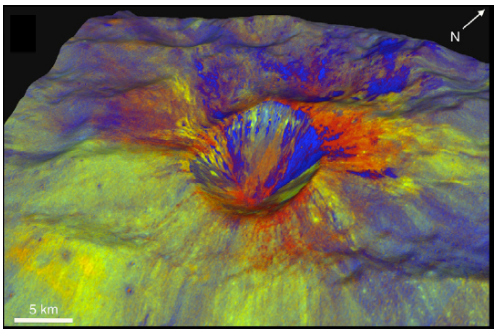

Figure 3: *Perspective view of the Rubria crater as seen by FC and overlaid on topography.*

Color properties: Based on analysis of FC data, we found that all orange material deposits have similar color spectra with a red slope. The only difference between them is the depth of the pyroxene Band I, which can vary with the background: weaker for darker surface, and deeper for brighter surface. Generally, orange patches have higher 0.75-µm albedo than other orange deposits.

Composition: We explored several options for the composition of this material (that could explain the red spectral slope) and after analyzing the Dawn data we ruled out the olivine option [11] and the metal option. Our detailed reasoning is described in [12].

Mineralogy and HEDs. The range of pyroxene "compositions" that we derived for 17 sites of orange material is between $Fs_{38\text{-}46}Wo_{8\text{-}11}$ with an average of $Fs_{42}Wo_{9}$ (Fig. 4). This narrow pyroxene chemistry range observed among the 17 sites suggests similar composition and formation mechanism. The pyroxene chemistry plot in the transition region between cumulate eucrites (CE) and basaltic eucrites and at the upper end of basaltic eucrite-rich howardites (Fig. 4).

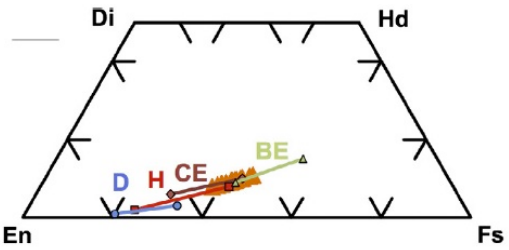

Figure 4: *Pyroxene quadrilateral including the orange material sites from the VIR data and the ranges of mean pyroxene compositions for cumulate eucrite (CE), basaltic eucrite (BE), diogenite (D) and howardite (H). It is important to note that the ranges shown here represent mean pyroxene chemistries derived from spectral data and not laboratory data.*

In addition, Band I center and BAR values of the orange material sites are most consistent with those of basaltic eucrites and not with diogenites. Using preliminary total iron (wt.%) calibration developed with HED spectral data we estimated the iron abundance for the 17 sites for which we extracted VIR spectra. The range of iron abundance for these sites is very narrow (13.5–14.2 wt.%) with a mean of 13.8 wt.%, consistent with basaltic eucrites and/or howardites.

Elemental composition. Arruntia and Octavia ejecta are found to have compositions consistent with howardites with no CE admixture according to C_p analysis (Fig. 5). Oppia also has a howardite-like composition, however a CE admixture of ~25% is allowed by the GRaND measurements. Using the Fe counting rate translated in Fe abundance, we found that the three sites are consistent with howardites/polymict eucrite, with Octavia matching some basaltic eucrites and Oppia getting close to cumulate eucrite data points.

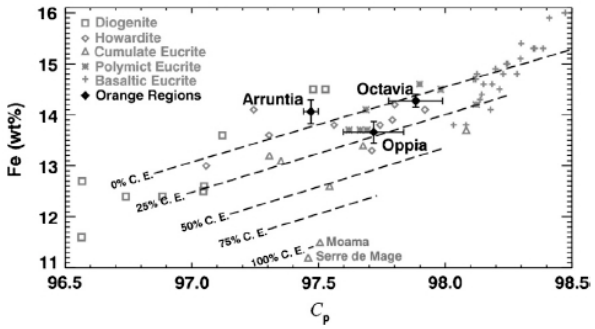

Figure 5: *Fe abundances plotted against the high-energy gamma-ray derived Cp values for 57 HED whole-rock elemental compositions. Arruntia, Octavia, and Oppia regions of interest are represented in black diamonds. Black dash lines indicate trendlines for non-CE and CE admixtures.*

Impact melt hypothesis: The two HED impact melt samples that plot closest to the orange material in BI center vs. BAR in both parameter spaces are LEW85303 (impact melt matrix) and Macibini (impact melt clast). The diversity of BI center positions of the samples could reflect the different nature of the original material that has been impacted and melted. Combining the interpretations from topography, geomorphology, color parameters from the FC, curve matching and band parameters from the VIR spectral data, the most probable analog for the orange material on Vesta is impact melt dominated howarditic material.

References:

[1] Bobrovnikoff 1929. [2] Li et al. 2010 *Icarus*. [3] Reddy et al. 2013 *Icarus*. [4] Reddy et al. 2012 *Science*. [5] Reddy et al. 2012 *Icarus*. [6] Sierks et al. 2011 *Space Sci. Rev*. [7] DeSanctis et al. 2011 *Space Sci. Rev*. [8] Prettyman et al. 2013 *MAPS*. [9] Yamashita et al. 2013 *MAPS*. [10] Peplowski et al. 2013 *MAPS*. [11] Gaffey et al. 1997 *Icarus*. [12] Le Corre et al. 2013 *Icarus*.

The Photometric Properties of Vesta and the Implications. Jian-Yang Li[1], B.J. Buratti[2], C.M. De Sanctis[3], B.W. Denevi[4], M. Hoffmann[5], A. Longobardo[3], S. Mottola[6], A. Nathues[5], V. Reddy[1], C.T. Russell[7], S.E. Schröder[6], [1]Planetary Science Institute, jyli@psi.edu, [2]Jet Propulsion Laboratory, California Institute of Technology, [3]Istituto di Astrofisica e Planetologia Spaziali, INAF, Rome, Italy, [4]Johns Hopkins University, Applied Physics Laboratory, [5]Max Planck Institute for Solar System Research, Katlenburg-Lindau, Germany, [6]Deutsches Zentrum für Luft- und Raumfahrt (DLR), 12489 Berlin, Germany, [7]Institute of Geophysics and Planetary Physics, University of California Los Angeles.

Introduction: The visual geometric albedo of 0.38 [1, 2] makes Asteroid Vesta the brightest rocky body of its size in the solar system. All other large planetary bodies in the solar system that are brighter than Vesta have mostly icy surfaces. For the less than 1% of asteroids that are brighter than Vesta, all are much smaller and considered collisional fragments from their parent bodies. Ample evidence suggests that Vesta, instead, is a protoplanet that failed to accrete to a full-sized planet, and has an ancient surface that retains the impact records over the past four billion years [e.g., 3, 4]. Li et al. [1] performed a detailed global photometric analysis of the surface of Vesta in the visible wavelengths using the images collected by the Framing Camera (FC) onboard NASA's Dawn spacecraft during its year-long stay in orbit around Vesta. We will summarize the photometric properties of Vesta, and discuss the implications of both our understanding of the photometric properties of Vesta and asteroids in general, and the photometric modeling of solar system rocky bodies. Vesta shows relatively large and interesting variations in its local photometric properties [e.g., 5, 6]. In this paper, we shall restrict ourselves to the globally averaged photometric properties. We note that some hypotheses we proposed in this paper can be further tested with in-depth, comparative studies of the photometric variations on the highly heterogeneous surface of Vesta in the future.

Photometric Properties of Vesta: Based on Li et al. [1], the albedo of Vesta is about twice as high as that of average S-type asteroids, and shows a strong dependence on wavelength from its pyroxene composition [7, 8]. Other than albedo, the globally averaged photometric properties of Vesta are similar to those of S-type asteroids. The wavelength dependence of those photometric parameters is weak between 0.4 and 0.98 μm wavelengths. The Hapke photometric roughness of Vesta is 18º. The histogram of the albedo distribution of Vesta at a pixel size of 1 km is single peaked, with a full-width-at-half-maximum of 17% of the average albedo, compared to the total range of albedo >4x wider. Models from FC data suggest similar or slightly stronger phase reddening as compared to Eros, an S-type near-Earth asteroid with a mean dimension of 17 km [9]. However, previous ground based observations and laboratory measurements of HED meteorites suggested the same trend but twice as strong phase reddening [10].

Implications: While the physical interpretations of photometric behavior, especially under the Hapke's theoretical framework, are still under debate and further laboratory investigation [e.g., 11], comparisons between different objects are still revealing. The albedo of Vesta puts it between the generally darker rocky and the generally brighter icy bodies. It is therefore also informative to consider the implications in terms of photometric modeling.

Phase Function: It is interesting to note that, despite the nearly 2x albedo difference, the single-particle phase function of Vesta is similar to that of average S-type asteroids [1]. However, dark, primitive type asteroids have steeper phase functions than Vesta, and brighter, icy satellites have comparable or shallower slopes. Based on McGuire and Hapke [12] and Souchon et al. [13], the single-scattering phase functions of Vesta and S-type asteroids are most consistent with irregular, rough, and opaque solid or hollowed particles that have a large fraction of internal impurity, but not consistent with smooth or transparent particles. The similar disk-averaged phase functions of large and ancient Vesta and various small, possibly fragment S-type asteroids indicate that phase function of asteroids seems to be independent of their average surface ages.

Hapke Roughness Parameter: The exact physical meaning of Hapke's roughness parameter is not clear. Some laboratory studies [14] suggested that roughness parameter is determined by the smallest structures that cast shadows. In the visible wavelengths, almost all asteroids, and even comets, that have been carefully modeled with disk-resolved data have roughness parameters within a range of 15º-30º [1, 15]. This fact seems to suggest that, despite the vastly different surface morphology of these objects, the small-scale (<mm) macroscopic structures of all solar system objects are similar. If this conclusion is true, then it further suggests that photometric roughness is dominated by small-scale regolith processes, such as micrometeorite gardening, rather than large-scale impacts. Or, alternatively, the small range of modeled roughness values compared to the possible full range (0º-60º) could suggest that the Hapke model itself is not very sensitive to roughness at all.

Multiple Scattering: Li et al. [1] estimated that, even for the relatively high single-scattering albedo of Vesta (~0.5 at 550 nm), multiple scattering accounts for only up to 30% of the total reflectance, which in turn still linearly depends on single-scattering albedo within ±30% of the average albedo. The majority of rocky bodies in the solar system are darker than Vesta. Therefore, this result for Vesta validates the approach that uses photometricaly corrected reflectance maps to approximate albedo maps by assuming a linear relationship between reflectance and various albedos for most rocky bodies.

In addition, Li et al. [1] compared Hapke model using an isotropic multiple scattering approximation and that partially accounting for anisotropic multiple scattering [c.f. 16], and reported that the level of multiple scattering for Vesta does not generate appreciable deviation between the two models. Although this result could be due in part to the large photometric variations on the surface of Vesta that hide the effect of multiple scattering, it still suggests that the effect of anisotropic multiple scattering can be ignored in the photometric modeling of almost all rocky bodies.

Phase Reddening: The similar phase reddening effect for Vesta compared to Eros is consistent with the similar photometric properties of Vesta with average S-type asteroids and the similar characteristics in their visible spectrum. But it is a puzzle that the phase reddening measured from FC data appears to be much weaker than those observed from the ground and measured for HED meteorites [10]. Assuming that all instruments are well inter-calibrated, then the discrepancy must lie on their different spatial resolutions and the associated geometric characteristics: Ground-based observations are hemispheric in scale, with the total flux integrated at a particular phase angle but over the whole range of incidence and emission angles in the illuminated and visible part of the surface. FC data used in Li et al. [1] have a field-of-view (FOV) of ~200 km, with relatively limited range of relatively low emission angles in each pixel. While laboratory measurements essentially eliminate all of the variations in the scattering geometry, the samples are artificially prepared and might have different photometric properties from the natural surface on Vesta.

Recent studies suggest that multiple scattering could cause phase reddening [17]. The fraction of multiple scattering is higher at higher phase angles [e.g. 1]. The overall increasing albedo of Vesta with wavelength means that at longer wavelength, increasing multiple scattering will result in a relatively shallower phase function, resulting in phase reddening. We suggest that the high emission angle areas on Vesta included in ground-based, disk-integrated data might be the cause of stronger phase reddening observed as compared to FC data. Hapke model calculations showed that the relative contribution of multiple scattering increases with phase angle faster near the limb/terminator than the center of disk (low emission angles). We plan to compare the phase reddening observed from the ground with those derived from FC data with the full disk of Vesta in the FOV and with the highest resolution data with 20 km FOV to quantitatively assess this explanation.

Conclusions: The similar phase functions and Hapke photometric roughnesses of Vesta and many S-type asteroids might be an indication that the globally averaged photometric properties are probably not sensitive to geologic processes of the overall surface. If photometric properties are affected by any global scale geologic processes, then the "photometric equilibrium" might be reached in a much shorter time scale than geologic time scale. This conclusion is similar to that suggested by Li et al. [15] with the study of similar photometric properties of cometary nuclei and the comparisons with dark type asteroids.

The phase reddening behavior of Vesta seems to be consistent with a multiple scattering origin of phase reddening, although we cannot rule out any other possible causes. On the other hand, the level of multiple scattering on Vesta is not sufficiently strong to cause an appreciable non-linear effect in photometric modeling. Since the albedo of Vesta is higher than most rocky bodies, the above conclusions about multiple scattering should be applicable to most rocky bodies in the solar system.

Acknowledgement: This work is supported by NASA Dawn at Vesta Participating Scientist Program, Grant NNX13AB82G to Planetary Science Institute.

References: [1] Li, J.-Y., et al. (2013) Icarus, 226, 1252. [2] Tedesco, E.F. (1998) Asteroids II, pp. 1090. [3] Russell, C.T., et al. (2012) Science 336, 684. [4] Marchi, S., et al. (2012) Science 336, 690. [5] Schröder, S.E., et al. (2013) Icarus 85, 198. [6] Buratti, B.J., et al. (2012) 43rd LPSC, Abstract 1659. [7] De Sanctis, M.C., et al. (2012) Science, 336, 697. [8] De Sanctis, M.C., et al. (2013) M&PS, in press. [9] Clark, B.E., et al. (2002) Icarus 155, 189. [10] Reddy, V., et al. (2012) Icarus 217, 153. [11] Shepard, M.K., and Helfenstein, P. (2007) JGR, 112, E3. [12] McGuire, A., Hapke, B. (1995) Icarus, 113, 134. [13] Souchon, A.L., et al. (2011) Icarus, 215, 313. [14] Shepard, M.K., and Campbell, B.A. (1998) Icarus, 134, 279. [15] Li, J.-Y., et al. (2013) Icarus 222, 467. [16] Hapke, B. (2012) Theory of Reflectance and Emittance Spectroscopy, Cambridge Univ. Press. [17] Hapke, B., et al. (2012) JGR, 117, E00H15.

RETRIEVAL OF DISK-RESOLVED PHASE FUNCTIONS OF VESTA AND COMPARISON WITH OTHER ASTEROIDS. A. Longobardo[1], F. Capaccioni[1], E. Palomba[1], M.C. De Sanctis[1], F.Tosi [1], S.E. Schroeder[2], J.-Y. Li[3], M.T. Capria[1], E. Ammannito[1], C.A. Raymond[4] and C.T. Russell[5]. [1]INAF-IAPS, via Fosso del Cavaliere 100, Rome, Italy (andrea.longobardo@iaps.inaf.it), [2]Deutsches Zentrum für Luft und Raumfahrt (DLR), Berlin, Germany, [3]Planetary Science Institute, Tucson, AZ, USA [4]California Institute Technology JPL, Pasadena, CA, USA, [5]UCLA, Los Angeles, CA, USA.

Introduction: The NASA-Dawn mission has observed for one year the Vesta surface, taking hyperspectral data by means of the Visible and InfraRed (VIR) spectrometer [1].

The calibration of VIR data [2] allowed us to record the surface reflectance in both visible and infrared domains of the VIR instrument. The analysis revealed that Vesta has a large visual albedo (0.38 on average [3]) and shows the largest reflectance variations on its surface, with presence of high-albedo (bright) [4] and low-albedo (dark) units [5], which have been associated to uncontaminated HED (whose Vesta is believed to be the parent body) and presence of carbonaceous chondrites, respectively.

The measured reflectance strongly depends on the observation geometry, i.e. the solar incidence angle i, the emission angle e and the solar phase φ. The understanding of these behaviors is essential in the interpretation of data, because it allows: a) to apply a photometric correction to images/spectra, in order to rely on their comparison (meaningless in absence of this correction); b) to provide information on the physical and optical properties of the surface regolith, such as grain size, roughness, role of single and multiple scattering, and composition.

In this work we focus on the behavior of reflectance measured at two wavelengths (0.75 μm and 1.2 μm) as a function of phase angle. We studied the 20°-60° phase slope variations across the Vesta surface and compared the inferred values with those found in other asteroids of different spectral types (C, S, E), in order to find a "photometric equivalent" for the dark and bright endmembers. In this study, we considered the Lutetia asteroid, too, by analyzing the data provided by the VIRTIS (Visible InfraRed Thermal Imaging Spectrometer) instrument [6] onboard the Rosetta mission. This is an interesting case since the Lutetia spectral class is still debated (C, D, E or a combination of them [7]).

Vesta phase functions: [8] performed a photometric correction of VIR reflectance at 0.75 μm and 1.20 μm, by combining a disk function and phase function. The former removes the topography effects on the measured reflectance (primarily due to i and e variations), whereas the latter reproduces the brightness variations with phase.

The considered disk function is the parameter-less Akimov function [9], which is wavelength independent, while it depends only on the illumination and observation angles (i, e, φ). The calibrated radiance factor I/F has been then divided for the disk function in order to obtain the equigonal albedos at the considered wavelength.

The phase functions have been calculated over ten families of equigonal albedos. These have been empirically defined, by means of a statistical analysis on the whole VIR dataset (containing 20 million spectra) [8]. This analysis allowed to study the phase function variation across Vesta.

The reflectance decrease with phase has been found to be steeper in low-albedo regions and more moderate as reflectance increases (Figure 1). This has been ascribed primarily at the more important role in bright units of multiple scattering, which redistributes the incident radiation, causing a flattening of the phase curve.

To allow a comparison between phase functions of Vesta and other asteroids, these have been recalculated, considering the radiance factor instead of the equigonal albedo (Figure 1). These new phase functions are steeper than the previous ones, since the application of the disk function reduces the reflectance changes with phase.

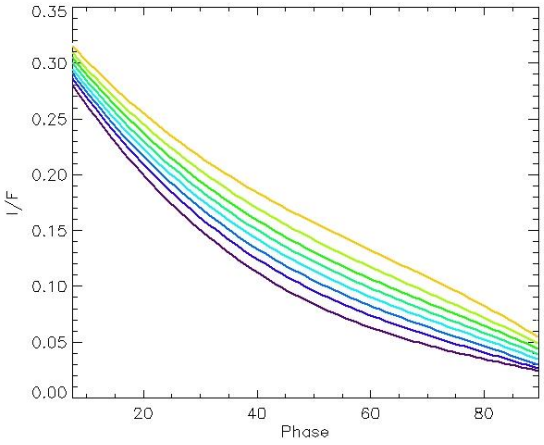

Figure 1: Radiance factor as function of phase angle for different Vesta reflectance families (reflectance increases from purple to yellow).

Lutetia phase function: The radiance factor behaviour with phase has been similarly studied on the dataset of VIRTIS observations of Lutetia, including about eighteen thousand spectra. The analysis has been performed at different infrared wavelengths, i.e. 1.00 μm, 1.28 μm, 1.56 μm, 1.85 μm and 2.13 μm [10].

The phase function has been found to be independent of wavelength (at least for $\varphi > 20°$). Since the reflectance variations across Lutetia are much lower than those observed on Vesta, we did not consider reflectance families, but the mean phase curve for each wavelength (producing specific disk-integrated phase functions).

Comparison with other asteroids: preliminary results. We define the phase slope as the reflectance decrease from 20° to 60°, relative to the reflectance at 20°. We calculated it on the phase functions averaged on Vesta bright regions, Vesta dark regions and the whole Vesta surface, as well as on the disk-integrated phase function of Lutetia. Finally, we considered phase slopes from phase functions obtained in literature of asteroids visited by spacecrafts, e.g. the S-type Gaspra, Ida, Eros and Annefrank, the C-type Mathilde and the E-type Steins.

These phase functions were obtained at different wavelengths of the visible and/or infrared domain. However, we can consider in a first approximation that phase functions do not present large spectral variations as long as they are calculated at wavelengths far from absorption bands. This assumption is justified by different photometry studies performed on Vesta (e.g. [8], [3]) and other asteroids (e.g. [10], [11]).

The phase slope comparison is shown in Table 1.

A preliminary analysis evidences that the Vesta average photometric properties are comparable with S-type asteroids, in agreement with [3].

The phase slope of the Vesta darker regions tends to values typical of the C-type asteroid Mathilde. This would be explained by the presence of charbonaceous chondrites in the Vesta dark units.

No equivalent asteroid spectral types are instead found for the Vesta bright regions, characterized by a lower phase slope. This may indicate that the multiple scattering has a more important role in the uncontaminated HED than in the chondrites, due to their larger albedo. However, it should be noted that Steins has a mean visible albedo similar to Vesta bright units [12], but a disk-integrated phase slope more similar to the Vesta average.

Finally, Lutetia shows a phase slope intermediate between the Vesta average and bright units, making it quite similar to the E-type Steins and much different from the C-type Mathilde. This would evidence that Lutetia could not be a C-type asteroid, as asserted by [16].

Asteroid	Type	λ(μm)	Phase slope	Ref
Mathilde	C	0.70	69%	[13]
Vesta dark units	V	0.75	68%	[8]
		1.20	67%	[8]
Eros	S	0.56	66%	[13]
		1.49	62%	[11]
Ida	S	0.56	62%	[11]
Annefrank	S	0.63	62%	[15]
Vesta average	V	0.75	56-60%	[8], [3]
		1.20	56%	[8]
Steins	E	0.63	57%	[12]
Lutetia	C, D or E	IR	50%	[10]
Vesta bright units	V	1.20	45%	[8]
		0.75	41%	[8]

Table 1: Phase slope of different asteroids (in decreasing phase slope order). The Lutetia phase slope is the same at all the five infrared wavelengths considered.

References:

[1] De Sanctis M.C. et al. (2011) *SSR, 163,* 329-369. [2] Carraro F. et al. (2012) *LPSC XLIII*, 1439. [3] Li J.-Y. et al. (2013) *Icarus, 226*, 1252-1274. [4] Zambon F. et al. (2013) *Icarus, Under Review*. [5] Palomba E. et al. (2013) *Icarus, Under Review*. [6] Coradini A. et al. (2007) *SSR*, *128*, 529-559. [7] Barucci M.A. et al. (2012) *PSS*, *66*, 1, 23-30. [8] Longobardo A. et al. (2013) *Icarus, Under Review*. [9] Shkuratov Y.G. et al. (1999) *Icarus, 141*, 132-155 [10] Capaccioni F. et al. (2013) *LPSC XLIV*, 2229. [11] Clark B.E. et al. (2002) *Icarus, 155*, 1, 189-204. [12] La Forgia F. et al. (2012) *MemSAIT*, *20*, 15. [13] Clark B.E. et al. (1999) *Icarus, 140,* 1, 53-65. [14] Domingue et al. (2002) *Icarus, 155,* 1, 205-219. [15] Hillier J.K. et al. (2011) *Icarus, 211*, 1, 546-552. [16] Coradini A. et al. (2011) *Science, 334*, 6055, 492.

Acknowledgements:

VIR is funded by the Italian Space Agency–ASI and was developed under the leadership of INAF-Istituto di Astrofisica e Planetologia Spaziali, Rome-Italy. The instrument was built by Selex-Galileo, Florence-Italy. The authors acknowledge the support of the Dawn Science, Instrument, and Operations Teams. This work was supported by ASI and NASA.

New Insights on the Differentiation of Asteroid Vesta.

S. Marchi[1], M. C. De Sanctis[2], E. Ammannito[2], H. Y. McSween[3], L. A. McFadden[4], C. A. Raymond[5], L. T. Elkins-Tanton[6], W. F. Bottke[7] and C. T. Russell[8]. [1]Solar System Exploration Research Virtual Institute, Southwest Research Institute, Boulder, CO, USA (marchi@boulder.swri.edu), [2]Istituto Nazionale d'Astrofisica, Rome, Italy, [3]University of Tennessee, Knoxville, TN, USA, [4]NASA, Goddard Space Flight Center, Greenbelt, MD, USA, [5]Jet Propulsion Laboratory, Pasadena, CA, USA, [6]Carnegie Institution for Science, Washington DC, USA, [7]Southwest Research Institute, Boulder, CO, USA, [8]University of California, Los Angeles, CA, USA.

Introduction: Asteroids offer an unique opportunity to study processes of planetesimal accretion and differentiation that took place at the dawn of our Solar System. Fortunately, the current main belt -a reservoir of rocky asteroids between the orbit of Mars and Jupiter- contains planetesimals that survived the latest stages of planetary accretion [1-4]. Among the multitude of main belt asteroids, the 500-km Vesta emerges as one of the best bodies to study the early processes of accretion, differentiation, and subsequent collisional evolution of planetesimals. Much of our ability to study and constrain Vesta's internal structure and differentiation processes come from Howardite, Eucrite and Diogenite (HED) meteorites [e.g., 6].

Pre-Dawn models based on HEDs petrology were consistent with both a i) vertically layered body resulting from the solidification of a magma ocean having a deep olivine-rich mantle [e.g., 7], or ii) heterogeneous internal structure due to serial magmatism resulting in fractional crystallization of diogenitic plutons at the base or within the mantle-crust boundary [e.g., 8].

Olivine on the surface of Vesta: The Dawn spacecraft [9] acquired high-resolution global imaging and spectral and elemental mapping from which surface composition is derived, which enabled us to narrow down differentiation models. In particular, the global mapping unveiled the collisional history of Vesta [10], providing geological setting for the HEDs source location and the observed heterogeneity of the surface composition. The latter data showed the presence of olivine-rich (~50-70%) terrain admixed with howarditic material distributed on the surface at high northerly latitudes [11].

A possible explanation for this unexpected discovery is that the olivine-rich material has been accreted by a collision with an olivine-rich asteroid. While Dawn data cannot definitely rule out this scenario, it appears unlikely given the scarcity of such asteroids within the main belt [12].

On the other hand, the geological setting of this olivine-rich terrain -apparently not associated with the largest Rheasilvia and Veneneia basins- precludes that it is the result of material excavated from the mantle [12], unless some of the degraded large craters seen on the northern hemisphere were capable of exposing mantle rocks. The latter possibility cannot be ruled out with present data, but it seems unlikely given the shallow excavation depth of such impact structures.

Conclusions: Therefore, these results favor both classical and recent magma ocean models [e.g., 13] that predict i) the formation of olivine diogenite in the lower crust, and ii) an internal heterogeneous distribution of lithologies, perhaps due to a non-uniform crustal thickness or to the presence of magma chambers. Interestingly, the presence of crustal non-uniformities may be inferred with the aid of a recent Bouguer gravity map obtained by Dawn [14] and by the distribution of large-scale troughs [15].

References: [1] Safronov, V.S., 1969. Evolution of Protoplanetary Cloud and Formation of the Earth and Planets. Nauka, Moscow. [2] Greenberg, R., et al., Planetesimals to planets. Numerical simulation of collisional evolution, 1978, Icarus 35, 1. [3] Wetherill, G.W., Stewart, G.R., Accumulation of a swarm of small planetesimals, 1989, Icarus 77, 330. [4] Wetherill, G.W., 1989. Origin of the asteroid belt. In: Binzel, R.P., Gehrels, T., Matthews, M.S. (Eds.), Asteroids II. Univ. of Arizona Press, Tucson, 661. [5] Keil, K., Geological history of Asteroid 4 Vesta: the "smallest terrestrial planet.", 2002, In: Bottke, W.F., Cellino, A., Paolicchi, P., Binzel, R. (Eds.), Asteroids III. Univ. Arizona Press, Tucson, 573. [6] McSween H.Y., Meteorites and Their Parent Planets, 1999, Cambridge Univ. Press, 310 p. [7] Righter, K., & Drake, M. J. A magma ocean on Vesta: Core formation and petrogenesis of eucrites and diogenites, 1997, MAPS 32, 929. [8] Barrat, J.-A et al. Relative chronology of crust formation on asteroid Vesta: Insights from the geochemistry of diogenites, 2010, Geo. et Cosmo. Acta 74, 6218. [9] Russell, C. T. et al., Dawn at Vesta: testing the protoplanetary paradigm, 2012, Science 336, 684. [10] Marchi, S. et al. The violent collisional history of asteroid 4 Vesta, 2012, Science 336, 690. [11] De Sanctis, M. C., et al. Possible Detection of Olivine on Vesta. 2013, LPI Science Conf. Abs., 44, 1460. [12] Ammannito, E. et al. Olivine in an unexpected location on Vesta's surface, 2013, Nature. [13] Mandler, B.E. & Elkins-Tanton L.T., The origin of eucrites, diogenites and olivine diogenites, 2013, MAPS, in press. [14] Raymond, C. A. et al., submitted. [15] Buczkowski, D. L. et al., GRL 39, L18205, 2012.

EXPERIMENT TO DETERMINE THE UPPER LIMITS OF THE SEARCH FOR SATELLITES OF VESTA. L. A. McFadden[1], D. R. Skillman[1], N. Memarsadeghi[1], J.-Y. Li[2], M. Mutchler[3], B. McLean[3], U. Carsenty[4], S. Mottola[4], S. Hellmich[4], M.V. Sykes[2], P. Tricarico[2], E. Palmer[2], C.T. Russell[5], C. A. Raymond[6] [1]NASA Goddard Space Flight Center, Greenbelt, MD,[2]Planetary Science Institute, Tucson, AZ [3]Space Telescope Science Institute, Baltimore, MD, [4]DLR, Berlin, [5]IGPP, UCLA, Los Angeles, CA, [6]Caltech/Jet Propulsion Lab, Pasadena, CA.

Introduction: The Dawn mission executed a satellite search between May and July 2011 because the presence or absence of natural satellites provides a piece of the collisional and dynamical history of Vesta. The collisional history of Vesta has been active as recently as 1 BY ago [1,2] and the existence of the Vesta family [3] also provides many candidate bodies to be held in orbit around Vesta. The deepest satellite search prior to this was conducted using Hubble Space Telescope and searched to a detection limit of 44 m diameter [4]. Data acquisition, processing and multiple search approaches have been described in [5]. No satellites were found in two types of searches described below. Here we describe the experiment designed to determine the limits of the search in which artificial satellites of random orbits were implanted in two sets of images. Our purpose was to find the limiting magnitude of the Vesta satellite search and determine the completeness of the search.

Artificial Satellite Generation: We first worked with the Optical Navigation imaging sequence 16 (OpNav16) acquired with Dawn's Framing Camera [6]. This is the last sequence in which Vesta does not fill the camera's field of view (Fig.1). Satellites with random circular orbits of 1.1 to 10 Vesta radii, with random inclinations, centered on Vesta were implanted into the sequence of 20 images calculating the position of the satellite with respect to Vesta's center for each image at each time. A dedicated satellite search mosaic was also carried out. To assess the limits of searching this series, we took Station 5 images in all three mosaics and inserted simulated satellites. The satellites are in arbitrarily oriented circular orbits with radii 1.1 to 100 Vesta radii. They cover a range of magnitudes and the motions are consistent over all images. Synthetic satellites were also generated using the software image simulator developed for the proposed German "AsteroidFinder" space mission [7] realistically reproducing the basic steps of the image formation process: optical transfer through the optics, image projection onto the detector, charge accumulation in the CCD, charge transfer and readout process.

Results: We had five searchers look for satellites in OpNav 16 images and six co-authors searched the station 5 mosaics. For the OpNav 16 sequence, the 50% completeness instrumental magnitude is 8. The magnitude equation calculated against UCAC3 catalogue stars is y=0.9977x + 12.555. Our 50% completeness apparent visual magnitude is 20.54.

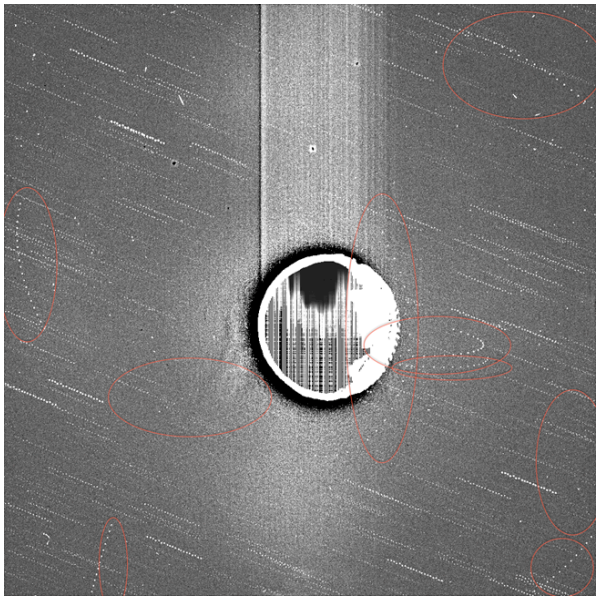

Fig. 1 Randomly Implanted satellites in OpNav16 appear as curved arcs when the sequence of 20 images is stacked and summed. Red circles guide the viewer to them.

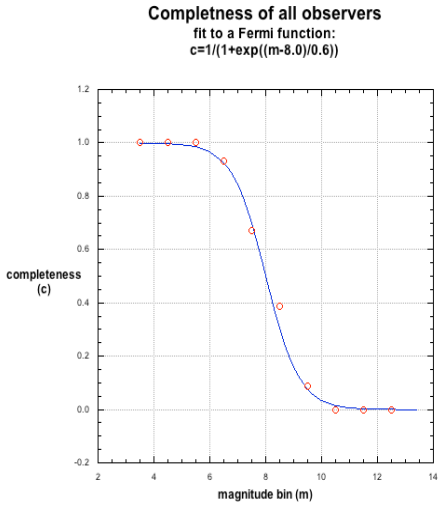

Fig. 2 Completeness of OpNav 16 search in instrumental magnitude.

References:

[1] Schenk P. et al. (2012) *Science, 336,* 694. [2] Marchi S. et al. (2012) *Science, 336,* 690. [3] Binzel R. P. and Xu, S. (1993) *Science, 260,* 186. [4] McFadden, L.A. et al. (2012) *Icarus, 220*, 305. [5] Memarsadeghi, N. et al. (2012) *Proc. SPIE, 8296,* Computational Imaging X*, 82960H.* [6] Sierks et al. 2011, *Space Sci. Rev. 163*, 263. [7] Mottola et al. 2008 In *ACM 2008* held July 14-18, 2008, Baltimore, MD. *LPI Contribution No. 1405*, paper id. 8140.

Additional Information: This work was supported by the Dawn project and the DLR. Space Telescope Science Institute contributed the time of MM and BM. Support from the framing camera team is appreciated.

VESTA IN THE LIGHT OF DAWN, BUT WITHOUT HEDS? H. Y. McSween[1], D. W. Mittlefehldt[2], and the Dawn Science Team, [1]Department of Earth and Planetary Sciences, University of Tennessee, Knoxville, TN 37996-1410, mcsween@utk.edu, [2]KR/Astromaterials Research Office, NASA/Johnson Space Center, Houston, TX 77058.

Introduction: The derivation of HEDs from Vesta is strongly supported by Dawn data [1], and these meterorites have made interpretations of Dawn spectra much more rigorous. Compared to the Moon, where samples became available *after* geologic mapping, the exploration of Vesta has been backwards. But what if HEDs had not been available or identified as vestan samples? What petrologic and geochemical predictions would have been possible using Dawn data, without the benefit of HEDs?

Compositional Mapping: VIR , FC, and GRaND compositional maps of Vesta [2,3,4] reveal that the regolith consists of regionally varying combinations of basalt and orthopyroxenite, based on comparisons with HEDs. But would these specific lithologies have been identified from VISNIR spectra indicating only Fe-bearing pyroxenes of varying composition, or from neutron absorption values or global Fe/O and Si/O ratios? And without the ability to analyze the mineralogy and chemistry of eucrite and diogenite end members, modeling regolith mixing and the petrogenesis of the igneous rocks would be qualitative at best. Assuming that samples had been extracted and launched from the 500 km diameter Rheasilvia basin (as inferred from observations of the Vestoids [5]), we probably would have predicted, based on petrologic reasoning, that crustal basalts or gabbros (eucrites) would be the most abundant lithologies, as observed. However, the high abundance of basaltic eucrites (63%) relative to cumulate (3%) and polymict (34%) eucrites would probably not be predicted. An estimate of regolith thickness ($\leq$1 km) [6] predicts that regolith breccias (howardites) would be less abundant, as observed.

Regolith Properties: Without the observation of CM clasts in howardites, it is arguable whether the unexpected discovery of H-rich [7] and OH-rich [8] regions on Vesta would have been interpretable in terms of exogenic carbonaceous chondrite containing hydrous minerals, although their occurrence as low-albedo regions might suggest a foreign component. The low amounts of impact melt in fresh craters seen in FC images [6] is consistent with models that imply limited melting due to low impact velocities, and would have correctly predicted limited amounts of impact melts in howardites. Recognizing the distinctive character of space weathering on Vesta [9] did not require HEDs, although the lack of agglutinates and nannophase iron in howardites provides confirmation of the spectral interpretation.

Magma Ocean: Dawn's observation that orthopyroxenite (if that lithology could have been identified) on Vesta has been excavated from the Rheasilvia basiin (with a 30-45 km deep transient cavity, twice the estimated thickness of Vesta's crust [10]) would likely have led to the hypothesis of a global magma ocean, by analogy with the Moon. However, the complexity of vestan magma ocean models [11], involving a period of equilibrium crystallization followed by continuous extraction of residual melts into fractionating plutons at higher levels, is required by HED geochemistry. The homogeneity of oxygen isotopes in HEDs [12] is a predictable consequence of pervasive melting.

Mantle Composition: The lack of spectrally detectable olivine in Rheasilvia [13] might have led to a prediction of an olivine-free upper mantle. However, harzburgitic diogenites contain olivine [14], a discrepancy now reconciled by experiments showing the difficulty of spectrally detecting <25% olivine in the presence of orthopyroxene [15].

Core Size and Bulk Composition: The estimated core mass fraction of Vesta is ~18%, based on fitting of Dawn's determination of the gravitational moment J_2 [16]. We now know that this is in remarkable agreement with meteorite-based models of the HED parent body, with core mass fractions of 15-20% [17]. The core size is a critical constraint on Vesta's bulk composition, recently modeled as Na-depleted H chondrite with ~25% admixed CM chondrite [18]. This compositional model can yield eucrite-like melts, and has an Fe/Mn ratio, an oxygen isotopic composition, and a redox state like HEDs, but none of those constraints would be available without HEDs. Estimating this bulk composition is a necessary step in devising models for the thermal evolution [19] and magmatic differentiation [11] of Vesta.

Chronology: From the crater-saturated surface of Vesta and from crater-counting chronology of vestan units as >3.5 Ga [20], the ancient crystallization ages of HEDs [21] were predictable but not precisely quantifiable. Without $^{40}Ar/^{39}Ar$ measurements of HED breccias [22], the late bombardment by high-velocity impactors on Vesta [23] would not be recognized.

Conclusion: Our understanding of Vesta's geology and evolution is so inextricably linked to HEDs [24] that it is difficult to imagine a Dawn mission not informed by these samples. Vesta now joins the Moon and Mars as the only extraterrestrial bodies that have been geologically, petrologically, and geochemically characterized. Not coincidentally, samples are available for all three bodies.

References: [1] McSween H.Y. et al. (2013) *MAPS*, in press. [2] Ammannito E. et al. (2013) *MAPS*, in press. [3] Thangiam G.S. et al. (2013) *MAPS*, in press. [4] Prettyman T.H. et al. (2013) *MAPS*, in press. [5] Binzel R.P. and Xu S. (1993) *Science* 260, 186-191. [6] Jaumann R. et al. (2012) *Science* 336, 687-694. [7] Prettyman Y.H. et al. (2012) *Science* 338, 242-246-. [8] De Sanctis M.C. et al. (2012) *Ap.J. Lett.* 758, L36. [9] Pieters C.M. et al. (2012) Nature 491, 79-82. [10] McSween H.Y. et al. (2013) *JGR* 188, 335-346. [11] Mandler B. and Elkins-Tanton L (2013) *MAPS*, in press. [12] Greenwood R.C. et al. (2005) *Nature* 435, 916-918. [13] Ammannito E. et al. (2013) *Nature*, doi:10.1038/nature12665. [14] Beck A.W. and McSween H.Y. (2010) *MAPS* 45, 850-872. [15] Beck A.W. et al. (2013) *MAPS*, in press. [16] Russell C.T. et al. (2012) *Science* 336, 684-686. [17] Righter K. and Drake M.J. (1997) *MAPS* 32, 929-934. [18] Toplis M.J. et al. (2013) *MAPS*, in press. [19] Formissano M. et al. (2013) *MAPS*, in press. [20] Marchi S. et al. (2012) *Science* 336, 690-694. [21] McSween et al. (2011) *Space Sci. Rev.* 163, 141-174. [22] Bogard D.D. (2011) *Cheme de Erde* 71, 201-226. [23] Marchi S. et al. (2013) *Nature Geosci.* 6, 303-307. [24] Keil K. (2002) *Asteroids III*, 573-584.

GEOLOGICAL STRUCTURES IN THE WALLS OF VESTAN CRATERS. D. W. Mittlefehldt[1], A. Nathues[2], A. W. Beck[3], M. Hoffmann[2], M. Schaefer[2],and D. A. Williams[4], [1]NASA/Johnson Space Center, Houston, TX, USA (david.w.mittlefehldt@nasa.gov) , [2]Max Planck Institute for Solar System Research, Katlenburg-Lindau, Germany, [3]Smithsonian Institution, Washington, DC, USA, [4]Arizona State University, Tempe, AZ, USA.

Introduction: A compelling case can be made that Vesta is the parent asteroid for the howardite, eucrite and diogenite (HED) meteorites [1], although this interpretation has been questioned [2]. Generalized models for the structure of the crust of Vesta have been developed based on petrologic studies of basaltic eucrites, cumulate eucrites and diogenites. These models use inferred cooling rates for different types of HEDs and compositional variations within the clan to posit that the lower crust is dominantly diogenitic in character, cumulate eucrites occur deep in the upper crust, and basaltic eucrites dominate the higher levels of the upper crust [3-5]. These models lack fine-scale resolution and thus do not allow for detailed predictions of crustal structure. Geophysical models predict dike and sill intrusions ought to be present, but their widths may be quite small [6].

The northern hemisphere of Vesta is heavily cratered, and the southern hemisphere is dominated by two 400-500 km diameter basins that excavated deep into the crust [7-8]. Physical modeling of regolith formation on 300 km diameter asteroids predicts that debris layers would reach a few km in thickness, while on asteroids of Vesta's diameter regolith thicknesses would be less [9]. This agrees well with the estimated ≤1 km thickness of local debris excavated by a 45 km diameter vestan crater [10]. Large craters and basins may have punched through the regolith/megaregolith and exposed primary vestan crustal structures. We will use Dawn Framing Camera (FC) [11] images and color ratio maps from the High Altitude and Low Altitude Mapping Orbits (HAMO, ~65 m/pixel; LAMO, ~20 m/pixel) to evaluate structures exposed on the walls of craters: two examples are discussed here.

Marcia Crater: Marcia is a young crater 68×58 km in size centered at latitude, longitude 9º, 190º [12] (Fig. 1a). Formation of Marcia partially obliterated the rim of 53 km diameter Calpurnia crater. Topographic prominences forming semi-continuous layers are visible at many locations high on Marcia crater walls. On the western wall where illumination was most favorable, semi-continuous layers of bright material overlie a discontinuous layer and/or scattered blocks of dark material (Fig. 1b). In one area bright material layers meet the underlying dark material layer at acute angles and appear to be truncated (black arrows, Fig. 1c). However, talus obscures the underlying structure below the dark band.

Fig. 1 FC images of Marcia crater. a. Portion of HAMO global mosaic showing the general region. b. Portion of a LAMO image showing discontinuous dark layer and blocks topographically below semi-continuous bright layers. c. Region showing angular junctures between bright and dark materials (arrows).

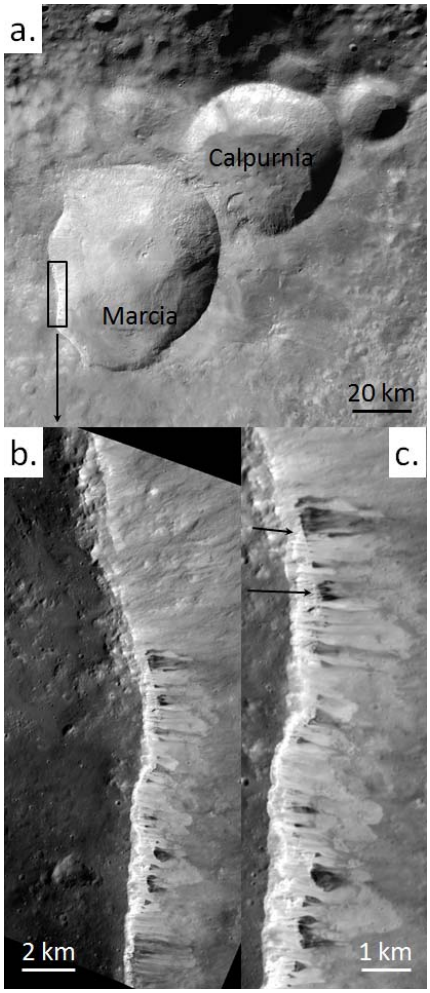

Rubria Crater: Rubria is a young crater ~10 km in diameter centered at latitude, longitude -7.5º, 18.5º within the Divalia Fossa, a region of troughs engendered by the Rheasilvia basing-forming impact [13] (Fig. 2a). Rubria crater was formed on a slope. The upslope northern crater wall has numerous prominences of bright material with some areas showing semi-continuous bright material bands (Figs. 2b-d; yellow arrows). Locally scattered within the bright material prominences are 100-400 m patches and short bands of

dark material. Some are below bright material prominences suggesting they may be resistant to mass wasting and possibly supporting the prominences (black arrows; Figs. 2c, d). None of the boulders ejected onto the rim or mass-wasted to the south appear to be dark material (Fig. 2b) as might be expected if that material was mechanically strong.

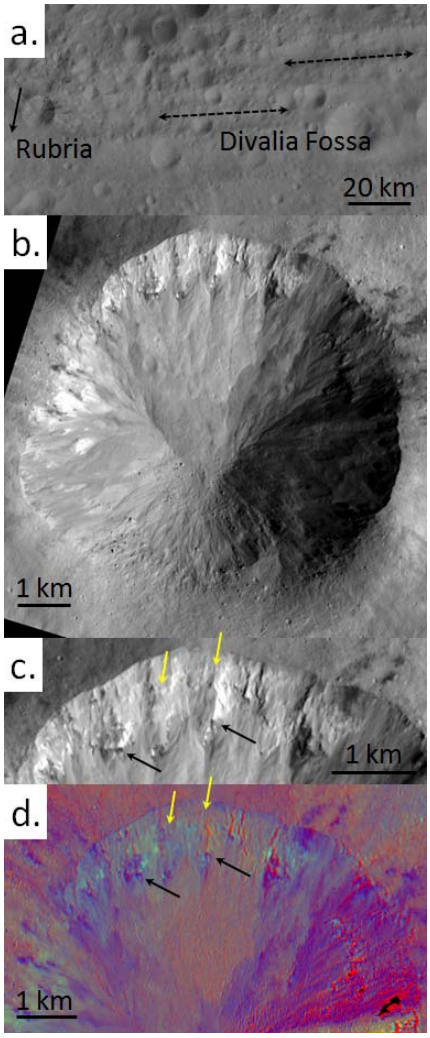

Fig. 2 FC images of Rubria crater. a. Portion of HAMO global mosaic showing the relationship between Rubria crater and equatorial troughs (dashed arrows) and the general downslope direction (solid arrow). b. Portion of a LAMO image. c. Expanded view of the north wall showing dark materials below prominences (black arrows), and semi-continuous layers of bright material (yellow arrows). d. Portion of a LAMO Clementine color ratio mosaic showing lithologic diversity.

Discussion: In general, dark materials on Vesta are interpreted to be fragments of carbonaceous chondrite impactors [14] while bright materials have spectral characteristics indicating that they are the most pristine vestan lithologies [15]. The thin layer of dark material in Marcia crater may have a different origin. The crosscutting relationship with bright material layers suggests a possible sill-like intrusion. However, the dark material band is at a depth of <2 km from the rim, within the depth range of a megaregolith assuming asteroid regolith formation models [9] are accurate. Thus, the bright layers may be ejecta draped onto a surface of preexisting dark material. The morphology of the thin layer of dark material in Marcia crater (Fig. 1c) is not that expected of carbonaceous chondrite debris. These fragile rocks ought to be efficiently disrupted during impact and mixed within vestan ejecta as scattered blocks; this morphology is observed in other craters on Vesta [16]. The thin, ~1 km long layer of dark material in Marcia crater could represent ponded impact-melt or melt-breccia from an earlier impact. Melt-breccia clasts in HEDs are typically dark brown to black [e.g., 17]. The dark material that appears to form a thin band supporting a prominence in Rubria crater (left black arrow, Fig. 2c, d) may be another instance of impact-melt or melt-breccia.

At present, all of the structures examined in vestan crater walls are plausibly layers or blocks of ejecta material, impact-melts, melt-breccias and/or impactor debris from earlier impact events. If the dark layer in Marcia crater is in fact composed of chondritic debris, this only strengthens the conclusion that the structures are not primary. We have yet to find unequivocal evidence for primary crustal structures on Vesta.

Acknowledgement: Images are courtesy of NASA/JPL-Caltech/UCLA/MPS/DLR/IDA.

References: [1] McSween H. Y. Jr. et al. (2013) *Meteoritics & Planet. Sci.,* in press. [2] Wasson J. T. (2013) *Earth Planet. Sci. Lett., 381,* 138. [3] Takeda H. (1979) *Icarus, 40,* 455. [4] Righter K. and Drake M. J. (1997) *Meteoritics & Planet. Sci., 32,* 929. [5] Mandler B. E. and Elkins-Tanton L. T. (2013) *Meteoritics & Planet. Sci.,* doi: 10.1111/maps.12135. [6] Wilson L. T. and Keil K. (2012) *Chem. d. Erde Geochem., 72,* 289. [7] Marchi S. et al. (2012) *Science, 336,* 690. [8] Schenk P. et al. (2012) *Science, 336,* 694. [9] Housen K. R. and Wilkening L. L. (1982) *Ann. Rev. Earth Planet. Sci., 10,* 355. [10] Jaumann R. et al. (2012) *Science, 336,* 687. [11] Sierks H. et al. (2011) *Space Sci. Rev.,* doi: 10.1007/s11214-011-9745-4. [12] Williams D. A. (2013) *Icarus,* submitted. [13] Buczkowski D. L. et al. (2012) *Geophys. Res. Lett., 39,* L18205. [14] McCord T. B. et al. (2012) *Nature, 491,* 83. [15] Li J.-Y. et al. (2012) *LPS, XLIII,* Abstract #2381. [16] Reddy V. et al. (2012) *Icarus, 221,* 544. [17] Labotka T. C. and Papike J. J. (1980) *Proc. 11th Lunar Planet. Sci. Conf.,* 1103.

THE IMPACT HISTORY OF VESTA. D. P. O'Brien[1], S. Marchi[2], A. Morbidelli[3], W. F. Bottke[2], P. Schenk[4], C. T. Russell[5], C. A. Raymond[6], [1]Planetary Science Institute, 1700 E. Ft. Lowell, Suite 106, Tucson, AZ 85719 (obrien@psi.edu), [2]NASA Lunar Science Institute, Southwest Research Institute, Boulder, CO, [3]Observatoire de la Cote d'Azur, CNRS, Nice, France, [4]Lunar and Planetary Institute, Houston, TX, [5]Institute of Geophysics and Planetary Physics, University of California, Los Angeles, CA, [6]Jet Propulsion Laboratory, California Institute of Technology, Pasadena, CA.

From radiometric dating of HED meteorites, we know that Vesta dates back to the beginning of the Solar System [e.g. 1], and hence its cratered surface may potentially hold a record of impacts dating back to that early era. Understanding Vesta's impact record requires a crater chronology curve that relates crater density to surface age (which may either be the formation age of the local crust or the time since the last major resurfacing event).

It is common practice to scale the crater production rate from one body (generally the Moon) to another in the inner Solar System using estimates of the orbital distribution of impactors (namely the Near-Earth Asteroids, NEAs) and scaling laws for crater production [eg. 2]. While this is not without its difficulties and uncertainties, it is generally a reasonable approach given that the different terrestrial bodies are all targets being hit by a single source population, the NEAs. The same scaling approach can not be applied to adapt the lunar crater production rate to the asteroid belt, however, since in the former case the source of projectiles on the Moon and terrestrial planets is the subset of bodies that leak out of the asteroid belt, while in the latter case the entire asteroid belt is the source of impactors on Vesta. A simple scaling from the moon to the asteroid belt ignores the fact that the dynamical history that delivers impactors from the main belt to the terrestrial planet region may imply a much different collisional history for the asteroid belt itself.

We have developed a chronology based on models of the primordial depletion and subsequent dynamical evolution of the main belt under the influence of giant planet migration and chaotic diffusion processes. The asteroid belt since ~4.1 Ga likely experienced a factor of ~4 depletion due to the combined effects of the resonance sweeping during the Nice Model instability [3] and the subsequent decay of unstable asteroids [4]. The E-Belt hypothesized by [5], while it would have dominated the impacts on the terrestrial planets, would have only been a relatively small fraction of the mass in the primordial belt, although E-belt bodies that hit Vesta would have likely had high velocities and may be responsible for resetting the Ar-Ar ages of HED meteorites [6].

At the earliest times, immediately following the formation of the Solar System, the asteroid belt may have had significantly more mass than it currently does, which would have been depleted over the first ~100 Myr [7-9] and led to an increased impact rate in the belt during that time. Another possible contributor to the early impact rate in the asteroid belt could be leftover scattered planetesimals from the terrestrial planet region, although the effect of such bodies on the asteroid belt has not been fully quantified. Regardless of the source of these earliest impactors, it is likely that there was a somewhat larger impact rate in the asteroid belt immediately following the formation of the Solar System, which would have decayed to ~4 times the current rate and stayed at that level until ~4.1 Ga, then decayed to its current rate following the destabilization of the asteroid belt and E-Belt. This destabilization and depletion at ~4.1 Ga would correspond to the beginning of the Late Heavy Bombardment on the Moon.

The largest uncertainty in this model chronology is the initial mass of impactors (which is related to this initial impact rate). If we assume that the largest craters on Vesta, impact basins larger than ~200 km in diameter, represent all craters of that size that have formed over its history (ie. no basins of that size have been erased), we can place a constraint on the initial impact rate and hence constrain the chronology curve. Using this approach suggests a primordial impacting mass in the asteroid belt region of roughly 1 Earth mass, broadly consistent with other estimates of the mass that would have been initially present in that region [7-9, see 10 for a review]

The resulting model chronology curve is plotted on the following page in normalized form $N^*(T)$, which gives the number of craters of a given size that accumulate over a given time for every one crater of that size formed per billion years. Also shown on the plot for comparison are a linear chronology curve, in which the rate of crater formation is the same at all times (no increased flux in the past), and a scaled version of the lunar chronology curve [eg. 11]. The dashed section prior to 4.1 Ga is an extrapolation, as the lunar impact history is not well-constrained prior to that time.

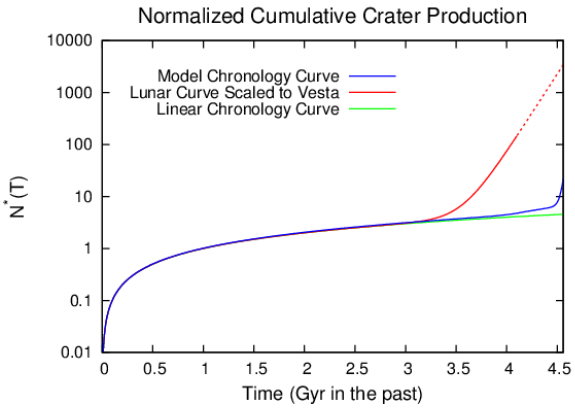

The Model Production Function (MPF) for Vesta derived by [12] can be used to convert the normalized $N^*(T)$ curves to actual crater densities on Vesta, and hence for a given crater density we can estimate the absolute age of a surface. We find an age of ~1 Ga for Rheasilvia using our model chronology, consistent with previous estimates [12]. This young age is also consistent with several other lines of evidence. Rheasilvia has a very fresh appearance relative to all other large impact basins. The size distribution of the Vesta family members, or "vestoids," is quite steep compared to the background population. This steep size distribution would collisionally grind down if the family were older than ~1 Gyr, suggesting its relatively recent formation [13,14]. A young age is also consistent with the much lower abundance of exogenic hydrogen within Rheasilvia Basin compared to the rest of the surface, as found by the Gamma Ray and Neutron Detector (GRaND) on Dawn [15]. For the Hghly Cratered Terrain (HCT) regions in the northern hemisphere identified by [12], we find an age of ~4.3 Ga, consistent with them being amongst the oldest terrains on Vesta. It is somewhat odd that an age of 4.5 is not obtained for that region. [12] find that while the HCT regions are not saturated (such that for every crater created, another is erased), they may be close enough to saturation that erasure processes may be affecting the crater counts and the measured crater population may be somewhat lower than the production population. Thus, the actual age of the HCT regions could be closer to 4.5 Ga, the age of Vesta itself.

In contrast to our model chronology, the scaled lunar chronology [eg. 11] predicts a much larger impact rate prior to ~3.5 Ga, such that even the entire surface of Vesta, as dated by its largest impact basins, is only ~4 Ga. This is difficult to reconcile with its radiometric age of ~4.5 Ga, and would require either that there were no impacts on its surface prior to ~4 Ga, which is hard to fathom from a dynamical standpoint, or that the impact rate prior to 4 Ga was so intense that the entire surface (even craters on the scale of Rheasilvia) was reset, which would have likely eroded away Vesta's basaltic crust.

In addition to the cratering record, we have meteorites from Vesta, the HEDs, that record the ages of major impact events in their Ar-Ar ages. The Ar-Ar ages of eucrites suggest that several such events occurred between 3.4 and 4.1 Gyr ago, and that an especially large impact event (or events) occurred 4.48 Gyr ago, but few impacts capable of resetting the Ar-Ar chronometer occurred in the interval from 4.1 to 4.5 Ga [16]. Zircons in HED meteorites also suggest a period of very early impacts [17]. The scaled lunar chronology, if extrapolated back to 4.5 Ga, would predict a much larger number of resetting events in the 4.1 to 4.5 Ga timespan than in the 3.4 to 4.1 Ga timespan, which would be difficult to reconcile with the meteorite data. On the other hand, dynamical and impact modeling consistent with the theoretical chronology discussed here is able to reproduce the main features of the eucrite Ar-Ar age distribution [6].

Acknowledgements

D. P. O'Brien is supported by grant NNX10AR21G from NASA's Dawn at Vesta Participating Scientist Program.

References

[1] L. E. Nyquist (2009) *Geo. Cos. Acta* **73,** 5115.
[2] B. A. Ivanov (2001) *Space Sci. Rev.* **96**, 87.
[3] A. Morbidelli (2010) *AJ* **140**, 1391.
[4] D. A. Minton (2010) *Icarus* **207**, 744.
[5] W. F. Bottke (2011) *Nature* **485**, 78.
[6] S. Marchi (2013) *Nat. Geosci.* **6**, 303.
[7] G. W. Wetherill (1992) *Icarus* **100**, 307.
[8] J.-M. Petit (2001) *Icarus* **153**, 338.
[9] D. P. O'Brien (2007) *Icarus* **191**, 434.
[10] D. P. O'Brien (2011) *Space Sci. Rev.* **163**, 41.
[11] N. Schmedemann (2013) LPSC 44, 2155.
[12] S. Marchi (2012) *Science* **336**, 690.
[13] F. Marzari (1996) *A&A* **316**, 248.
[14] F. Marzari (1999) *Icarus* **142**, 63.
[15] T. H. Prettyman (2012) *Science* **338**, 242.
[16] D. D. Bogard (2011) *Chemie der Erde* **71,** 207.
[17] M. D. Hopkins (2012) LPSC 43, 2109.

MASS-WASTING FEATURES IN VESTA'S SOUTH POLAR REGION. K. A. Otto[1] (katharina.otto@dlr.de), R. Jaumann[1, 2], K. Krohn[1], K.-D. Matz[1], F. Preusker[1], T. Roatsch[1], P. Schenk[3], F. Scholten[1], K. Stephan[1], C. A. Raymond[4] and C. T. Russell[5], [1]Deutsches Zentrum für Luft- und Raumfahrt (DLR), Institute of Planetary Research, Rutherfordstraße 2, 12555 Berlin, Germany, [2]Institute of Geosciences, Freie Universität Berlin, Berlin, Germany, [3]Lunar and Planetary Science Institute, Houston, Texas, USA, [4]California Institute of Technology, Jet Propulsion Laboratory, Pasadena, California, USA, [5]Institute of Geophysics and Planetary Physics, University of California, Los Angeles, California, USA

Introduction: The DAWN spacecraft orbited asteroid (4) Vesta from August 2011 until September 2012 [1]. The Framing Camera (FC) on board the space craft collected image data of the asteroids surface with a resolution of about 70 m/pixel in the High Altitude Mapping Orbit (HAMO) and up to 20 m/pixel in the Low Altitude Mapping Orbit (LAMO). The FC obtained multiple images of the same area with different viewing geometries in HAMO resolution. Based on this stereo data set, a three-dimensional Digital Terrain Model (DTM) has been constructed on a reference spheroid of 285 km by 229 km [2]. Vesta's southern hemisphere exhibits two large basins, Rheasilvia and underlying Veneneia [3, 4]. The region around these basins shows various types of mass-wasting features that can be correlated to the basin formation and degradation processes [5]. We used LAMO images and the DTM to identify and map six different types of mass-wasting features.

Intra-crater Mass Wasting:

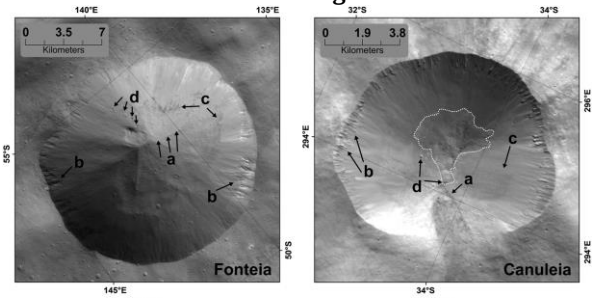

(a) (b)

We considered five intra-crater mass-wasting features. These include lobate downslope movement of debris (arrows a), spurs along the rims of the craters (arrows b), dark albedo patches overrun by brighter material (arrows c), boulders accumulated on the craters' floors and walls (arrows d), and talus material (dotted white line in (b)) [5].

The intra-crater mass-wasting features are distributed almost homogenously throughout the southern hemisphere indicating similar material properties. Older impact craters often lack fragile intra-crater mass-wasting features such as boulders, spurs and dark patches. It is likely that they have been eroded by intra-crater landslides triggered by local seismic shaking of subsequent impacts [5].

Flow-Like Features:

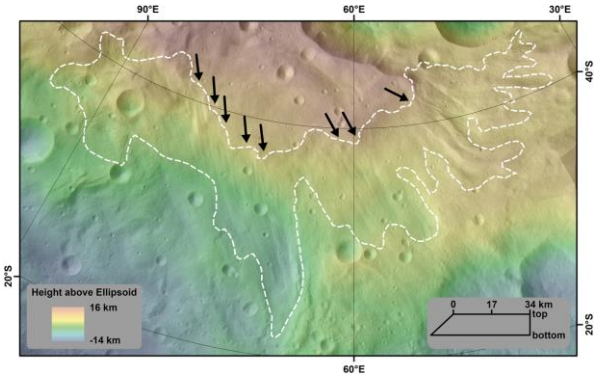

The Rheasilvia basin exhibits flow-like mass movements (dashed white line), which show a flume-like pattern with striations parallel to the direction of travel (arrows) and lobate scarps at the front of the features. The striations suggest fluid-like flow behavior, indicating that the frictional forces between the particles are small [5].

Creep-Like Features:

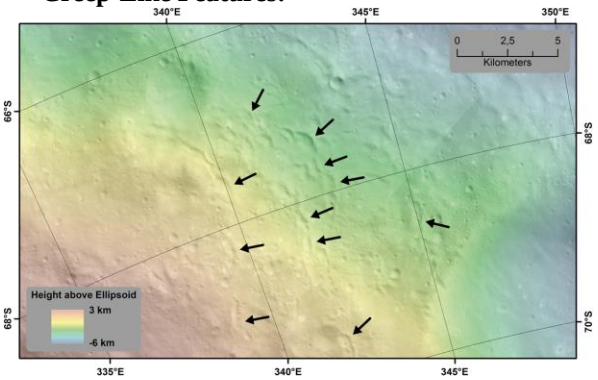

Other mass-wasting features occurring on Vesta's southern hemisphere are creep-like mounds on the regolith covered surface (arrows). These mounds are elongated features with a straight or slightly curved shape. Their lengths vary from a few hundred meters to several kilometers and they often appear in clusters with a curved alignment perpendicular to the slope [5].

Flow-like and creep-like features cluster within the region of 0°E and 90°E on the southern hemisphere. This is an area where the Rheasilvia impact ejecta has been proposed [7, 8]. It is probably that this highly

shocked and fractured material exhibits properties different from the other extant surface material [5].

Slumping:

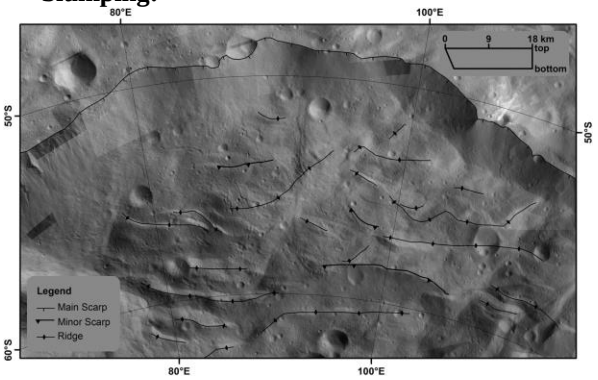

Rheasilvia has degraded due to slumping in various regions. Slumping features include almost vertical scarps, heads that are tilted backward toward the scarp, transverse cracks, ridges, and toe features at the front of the slumping bodies. A prominent and relatively young area of rotational slumping blocks appears along the Matronalia Rupes scarp toward the center of the Rheasilvia basin [5, 6].

Slides:

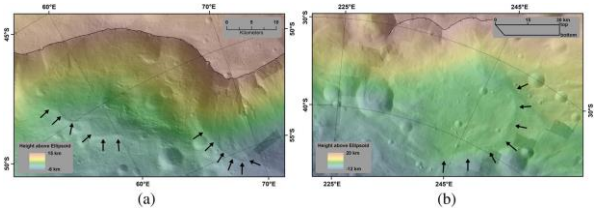

The Rheasilvia basin exhibits multiple ancient and recent landslides (arrows). The less eroded and younger landslides tend to be less massive in volume and run-out length. The landslides migrated from the rim and central peak of Rheasilvia toward the basin floor. For most identified slides, an eroded scarp can be observed. The resting bodies of the slides consist of elongated lobes or widened fans of material [5].

Slumping and sliding areas are mutually exclusive due to their compact and granular material properties, respectively [5].

Curved Ridges:

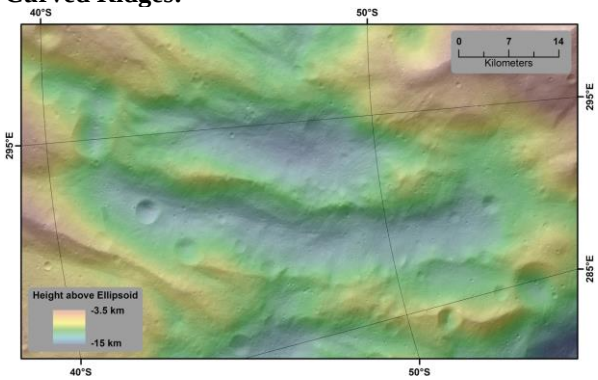

The Rheasilvia floor is characterized by numerous ridges and grooves that extend radially over the impact basin. The radial ridges are curved and up to 100 km long. They often run in parallel, with valleys separating them. In some cases, the valleys exhibit flow-like structures, indicating material migration [5].

The Rheasilvia basin also exhibits concentric ridges parallel to the crater rim. They are generally smaller than the radial ridges with lengths of up to 10 km. They often occur perpendicular to the slope which makes it likely they originated from the concentric crater collapse and relaxation after Rheasilvia had formed [5].

Conclusions: We identified six different types of mass-wasting features within the south polar region of Vesta. These features are evidence for the collapse and degradation of the Rheasilvia and Veneneia basins. Intra-crater mass wasting is present in smaller craters throughout the basins. Flow-like and creep-like features show the material behavior of highly fractured and shocked material produced by the Rheasilvia impact. Slumping and sliding are the most effective degradation processes due to their number and size. Curved radial and concentric ridges are the remnants of the early mass wasting in the modification stage of the Rheasilvia basin and the collapsed Rheasilvia wall, respectively.

References: [1] Russell et al. (2013) *Meteoritics & Planet. Sci.,* doi: 10.1111/maps.12091. [2] Preusker et al. (2012) EPSC *VII*, Abstract #EPSC2012-428-1. [3] Jaumann R. et al. (2012) *Science, 336,* 687-690. [4] Schenk P. et al. (2012) *Science, 336,* 694-697. [5] Otto et al. (2013) *JGR, 118*. [6] Reddy V. et al. (2012) *Science, 336,* 700-704. [7] De Sanctis C. et al. (2012) *Science, 336,* 697-700. [8] Krohn et al. (2013) EGU *XV*, Abstract #EGU2013-3213.

NATURE OF DARK MATERIAL UNITS ON VESTA: IMPLICATIONS FOR REGOLITH FORMATION AND CARBONACEOUS MATERIAL DELIVERY

E. Palomba (1), A. Longobardo (1), M.C. De Sanctis (1), S. Marchi (1,2), F. Zambon (1), F. Tosi (1), E. Ammannito (1), F. Capaccioni (1), M.T. Capria (1), C.T. Russell (3), C.A. Raymond (4)
(1) INAF-IAPS, Rome, Italy, ernesto.palomba@iaps.inaf.it, (2) Solar System Exploration Research Virtual Institute, Southwest Research Institute, Boulder, USA, (3) UCLA, Los Angeles, USA, (4) Cal. Inst. Tech JPL, Pasadena, USA

Introduction: Recent studies of the dark material (DM) and bright material (BM) units revealed that the Vesta surface have undergone intense fracturing, production and comminution of regolith [1,2,3]. Geomorphological analysis of DM units and their spatial distribution suggest that patches of dark materials are buried at various depth in the subsurface (down to ~2 km). DM is excavated and brought to the surface by impacts [1]. The results is an uneven distribution of DM on Vesta that is covered by a fine regolith composed of a mixture of dark and bright, fresher materials. By using Framing Camera images and VIR hyperspectral data two different catalogues of Dark material units were built [1,2]. Even if the two instruments have different spatial resolution and their spectral regimes are only partially overlapped, the two catalogues show large consistency, and both show larger concentration of DM units around the Veneneia impact basin.

Nature of DM units: More than 100 DM units are listed in the VIR catalogue [1]. Their spectra are dominated by the two large absorption band at 1 and 2 μm, typical of the pyroxenes, with variable band depths (BD) and reflectance, similar to the average Vestan surface. The inferred composition of the different dark deposits is very homogenous among them, i.e. a mixture of eucritic and darkening agents in various proportions.

The majority of DM units show a weak, but well identified, 2.8 μm band due to OH, that indicates the hydrated carbonaceous chondrite material as the most probable darkening agent, as suggest by earlier studies, too [4,5,6]. These studies claim that the DM originated in a low-velocity (<2 km/s) carbonaceous body impact during the formation of the 400 km diameter Veneneia basin ([4] delivery).

Hoewever, few DM (<10%) do not show a detectable OH absorption feature. This could imply the presence of a dehydrated CC or a material of different origin (e.g. impact melts, or metal rich materials). It will be important to assess what kind of darkening agent is present here and if it is different from the CC.

Regolith grain size and CC abundance: Typically for pyroxene rich material, reflectance is inversely related to grain size and directly to band depths [7]. For Vesta we observe a similar behavior at least for the band depths, being the grain size an unknown parameter.

The reflectance vs BDII scatterplot allow to disentangle the combined effect of these two parameters since it is very sensitive both to the grain size and to the abundance of a darkening agent. In Fig.1 we show how the bright and dark materials behave in this scatterplot. These behaviors have been compared with those of mixtures of eucritic material and carbonaceous chondrite contaminant (with different CC amount), together with those of three eucrites at different grain size. Two arrows indicate the CC amount increasing and the smaller size direction. The different grain sizes/darkening agent abundance in the considered dataset allows us to build boundaries for these two parameters that we use to evaluate grain size and CC abundance on Vesta.

With only very few exceptions, the Vestan dark and bright materials lies between the 0-25 and 25-45 micron size boundaries. Therefore on Vesta, the regolith grain size seems to be nearly homogeneous, suggesting that the difference between the dark and bright stands in the abundance of the dark contaminant, only.

If the considered mixture is representative of HED+CC mixtures, nearly all the DMs on Vesta would be located within the boundaries of 10-30 vol% of CC. This global result does not exclude that on a local scale, single units may show larger abundance of carbonaceous material. However, it is important to remark that at spatial resolution of the data among all the DM units we were not able to find a single unit composed of a pure carbonaceous chondrite. Extrapolating this result to the bright units, it seems that many of them are still contaminated by smaller amounts (<10 %) of carbonaceous chondrite material and that it is very difficult to find bright materials completely uncontaminated.

Implications for regolith formation and carbonaceous chondrite delivery: The apparent size homogeneity observed on the surface of Vesta indicates that the regolith is well mixed horizontally and vertically, at least in the first hundreds of meters beneath the surface. Moreover, the fact that thick patches of DM are found at depth, suggest that their fine grain size is not

the result of subsequent evolution (e.g. collisional erosion), but rather it is the original accreted size. If true, this result argues against the scenario of large blocks of spall material from impacts with carbonaceous asteroids at the origin of the DM units, and supports the idea that DM was accreted in the form of dust [8]. The burial further constrains the accretion to be older than Rheasilvia basins (the last major event that may have generated a thick layer of regolith) but not necessarily older that Veneneia basin. A model of regolith redistribution due to the major observed craters [9] is needed in order to see if this scenario is consistent with the spatial distribution of the DM units.

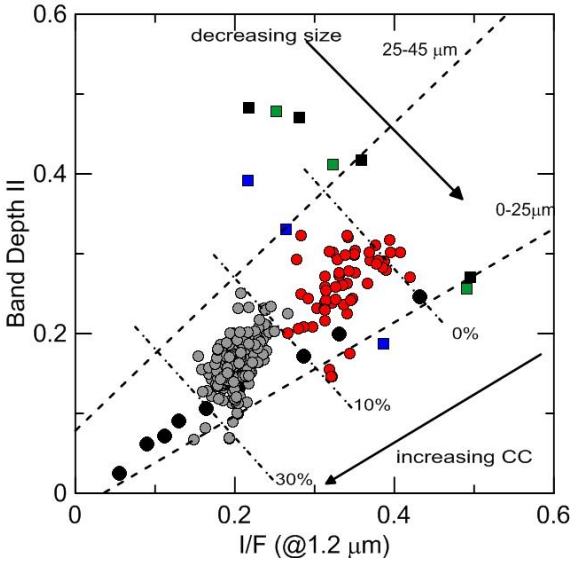

Fig.1 The black circles represent the mixture of a eucritic material (Millbillillie) and the Murchison meteorite at increasing abundance of the carbonaceous chondrite contaminant and with grain size (0-25 μm) [7]. The three eucrites are Juvinas (black square), Y-74450 (blue square), ALH78132 (green square) in the grain sizes interval (0-25, 25-45, 45-75μm). The BM cluster (red circles) is located in the eucrite region and is placed together with the DM cluster (grey circles). The dashed lines are the 0-25 and the 25-45 μm boundaries. The dash-dotted lines are the 0%, the 10% and the 30% boundaries.

References:

[1] Jaumann R. et al. (2013) *Icarus, Under Review*. [2] Palomba E. et al. (2013) *Icarus, Under Review*. [3] Zambon F. et al. (2013) *Icarus, Under Review*. [4] Reddy V. et al. (2012) *Icarus, 221*, 2, 544-559 [5] McCord T.B. et al. (2012) *Nature, 491*, 7422, 83-86. [6] De Sanctis M.C. et al. (2012) *ApJ Letters, 758*, 2, L36. [7] Cloutis, E.A. et al. (2013) *Icarus, 223*, 850-877. [8] De Sanctis M.C. et al. (2012) *Science, 336*, 6082, 697. [9] Marchi S. et al. (2012) *Science, 336*, 690.

VESTA'S ELEMENTAL COMPOSITION. T.H. Prettyman,[1] A.W. Beck,[2] W.C. Feldman,[1] D.J. Lawrence,[3] T.J. McCoy,[2] H.Y. McSween,[4] D.W. Mittlefehldt,[5] P.N. Peplowski,[3] C.A. Raymond,[6] R.C. Reedy,[1] C.T. Russell,[7] T.N. Titus,[8] M.J. Toplis,[9] N. Yamashita,[1] [1]Planetary Science Institute (1700 East Fort Lowell, Suite 106, Tucson, AZ 85719-2395, prettyman@psi.edu), [2]Smithsonian Institution, [3]Johns Hopkins University Applied Physics Laboratory, [4]University of Tennessee, [5]NASA Johnson Space Center, [6]Jet Propulsion Laboratory, Caltech, Pasadena, CA, [7]University of California, Los Angeles, [8]USGS Astrogeology Science Center, [9]University of Toulouse.

Introduction: Many lines of evidence (e.g. common geochemistry, chronology, O-isotope trends, and the presence of different HED rock types in polymict breccias) indicate that the howardite, eucrite, and diogenite (HED) meteorites originated from a single parent body.[1] Meteorite studies show that this protoplanet underwent igneous differentiation to form a metallic core, an ultramafic mantle, and a basaltic crust.[1] A spectroscopic match between the HEDs and 4 Vesta [2] along with a plausible mechanism for their transfer to Earth, perhaps as chips off V-type asteroids ejected from Vesta's southern impact basin, supports the consensus view that many of these achondritic meteorites are samples of Vesta's crust and upper mantle.[3]

The HED-Vesta connection was put to the test by the NASA Dawn mission, which spent a year in close proximity to Vesta.[4] Measurements by Dawn's three instruments, redundant Framing Cameras (FC), a Visible-InfraRed (VIR) spectrometer, and a Gamma Ray and Neutron Detector (GRaND), along with radio science have strengthened the link. Gravity measurements by Dawn are consistent with a differentiated, silicate body, with a dense Fe-rich core.[4] The range of pyroxene compositions determined by VIR overlaps that of the howardites.[5] Elemental abundances determined by nuclear spectroscopy are also consistent with HED-compositions.[6] Observations by GRaND provided a new view of Vesta inaccessable by telescopic observations. Here, we summarize the results of Dawn's geochemical investigation of Vesta and their implications.

A GRaND View of Vesta. Dawn's nuclear spectrometer (GRaND) was originally intended to be a "carbon-copy" of the Lunar Prospector Gamma-Ray Spectrometer (LP-GRS); however, the placement of the instrument on the deck of the spacecraft necessitated some design changes.[7] Like LP-GRS, GRaND contains a large-volume bismuth-germanate (BGO) scintillator, which serves as the primary gamma ray detector; however, unlike LP-GRS, GRaND's boron-loaded plastic (BLP) anti-coincidence shield and neutron spectrometer is segmented to enable contributions from Vesta (and Ceres) to be separated from spacecraft background. In addition, Li-loaded glass scintillators and Gd metal were strategically-added to the faces of the downward- and upward-facing BLP segments to enable separation of thermal and epithermal neutron components. Finally, an array of room-temperature semiconductors (CdZnTe), with better gamma-ray energy-resolution than BGO, was flown as a demonstration technology. The selected arrangement of sensors enables gamma ray spectroscopy up to ~10 MeV, a range that includes signatures for major elements such as Fe, Si, Mg, and O and radioelements K, Th, and U. GRaND's neutron measurements are sensitive to moderation by H, neutron absorption, and the average atomic mass of Vesta's regolith.

Close proximity and long integration times are required for nuclear spectroscopy. Thus, Dawn spent ~5 months in a low altitude circular, polar mapping orbit (about 1.79 body radii from center), which enabled full global mapping of selected elemental signatures. Despite similarities in spectrometer design, the sensitivity of these measurements was lower than that of Lunar Prospector, which flew much closer to the Moon (1.02 body radii from center). For Vesta, the intrinsic spatial resolution of map products was on the order of 300 km, somewhat smaller in scale than the Rheasilvia impact basin. The measurements are sensitive to regolith composition to depths of several decimeters.

The global regolith. The Fe/O and Fe/Si mass ratios for Vesta's global regolith, determined by gamma ray spectroscopy (BGO), are consistent with HED compositions (howardite).[6] The error ellipses exclude most other achondrite compositions, all chondrites and stony-iron meteorites. These observations indicate that Vesta's howarditic regolith does not contain significant exogenic Fe-Ni metal, beyond that observed in howardite, which implies that Vesta is not the source of the mesosiderites. The detection limit for the radioelement K (<1 mg/g),[6] abundant in glass spherules found in some howardites,[8] is consistent with the low concentrations found in HEDs,[6] ruling out evolved, K-rich lithologies as a major crustal component.

Exogenic hydrogen. Vesta's regolith contained unexpectedly high concentrations of hydrogen, as determined by measurements of epithermal neutrons [6] and confirmed by an analysis of fast neutron counting data.[9] The range of hydrogen on Vesta is about 400 μg/g, with the highest concentrations found in Vesta's dark hemisphere near the equator.[6] In these locations, water ice is not stable within the depths sensed

by GRaND. Furthermore, the global maximum is much higher than for lunar soils, which contain solar-wind hydrogen (typically <100 μg/g H).[6] Comparative analyses of Ne isotope ratios in lunar samples and regolithic howardites show that hydrogen content of Vesta's regolith that is derived from the solar wind must be much smaller than that of the Moon.[6] Although Vesta's magmas incorporated some water,[10] the source of surficial H seen by GRaND is not likely endogenic as Vesta formed from volatile-poor materials.[6] Rather, the observed anticorrelation of H with albedo points to the infall of exogenic carbonaceous chondrite material as the probable source.[6]

This hypothesis is supported by additional observations. The distribution of H is correlated with the 2.8 μm absorption band areas mapped by VIR, which is sensitive to OH content.[11] Carbonaceous chondrites contain hydrated phyllosilicates, which could serve as a stable reservoir of hydrogen. Some howardites contain clasts of carbonaceous chondrite, which have not undergone significant dewatering by impacts. C-type asteroids, some of which are located nearby, likely contributed hydrogen-rich material to Vesta. Finally, Vesta is the only asteroid for which evidence of surface alteration by volatiles has been found.[12] Pitted terrain found in the floors of young impact craters such as Marcia may have formed in high-velocity impacts that released volatiles from a regolith containing exogenic, hydrated minerals.[12, 13]

Elemental variegation. Vesta has long been known as a "colorful" asteroid,[14,15] and GRaND's measurements reveal broad, spatial patterns that track with those seen by optical spectroscopy. A suite of elemental maps was recently published [6, 9, 16-18] and is now available from the NASA Planetary Data System Small Bodies Node. The archive includes maps of H, Fe, the effective thermal neutron macroscopic absorption cross section (Σ_{eff}), contributions of fast neutrons to average atomic mass (<A>), and the high-energy gamma ray (HEGR) continuum. The latter three quantities are weighted averages of elemental abundances and are sensitive to different aspects of Vesta's composition. For example, Σ_{eff} is sensitive to Fe, which is primarily found in pyroxene, as well as Ca and Al, which are components of plagioclase.[18] Together, Fe and Σ_{eff} constrain the proportion of pyroxene and plagioclase in Vesta's surface.

The maps can be interpreted in terms of howardite petrology (e.g. see Fig 1). The Rheasilvia basin is diogenite-rich; whereas, the older terrane within Vesta's dark hemisphere is eucrite-rich. A lobe of diogenite-rich material extending northward from the Rheasilvia basin in the eastern hemisphere may be part of the ejecta blanket, perhaps diagnostic of an oblique impact. A similar lobe is seen in compositional indices derived from FC and VIR data. The impact that formed Rheasilvia may have excavated portions of Vesta's harzburgitic mantle [19]; however, an elemental signature for olivine-rich lithologies within the basin is lacking.[18] A region of low-Fe and intermediate neutron absorption has been interpreted as a possible signature for cumulate eucrites [16]; however, the range of compositions sensed by GRaND is consistent with howardite. Vesta's pristine, ancient crust has been pulverized by impacts to produce a howarditic regolith.

References: [1] McSween, H.Y. et al. (2011) *Space Sci. Rev.* 163, 141-174. [2] McCord, T.B., J.B. Adams, T.V. Johnson (1970) *Science*, 168, 1445-1447. [3] Binzel, R.P., S. Xu (1993) *Science* 260, 186-191. [4] Russell, C.T. et al. (2012) *Science* 336, 684-686. [5] De Sanctis, M.C. et al. (2012) *Science* 336, 697-700. [6] Prettyman T.H. et al. (2012) *Science* 338, 242-246. [7] Prettyman T.H. et al. (2011) *Space Sci. Rev.* 163, 371-459. [8] Barrat et al. (2009) *Meteorit. Planet. Sci.* 44:359-374. [9] Lawrence et al. (2013) *Meteorit. Planet. Sci.* in press. [10] Sarafian, A.R., M.F. Roden, A.E. Pati (2013) *Meteorit. Planet. Sci.* doi: 10.1111/maps.12124. [11] De Sanctis M.C. et al. (2012) *Ap. J. Lett. 758*, L36. [12] Denevi et al. (2012) *Science* 338, 246-249. [13] Boyce et al. (2013) *Icarus* 221, 262–275. [14] Bobrovnikoff, N.T. (1929) *Lick Obs. Bull.* 14, 18. [15] Reddy, V. et al. (2012) *Science* 336, 700-704. [16] Yamashita, N. et al. (2013) *Meteorit. Planet. Sci.* doi:10.1111/maps.12139 [17] Peplowski et al. (2013) *Meteorit. Planet. Sci.* in press. [18] Prettyman et al. (2013) *Meteorit. Planet. Sci.* in press. [19] McSween et al. (2013) *J. Geophys. Res.* 118, 335-346.

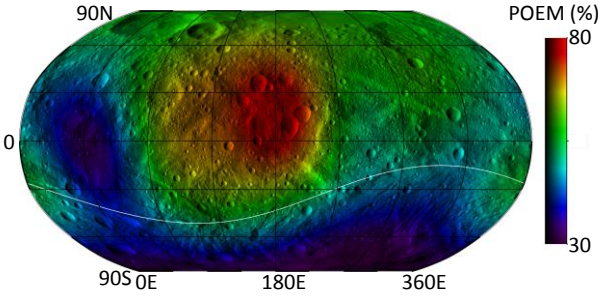

Fig. 1. The percentage of eucritic material (POEM) in Vesta's regolith determined by neutron spectroscopy [18] (color) is superimposed on shaded relief. Red regions are eucrite-rich; whereas, blue regions are rich in diogenite. The boundary of the Rheasilvia impact basin is shown (white line). Claudia longitudes [4] are shown.

Global Shape of (4) Vesta from Dawn FC stereo images. F. Preusker[1], F. Scholten[1], K.-D. Matz[1], T. Roatsch[1], R. Jaumann[1], C. A. Raymond[2], and C. T. Russell[3], [1]German Aerospace Center, Institute of Planetary Research, D-12489 Berlin, Germany (Frank.Preusker@dlr.de), [2]Jet Propulsion Laboratory, California Institute of Technology, Pasadena, CA 91109-8099, USA, [3]UCLA, Institute of Geophysics, Los Angeles, CA 90095-1567, USA.

Introduction: NASA's Dawn mission has observed the inner main belt asteroid (4) Vesta from July 2011 until September 2012 [1,6]. One of the prime science goals was the determination of the global shape of (4) Vesta represented by a digital terrain model (DTM). The DTM is particularly important, because it is essential for derivation of physical properties of (4) Vesta as well as for precise ortho-image registration, mosaicking, and map generation of monochrome/color framing camera images. In addition a DTM is needed for quantitative geomorphologic analysis and precise photometric analysis from detailed local surface inclination. For this purpose the entire illuminated surface was imaged stereoscopically using the Dawn Framing Camera (Dawn FC) [2].

Data: Starting from a Survey orbit at an altitude of about 2,700 km in August 2011, the Dawn FC acquired 1,179 clear filter images with an image scale of about 255 m/pixel. By end of September 2011, Dawn started its primary stereo image campaign from a high resolution mapping orbit (HAMO) at an altitude of about 700 km and completed the campaign after an extended stay in July 2012. During HAMO, the Dawn FC acquired about 5,550 clear filter images with an image scale of about 65 m/pixel and has imaged at least 95 % of Vesta's surface.

In both mapping phases the surface was imaged several times under similar illumination conditions (Sun elevation and azimuth), but different viewing conditions (by tilting the spacecraft). This allows to analyze the images stereoscopically and to construct stereo topographic maps as well as ortho-image mosaicks.

Methods: The stereo-photogrammetric processing for (4) Vesta is based on a software suite that has been developed within the last decade. It has been applied successfully to several planetary image data sets [3-6] and covers the entire workflow from photogrammetric block adjustment to DTM and map generation.

Differences in illumination	<10°
Stereo angle	15-55°
Incidence angle	0-85°
Emission angle	0-55°
Phase angle	5-160°

Table 1. Requirements for stereo processing.

Results: We constrained all HAMO clear filter images with our stereo requirements (Table 1) and achieved at least triple stereo image coverage for the entire illuminated surface. In total, about 35,000 independent multi-stereo image combinations were used to determine selected image tie points by multi-image matching for the set-up of a 3D control network of about 83,000 surface points. The control point network defines the input for the photogrammetric least squares adjustment where corrections for the nominal navigation data (pointing and position) are derived. The three-dimensional (3D) point accuracy of the resulting ground points have been improved from ±55 m to ±8 m (0.15 pixel). We have also refined Vesta's spin axis orientation, formerly determined from Earth-based observations [7, 8], to: right ascension = 309.0319° ± 0.005°, declination = 42.2229° ± 0.005°. Finally, 35,000 individual multi-image matching processes at full image resolution were carried out to yield ~2.5 billion object points. The achieved mean forward ray intersection accuracy of the ground points is ±8 m, which is comparable to absolute 3D point accuracy [9]. Finally, we have generated a DTM with a lateral spacing of 48 pixel/degree (92.7 m/pixel) and a vertical accuracy of about 6 m. The DTM covers approximately 95% of Vesta's surface.

Based on the entire DTM (Fig. 1), we determined a best-fit ellipsoid (285.3/277.7/223.8 km) with its body long axis at 40.6°E w.r.t. the new reference system [1]. Compared to results from Earth-based observations [8], these values are smaller by about 4%. Finally, ortho rectified Survey images and image mosaics have been derived based upon the adjusted orientations and the Survey DTM as the topographic reference [10].

References:

[1] Russell C.T. et al., (2012), *Science, 336*, pp. 684-686. [2] Sierks H. et al, (2011), *Space Science Review, 163*, pp. 263-327. [3] Gwinner K. et al., (2010), *Earth Planet. Science Letters, 294*, Issues 3-4, pp. 506-519. [4] Preusker F. et al., (2011), *Planetary Space Science, 59*, pp. 1910–1917. [5] Scholten F. et al., (2012), *JGR, 117*. [6] Jaumann R. et al., (2012), *Science, 336*, pp. 687-690. [7] Li J.-Y. et al., (2010), *Icarus, 211*, pp. 528-53. [8] Thomas P.C. et al., (1997), *Icarus, 128*,. 88. [9] Raymond C.A. et al., (2011) *Space Sci. Rev., 163*, 487-510. [10] Roatsch T. et al., (2013), *this session*

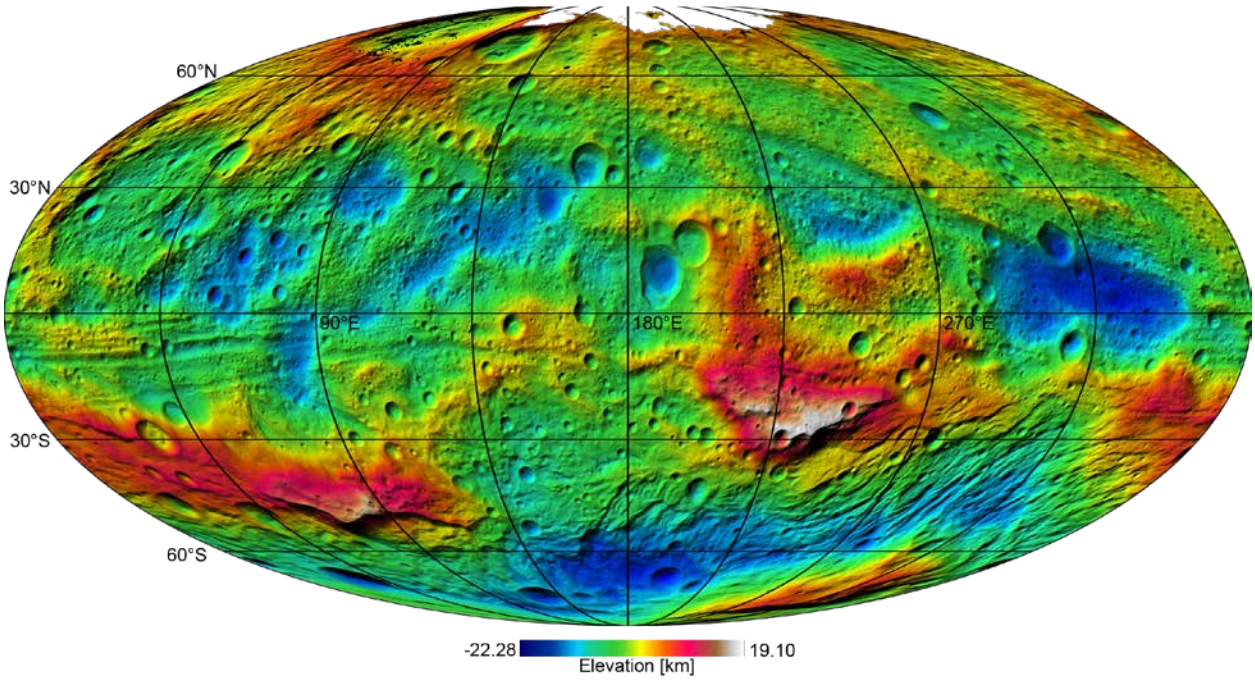

Global HAMO DTM of (4) Vesta with a lateral spacing of about 93 m (hill-shaded color-coded heights) in Mollweide Projection (equal-area). Heights refer to a biaxial ellipsoid (285x285x229 km).

CONSTRAINTS ON VESTA'S INTERIOR EVOLUTION FROM DAWN GEOPHYSICAL DATA. C. A. Raymond[1], R. S. Park[1], S. W. Asmar[1], A. S. Konopliv[1], M. C. De Sanctis[2], R. Jaumann[3], H. Y. McSween[4], C. T. Russell[5], D. E. Smith[6], M. Toplis[7], M. T. Zuber[6], [1]Jet Propulsion Laboratory, California Institute of Technology, Pasadena, CA, USA (carol.a.raymond@jpl.nasa.gov), [2]INAF, Istituto di Astrofisica e Planetologia Spaziale, Area di Ricerca di Tor Vergata, Roma, Italy, [3]DLR, Inst. of Planetary Research, Berlin, Germany, [4]Dep. of Earth and Planetary Sciences, University of Tennessee, Knoxville, TN, USA; [5]UCLA, Los Angeles, CA, USA, [6]MIT, Cambridge, MA, USA, [7]Uni. de Toulouse, France.

Introduction: Dawn's year-long stay at Vesta allowed comprehensive mapping of the shape, topography, geology, mineralogy, elemental abundances, and gravity field using its three instruments and high-precision spacecraft navigation. A gravity field accurate to degree and order ~20 [1] was obtained from high-accuracy data in the Low Altitude Mapping Orbit (LAMO). Multi-angle imaging in the Survey and High Altitude Mapping Orbits (HAMO-1 and HAMO-2) has provided adequate stereo coverage to develop a shape model accurate to ~10 m at 100 m horizontal spatial resolution [2]. The shape and gravity of Vesta can be used to infer the interior density structure and investigate the nature of the crust, informing models for Vesta's formation and evolution. The low degree gravity constrains the radial density structure, while the higher degree terms reflect variations in the structure of the crust and mantle. Significant Bouguer anomalies are found within the vestan crust and mantle that can be interpreted as crustal thickness or density variations, and likely reflect both sources. The Bouguer anomalies are associated with structural features such has the Vestalia Terra highland and the deep Saturnalia Fossae, as well as lithological provinces, such as the extensive dark material deposits at the Veneneia impact basin rim, and the diogenitic central mound of the Rheasilvia impact basin.

Vesta's Core, Mantle and Crust: The gravity field of Vesta at degree and order 20, excluding degree 1 and J_2, ranges from -1000 to 2000 mgals, and is highly correlated to the topography [1]. The J_2 term is consistent with Vesta being a solid body out of hydrostatic equilibrium; it also indicates a central mass concentration. Applying constraints from meteoritic studies, Vesta's core size has been estimated using a mass balance approach that matches the observed J_2. We find a core of average size 110-km assuming an average density of 7400 kg/m3, consistent with iron meteorite densities [3]. Such an approach also yields the bulk silicate density, which averages around 3100 kg/m3, and indicates porosity in the crust and mantle of ~10%. Combinations of mantle and crust densities tand layer dimensions that satisfy the bulk silicate density and J_2, are used to derive the Bouguer gravity field by subtracting the predicted gravity from the observed. Applying a Bouguer correction results in an anomaly field ranging over hundreds of mgal, roughly 10% of the gravity field (Fig. 1). The three-layer model used to calculate the Bouguer field uses the core radius of 110 km and a crustal layer that averages, with the top surface following the shape model and bottom defined by the ellipsoidal mantle layer. The crustal layer is assumed to have zero thickness in the deepest point of the Rheasilvia basin, and averages ~19 km in thickness, consistent with a chondritic bulk composition [4].

The Bouguer anomalies reflect the modification of the vestan crust and mantle by impacts that have extensively fractured and pulverized it while also exposing deep-seated material and mixing it with the original crust; they also reflect the addition of low-density exogenic material to Vesta's surface. However, impacts alone can't account for the all of the density (and/or crustal thickness) variations implied by the Bouguer gravity field. The presence of significant density anomalies in concert with broad compositional and geologic variations is consistent with heterogeneity in the original crust and mantle of Vesta.

Considerable variation is seen in the crust/mantle density contrast that minimizes the major Bouguer anomalies in different regions of Vesta, indicating variations from the assumed layer thicknesses and/or variations in the density. Given the intense pummeling of Vesta by impacts, it is likely that the original crustal layering has been largely overprinted by impact gardening. Density variations include variations in porosity as well as compositional variations that may be related to the original crustal architecture. Several features are examined to probe the interior structure.

Vestalia Terra: A very strong positive Bouguer anomaly is seen over the southern postion of Vestalia Terra (Fig 1: -150 to -120 E; 15-30 S). Vestalia Terra (VT) is a large topographic rise that contains the highest topography on Vesta. It is recognized that VT is an ancient terrain, pre-dating the Rheasilvia and older Veneneia impacts as these basins carve the edges of VT [5]. The Bouguer anomaly of southern VT represents a significant mass concentration relative to the average bulk silicate density of Vesta; the estimated crustal density for southern Vestalia Terra is ~3200

kg/m^3 [6], which is an average of the crust and its ejecta blanket. The gravity data indicate that the Rheasilvia ejecta are resting on a dense topographic rise that likely is composed of ultramafic mantle material. The density of the underlying rise also appears higher than the mantle elsewhere in the southern hemisphere. Thus, the density structure of Vestalia Terra may be indicative of a more primordial state of the vestan interior. It is difficult to probe the nature of the bedrock beneath the mantling RS ejecta, but several small impact craters indicate at least localized presence of diogenitic material [5]. The origin of VT could be the result of magmatic processes during Vesta's early evolution, or may be explained by variable impact gardening of the vestan crust and mantle.

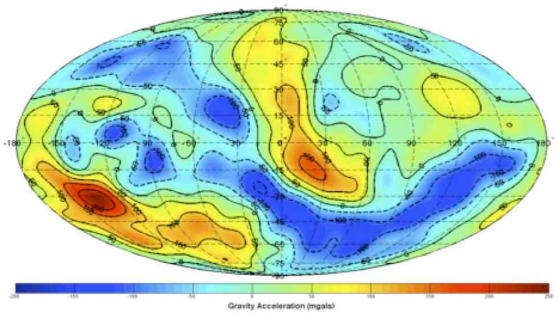

Figure 1. Color contour Bouguer anomaly map in mgals calculated using crustal density of 2800 kg/m^3 and mantle density of 3300 kg/m^3 [1].

Rheasilvia Basin: The higher density implied for the RS central mound indicates thin crust and uplifted mantle at the central mound, in agreement with the presence of diogenitic material identified in VIR data [7]. The dense material extends beyond the central topographic mound, however, and may indicate crustal inhomogeneity that pre-dated the formation of RS.

Eastern Equatorial Troughs: The are to the north of the prominent RS basin eastern rim is an area of well-defined troughs (0-60E; 0-30S). There is a strong positive Bouguer anomaly associated with this area, which is part of a broad swath of positive anomalies that extends northward to the area where olivine was identified [8]. The positive Bouguer gravity generally follows the topography, but otherwise there is nothing that is unique about this region. The strong anomaly near the equator may indicate a buried dense body.

Features such as southern Vestalia Terra and similar high-density features suggest intracrustal plutons consistent with evidence from the trace element geochemistry of HED meteorites, and genetic models that include multiple magma chambers.

References: [1] Konopliv, A. S. et al. (2013), *Icarus in press*. [2] Preusker F. et al. (2012), *AGU Fall Mtg.* [3] Russell, C. T. et al. (2012), *Science 336, 697.* [4] McSween, H. Y. et al., *Space Science Reviews, 163*. [5] Buczkowski, D. L., et al., (2012), *LPS XLIV*. [6] Park, R.S. et al. (2014), *Icarus, in press*. [7] De Sanctis, M. C. et al. (2012). *Science 336, 697.* [8] De Sanctis, M. C. et al. (2013). *Nature.*

Acknowledgements: A portion of this research was carried out at the Jet Propulsion Laboratory, California Institute of Technology, under contract to the National Aeronautics and Space Administration.

Vesta Surface Colors and Mineralogy. V. Reddy[1], L. Le Corre[1], A. Nathues[2], J.-Y. Li[1], T. B. McCord[3], M. J. Gaffey[4], C. T. Russell[5] and C. A. Raymond[6], [1]Planetary Science Institute, 1700 E. Fort Lowell Road, Tucson, Arizona 85742, reddy@psi.edu; [2]Max-Planck Institute for Solar System Research, Katlenburg-Lindau, Germany; [3]Bear Fight Institute, Washington; [4]University of North Dakota, North Dakota; [5]University of California Los Angeles, California; Jet Propulsion Laboratory, [6]California Institute of Technology, California.

Introduction: Surface colors and mineralogy of Vesta are unique among asteroids visited so far by spacecraft. Dawn Framing Camera observed the asteroids in seven color (0.4-1.0 microns) and a clear filter during its year-long orbital mission mapping the surface at a resolution as high as 16 meters/pixel. These seven filters help identify different geologic units, constrain lithologies and understand Vesta's composition and surface heterogeneity.

Dawn FC images revealed a surface with the most diverse albedo variation of any asteroid observed so far. While ground based observations of Vesta had shown large hemispherical scale dichotomy, regional and local scale albedo variations were unexpected [1]. Unlike the Moon, where albedo and topography are intimately correlated with the mineralogy of lower albedo maria and higher albedo highlands, no such relationship was observed on Vesta [1].

Albedo: Li et al. (2013) studied the photometric properties of Vesta in the visible wavelengths using FC data, and found that its photometric properties show weak or no dependence on wavelengths, except for the albedo. At 0.554 microns, the global average geometric albedo of Vesta is 0.38±0.04; the Bond albedo is 0.20±0.02. The bolometric Bond albedo is 0.18±0.01. Vesta's phase function is similar to those of S-type asteroids. Vesta's surface shows a single-peaked albedo distribution with a full-width-half-max ~17% relative to the global average, much smaller than its full range of albedos (from ~0.55× to >2× global average) in localized bright and dark areas of a few tens of km in sizes, and is probably a consequence of significant regolith mixing on the global scale. Rheasilvia basin is ~10% brighter than the global average [2]. Vesta's phase reddening measured from Dawn FC is comparable or slightly stronger than that of Eros as measured by the Near Earth Asteroid Rendezvous mission, but weaker than previous measurements based on ground-based observations of Vesta and laboratory measurements of HED meteorites [2].

Color Units: Ground-based and HST observations of Vesta revealed several color and albedo units that were confirmed by the Dawn spacecraft [3]. The largest of these units include the hemispherical scale dichotomy which has been attributed to 'age-related darkening effect' [4]; "domination by iron-rich and relatively calcium-rich pyroxene" similar to basaltic flows like eucrites [5]; and impact craters/basins filled with dark material similar to lunar mare [6]. Dawn FC and GRaND observations of the dark Western hemisphere shows that it is composed of a mixture of exogenic carbonaceous chondrite material with HEDs [7,8] while the brighter Eastern hemisphere was primarily sculpted by impact processes.

Apart from hemispherical scale dichotomy in albedo and composition, several distinct color units have been identified on Vesta. These include: Dark, Bright, background gray and Orange material.

Dark Material. Dark material has lower albedo (~8%) than average Vesta surface and is found on the walls of impact craters, ejecta, and crater rims (Fig. 1). Color properties of dark material in small craters are similar to lower albedo Western hemisphere. Apart from lower albedo, pyroxene absorption bands in dark material are also weaker. Laboratory mixtures of HED meteorites and carbonaceous chondrites mimic the color properties of dark material on Vesta [7]. Independent observations by VIR spectrometer and GRaND instrument confirmed the exogenous origin on dark material on Vesta [8,9]. The distribution of dark material coincides with the concentration of OH [8]. Exogenous material in HEDs have been observed and quantified. A majority of these exogenous materials are in the form of dark hydrous clasts (primarily composed of CM2 and CR carbonaceous chondrite meteorites) in howardites [4]. These clasts typically comprise ≤5 vol.% but more recent Antarctic meteorite finds such as PRA 04401 have up to 60 vol.% dark carbonaceous clasts [7]. An hydration feature associated with dark material has been observed from ground-based telescope prior to arrival of Dawn on Vesta. Hasegawa et al. (2003) noting the presence of a 3-μm absorption suggested contamination from impacting carbonaceous chondrites as possible cause of this feature.

Bright Material: Bright material on Vesta is pristine with little or no contamination from exogenous carbonaceous material or impact melt/shocked material [10]. Composition of bright material is predominantly dictated by its location with more diogenitic material associated with bright material in the South Pole Rheasilvia basin and more howarditic material outside the basin and its associated ejecta [11].

Gray Material: Mixed bright and dark material is the predominant cause of the background gray material on Vesta [1]. Composition of gray material is dependent on the local abundances of eucrite and diogenite

components with more diogenitic material closer to the Rheasilvia basin.

Orange Material: While bright, dark and gray material were identified using clear filter images from the Framing Camera, additional color units were identified using color filter ratio images. One such color composite is the Clementine RGB color composite in which CR= R(0.75)/R(0.45), CG= R(0.75)/R(0.92), and CB= R(0.45)/R(0.75); where R(λ) is the reflectance in a filter centered at λ(μm) and CR, CG, CB are the red, green and blue channels respectively. Greener areas in this color ratio have deeper pyroxene absorption bands (typical of diogenites) and redder areas have steeper visible slopes relative to bluer areas. Two large impact craters (Oppia and Octavia) that showed prominent red/orange ejecta in Clementine color ratio. Le Corre et al. (2013) also noted several brighter orange patches around Oppia. The orange/red color of these craters and surrounding patches appears to come from a steeper visible slope (R(0.75)/R(0.45)) compared to surrounding areas.

Ground based observations of Vesta showed a distinct feature on Vesta, which was interpreted to be an olivine-rich unit [4]. This unit corresponds to the location of Oppia (Fig. 2) on Dawn FC Clementine color ratio maps [3]. HST observations of Vesta label this feature as #15 and noted distinct red slope in its color spectrum [12]. Based on this red slope, [12] suggested space weathering as a possible mechanism for explaining it. Detailed compositional analysis using all three instruments on Dawn by [13] suggests that the most probable analog for the orange material on Vesta is impact melt. Orange patches, which seem to be distributed around the South Pole, are thought to be impact melt splash from the formation of the Rheasilvia basin [13]. While the observations of Oppia from ground by [13] and HST by [12] are consistent with those from Dawn FC and VIR spectrometer, the interpretations (olivine vs. space weathering vs. impact melt) are different primarily due to the improved spatial context provided by spacecraft data.

References: [1] Reddy et al. 2012. *Science,* [2] Li et al. 2013. *Icarus,* [3] Reddy et al. 2013. *Icarus,* [4] Gaffey 1997. *Icarus,* [5] Binzel et al. 1997. *Icarus,* [6] Zellner et al. 2005 *Icarus* [7] Reddy et al. 2012. *Icarus,* [8] McCord et al. 2012. *Nature,* [9] Prettyman et al. 2012. *Science,* [10] Li et al., 2012. ACM abstract, [11] Zambon et al. 2014. *Icarus,* Submitted, [12] Li et al., 2010. *Icarus,* [13] Le Corre et al. 2013. *Icarus.*

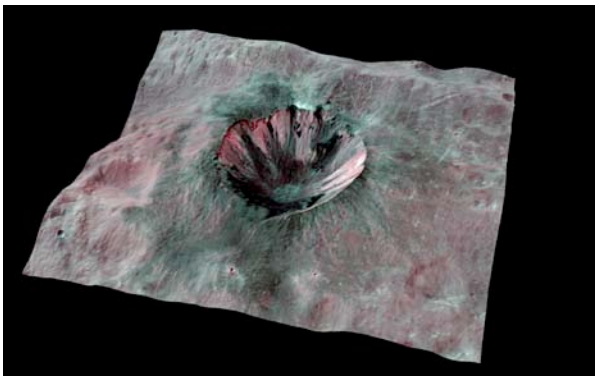

Figure 1. Dark material associated with impact crater Cornelia shown here overlaid on topography.

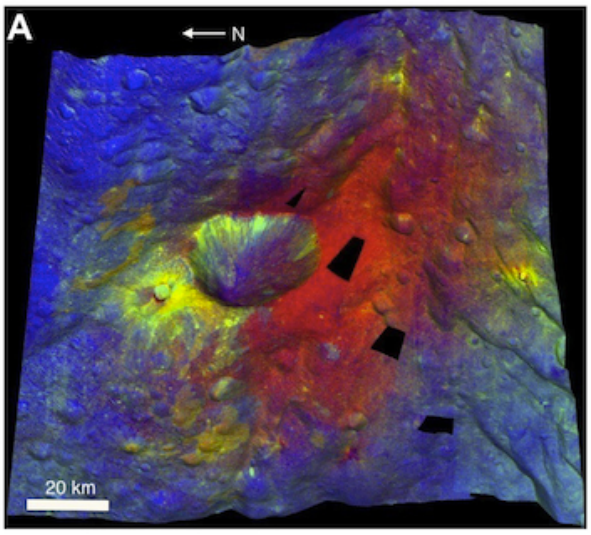

Figure 2. Orange material associated with impact crater Oppia shown in this Clementine color ratio image overlaid on topography.

PEAKS IN DAWN GAMMA-RAY SPECTRA AT AND NEAR VESTA. R. C. Reedy[1], T. H. Prettyman[1], and N. Yamashita[1], Planetary Science Institute, Northern Rio Grande Contingent, New Mexico, USA. <reedy@psi.edu>.

Summary: The peaks in gamma-ray spectra at various distances from Vesta are presented and summarized. Spectra from Vesta for low- and high-neutron leakage fluxes are also presented.

Introduction: The Gamma Ray and Neutron Detector (GRaND) instrument was on the Dawn spacecraft that orbited the asteroid 4 Vesta in 2011-2012 [1,2,3]. Some results from GRaND gamma-ray spectra have been reported [3,4].

The big advantage of gamma rays for planetary compositional studies is that it directly senses elements from the unique energies of the gamma rays. Planetary elemental mapping has previously been done for the Moon [5,6,7], Mars [8], Mercury [e.g., 9], and the asteroid Eros [10]. The observed gamma-ray spectra were studied after having determined the locations of the peaks in the observed gamma-ray spectra.

All planetary spectra (e.g., [5-10]) are calibrated using peaks measured during the mission, as laboratory calibrations are hard to apply to the very different conditions in space, especially the many effects of cosmic rays. The sources of the stronger gamma rays in planetary spectra were well known, including the major gamma rays from Fe, O, C, and Si. Often, gamma rays from material in or near the GRS produce strong peaks. For GRaND, those nearby elements include Al and, to a lesser degree, C and Si.

We present results for peak identifications using gamma-ray spectra measured by GRaND for 3 altitudes during the Vesta encounter. A spectrum during a solar-particle event during cruise to Vesta is included as it shows gamma rays from material within a few millimeters of space, the only parts of a spacecraft irradiated by the low-energy particles in solar-cosmic-ray events.

Spectra: The gamma rays from the surface of Vesta were split into those for regions with low and high densities of leakage neutrons (ND) and latitudes above 70N and below 70S. Spectra from the 3 main orbits about Vesta were included: survey (2750 km), high altitude mapping orbit (HAMO) at 680 km, and low altitude mapping orbit (LAMO) at 210 km. A spectrum during a solar cosmic ray (SCR) event during cruise was also used. These spectra are plotted in Fig. 1.

Fig. 2 shows the spectrum between 1000 and 3500 keV, the part of the spectrum with the most peaks. Fig. 3 shows the specrum for the higher enegies.

The decrease at the highest energies is a known effect of the electronics and how the data was processed.

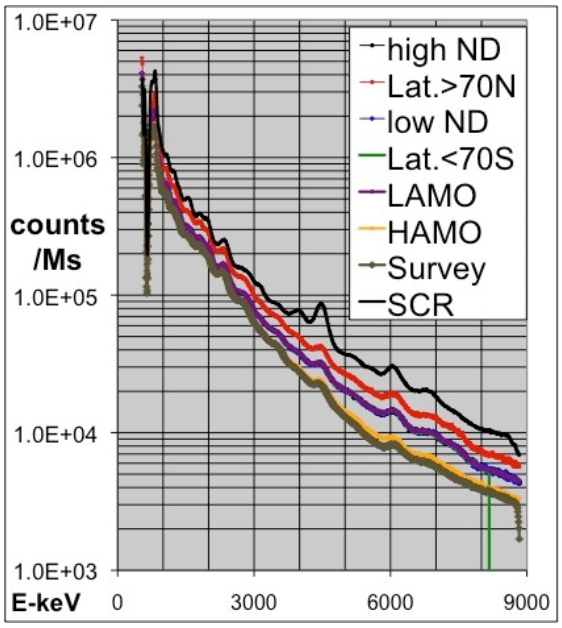

Fig. 1. The gamma-ray spectra from GRaND on the Dawn spacecraft near the asteroid Vesta for several compostional regions on Vesta and different altitude above Vesta, including one during a solar cosmic ray (SCR) event in cruise to Vesta. Some spectra plot under the LAMO spectrum (Ms is megaseconds, ND is neutron density.)

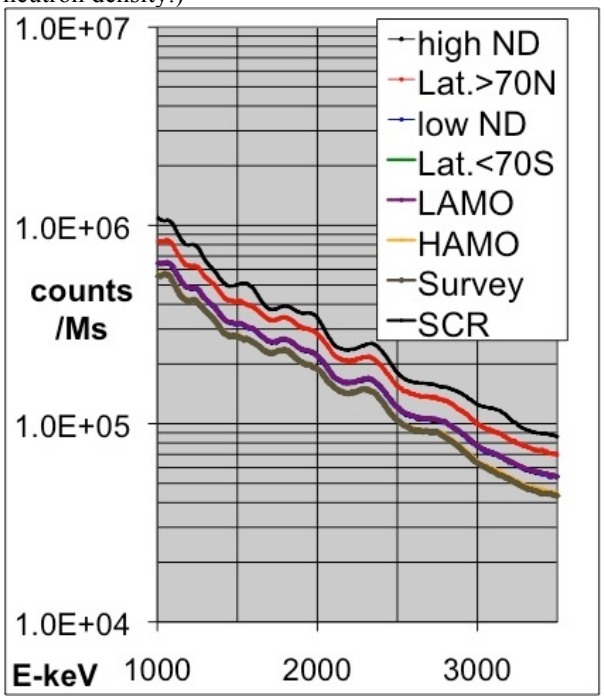

Fig. 2. The low-energy part of the GRaND gamma-ray spectra shown in Fig. 1.

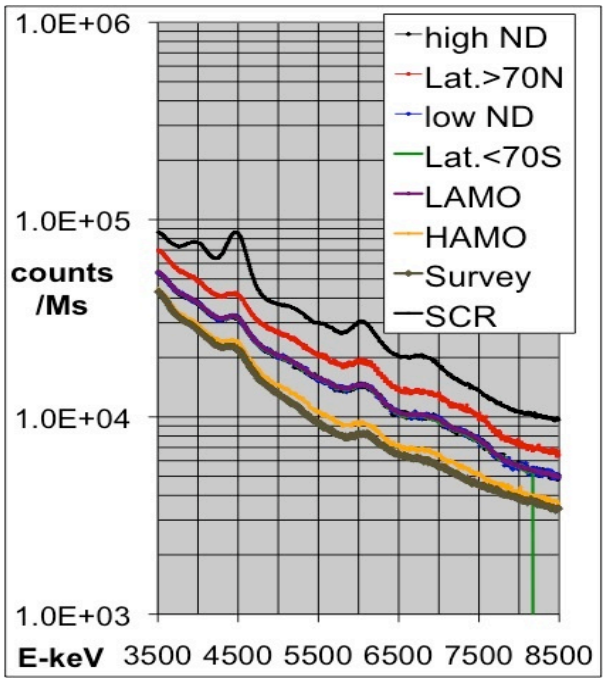

Fig. 3. The high-energy part of the GRaND gamma-ray spectra shown in Fig. 1.

Ch	E-cal	E-ref	ΔE	Source	Alt. source
87	1088	1014	-74	^{27}Al*	
124	1409	1369	-40	^{24}Mg*	^{24}Na
151	1643	1634	-9	^{20}Ne*	
175	1851	1809	-42	^{26}Mg*	^{28}Si*-1779
218	2223	2211	12	^{27}Al*	^{1}H(n,γ)-2111
269	2665	2685	20	^{208}Pb*	^{24}Mg*-2754
363	3479	3539	60	Si(n,γ)	
471	4414	4438	24	^{12}C*	^{16}O
563	5211	5240	29	^{15}O*	^{15}N*-5269
669	6129	6129	0	^{16}O*	
769	6995	7015	20	^{16}O*	
850	7696	7638	-58	Fe(n,γ)	

Table 1. The strong gamma-ray peaks in GRaND spectra. The calculated energy is that in the spectra. The reference energies are for the most like source or sources. Energies are in keV. A * indicates the gamma ray is from an excited level in that nucleus, which often can be made by several reactions.

All but the SCR spectra are similar in shape. Those for low and high neutron densities (ND) and Lat.<70S are very close and can't be distinguished in Figs. 1-3. The Lat.>70N region has spectra collected when Dawn was closer to the surface.

Peaks in GRaND Gamma-Ray Spectra: The most-likely and most-intense sources for the stronger peaks in the spectra in Fig. 1 have been identified and listed in Table 1. The gain (slope) and zero (offset) was calculated using the 2 strong gamma rays at 6129 and 2.21 MeV. The differences of the calculated and reference energies are plotted in Fig. 4. The trend is curved, a feature of many planetary gamma-ray spectra. The differences in energies are of the same magnitude as that from the laboratory calibration of GRaND [1] and probably reflect the uncertainties of peak positions for bismuth germanate (BGO) spectra.

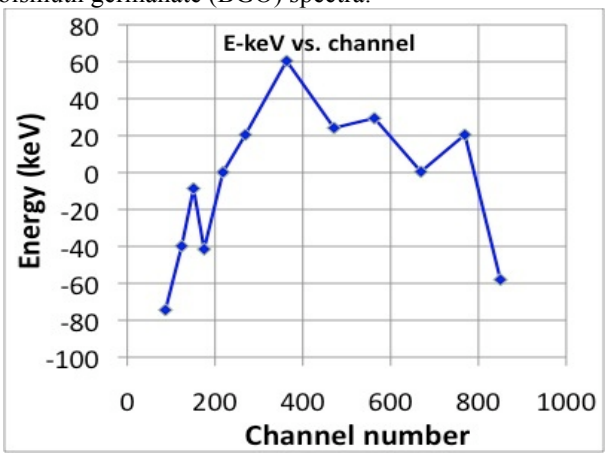

Fig. 4. Differences in calculated and expected energies versus spectral channel.

Many Al and C peaks appear in the spectrum during a solar-cosmic-ray (SCR) particle event, probably because those elements were near the very surfaces of GRaND or the spacecraft.

Summary: The major peaks in GRaND gamma-ray spectra have been identified. The trend for the differences of the actual and spectral energies is not linear but has a good systematic trend with delta energies similar to those in [1]. The energies of peaks in features are well known and provide confidence in locating peaks for other gamma rays of interest, such as from Si, Mg, and ^{40}K.

Acknowledgments: NASA supported this work through the Dawn at Vesta Participating Scientist program (RCR) and the Dawn program (THP and NY).

References: [1] Prettyman T.H. et al. (2011) *Space Sci. Rev.*, 163, 371. [2] Prettyman T.H. et al. (2012b) *Science*, *338*, 242. [3] Yamashita, N. et al. *Meteoritics & Planet. Sci.*, in press. [4] Peplowski P.N. et al. (2013). *Meteoritics & Planet. Sci.*, in press. [5] Bielefeld M. et al. (1976) *Proc. Lunar Sci,. Conf. 7*, p. 2661. [6] Prettyman T.H. et al. (2006) *J. Geophys. Res.* 111, E12007. [7] Yamashita N. et al. (2012) *Lunar Planet. Sci.* 43, #1283. [8] Evans L. G. et al. (2006) *J. Geophys. Res.* 111, E03S04. [9] Evans L. G. et al. (2012) *J. Geophys. Res.* 117, 0L07E. [10] Evans L. G. et al. (2001) *Meteoritics & Planet. Sci.*, 36, 1639.

EXOGENIC OH ON VESTA: IMPLICATIONS FROM AND FOR OTHER ASTEROIDS. A S. Rivkin, [1]JHU/APL (andy.rivkin@jhuapl.edu).

Introduction: The HED (howardite, eucrite, diogenite) meteorites, generally thought to be from Vesta, are by and large free of hydrated phases. This gave rise to an expectation that Vesta itself would currently be free of hydrated minerals (regardless of what may have occurred earlier in its history).

Initial observations of Vesta in the 3-μm spectral region, where diagnostic absorptions due to OH and H_2O are found, were consistent with an anhydrous surface [1], but later observations at higher spectral resolution showed a shallow absorption that was interpreted as due to infall of carbonaceous material [2]. While confirmation of the 3-μm band was stymied by a lack of suitable laboratory spectra for comparison, the infall idea was supported by the albedo distribution on Vesta's surface [3].

Dawn's arrival at Vesta firmly established the presence of hydrated minerals on Vesta via observations of a band at 2.8 μm that is obscured by Earth's atmosphere as well as hydrogen measurements by the GRaND neutron spectrometer [4,5]. This hydrogen/OH is associated with low albedo areas, and the interpretation that surviving remnants of carbonaceous impactors are responsible is still the leading theory [6].

C chondrites and C asteroids: Laboratory spectra of the CM, CI, and CR subgroups of carbonaceous chondrites (CC) show absorptions due to phyllosilicates, with band minima in the 2.7-2.8 μm range depending on mineralogy [7-8]. The C-complex asteroids are seen to have a variety of spectra in the 3-μm region, including a group that looks like the hydrated CC at the wavelengths where the Earth's atmosphere allows good data to be collected [9,10].

While data in the 3-μm region has only been obtained for roughly 100 C-complex asteroids, visible and near-IR (0.5-2.5 μm) data is available for many more, and the WISE mission has obtained high-quality albedos for thousands of asteroids. All told, evidence suggests that the C complex objects dominate the asteroid belt, accounting for half of the objects even in the inner belt where they are least common [11,12]. Statistical arguments based on a shallow absorption near 0.7 μm suggests that the CM group may constitute upward of 30% of the C-complex population [13].

All told, hydrated carbonaceous material would be very common impactors, and their low-albedo, neutral spectra would be very effective in providing a 3-μm absorption while leaving shorter wavelengths more or less unaffected.

What this might help explain: There is no obvious reason to think that Vesta alone would feel the effects of carbonaceous impactors. Surfaces throughout the asteroid belt will potentially accumulate the kind of carbonaceous material that is thought to be present on Vesta. Accordingly, the prospect of impactor contamination causing a 3-μm band on asteroids is prompting a reevaluation of our interpretations of other asteroid spectra.

Some M-class asteroids, once generally considered to be parent bodies for iron meteorites, were reinterpreted due to the presence of a 3-μm band. Given the association of OH and water with aqueous alteration, and the incompatibility of iron meteorites with aqueous alteration, it was thought that the presence of a 3-μm band precluded an object from being analogous to iron meteorites [14,15].

In-depth studies of M asteroids have established that many have radar albedos consistent with rocky or partially-rocky rather than metallic natures. However, an accumulation of carbonaceous chondrite debris could plausibly explain those objects for which 3-μm bands and high radar albedos coexist [16].

In addition to the M asteroids, carbonaceous impactors may be responsible, or partially responsible, for the spectra of two large S-class near-Earth objects (NEOs), 433 Eros and 1036 Ganymed. These were not expected to have hydrated minerals, but have 3-μm bands a few percent in depth [17]. In addition, Eros was observed by NEAR Shoemaker to have accumulations of darker material on its surface, though it was interpreted as vapor-deposited nanophase iron coatings on native material, created through micrometeorite impacts [18].

The Eros/Ganymed observations also present an additional challenge. While GRaND measurements at Vesta can be used to argue that Vesta's hydrogen isn't delivered by the solar wind, similar measurements are absent for typical asteroids. Therefore, additional care must be taken to correctly interpret 3-μm absorptions as primarily solar wind-created (like those on the Moon are thought to be) or impactor-related (like those on Vesta are thought to be).

What this doesn't explain and makes more complicated: In addition to Vesta, one other asteroid has been recently visited by a spacecraft with spectral capability in the 3-μm region: 21 Lutetia by Rosetta. Unlike the objects discussed above, the data returned from Lutetia is difficult to reconcile with the idea that asteroids are commonly accreting carbonaceous debris.

Contrary to the Dawn findings at Vesta, the Rosetta spectra of Lutetia are reported to have no absorption in the 3-µm region within 2% [19], and thus no OH or water is interpreted as present.

Given that Lutetia orbits in the same part of the belt as Vesta, we would expect its impactor population to be largely the same as Vesta's. Furthermore, the retention of impactor material would seem to be more a function of impact speed and whether it survives the impact than a matter of escape speed and keeping ejecta. Making sense of both Lutetia and Vesta is still work to be done.

It also seems likely that impactor contamination could be a factor at Ceres. Ceres resides in a more C-asteroid rich part of the asteroid belt, and would presumably have as much material survive as does Vesta.

However, unlike Vesta, which has a native composition and spectral properties that provided a strong contrast with carbonaceous impactor material, it is less obvious how best to account for this material at Ceres. Ceres has a distinct reflectance spectrum in the 3-µm region compared to what is seen in the CC meteorites, and while on large scales it is unlikely that an impactor-delivered component will cause much confusion, on small scales and in particular regions ambiguity is possible between a native, unusual area and impactor contamination. Calibration from Vesta may be necessary to allow accurate estimates of any exogenic contribution to Ceres' surface.

It is likely, at least, that Bennu is too young to have incorporated much endogenic material, and so the OSIRIS-REx sample return results seem unlikely to be spoofed by foreign material. Still, a more thorough study of S-class NEOs like Eros and Ganymed, and perhaps even a sample return with a significant mass returned may be necessary before this issue is fully understood.

References: [1] Lebofsky, L. A. (1980) *Ast. J, 85,* 573-575. [2] Hasegawa et al. (2003) *GRL, 30*. DOI 10.1029/2003GL018627 [3] Rivkin, A. S. et al. (2006) *Icarus, 180,* 464-472. [4] De Sanctis, M. C. et al. (2012) *Ap. J. Lett., 758*, L36-40. [5] Prettyman, T. H. et al. (2012) *Science, 338,* 242-244. [6] McCord, T. B. et al. (2012), *Nature, 491,* 83-86. [7] Beck, P. et al. (2010), *GCA, 74,* 4881-4892. [8] Takir, D. et al. (2013) *Met. Plan. Sci., 48,* 1618-1637. [9] Takir, D. and Emery, J. P. (2012), *Icarus, 219,* 641-654. [10] Rivkin, A. S. et al. (2012) *EPSC*, abstract id EPSC2012-359. [11] Masiero, J. R. et al. (2012) *Ap. J. Lett., 759*, L8-12. [12] DeMeo, F. S. and Carry, B. (2013) *Icarus, 226,* 723-741. [13] Rivkin, A. S. (2013) *Icarus, 221,* 744-752. [14] Rivkin, A. S. (1995) *Icarus, 117,* 90-100. [15] Rivkin, A. S. (2000) *Icarus, 145,* 351-368. [16] Shepard, M. K. et al. (2013) *DPS 45*, abstract no. 201.01. [17] Rivkin, A. S. et al. (2013) *LPS XLIV* Abstract #2070. [18] Clark, B. E. et al. (2001) *Met. Plan. Sci., 36,* 1617-1637. [19] Coradini, A. et al. (2011), *Science, 334,* 492-494.

THE ATLASES OF VESTA. Th. Roatsch[1], E. Kersten[1], K.-D. Matz[1], F. Preusker[1], F. Scholten[1], R. Jaumann[1], C.A. Raymond[2], and C.T. Russell [3], [1]Institute of Planetary Research, German Aerospace Center (DLR), Berlin, Germany; [2]Jet Propulsion Laboratory, California Institute of Technology, Pasadena, CA; [3]Institute of Geophysics, UCLA, Los Angeles, CA. (Thomas.Roatsch@dlr.de)

Introduction: NASA's Dawn spacecraft entered orbit of the inner main belt asteroid 4 Vesta on July 16, 2011, and has spent 14 months in orbit to characterize the geology, elemental and mineralogical composition, topography, shape, and internal structure of Vesta before it departed to asteroid 1 Ceres in September 2012. One of the major goals of the mission is a global mapping of Vesta.

Data: The Dawn mission has been mapping Vesta from three different orbital heights during Survey orbit (2700 km altitude), HAMO (High Altitude Mapping Orbit, 700 km altitude), and LAMO (Low Altitude Mapping Orbit, 210 km altitude) (Russell and Raymond, 2011). The Dawn mission is equipped with a framing camera [FC (Sierks et al., 2011)], which was the prime instrument during the HAMO phase. The framing camera took about 1,100 clear filter images with a resolution of about 200 m/pixel during the Survey phase, about 2,500 images with a resolution of about 60 m/pixel during the first HAMO phase and about 10,000 images with a resolution of about 20 m/pixel during the LAMO phase. A second HAMO phase with about 2,100 images completed the imaging campaign. The second HAMO phase was necessary to image the Northern polar area during spring time.

Data processing: The first step of the processing chain is to ortho rectify the images to the proper scale and map projection type. This process requires detailed high-resolution information of the local topography of Vesta and high-accurate orbit and pointing information. Both the global topgraphy and the improved orbit and attitude data were calculated during the stereo processing of the HAMO images [3] and were used here. The shape model was used for the calculation of the ray intersection points while the map projection itself was done onto a sphere with a mean radius of 255 km. The next step was the mosaicking of the images from the different orbit phase to three global mosaics of Vesta, the so called basemaps.

Vesta map tiles: The Survey atlas was produced in a scale of 1:1,500,000 and consists of four quadrangles on 3 sheets (the sub-division of the synoptic format) [Fig.1.]. The HAMO atlas was produced in a scale of 1:500,000 and consists of 15 tiles [Fig.2] that conform to the quadrangle scheme proposed by Greeley and Batson [4] whereas the LAMO atlas consists of 30 tiles with a scale of 1:200,000 [Fig. 3].

Nomenclature: The dawn team proposed to the International Astronomical Union (IAU) to use the names of vestal virgins and famous Roman women as names for the craters and to use names of places and festivals associated with vestal virgins for other feature names. This proposal was accepted by the IAU and 65 names for geological features were approved by the IAU. 39 additional feature names are currently under review by the IAU. All approved feature names were applied to the map tiles. All three Vesta atlases are available to the public through this web page: http://dawn_gis.dlr.de/

References: : [1] Russell, C.T. and Raymond, C.A., Space Sci. Review, 163, 3-23; [2] Sierks, et al., 2011, Space Sci. Rev., 163, 263-327; [3] Preusker, F. et al., 2012, LPSC, # 2012; [4] Greeley, R. and Batson, G., 1990, Planetary Mapping, Cambridge University Press.

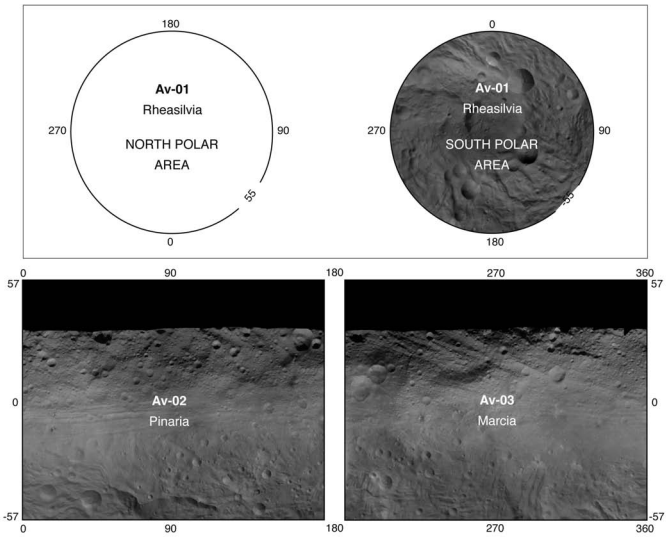

Fig. 1: Tiling scheme of Vesta's Survey atlas

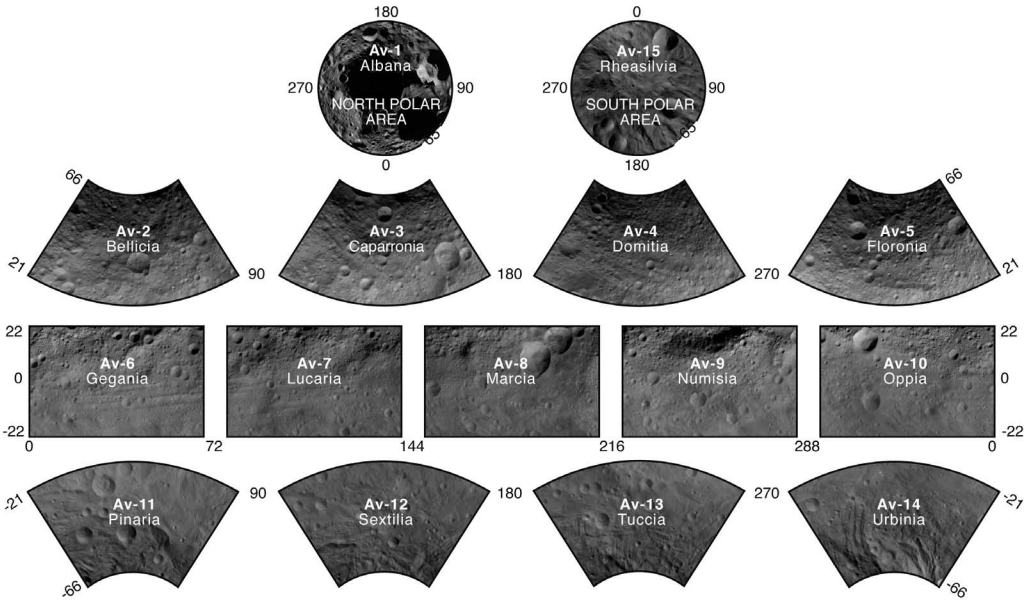

Fig. 2.: Tiling scheme of Vesta's HAMO atlas

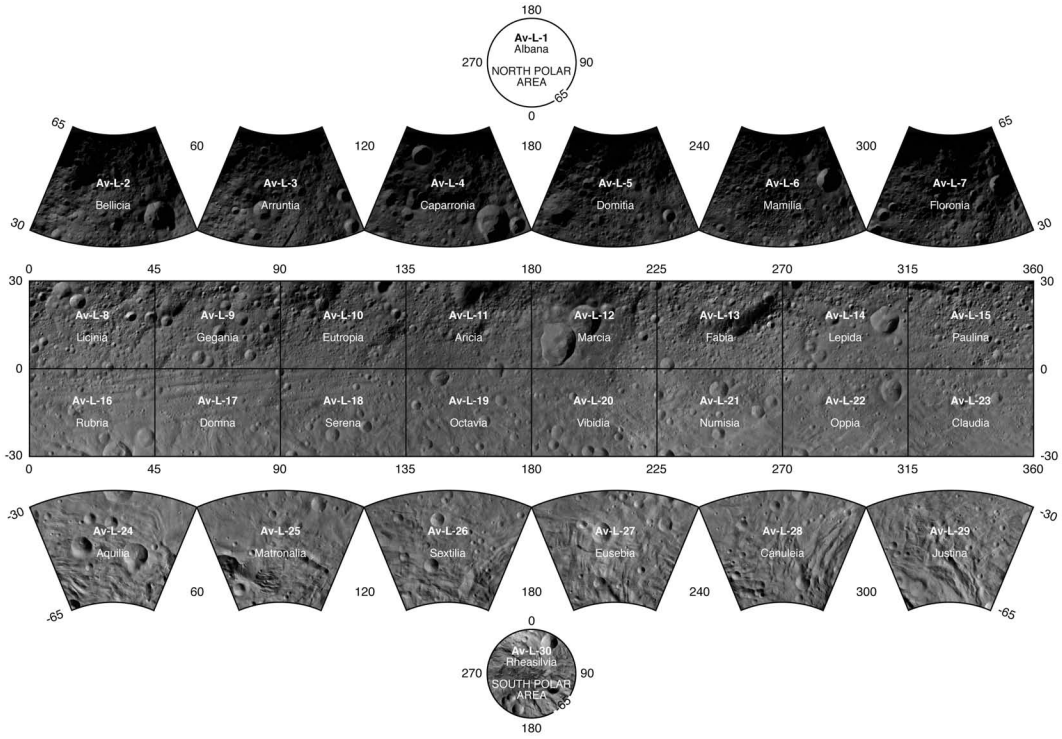

Fig. 3: Tiling scheme of Vesta's LAMO atlas

THE COLORS OF VESTA. Th. Roatsch[1] S.E. Schröder[1], S. Mottola[1], K.-D. Matz[1], E. Kersten[1], R. Jaumann[1], C.A. Raymond[2], and C.T. Russell[3], [1]Institute of Planetary Research, German Aerospace Center (DLR), Berlin, Germany; [2]Jet Propulsion Laboratory, California Institute of Technology, Pasadena, CA; [3]Institute of Geophysics, UCLA, Los Angeles, CA. (Thomas.Roatsch@dlr.de)

Introduction: NASA's Dawn spacecraft entered orbit of the inner main-belt asteroid 4 Vesta on July 16, 2011, and spent 14 months in orbit to characterize the geology, elemental and mineralogical composition, topography, shape, and internal structure of Vesta before it departed to asteroid 1 Ceres in September 2012. One of the major goals of the mission is a global color mapping of Vesta.

Data: The Dawn mission mapped Vesta from three different heights during Survey orbit (2700 km altitude), HAMO (High Altitude Mapping Orbit, 700 km altitude), and LAMO (Low Altitude Mapping Orbit, 210 km altitude) [1]. The Dawn mission is equipped with a framing camera (FC) with one clear and seven narrow band color filters [2]. The FC took about 6,500 color images in all seven filters with a resolution of about 60 m/pixel during the two HAMO phases, which resulted in almost complete coverage of Vesta.

Data processing: The first step of the processing chain is an accurate radiometric calibration of the images. The camera was calibrated on ground but it became necessary to improve this procedure with an extended in-flight calibration [3]. Images taken through the narrow band filters are plagued by in-field stray light, which must be subtracted after the standard radiometric correction [4]. The next step in the processing chain is the photometric correction of the images [4,5]. The following steps are the same as those for clear filter images: ortho rectification and mosaicking [6].

True color: The global true color mosaic in Mollweide projection is shown in Fig.1. True color was achieved by scaling FC images acquired through the red, green, and blue filters to RGB values calculated from the CIE color matching functions and a Vesta spectrum [7].

Clementine ratios: Clementine-type color ratio image mosaics were calculated using the mosaics of three different narrow band filters; Red: 750/430 nanometers (nm); Green: 750/920 nm; Blue: 430/750 nm. The color ratio image product serves to cancel out the dominant brightness variations of the scene (controlled by albedo variations and topographic shading) and enhances color differences related to soil mineralogy and, possibly, maturity.

Download: All color mosaics will become available to the public through JVesta, the Vesta version of the JMARS geographic information system [8].

References: : [1] Russell, C.T. and Raymond, C.A., 2011, Space Sci. Review, 163, 3-23; [2] Sierks, H. et al., 2011, Space Sci. Rev., 163, 263-327; [3] Schröder, S.E. et al., 2013, In-flight calibration of the Dawn Framing Camera, Icarus, 226, 1304-1317; [4] Schröder, S.E. et al., 2013, In-Flight calibration of the Dawn Framing Camera II: Flat fields and stray light correction, submitted to Icarus; [5] Schröder, S.E. et al., 2013, Resolved photometry of Vesta reveals physical properties of crater regolith, Planet. Space Science, 85, 198-213; [6] Roatsch, Th. et al., 2012, High resolution Vesta High Altitude Mapping Orbit (HAMO) Atlas derived from Dawn framing camera images, Planet. Space Science, 73, 283-286; [7] Xu, S. et al., 1995, Small main-belt asteroid spectroscopic survey: Initial results. Icarus 115, 1–35. [8] http://jmars.asu.edu.

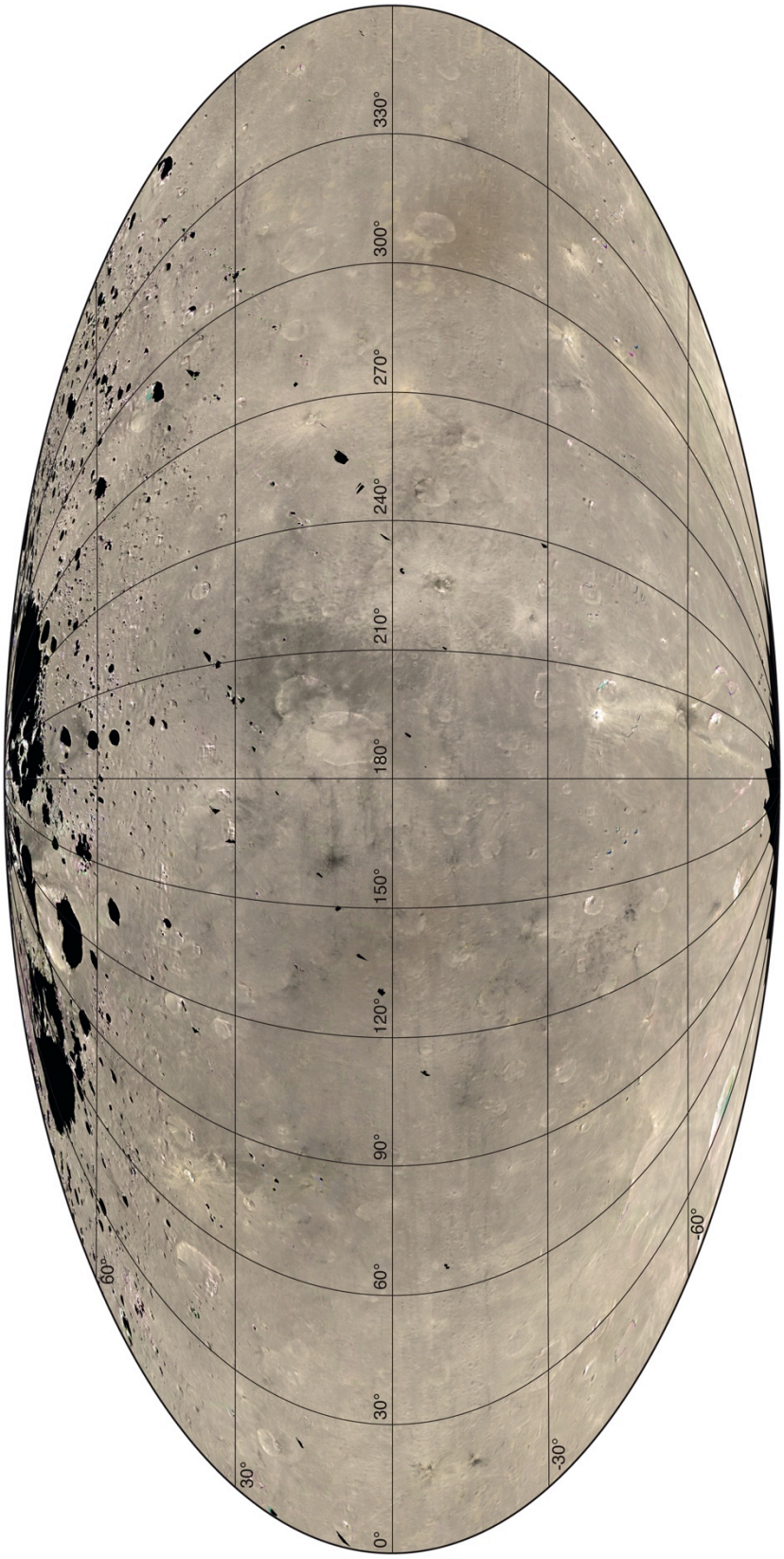

Fig. 1: Global true color mosaic in Mollweide projection

SOME MORE LOCATIONS OF POSSIBLE EXPOSED OLIVINE ON VESTA USING VIR/DAWN DATA.

O. Ruesch[1], H. Hiesinger[1], M. C. DeSanctis[2], E. Ammannito[2], E. Palomba[2], A. Longobardo[2], M. T. Capria[2], F. Capaccioni[2], A. Frigeri[2], F. Tosi[2], F. Zambon[2], S. Fonte[2], G. Magni[2], C. A. Raymond[3], C. T. Russell[4], [1]Institut für Planetologie, Westfälische Wilhelms-Universität Münster, Germany (ottaviano.ruesch@uni-muenster.de), [2]Istituto di Astrofisica e Planetologia Spaziali, INAF, 00133 Rome, Italy. [3]Jet Propulsion Laboratory, Caltech, Pasadena, California 91109, USA. [4]University of California, Los Angeles, California 90095, USA.

Introduction: The large asteroid Vesta underwent global-scale differentiation and intense magmatism. Although impact events on Vesta have oblitered the structure of the original igneous crust [1], the surface mineralogy (pyroxenes, olivine) has likely kept the record of the magmatic processes [2]. In addition to studying the surface mineralogy, a major contribution to the understanding of Vesta magmatism is provided by studies of mafic and ultramafic achondrites (the Howardite, Eucrite, Diogenite (HED) suite), that likely formed on Vesta [3, 4]. The diversity of pyroxene minerals and their spatial distribution across Vesta has been studied with the Dawn mission data and is broadly consistent with a pervasive melting of primordial Vesta, perhaps with the formation of a magma ocean [2]. More regional processes, however, also seem to have played a role during Vesta´s differentiation and crust formation [5,6]. Recently, using the Dawn mapping spectrometer (VIR) [7], olivine mineral was found to be rare and only locally exposed on Vesta´s surface [8]. In order to better understand the processes responsible for the origin and distribution of olivine on Vesta, we performed a detailed mapping of the olivine signature across the entire surface of Vesta. For such purpose, we developed a set of specific spectral parameters and specific thresholds to isolate and map the signature of olivine in the VIR/Dawn data.

Method: *Spectral parameters.* In the near-IR spectral range (0.6-2.5 μm) Vesta´s surface is a multicomponent surface dominated by pyroxenes absorption bands. We use the slope increase in the 1.1-1.6 μm range, measured by a parameter defined in [9] (hereafter named FoP), to detect increasing olivine content in pyroxene-dominated mixtures. Because the parameter is also sensitive to dark material, glass, and pyroxenes with Fe^{2+} in the M1 crystallographic site, additional parameters are developed in order to discriminate between olivine and the other components: (1) the band depth at 1 μm (BD1), (2) the band depth at 1.8 μm (BD1.8) and (3) at 2.2 μm (BD2.2), (4) the ratio BD2.2/BD1.8.

Thresholds on parameters. Two thresholds on the FoP parameter are defined to avoid spectral signatures of dark material and pyroxenes with Fe^{2+} in the M1 site. Their values are not chosen as constant, instead, they vary as a function of the parameter variations within each cube. To avoid effects of dark material, the threshold varies as a function of the BD1 parameter, which decrease with increasing dark material content [10]. To avoid Fe^{2+}/M1 pyroxenes, the threshold varies proportionally to the BD2.2/BD1.8 ratio, which increase with a higher amount of Fe^{2+}/M1 pyroxene [11]. Such parameter trends were verified using the available laboratory data on mineral mixtures. Variations due to grain size and observation geometry effects [12, 13] were constrained. Quantitatively, (1) a FoP moving average is calculated across the BD1 (and the BD2.2/BD1.8 ratio) variation range in each image, and (2) the threshold is defined by adding to the moving average the 3σ (chosen after visual analyses of numerous VIR cubes of various illuminations and locations) of the FoP parameter. Because each cube is treated separately, and the threshold values slightly vary across Vesta´s surface, this method allows detecting olivine enrichment at a local scale.

By comparison with potential glass-rich regions [14], we found that (1) the FoP increase due to potential glass is below the 3σ threshold and (2) the spatial pattern of relatively high FoP values is different from that of previously identified olivine-rich spots. With the current understanding of glass spectral characteristics on Vesta [14] we conclude that glass does not influence olivine detections with the above method.

Results: The analyses of more than 700 cubes (Survey and HAMO-1-2) with global coverage led to the identification of 13 different potential olivine-rich locations on Vesta (Fig. 2). 10 of the sites have been detected in at least two VIR cubes acquired at different times and spatial resolutions, thus excluding instrumental artifacts. 3 of the sites have been previously detected by [8]. Relative to surrounding olivine free/poor spectra, the 10 newly identified sites have the highest 1.1-1.6 μm spectral slope, a weaker band depth at 2 μm, and a high albedo. These key features, in addition to no changes in the band centers, indicate the presence (<~50 vol.%) of olivine (Fig. 1)

At each site, generally 2-5 km wide, the morphology is consistent with fresh, un-gardened, surface exposures. As seen in Figure 2, the global spatial distribution indicates a hemispherical concentration. The northern olivine-rich sites are found on the rims of 100-200 km large basins, possibly representing ejected ma-

terial from depth to 9-12 km (using [15]), as well as in areas with regionally higher elevations. At the equator, the sites are located within a large-scale trough and ridge system. The southern sites are found at the edge and within the Rheasilvia ejecta, with the southernmost sites having pyroxenes rich in Mg (diogenite-like). This latter geologic context is illustrated in the topographic profile of Figure 2.

Discussion and Conclusion: This study tentatively identified kilometers-sized olivine exposure, with the newly identified locations (olivine content <~50 vol%.) occurring around previously identified sites (>50 vol.% [8]). The hemispherically limited distribution suggests a regional/local formation process. The relatively shallow depths of origin and the geologic context of the olivine-rich spots found in this study are less consistent with a mantle origin. Thus, if an olivine-dominated mantle is present on Vesta, it should be at depth greater than the excavation depth of Rheasilvia (30-45 km [16]). Olivine in association with a diogenite-like pyroxene composition is interpreted as a deep seated magmatic lithology being overturned by the Rheasilvia impact event, as schematically illustrated in Figure 2 cross section (layer 2). Olivine-rich material lacking enrichment in Mg-rich pyroxenes (howardite-like) could have been ejected from shallower depths (Figure 2 layer 1).

Future investigations will need to focus on quantitative analyses of the olivine abundances on the detected sites.

[1] Williams D.A. et al. (2013) *Planetary and Space Science*, in press. [2] DeSanctis M.C. et al. (2012) *Science, 366, p. 697*. [3] Righter and Drake (1997) *MPS* 32, 929-944. [4] Barrat J.-A. et al. (2008) *MPS* 43, 1759-1775. [5] Buczkowski D.L. et al. (2013) *44th LPSC abstract #1996* [6] Stephan K. et al. (2013) JGR. [7] DeSanctis M.C. et al. (2011) *SSR* doi10.1007/s11214-010-9668-5. [8] Ammannito E. et al. (2013) *Nature* doi:10.1038/nature12665. [9] Poulet F. et al. (2007) *JGR 112* E08S02. [10] Reddy V. et al. (2012) *Icarus 221, 544-559.* [11] Klima R.L. et al. (2011) *MPS 46, 379-395.* [12] Cloutis E. et al. (2012) *Icarus 223, 850-877.* [13] Ruesch O. et al. (2013) *44th LPSC abstract #2236.* [14] LeCorre L. et al. (2013) *Icarus 226, 1568-1594.* [15] Melosh, (1989) *Exford Univ. Press.* [16] Ivanov and Melosh (2013) *JGR 118, 1545-1557* [17] Yingst A. et al. (2013) *Icaurs* In revision.

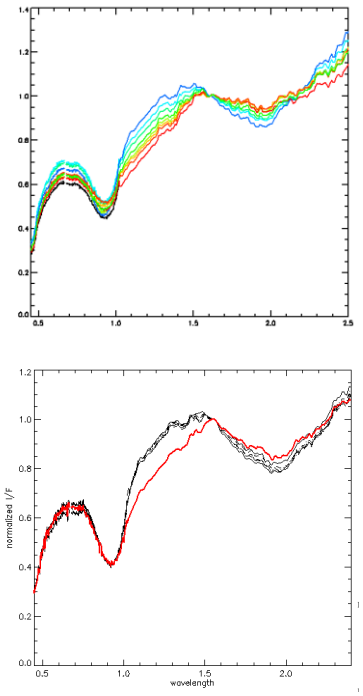

Figure 1. (top) Visible and near-IR spectral variations of an olivine free/poor area an an olivine-rich spot [7], as revealed by VIR/Dawn data. (bottom) VIR spectrum of a newly identified olivine-rich spot (red) compared to surrounding olivine free/poor spectra (black).

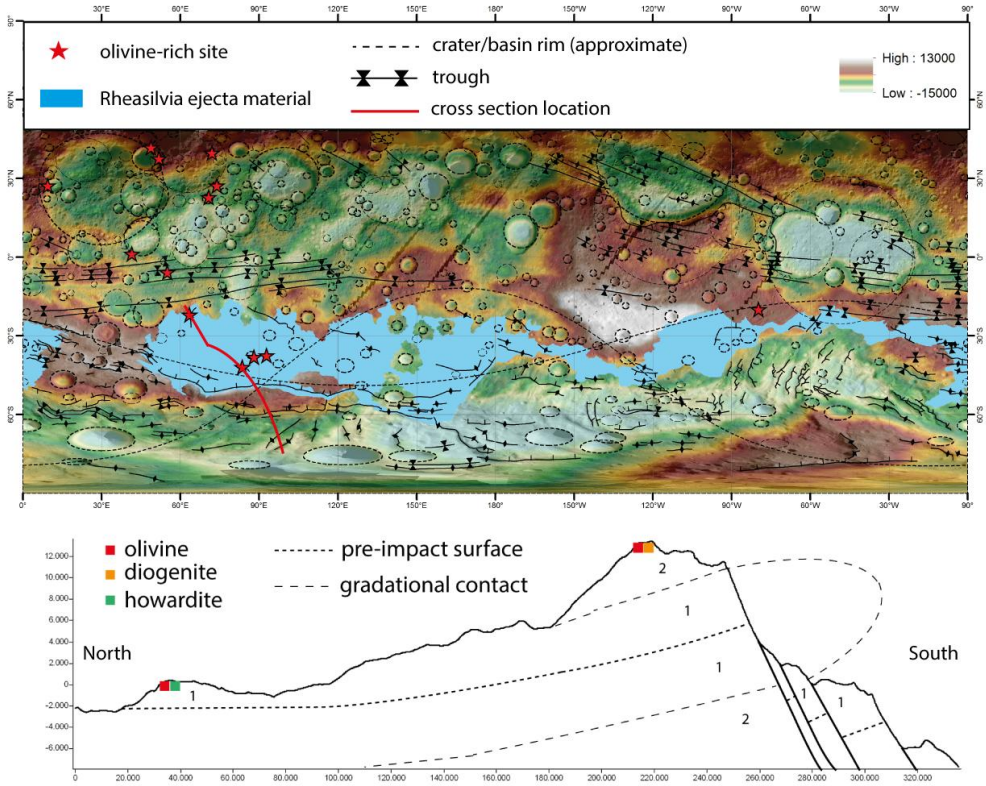

Figure 2. (top) Location of olivine-rich sites on a global topographic map of Vesta, identified in VIR/Dawn data. Rheasilvia ejecta material map from [17]. (bottom) Topographic profile and interpreted structure of the Rheasilvia ejecta and associated olivine-rich site with their pyroxene compositions.

A JOURNEY IN SPACE AND TIME: FIRST STOP VESTA. C. T. Russell, Earth Planets and Space Sciences, University of California, Los Angeles, CA 90095 USA

Summary: To uncover unwritten history one talks to the oldest survivor of the battle. To go back in time in the solar system we also need to converse with the oldest survivor, Vesta that formed within 2 million years of the first primitive meteorites. Vesta has seen the ravages of solar system time, the evolution of a protostar, the formation and migration of giant planets, the bombardment by energized neighboring asteroids, the transport of alien material to its pristine surface, global tectonic, basin forming events, global if not total melting and the evolution, erosion, and total fracturing of its crust and deep regolith. Vesta has seen mountains built, rift valleys form, giant landslides occur. Dry and airless but with curvilinear gullies and pits speaking of devolitization, Vesta pours out its soul with stories of a complex history rivaling those of larger bodies. This workshop is devoted to detailing this voyage outward in space and backward in time.

MEGASCALE IMPACTS INTO VESTA'S SOUTH POLE: THE MORPHOLOGIC CONSTRAINTS. P. Schenk,[1] D. O'Brien[2], H. McSween[3], D. Buczkowski[4], R. Gaskell[5], K. Otto[6], F. Preusker[6], S. Marchi[7], A. Yingst[2], S. Mest[2], C. Raymond[8], C. Russell[9], and the Dawn Science Team. [1]Lunar and Planetary Institute, Houston (schenk@lpi.usra.edu), [2]Planetary Science Institute, Tucson, [3]University of Tennessee, Knoxville, [4]JHU/Applied Physics Laboratory, Laurel, [5]Planetary Science Institute, Pasadena, [6]DLR, Institute of Planetary Research, Berlin, [7]NASA Lunar Science Inst., Boulder, [8]Jet Propulsion Laboratory, Pasadena, [9]Univ. of California, Los Angeles.

Introduction: The large 505-km-wide South Polar impact basin, Rheasilvia, on Vesta is the largest impact feature with respect to planet diameter observed to date. As such, it provides a unique window into large impacts into planetary scale bodies under near disruption conditions. Here we present an overview of Dawn mission findings for these large impact features and the constraints they place on impact models and HED's.

Description: A 450-km class impact feature on Vesta was first observed in HST data [1]. The first discovery by Dawn on approach in 2011 was that the impact feature actually consisted of two large overlapping basins [2], part of the complex impact history of Vesta [3]. The older Veneneia basin is 395-km across and is half obliterated by the younger 505-km Rheasilvia basin. The floor of Veneneia is highly disrupted and partially covered by Rheasilvia ejecta so we will focus mostly on Rheasilvia, except to note that Veneneia is associated with outcrops of dark material.

Rheasilvia: This large basin, centered at 72°S, 279°W (Claudia system), has a "complex" morphology, with a narrow rim scarp, broad floor material, quasi-conical central peak or complex. We will describe each briefly. The rim is relatively simple but variable along its circumference. In some regions it is a low ridge reflecting a break in slope. In other areas it is a narrow inward-facing scarp of a few hundred meters to ~25 km relative heights. A few large slump features have been identified, but they are not contiguous around the rim and absent in some quadrants.

The basin floor is not flat anywhere but slopes gently inward. It is highlighted by numerous minor landslides and by prominent linear to arcuate (1-2 km) scarps. These form an integrated (non-crosscutting) pattern across the entire floor arcing away from the central complex in a clockwise fashion, forming a spiral pattern nearly unique in the Solar System.

The central complex is ~200 km wide and 22 km high on average and has a rugged morphology. Hollows could be indications of impact melt but regolith formation precludes confirmation. Arcuate scarps suggest partial collapse of the complex on one side.

Varying thicknesses of heavily striated material mantles areas north of Rheasilvia, extending to the equator and beyond. This material is interpreted as ejecta 1-10 km thick (provisionally), consistent with decreasing degrees of crater erasure [3].

A set of spectacular large troughs extend along the equator. The geographic centers of these arcs are located within the basins, suggesting a causal relationship. We note that the troughs are not perfectly centered on the basins, however, suggesting a complex relationship. The only apparent radial features are a few sets of north-south crater chains.

Compositionally, the floor of Rheasilvia is heterogeneous [5]. Part of the floor is dominated by a diogenitic signature, which extends to the north beyond the rim suggesting partial excavation and ejection of deep crustal material. No unambiguous olivine signature has as yet been identified. The age of the basin is currently estimated at 1-2 Gyr [3].

Discussion: Volume calculations confirm that Rheasilvia was more than capable of ejecting enough material to form the Vestoid asteroid family and the HED meteoritie suite with it [2]. The lack of an olivine signature is not well understood, though gravity data are being interpreted with this question in mind. Impact modelers are working on refining their models using the new constraints, including trough formation. The high crater density on the troughs can be explained by ejecta landing after the stress waves pass.

One of the most surprising aspects of Rheasilvia has been the arcuate/spiral scarp pattern on the floor. These are interpreted as a record of the deformation pattern and stress field as the basin floor rebounded (and not to post-impact mass-wasting). The spiral pattern has been interpreted as due to failure during inward movement of floor material during post-excavation rebound. Two possible causes of the pattern have been suggested: coriolis deflection of floor material (the sense of rotation is correct) and failure patterns found in nature and experimentally in converging material. Both may be possible but discovery of similar patterns in natural crates suggests that coriolis may not be necessary. In the case of Rheasilvia, the absence of large volumes of impact melt leave these patterns exposed to view.

References: [1] P. Thomas, and others (1997), *Science* 277, 1492-1495. [2] P. Schenk, and others. (2012) *Science, 336,* 694-696. [3] S. Marchi and others. (2012) *Science, 336,* 690-693. [4] D. Buczkowski, and others (2012) *Geophys. Res. Lett., 39,* L18205. [5] H. McSween and others (2013) *J. Geophys. Res.*, 118, 335-346.

CRATERING ON A SMALL PLANET: MORPHOLOGIES OF FRESH CRATERS AND THE SIMPLE-COMPLEX TRANSITION ON VESTA. P. Schenk[1], J.-B. Vincent[2], V. Bray[3] and G. Kramer[1], and the Dawn Science Team [1]Lunar & Planetary Institute, Houston (schenk@lpi.usr.edu), [2] Max-Planck Inst., Katlenburg-Lindau, Germany, [3]Univ. of Arizona, Tucson, AZ.

Introduction: Dawn mapping [1] of Vesta has provides our first close look at impact crater formation processes on the previously unexplored largest asteroids / dwarf planets. Mapping of the largest previously visited asteroids (e.g., Lutetia) revealed only simple craters [2], and Vesta is the first silicate–rich asteroidal body examined significantly smaller than the Moon yet large enough to have complex craters, or predicted to do so.

Vesta is heavily cratered [3]. The morphology of craters of all classes and erosion states is examined by [4], but in this report we describe the shapes and morphologies of both simple and complex craters. This serves three objectives. The first is to examine the question of whether complex craters actually formed on Vesta and establish a reference shape of intact craters for determining the degree of erosion, mantling or relaxation of older craters, the second is to provide for comparison of complex crater formation processes on Vesta with other silicate bodies (e.g., the Moon), and third to determine the simple-to-complex crater transition in relatively fresh unmodified craters in comparison with prediction and with other terrestrial bodies, which from extrapolation of other data [5, 6] would be ~60-70 km on Vesta.

Impact crater morphologies on Vesta are determined from the global Framing Camera (FC) mosaic of Vesta at 20 meter resolution (except north of 55°N latitude where resolution is 65 meters). Shapes are determined using topographic data mapped at 65 m resolution from FC stereo imaging [7].

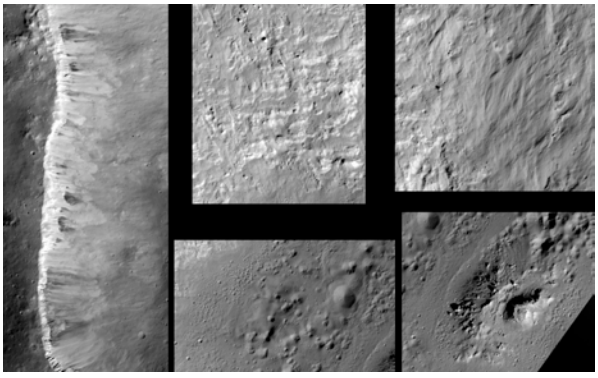

Figure 1: Elements of crater Marcia, the largest well-preserved crater on Vesta.

Crater Morphology: We focus here on those craters unmodified by erosion or mantling. While ancient craters as large as 250 km have been identified on Vesta [3,7], the global effects of ejecta produced from the two large impact basins at the south pole, Rheasilvia and Veneneia (D 505 and 395 km, respectively), have effectively mantled most impact craters formed prior to Rheasilvia with up to several kilometers of debris in many places (Schenk et al., 2012). Rheasilvia itself is estimated at roughly 1 Gyr in age [3,7], which is relatively young, and as a result, large intact, unmantled post-basin complex craters are relatively few. The largest such crater, Marcia, is only 65 by 72 km in size (Fig. 1), approximately the predicted diameter of the simple-to-complex transition on Vesta.

Simple Craters: Impact craters on Vesta smaller than ~30 km have a classic simple crater morphology, not radically dissimilar from lunar craters. Such craters have a bowl or inverted-cone profile shape highlighted by a sharply defined roughly circular rim scarp with outcrops of possible bedrock along the inner rimwall and lobate debris slides extending from the rim down to the bottom of the crater. Simple craters have depth/diameters that may be ~15% deeper than lunar equivalents (Fig. 3). Rim heights may be 30% higher on Vesta compared to lunar craters, pending reevaluation of the lunar crater data.

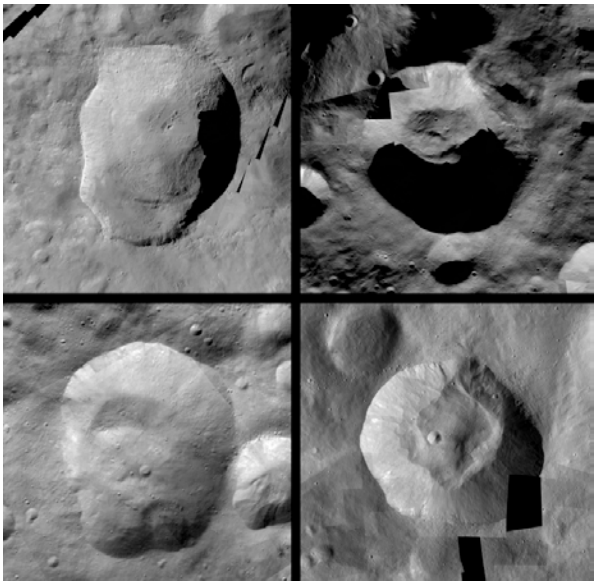

Figure 2: Examples of transitional/complex craters on Vesta. From top left: Marcia, D~62 km; unnamed, D=58 km; Caparronia, D=49 km; Pinaria, D=39 km.

Transitional Craters: Of well-preserved impact craters on Vesta larger than 30 km, only 505-km diam-

eter Rheasilvia has a fully expressed complex crater morphology (Veneneia being obscured or obliterated by the later Rheasilvia). Rheasilvia is broadly bowl-shaped but also has a prominent modified-conical central uplift and isolated slump features along the inner rim crest [8].

Among intact post-Rheasilvia impact craters larger than ~30 km, morphologies are neither simple nor complex (Fig. 2). These craters are broadly bowl-shapes with steep inner rimwalls and debris slides but most have a rounded but distinctly noncircular shape. They also have either broad flat floors or large arcuate to irregular mounds covering a broad crater floor (Fig. 2). The largest of these, Marcia (D~65 km) is broadly flat floored but also has a small central mound or massif that may be a putative central peak, but otherwise classical conical central peaks are not developed or preserved in any Vesta craters other than Rheasilvia. All craters identified as having "transitional" morphologies are also significantly shallower than the similar-sized simple craters (Fig. 3).

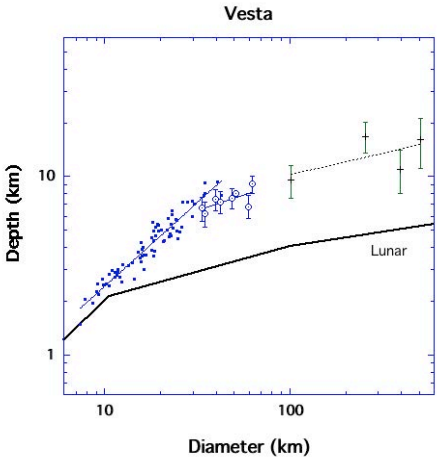

Figure 3. Observed crater shapes for fresh unmodified impact craters on Vesta. Solid circles are simple craters; open circles are 'transitional' craters. Largest basins are also shown separately.

Accepting the transitional crater *d/D* curve (and the associated large basin *d/D* measurements) as the only preserved segment of the complex crater curve on Vesta, we can estimate the transition diameter *Dtr* for Vesta from the intersection of this with the well-defined simple crater *d/D* curve (Fig. 3). This intercept or inflection occurs at *Dtr* ~ 28 km, roughly half that predicted from simple extrapolation of the measured *Dtr* of other silicate-rich planets (Fig. 1).

Discussion: In addition to detailed descriptions of crater morphologies and some lunar comparisons, we will discuss the apparent morphologic transitions. At face value, the new *Dtr* trend for silicate targets when Vesta is included is *Dtr* ~ *D*^-0.7, indicating a weaker but still significant dependence on complex crater formation on surface gravity (Fig 4).

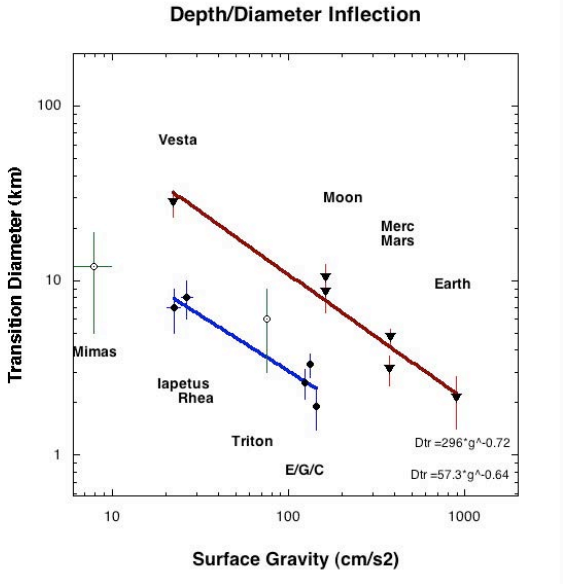

Figure 4: Updated simple-to-complex transition diameters for Solar System objects, based on the observed Vesta data and updated Cassini data [9]. Lines are best fits to icy and rocky targets. Assuming a g^{-1} relationship, the differences in transition diameter may reflect differences in effective regolith strength on the various bodies.

One interpretation of Figure 4 is that we are seeing the combined influence of gravity and strength on crater collapse and complex crater initiation. (The role of impact velocity remains indeterminant. It is also possible that even 60-km craters on Vesta formed in the strength rather than the gravity regime.) Thus the *g-Dtr* relationship may remain valid for all bodies but that strength is very important (as evidenced by the different ice and rock trends in Fig. 4) and that Vesta and the icy satellites of Saturn all have significantly weaker crustal strengths than their larger cousins; why is unclear.

Acknowledgements: The author thanks the Dawn at Vesta Participating Scientist program.

References: [1] Russell, C., et al., *Science*, 336, 684-687 (2012). [2] Vincent, J.-B., *PSS*, 66, 79-86 (2012). [3] Marchi, S., et al., *PSS*, 66, 87-95 (2012). [4] Vincent, J.-B., et al., *LPSC 43rd*, id 1415 (2012). [5] Pike, R., Proc. *11th LPSC*, 2159-2189 (1980). [6] Schenk, P., et al., in *Jupiter*, p. 427 (2004). [7] Jaumann, R., et al., *Science*, 336, 688-691 (2012). [8] Schenk, P., et al., *Science*, 336, 693-695 (2012). [9] White, O. et al., 223, 699-709, Icarus, (2013).

VESTAN GULLIES AND THEIR FORMATION MECHANISMS. J. E. C. Scully[1], C. T. Russell[1], A. Yin [1], R. Jaumann[2], E. Carey[3], H. Y. McSween[4], C. A. Raymond[3], V. Reddy[5,6], L. Le Corre[5,6,], J. Castillo-Rogez[3], [1]Dept. of Earth and Space Sciences, University of California, Los Angeles, CA, USA (jscully@ucla.edu), [2]DLR, Berlin, Germany, [3]Jet Propulsion Laboratory, California Institute of Technology, Pasadena, CA, USA, [4]University of Tennessee, Knoxville, TN, USA, [5]Max Planck Institute, Katlenburg-Lindau, Germany, [6]PSI, Tuscon, AZ USA.

Introduction: The view that airless solar system bodies are completely dry is changing with the discovery of water on the Moon [e.g. 1] and Mercury [e.g. 2]. Vesta too has evidence for water: its meteorites contain evidence for aqueous alteration [3,4] and water in primitive melts [5]. Furthermore, Dawn's observations detected a 2.8 μm OH absorption [6] and mineralogically bound OH and/ or H_2O [7]. Also, pitted terrain, interpreted as evidence for degassing of volatile-bearing material, is found in some recent craters [8].

Flow conditions and morphology: Morphology of terrestrial flow features is used to indicate the flow conditions under which they formed [9]. This approach is adopted by planetary geologists, who have used surface morphology, amongst other characteristics, as an indicator of the formational flow conditions of gullies on the Moon and on Mars [10,11,12].

Lunar gullies are straight, parallel to one another and do not intersect to form networks, which is indicative of their formation by dry flow of granular material [11,12]. Martian gullies have a generic form of a head alcove, curvilinear channels and a depositional apron [10] and many formation mechanisms for them have been proposed [e.g. 13]. A specific set of young Martian gullies, called surficial gullies, are located in and around Gasa crater and are proposed to form by the flow of impact-melted water sourced in ice-rich mantle deposits [14]. These surficial gullies have some morphologies that are different from generic Martian gullies: they are shallowly incised and can originate in the crater walls without alcoves [14].

Observations: Gullies on Vesta are classified, based on morphology, into two types: linear, identified in 50 locations, and curvilinear, identified in 8 locations. Both are chiefly found on the sloping walls of young impact craters.

Linear gullies. Linear gullies are straight, parallel to each other, rarely intersect and have simple network geometries that form parallel networks. They typically originate in alcoves below spurs of more coherent material and are often bounded by talus material levees.

Curvilinear gullies. The type area curvilinear gullies are found in two craters: Cornelia and Marcia. In these craters the gullies are sinuous, frequently intersect and have complex network geometries that form sub-dendritic and sub-parallel networks. They typically originate below slumped deposits or in the crater walls and commonly end in deposits that are lobate in shape. These lobate deposits partially superpose one another and are morphologically similar to terrestrial alluvial fans formed by debris flows.

Pitted terrain: The four craters with pitted terrain on their floors [8] also contain curvilinear gullies in their walls. Sometimes, pitted terrain is observed on the lobate deposits of curvilinear gullies as well as on the rest of the crater floor. Pitted terrain is not observed in craters containing only linear gullies. Pitted terrain is morphologically similar to Martian pitted terrains [15] and both are interpreted to form by impact-heated degassing of volatile-bearing material [8,15].

Quantified observations: The morphologic dissimilarity between the two gully types can also be quantified. The length to width ratio of curvilinear gullies, on average 30, is higher than that of the linear gullies, on average 13. Also, the junction angles between connecting gullies, on average 33° for curvilinear gullies, is higher than that of the linear gullies, on average 16°. The number of connections between gullies is also highest for curvilinear gullies.

Interpretations: There are a number of different possible interpretations for the formation mechanism of the vestan gullies, which are discussed below.

Interpretation A: flow of impact melt. Flow of impact melt is considered the least likely formation mechanism for either type of gully due to the low volumes of impact melt observed and predicted based on calculations [e.g. 16]; the spectral characteristics of the gullies being inconsistent with impact melt; and the paucity of impact melt morphologies associated with the gullies (although melt may be incorporated within some of the pitted terrain regions).

Interpretation B: dry flow. The morphology of the linear gullies is analogous to lunar gullies and it is likely that they formed by flow of dry granular material. However, since the morphologies of the linear and curvilinear gullies are dissimilar, the principle of morphology indicating flow conditions suggests that some flow condition(s) that formed the linear gullies must be different from the flow condition(s) that formed the curvilinear gullies. In searching for the different flow condition(s), it is found that both types of gullies: i) form on the same ranges of slopes; ii) have similar amounts of material available for flow; and iii) have similar compositions. Also, thermal inertia data [17] indicates that the curvilinear gullies are not formed by flow of relatively finer grained material. Thus, it seems

likely that linear gullies are formed by flow of dry granular material, but no varying flow condition can be found to explain how flow of dry granular material could also form the morphologically dissimilar curvilinear gullies.

Interpretation C: dry flow and transient flow of liquid water.

Since no varying flow condition(s) can be found to explain the flow of dry granular material forming the curvilinear gullies, it is proposed that dry granular flow formed the linear gullies but that flow of transient liquid water was involved in the erosion of the curvilinear gullies. Observations that support this proposal are the morphologies of the curvilinear gullies, their formation of complex networks, their similarity to the Martian surficial gullies and their association with pitted terrain.

Proposed formation mechanism of curvilinear gullies: Water will be stable in the gaseous state at vestan surface conditions and could be trapped and survive for billions of years in ice form as shallow as a few meters in the regolith [18]. It is proposed that the water is sourced in sub-surface ice-bearing deposits (Fig. a). The sub-surface distribution of these deposits may be represented by the two clusters of craters containing curvilinear gullies.

The preferred source of the sub-surface ice-bearing deposits is accretionary rather than later deposition by water-rich bodies, because it would be difficult to retain and bury exogenous ice on the surface of Vesta before it changed phase to a gas and was lost to space. Even though water and other volatiles originally present in the bodies that completely melted, such as Vesta, are usually assumed to be completely lost [19], quartz veins in a eucrite meteorite have been dated to be older than 4.4 Ga [3], which suggests that at least some water was present early on in Vesta's history.

Sub-surface ice-bearing deposits can be tapped by small-medium impacts that excavate material and sufficiently increase the temperatures and pressures so that part/ all of the ice-bearing deposit melts (Fig. b). Once water leaves the ice-bearing deposit and reaches the crater wall it begins to evaporate. However, not all will instantaneously evaporate. Only the top layer will be exposed and evaporating at any one time, which hinders the evaporation of lower levels (Fig. c). This process is enhanced because low surface temperatures also cause the water surface to partially freeze. Thus, water can transiently flow under a temporary protective evaporating and/ or freezing barrier before it finally all evaporates and is lost. Observations support this scenario because no curvilinear gullies are found on escarpments outside of impact craters. Experiments are underway at vestan surface temperatures and pressures to demonstrate this transient flow process. After the transient flow, loss, through evaporation, of the water on the crater floors may contribute to pitted terrain formation (Fig. d).

Conclusions: We propose that curvilinear gullies are morphological evidence for localized water on Vesta, which is in keeping with recent meteorite and remote sensing evidence.

References: [1] Saal A. E. et al. (2008) *Nature, 454*, 192. [2] Lawrence D. J. et al. (2013) *Science, 339*, 292. [3] Treiman A. H. et al. (2004) *Earth Planet. Sci. Lett., 219*, 189. [4] Warren P. H. et al. (2013) *LPSC XXXXIV*, Abstract #2875. [5] Sarafian A. R. (2012) *LPSC XXXXIII*, Abstract #1175. [6] De Sanctis M. C. (2012) *Astrophys. J. Lett., 758*, 1. [7] Prettyman T. H. et al. (2012) *Science, 338*, 242. [8] Denevi B. W. et al. (2012) *Science, 338*, 246. [9] Horton R. E. (1945) *Bull. Geol. Soc. Am., 56*, 275. [10] Malin M. C. and Edgett K. S. (2000) *Science, 288*, 2330. [11] Bart G. D. (2007) *Icarus, 187*, 417. [12] Kumar P. S. et al. (2013) *J. Geophys. Res. Planets, 118*, 1. [13] Carr M. H. (2012) *Phil. Trans. R. Soc. A, 370*, 2193. [14] Schon S. C. and Head J. W. (2011) *Icarus, 213*, 428. [15] Mouginis-Mark P. J. and Garbeil H. (2007) *Meteroit. Planet. Sci., 42*, 1615. [16] Jaumann R. et al. (2012) *Science, 336*, 687. [17] Capria M. T. et al. (2013, submitted). [18] Stubbs T. J. and Wang Y. (2012) *Icarus, 217*, 272. [19] Elkins-Tanton L. T. (2013) *Eos, 94*, 149.

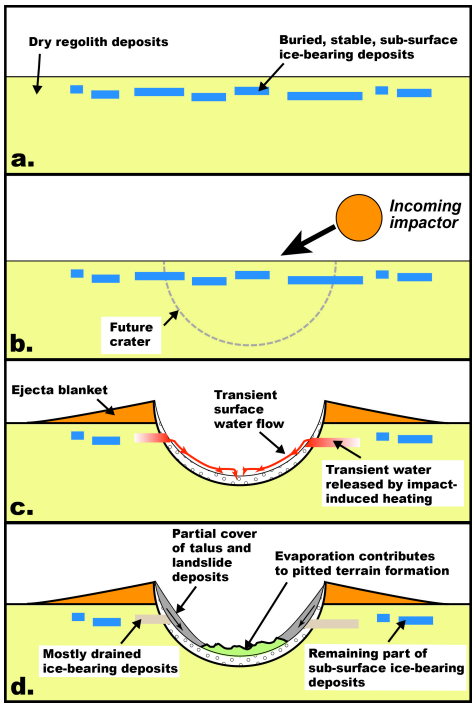

Figures a-d. Schematic illustration of proposed formation mechanism of curvilinear gullies.

GEOMORPHOLOGY AND STRUCTURAL GEOLOGY OF SATURNALIA FOSSAE AND ADJACENT STRUCTURES IN THE NORTHERN HEMISPHERE OF VESTA. J.E.C. Scully[1], A. Yin[1], C.T. Russell[1], D.L. Buczkowski[2], D.A. Williams[3], D.T. Blewett[2], O. Ruesch[4], H. Hiesinger[4], L. Le Corre[5], C. Mercer[3], R.A. Yingst[5], W.B. Garry[5], R. Jaumann[6], T. Roatsch[6], F. Preusker[6], R.W. Gaskell[5], S.E. Schröder[6], E. Ammannito[7], C.M. Pieters[8], C.A. Raymond[9], [1]Dept. of Earth and Space Sciences, University of California, Los Angeles, California, USA (jscully@ucla.edu), [2]JHU-APL, Laurel, MD, USA, [3]ASU, Tempe, AZ, USA, [4]Westfälische Wilhelms-Universität, Münster, Germany, [5]PSI, Tucson, AZ, USA, [6]German Aerospace Center (DLR), Berlin, Germany, [7]Istituto di Astrofisica e Planetologia Spaziali, Istituto Nazionale di Astrofisica (INAF/IFSI), Rome, Italy, [8]Brown University, Providence, RI, USA, [9]Jet Propulsion Laboratory, California Institute of Technology, Pasadena, CA, USA.

Introduction: Vesta's size and surface gravity, 0.25 m/s^2, place it in an intermediate category between terrestrial planets and small asteroids [e.g. 1]. Unlike Earth or Mars, Vesta lacks a protective atmosphere and consequently the dominant geologic process is impact cratering [e.g. 1,2,3]. The two most prominent impact features are large impact basins near Vesta's southern pole: Rheasilvia (500 km wide), which partially overlies an older basin, Veneneia (450 km wide) [3].

Previous studies have shown that impact processes not only form numerous craters on Vesta, but also induce the formation of large structural features termed fossae: the Saturnalia Fossae in the northern hemisphere and the Divalia Fossae around the equator [1,4,5]. It is proposed that Vesta's differentiated interior amplified and reoriented the stresses induced by the impacts and allowed the fossae, which are interpreted to be graben, to form [4]. Such amplification and reorientation does not occur on smaller, undifferentiated asteroids, like Lutetia, Eros and Ida, where smaller-scale impact-induced lineaments and grooves form [4].

This work expands upon the link between impact cratering processes and structural features on Vesta by presenting findings of a structural mapping study of the Saturnalia Fossae and a variety of other, smaller-scale, adjacent structural features. These structures are located in the northern hemisphere, primarily in two of Vesta's fifteen quadrangles, Caparronia and Domitia.

Methods: This work mainly uses clear filter Framing Camera images and mosaics from the Low Altitude Mapping Orbit (~20 m/pixel), overlain onto High Altitude Mapping Orbit 2 (~65 m/pixel) data to fill in coverage gaps. Geological mapping was carried out using ESRI ArcMap 10.0 software, the Small Body Mapping Tool [6] and JMARS (for Vesta).

Results: Full geological maps of Caparronia and Domitia quadrangles were produced, along with structural maps of the Saturnalia Fossae in the whole northern hemisphere and of the adjacent structures in Caparronia, Domitia and Floronia quadrangles.

Definition of Map Units. The geologic units in Caparronia and Domitia quadrangles were characterized and ordered from oldest to youngest, based mainly on cross-cutting relationships [further information in 7]: 1) Vestalia Terra unit, 2) cratered highlands unit, 3) Saturnalia Fossae trough unit, 4) Saturnalia Fossae cratered unit, 5) undifferentiated lobate unit, 6) dark lobate unit, 7) dark linear unit and 8) confined lobate unit. All units are either modified by impact cratering processes, directly formed by impact cratering processes or induced by impact-induced processes.

Observation and interpretation of structures.

i. Saturnalia Fossae. The Saturnalia Fossae are the principal structure in Vesta's northern quadrangles. There are a maximum of 5 fossae within the group, of which Saturnalia Fossa A is the largest structure, with a maximum width of ~43 km. In cross section Saturnalia Fossa A is an approximately symmetrical rounded depression, while fossae B–E are more asymmetric rounded depressions. Saturnalia Fossa A is also deeper than fossae B–E, with a maximum depth of ~4.5 km. The mean orientation of the fossae is ESE-WNW (Fig. a).

Tight clustering of the orientations of the fossae suggests a related formation mechanism. It has been previously suggested that Saturnalia Fossa A is a graben [4]. In profile Saturnalia Fossa A is the deepest fossae and is symmetrical, which is interpreted to be due to the presence of two large, symmetrical normal faults on either side, which form a graben. Fossae B-E are asymmetric in profile and significantly shallower than Saturnalia Fossa A and are consequently interpreted to be half-grabens. It is likely that they are formed by synthetic faults that may connect to the southernmost Saturnalia Fossa A fault at depth.

ii. Adjacent structures: minor ridges. The minor ridges are ~2-25 km long, are linear to curvilinear and are shallower than the fossae. Some minor ridges are observed to cross-cut impact craters. The mean orientation of the minor ridges is NE-SW (Fig. d). The orientations of the minor ridges can be divided into two dominant groupings of orientations: E-W, which is approximately parallel to the regional slope and NE-SW and N-S, which is not approximately parallel to regional slope.

The two groupings of minor ridges are interpreted to have two different formation mechanisms. The group of minor ridges aligned approximately parallel

to regional slope, E-W, may be accumulations of regolith that piled up as the material flowed under the control of the regional slope. However, this formation mechanism cannot be invoked for the minor ridges approximately aligned NE-SW and N-S. The morphology of the minor ridges closely resembles wrinkle ridges/ thrust scarps observed on the Moon [8], Mercury [9] and Mars [10]. Also, the observation that some minor ridges cross-cut impact craters is interpreted as further evidence that the minor ridges aligned NE-SW and N-S are the surface expression of thrust faults that thrust over older craters.

iii. Adjacent structures: grooves and crater chains. The grooves and crater chains are ~1-25 km long, are linear to curvilinear and are shallower than the fossae. Both have mean orientations of E-W (Figs. b and c). In some locations, a feature begins as a groove and merges into a crater chain and vica versa. Some grooves and crater chains are orientated radially around Calpurnia and Marcia craters. However, there are many other groupings of grooves and crater chains that are not clearly radial to an impact crater.

It is likely that the grooves and crater chains are end-members of the same type of feature. Secondary material from an impact scouring and bouncing across the surface commonly forms ejecta ray systems, which consist of grooves and secondary crater chains [e.g. 11]. Grooves and crater chains radial to Calpurnia and Marcia craters are interpreted to form in this way.

However, many of the E-W trending grooves and crater chains and not oriented radially to an impact crater and may have a tectonic origin. Pit crater chains on Earth and Mars are proposed to form by unconsolidated material draining down into extension fractures and/ or dilational normal faults in a more consolidated material at depth [12,13]. In this scenario the crater chains are pit crater chains and are the surface expression of funnels of down-draining material and the grooves represent a more even distribution of down-drained regolith.

Discussion: The structural features are classified into stages of formation by the scale of impact interpreted to have formed them and by their relative temporal relationships.

Stage 1: Formation of Saturnalia Fossae by the Veneneia impact. The fossae are interpreted to be older than the adjacent structures because of cross-cutting relationships and morphology. As discussed in the Introduction, the Saturnalia Fossae were induced by the large (>100 km wide) Veneneia impact [1,4,5].

Stage 2a: Formation of a sub-set of adjacent structures by the Rheasilvia impact. The minor ridges interpreted as thrust faults are oriented NE-SW and N-S and are approximately orthogonal to the grooves and pit crater chains that also have a structural origin, which are oriented E-W. Thus, since extension fractures form approximately orthogonal to thrust faults in shear zones [14] these structures are oriented as if they formed due to simple shear. Consequently, the shear over most of the surface of Vesta, which was a result of the large (>100 km diameter) Rheasilvia-forming impact [1,4,5], may have formed these adjacent structures.

Stage 2b: Formation of a sub-set of adjacent structures by small- and medium-scale impacts. The formation of the remaining adjacent structures is interpreted to be induced: a) by ejected secondary material forming grooves and secondary crater chains and b) by impact-induced seismic shaking [1] inducing the flow of regolith under the control of the regional slope, which formed E-W minor ridges. Near-by likely source craters are <100 km in diameter, i.e. small and medium scale.

References: [1] Jaumann R. et al. (2012) *Science, 336*, 687. [2] Russell C. T. et al. (2012) *Science, 336*, 684. [3] Schenk P. et al. (2012) *Science, 336*, 694. [4] Buczkowski D. L. et al. (2012) *Geophys. Res. Lett., 39*, L18205. [5] Bowling T. et al. (2013) *J. Geophys. Res-Planet., 118*, 1. [6] Kahn E. G. et al. (2011) *LPSC XXXXII*, Abstract #1618. [7] Scully J. E. C. et al. (2013) *Icarus*, in revision. [8] Watters T. R. et al. (2010) *Science, 329*, 936. [9] Watters T. R. et al. (2009) *Earth. Planet. Sci. Lett., 285*, 283. [10] Golombek M. P. et al. (2001) *J. Geophys. Res., 106*, 23811. [11] Melosh H. J. (2011) *Cambridge University Press*, 245. [12] Ferrill D. A. et al. (2011) *Lithosphere, 3*, 133. [13] Wyrick D. et al. (2004) *J. Geophys. Res., 109*, E06005. [14] Sylvester A. G. (1988) *Geol. Soc. Am. Bull., 100*, 1666.

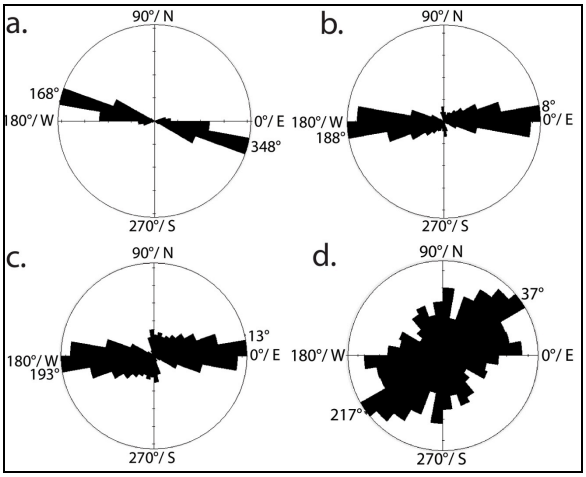

Figures a-d. Rose Diagrams displaying orientations of (a) Saturnalia Fossae, (b) crater chains, (c) grooves and (d) minor ridges.

GRAVITATIONAL DEFORMATION AND THERMAL HYSTORY OF VESTA. E. N. Slyuta[1] and S. A. Voropaev[1], [1]Vernadsky Institute of Geochemistry and Analytical Chemistry, Russian Academy of Sciences, 119991, Kosygin St. 19, Moscow, Russia. slyuta@mail.ru.

Introduction: Gravitational loading in small bodies in the form of stress deviator caused by mass and a nonequilibrium figure of bodies, is constant and actually exists from the moment of their formation [1]. There's no creep in small Solar system bodies. All small Solar system bodies irrespective of their structure from icy to metal including stony bodies are elastic bodies which possess ultimate and yield strength [2]. An analysis of mechanical properties of small stony bodies has been carried out with a model, which uses the elastic theory with ultimate strength for a three-dimensional self-gravity body, and allows the exact solution of differential stresses in a solid elastic body to be received and to carry out their analysis. The value and distribution of stress deviator in small body depends on mass, size, density, figure eccentricity and Poisson coefficient and defined by equation $\tau_{max}=\sigma_0 F(\varepsilon,\nu)$ (1), where dimension factor $\sigma_0 = \frac{9}{8\pi}\frac{GM^2}{a^2 bc}$, where G - gravitational constant, M – mass ($M = \frac{4}{3}\pi\rho_0 R_m^3$, where R_m – mean radius), a, b and c – main semiaxes, and $F(\varepsilon,\nu)$ – dimensionless function, which depends on figure eccentricity (ε) and Poisson coefficient (ν) [3]. If magnitude of stress deviator is greater than the compressive strength or yield point, the irregular figure of a small body as a result of gravitational deformation is transformed into a spherical equilibrium shape of a planetary body. Gravitational deformation is accompanied by gravitational densification and gravitational strengthening of a material at the entire body due to three-dimensional gravitational compression accompanied by two basic mechanisms of plastic deformation [1, 3].

Small stony bodies: Knowing the physical and mechanical properties of ordinary and carbonaceous chondrites [4], we can estimate (eq. 1) the critical mass and the size of small silicate bodies that undergo gravitational deformation. Small stony bodies composed of ordinary chondrites are characterized by compressive strength in the range of $105\leq\sigma_p\leq203$ MPa [5]. The critical size of a small body with the eccentricity of the figures typical of the small bodies of the S-type with an average axial ratio a/c=0.69 [2, 4], will be in the range of $(862\times595)\leq R_{cr}\leq(1198\times827)$ km, or in terms of the mean radius of a small body of equal volume - $R_{cr}\leq673\leq935$ km.

Small stony bodies of the C-type, consisting of carbonaceous chondrites are characterized by compressive strength in the range of $35\leq\sigma_p\leq70$ MPa [4]. The critical size of a small body with the eccentricity of the figures typical of the small bodies of the C-type with an average axial ratio a/c = 0.80 [2], will be in the range of $(784\times627)\leq R_{cr}\leq(1109\times887)$ km, or in terms of the mean radius of a small body of equal volume - $675\leq R_{cr}\leq956$ km. Thus, the critical radius of a small body of ordinary chondrites exceed 673 km and for carbonaceous chondrites - 675 km. With almost the same size, however, ordinary and carbonaceous chondrites differ significantly from each other in the critical mass and the threshold stress deviator (Fig. 1).

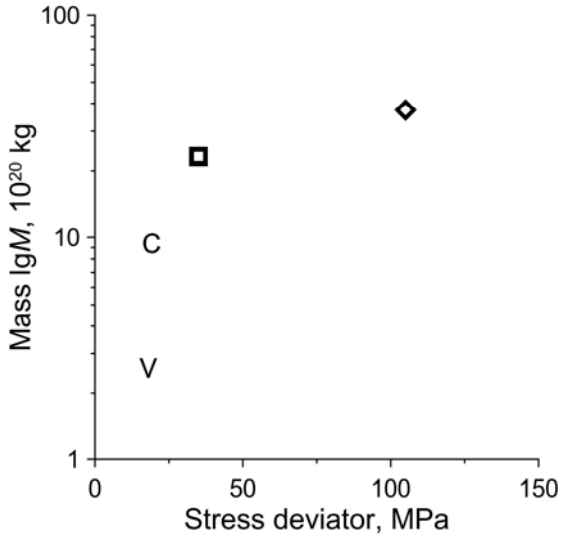

Fig. 1. The critical mass of small stony bodies, depending on the yield strength: ◇ - S-type small bodies (ordinary chondrites); ◘ - C-type small bodies (carbonaceous chondrites); V – Vesta; C – Ceres.

4 Vesta: The smallest silicate planetary body in the solar system is the asteroid 4 Vesta. Vesta has a spherical shape of radius R=286.3×278.6×223.2 km (R_m=262.7 km) and a high density ρ_0=3456 kg m^{-3} [6]. From geochemical point of view spectral mineralogical characterization of a surface generally corresponds to almost undamaged basaltic crust of a differentiated body [7]. It is assumed that mantle diogenity were dumped on the surface due to formation of impact basin, which struck eucrites (basaltic) crust of a differentiated asteroid [7]. Vesta's differentiation onto crust and mantle is a result of fairly active and complex

magmatic evolution of the asteroid, which is typical for planetary bodies.

If, in accordance with equation (1) we estimate the present value of stress deviator on Vesta, we will find that even in comparison with carbonaceous chondrites strength it is very small and is 18 MPa (Fig. 1). Strength properties of basaltic achondrites, perhaps, are similar to the basic and ultrabasic terrestrial rocks [1], or, at least, ordinary chondrites [5]. Such significant difference between the magnitude of the stress deviator and the yield strength of silicates confirms that Vesta in the early stages of its existence has subjected to strong heating, and, perhaps, even to complete melting. Otherwise, Vesta would never has acquired be the spherical equilibrium shape and, moreover, it would not has been differentiated.

But this is not the end of Vesta evolution. A very small stress deviator compared with the yield strength of silicates means that at the present time isostatic compensation mechanism, which is a necessary attribute of any planetary body, on Vesta does not work. As the cooling of the body and a corresponding increase in the yield strength of material, Vesta gradually from the category of planetary bodies has moved into the category of small bodies, and currently represents although spherical and differentiated (hot tracks of the past), but ordinary dead "cobble". To Vesta remained as planetary body and, like on other planetary bodies, an isostatic mechanism is continued to operate (i.e. gravitational deformation), the mass of Vesta should exceed its current value is more than an order of magnitude (Fig. 1) [1].

In a few billion years of collisional evolution spherical shape of Vesta without isostatic compensation will change to an irregular shape of a small body. And this process began back 2.1 billion years ago, when impact basin Veneneia in diameter of 400 km and a depth of 12 km has formed, and 1 billion years ago, when impact basin Rheasilvia, in diameter of 500 km and a depth of 19 km has formed [8]. Age of residual magnetization of eucrites (meteorite Allan Hills A81001), which is equal to 3.69 billion years old, suggests that Vesta was already cooled down at the time of formation of these impact basins. Since both the crater formed in South Pole, they are mechanically shortened rotation axis (c) on to 20 km, and oblateness ($(a-c)/c$) increased from 0.15 to 0.21 [9]. It is likely that formation of two systems of long troughs (graben) in the equatorial region of Vesta, one of which is oriented relative to the center of Veneneia, and the other is associated with Rheasilvia [10], is result of elastic deformation of solid Vesta in process of formation of large impact basins.

1 Ceres: There is another planetary body in the main belt [1], it is asteroid 1 Ceres in radius 487.3×454.7 км (R_m=476.2 km) [11]. Mineralogy of Ceres surface according to spectral data corresponds to carbonaceous chondrites, i.e. class C [12]. The diameter of Ceres is twice as much as Vesta, but due to the low density (ρ_0=2077 kg m^{-3}), the mass is only 7 times as much as mass of Vesta. Accordingly, a current value of stress deviator is also low and equal to 19.2 MPa, i.e. is slightly more than that of Vesta. It was assumed that bulk composition of Ceres could really be presented chondrites characterized by low strength [1]. However, the observed value of stress deviator is actually half of minimum compressive strength of carbonaceous chondrites (Fig. 1). Apparently, there is significant amounts even less durable material than carbonaceous chondrites in Ceres. It may be, for example, mixture of carbonaceous chondrites and ice. If strength of carbonaceous chondrites is significantly higher than the stress deviator on Ceres, then the yield strength of the ice, on the contrary, an order of magnitude less than the stress deviator [1]. Low density of Ceres also points to significant presence of ice in Ceres [6].

Summary: Significant difference between the magnitude of the stress deviator on Vesta and the yield strength of stony meteorites confirms that Vesta in the early stages of its existence has subjected to strong heating, and, perhaps, even to complete melting. But this is not the end of Vesta evolution. As the cooling of the body and a corresponding increase in the yield strength of material, Vesta gradually from the category of planetary bodies has moved into the category of small bodies, and currently represents although spherical and differentiated (hot tracks of the past), but ordinary dead "cobble". To Vesta remained as planetary body and, like on other planetary bodies, an isostatic mechanism is continued to operate (i.e. gravitational deformation), the mass of Vesta should exceed its current value is more than an order of magnitude.

References: [1] Slyuta E.N. and Voropaev S.A. (1997) *Icarus*, *129*, 401-414. [2] Slyuta E.N. (2013) *LPSC XXXXIV*, Abstr. #1117. [3] Slyuta E.N. and Voropaev S.A. (2014) *Icarus* (In press). [4] Slyuta E. N. (2014) *Sol. Sys. Res*. (In press). [5] Slyuta E. N. (2010) *LPSC XXXXI*, Abstr. #1103. [6] Russel et al. (2012) *Science*, *336*, 684-686. [7] De Sanctis et al. (2012) *Science*, *336*, 697-700. [8] Schenk et al. (2012) *Science*, *336*, 694-697. [9] Jaumann et al. (2012) *Science*, *336*, 687-690. [10] Thomas et al. (2005) *Nature*, *437*, 224-226. [12] Gaffey et al. (1989). In Asteroids II (Eds. R. P. Binzel, T. Gehrels, M. S. Matthews). Univ. Arizona Press, Tucson. 98–127.

VESTA – COMPOSITIONAL FINGERPRINT OF SMALL FRESH IMPACT CRATERS. K. Stephan[1], R. Jaumann[1,2], M. C. De Sanctis[3], F. Tosi[3], E. Ammannito[3], K. Krohn[1], F. Zambon,[3], S. Marchi[4], O. Ruesch[5], K.-D. Matz[1], T. Roatsch[1], F. Preusker[1], C.A. Raymond[6] and C. T. Russell[7], [1]Institute of Planetary Research, German Aerospace Center (DLR), Berlin, Germany (Katrin.Stephan@dlr.de), [2]Freie Universität Berlin, [3]INAF, Rome, Italy, NASA Lunar Science Institute, Boulder, CO, USA, [5]Westfälische Wilhelms-Univ. Münster, Germany, [6]Jet Propulsion Laboratory, California Institute of Technology, Pasadena, USA, [7]UCLA, Institute of Geophysics, Los Angeles, USA

Introduction: In order to further understand the composition of the upper as well as lower parts of Vesta's crust, small impact crater (< 10km in diameter), which show distinct ejecta and represent unweathered surface areas, have been identified and their spectral properties investigated with respect to their geological and geomorphological context [1]. The study was performed based on data acquired by the Visual and Infrared Spectrometer (VIR) [2], which observed Vesta's surface between 0.25 and 5.1µm with a pixel ground resolution of ~60 m/pixel. The geological and geomorphological context is provided by images acquired by the Framing Camera (FC) with a pixel ground resolution up to 20 m/pixel [3].

Spectral properties: The ejecta blankets of small fresh craters appear bright or dark in the visible light with a sharp contrast to the surrounding region (Fig. 1). Bright ejecta are dominated by howardite-like material as expected for Vesta's crust and/or ejecta of the southern impact basin Rheasilvia, which cover most of Vesta's southern hemisphere (Fig. 3). Dark ejecta associated with dark impact craters do not show a different pyroxene composition than the bright ejecta but an additional strongly absorbing, spectrally neutral compound, supporting an origin from carbon-rich impactors (Fig. 2).

Mostly, the crater itself is characterized by a similar albedo such as the ejecta. Only a few impact craters show bright ejecta and a dark crater floor (Fig. 1). Few of these impact craters could be identified to contain material that resembles diogenites, which are expected to exist in the deeper parts of Vesta's interior (Fig. 2+3). One of these impact craters is directly located at Matronalia Rupus (Fig. 1) allowing a direct view into the subsurface. This scarp is known to mark the rim of the Rheasilvia impact basin.

Intriguingly, both type of materials, i.e. the bright ejecta as well as the darker slumping material extending from the crater floor appear yellow in the ratio color composite classifying them as fresh (Fig. 1). Both materials also show a pronounced pyroxene signature.

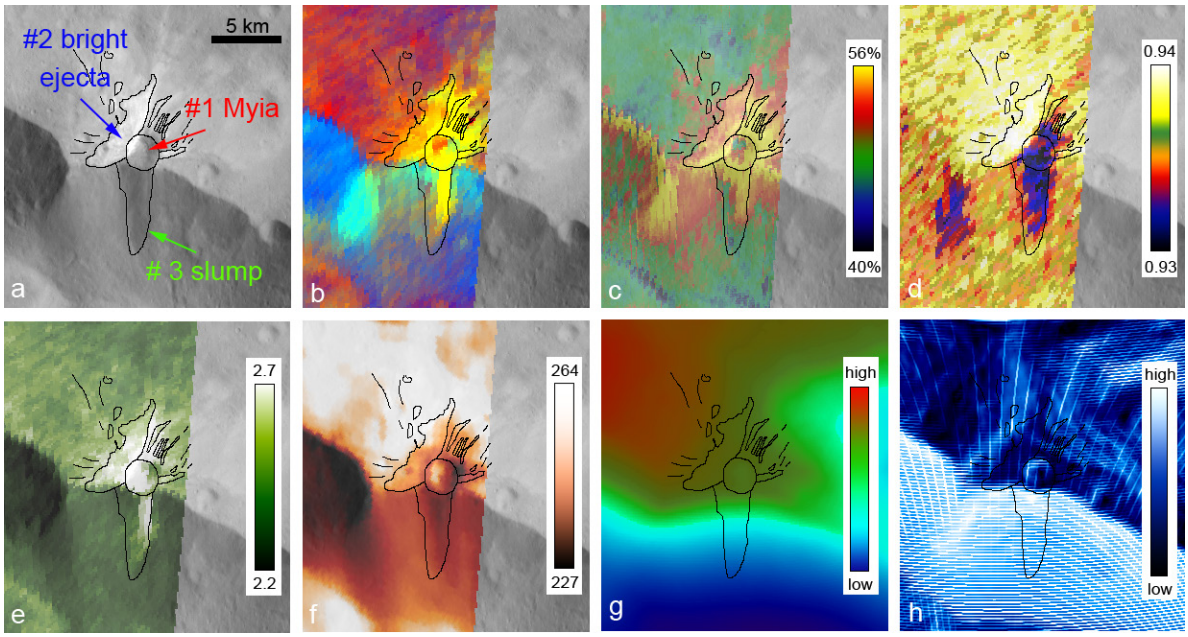

Figure 1

(Fig. 2+3), which is contrary to the variations in the spectral properties elsewhere on Vesta's surface. Usually, bright material corresponds to a strong pyroxene signature with deep absorptions near 1 and 2µm, whereas this signature is surpressed, where the visible albedo is low. Finally, VIR spectra show a possible slight shift in the position of the 1µm-pyroxene absorp-

tion toward shorter wavelength. This points a diogenitic composition of the material in the crater and the slump (Fig. 3).

Geological implications: The spectral variations mirror the global trend with a more diogenitic composition in the Rheasilvia basin and an eucrite-/howardite-like composition in the geologically older densely cratered equatorial region. This points to the interpretation that the bright ejecta might be related to the Rheasilvia basin whereas the darker material resembles excavated in-situ subsurface material. This interpretation is strengthend by the fact that the bright ejecta were formed only in the western part of the small impact crater in the direction of slightly higher elevation (Fig. 3) possibly representing an addional upper surface layer of former ejecta of Rheasilvia newly excavated.

References: [1] Stephan, K. et al. (2013) A compositional and geological view of fresh ejecta of small impact craters on asteroid 4 Vesta. submitted. [2] De Sanctis et al. (2011), The VIR Spectrometer, Space Science Reviews, 163, 329-369. [3] Sierks, H., et al. (2011), The Dawn Framing Camera, Space Science Reviews, 163, 263-327.

Figure captions:

Fig. 1: Spectral parameters near impact crater Myia: a) FC Clear filter images, b) color-ratio composite, c) BII band depth, d) BII position, e) VIS/UV ratio, f) local surface temperature [K], g) local topography, h) local topographic slope.

Fig. 2: VIR spectra of 1) bright, 2) dark and 3) diogenitic material in comparison to HED laboratory spectra and carbon as the darkening compound (RELAB spectral library); (lower left): comparison of the BI absorption band depth of the selected impact crater materials to the visual geometric albedo, and (lower right): BI and BII band center positions in comparison to the HED laboratory spectra (RELAB).

Fig. 3: Ratio spectrum enhancing the spectral characteristics of the bright ejecta compared to their "weathered" surroundings showing several small absorptions related to Fe2+ in comparison to laboratory spectra (USGS) of orthopyroxenes i.e. hypersthene of various grain sizes (a) 7, b) 23, c) 50, d) 180µm) and e) enstatite as well as clinopyroxenes f) hedenbergite, g) diopside and h) augite.

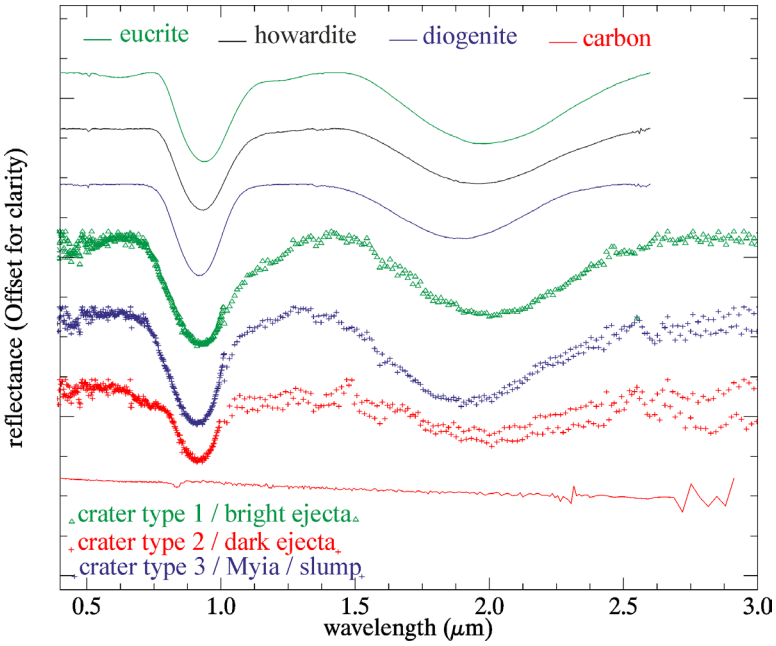

Figure 2

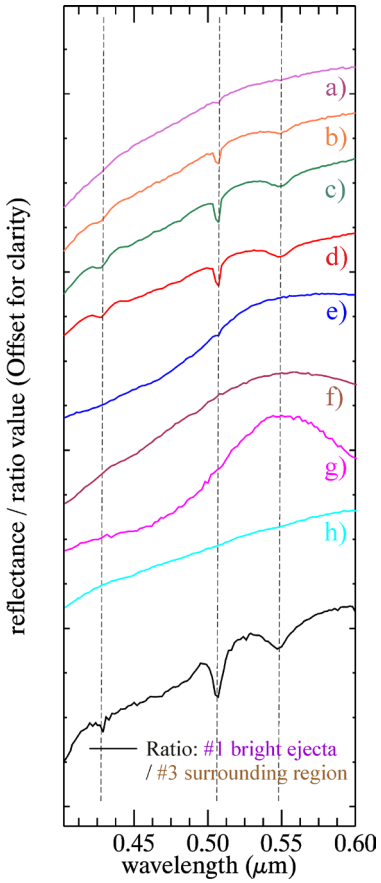

Figure 3

THE EFFECTS OF GIANT IMPACT INTO A DIFFERENTIATED VESTA: IMPLICATIONS FOR LARGE-SCALE TROUGH FORMATION. A. M. Stickle[1], P.H. Schultz[2], D.L. Buczkowski[1], and K.A. Iyer[1]. [1]Johns Hopkins University Applied Physics Laboratory, Laurel MD, angela.stickle@jhuapl.edu; [2]Brown University Geological Sciences, Providence, RI.

Introduction: The Dawn mission observed two sets of linear faults on the surface of the asteroid 4 Vesta [1-3]. Observations indicate that these features are likely related to the two large impact basins on the south pole of Vesta: Rheasilvia and Veneneia; though they appear to be slightly offset from the basin centers [2]. Our experimental and numerical results show that this is a natural consequence of oblique impacts into a spherical, differentiated target. Initial experiments and models show that large impacts result in different patterns of tensile stress and pressure for differentiated v. undifferentiated targets, and that sets of shear planes develop within the subsurface of the body following impact [4-5]. These subsurface features can propagate to the surface under combined tensile-shear loading to create sets of approximately linear faults on the surface.

Experimental Details and Model Setup: Impact experiments into spherical PMMA were performed at the NASA Ames Vertical Gun Range (AVGR) to track the time evolution of subsurface damage in spherical targets [e.g., 5]. For this study, a 6.35-mm Pyrex projectile impacted the spherical target at angles ranging from 40°-65° at 5 km/s. High-speed imaging allowed tracking the damage within the spheres at a high time resolution, which was then compared with three-dimensional CTH calculations [6].

For the direct comparison, the CTH calculations were done with identical impact conditions to the experiments to identify observed failure conditions observed inside the targets. Adaptive Mesh Refinement was used to track high-pressure regions in detail [6-7]. Pyrex was assumed to behave as a geologic material with a pressure-dependent yield surface; the PMMA spheres assume a von Mises plasticity model coupled to the Johnson-Cook Fracture damage model (JCF), which is used here to track shear deformation [8]. Tensile failure is considered separately.

While laboratory simulations provide important information about the processes occurring following oblique impacts, these direct comparisons also provide confidence for interpreting large-scale models. Specifically, we considered impacts into the asteroid 4 Vesta. To provide constraints on the formation of the trough systems, we examined the effects of impact angle (15°, 30°, 45°, and 90°), projectile size, internal structure of Vesta (e.g., un-, partially-, and fully- differentiated, as well as varying the core size), and material properties of the asteroid itself. Fully differentiated models included an iron core, dunite mantle and either basalt or basalt-analog crusts. The basalt-analog materials have fully described equation of state (EOS) and strength models known to undergo brittle fracture and have densities similar to the modeled basalt crusts. All impacts were at 5 km/s. Oblique impacts examined the effects of a 100-km dunite projectile into a fully differentiated Vesta, with structure after [9], and the calculation included self-gravity for the asteroid and the impactor. Normal impacts were simulated into three structures representing ancient Vesta: undifferentiated Vesta, and a two- or three-layer Vesta [after 10]. All models are of a ~530 km sphere, with core sizes ranging from 164-220 km.

Results and Discussion: The combination of laboratory experiments and numerical models allow us to track the state of the material, the modes of deformation, and the damage and fracture growth following impact (at both small and large scales).

Laboratory Experiments and Small-Scale CTH. Direct comparisons were made between observations of damage growth in the AVGR experiments and corresponding CTH models. A typical failure pattern from thr AVGR experiment is shown in Figure 1B. Observation of damage evolution coupled with CTH models of these experiments indicate that the near-surface failure haze is the result of incipient spallation at the farside of the target, the central damage stalk is a result of tensile strain, while the sub-parallel failure planes form due to high magnitudes of shear stress (Figure 1A). The orientation of these damage structures depends on impact angle and velocity, but they all evolve in the same manner.

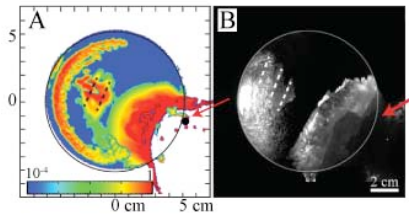

Figure 1. Comparison of lab-scale CTH simulations with AVGR experiment showing shear failure planes. (left) CTH simulation showing damage from both shear and spallation overlain onto each other, (right) Final damage from the AVGR experiment, with failure planes shown by white dotted lines. After [5]

Large-scale CTH models of Vesta. Large-scale CTH simulations, in conjunction with insights gained from laboratory experiments, provide new clues into the formation of the troughs on Vesta. Exploring a

large parameter space allows examination of the effects of impact parameters on subsurface damage and possible formation scenarios for the large-scale fracture systems.

Models examining the effect of differentiation on internal damage and fracture indicate that Vesta was likely differentiated at the time when Rheasilvia and Veneneia formed. The results of these models show that different patterns of fracture (Fig. 2) and pressure (Fig. 3) develop in a differentiated sphere (Fig. 2 center and right; Fig. 3, right) compared to an undifferentiated sphere of the same material and diameter (Figs. 2, 3, left). While these first-order models have yet to fully mimic the observations of troughs on Vesta, they do demonstrate that the density contrast in Vesta's differentiated interior affects the stresses resulting from the Rheasilvia and Veneneia impacts. It is this impedance mismatch that is suggested to be responsible for the development of Vesta's planet-like troughs [2]. Similar differences between differentiated and undifferentiated targets are seen for models of oblique impacts.

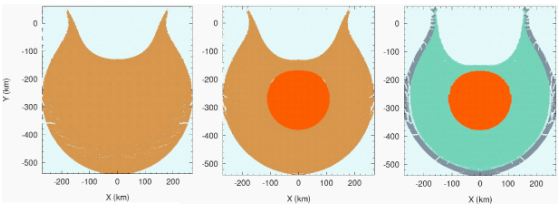

Figure 2. CTH hydrocode models of giant impact into Vesta showing materials following impact. Red is iron, green is dunite, brown is higher-density basalt analog and grey is lower-density basalt analog. Fracture due to tensile stresses changes depending on the amount of differentiation [4].

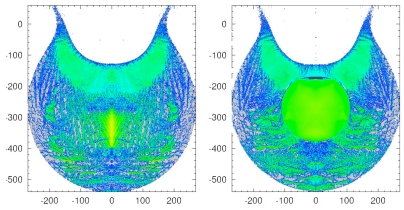

Figure 3. CTH models of a giant impact into an undifferentiated (left) and differentiated (right) Vesta yield very different pressure profiles depending on the presence or absence of a core. Though pressure values are not given in this image, changes in patterns of pressure can be observed [4].

In both normal and oblique impact cases, large regions of Vesta are subjected to tensile stresses great enough for fracture and failure. Because they are coupled to a damage model tracking shear deformation, the oblique impact models also show that these regions overlap with, or form directly prior to, regions of high shear stress. Temporally, the combination of these two stress states suggests that the subsurface of Vesta may be damaged or fractured due to tensile stresses but then fail and slide due to high shear-stresses set up behind the shock wave. This pattern is seen even to late times, as the shock, rarefaction, and shear waves reflect and coalesce throughout the body (Figure 4). The combination of high shear-stress magnitudes overprinting weakened or pre-damaged material lasts for hundreds of seconds, and during this time damaged material is continually subjected to high shear stress (Figure 4). This combination creates localized shear planes that then propagate to the surface. Thus, the linear features observed on Vesta may be the surface expression of large-scale subsurface shear failure and faulting from deep in the interior, similar to what is seen in laboratory experiments.

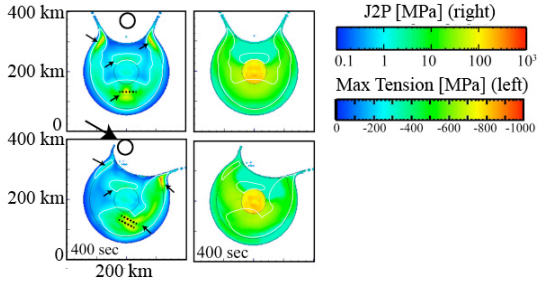

Figure 4. Large-scale time sequence of CTH simulation results showing maximum tensile stress (left) and the magnitude of shear stress (right) within Vesta. (top) center plane of Vesta on a plane perpendicular to the impact trajectory; (bottom) center plane parallel to the impact trajectory. The initial impactor size (100 km) and trajectory (30°) are shown for scale. Note here that the south pole of Vesta would be at the top of these images. After [5].

These general results are true for varying impact angle (30-45°) as well as impactor and core size (50-100 km and 164-220 km, respectively). At 15°, a large portion of the projectile decapitates and decouples from the impact, significantly reducing subsurface stress and damage formation. The results from differing impact angles also may allow constraints to be placed on impact trajectory. If the subsurface shear planes observed in the laboratory experiments are small-scale analogs to the trough features on Vesta, then the orientation of the damage region might also be used to constrain the impact trajectory and location by comparing the angle of the damage offset from the impact crater antipode.

References: [1] Jaumann, R. *et al.* (2012) *Science*, 336, 687-690; [2] Buczkowski, D. *et al.* (2012) *Geophys. Res. Let.*, 29, L18205; [3] Sierks, H. et al. (2011), *Space Sci. Rev.*, *163*, 263-327; [4] Buczkowski, D.L., et al. (2012) Paper presented at the GSA Annual Meeting; [5] Stickle, A.M. et al. (2013) *44th LPSC* Abs. 2417; [6] McGlaun, J.M. et al. (1990) *Int. J. Imp. Eng.* 10, 351-360; [7] Crawford, D.A. (1999) Paper presented at 15th US Army Symposium on Solid Mechanics, April 12-14; [8] Johnson, G.R. and W.H. Cook (1995) *Engr. Frac. Mech*, 21, 31-48; [9] Ruzicka, A.J *et al.* (1997) *Met. and Planet. Sci.* 32(6), 825-840; [10] Raymond, C.A., et al (2012) *43rd LPSC* Abs. 1007.

MEAN COMPOSITION OF FELDSPAR IN HED METEORITES AND IN PROTOPLANET VESTA. M. Szurgot, Lodz University of Technology, Center of Mathematics and Physics, Al. Politechniki 11, 90 924 Lodz, Poland, (mszurgot@p.lodz.pl).

Introduction: Feldspars are important minerals common in terrestrial and in extraterrestrial rocks. Data on the mean composition of feldspar in various meteorites, mainly chondrites and achondrites have been recently collected and analysed [1]. In our previous and present studies the mean composition of meteorites was the main source of data on feldspar, since the mean bulk elemental composition of meteorites contains important data on mean composition of various minerals, including plagioclase feldspar. HED meteorites and their parent body belong to very interesting and important extraterrestrial objects. Our intersts include also thermal properties of meteorites, asteroids and terrestrial planets. Specific heat capacity, heat capacity, and thermal capacity of Vesta have been recently estimated [2]. Dawn mission data enriche our knowledge on 4 Vesta, which is considered to be a parent body of HED meteorites. The aim of the paper was to determine and analyze the mean composition of feldspar in HED meteorites and in protoplanet Vesta.

Results: Data on the mean bulk elemental composition of HED meteorites and on predicted composition of HED parent body were used to calculate albite ($NaAlSi_3O_8$), anorthite ($CaAl_2Si_2O_8$) and orthoclase ($KAlSi_3O_8$) content. To determine albite (Ab), anorthite (An), and orthoclase (Or) content in feldspar the following relationships derived by Szurgot [1] were used:

$$Ab=100\cdot 2\cdot Na/[Al+Na+K], \quad (1)$$

$$An=100\cdot [Al-Na-K]/[Al+Na+K], \quad (2)$$

$$Or=100\cdot 2\cdot K/[Al+Na+K], \quad (3)$$

where Ab, An, and Or are expressed in mol%, and sodium (Na), potassium (K) and aluminum (Al) contents in at%. To derive eqs.(1)-(3) it was assumed that sodium is present only in albite, potassium only in orthoclase, and aluminum only in feldspar. Anorthite calcium content is expressed by Al content.

When sodium, potassium, and aluminum content are given in weight percent instead of atomic percent the modified equations are used:

$$Ab=100\cdot 2\cdot (Na^*/Al^*)\cdot (M_{Al}/M_{Na})/D, \quad (4)$$

$$An=100\cdot C/D, \quad (5)$$

$$Or=100\cdot 2\cdot (K^*/Al^*)\cdot (M_{Al}/M_K)/D, \quad (6)$$

where C and D are represented by

$$C=[1-(Na^*/Al^*)\cdot (M_{Al}/M_{Na})-(K^*/Al^*)\cdot (M_{Al}/M_K)], \quad (7)$$

$$D=[1+(Na^*/Al^*)\cdot (M_{Al}/M_{Na})+(K^*/Al^*)\cdot (M_{Al}/M_K)], \quad (8)$$

where M_{Al}, M_{Na}, and M_K represent elemental atomic weight of aluminum, sodium, and potassium, and Na*, Al*, and K* are sodium, aluminum and potassium content in wt%.

Our calculations reveal mean composition of feldspar determined for the three achondrite groups: eucrites Ab11An89Or0.6, howardites Ab10An89Or0.5, and diogenites Ab17An81Or1.4 (Tables 1-3). The mean composition of feldspar estimated by various models of HED parent body is Ab10An90Or0.5 (Table 4), and is very close to the eucrite mean feldspar, and to the howardite mean feldspar (Tables 1, 2). The range of anorthite content in eucrites amounts to An78-96, in howardites An87-91, and in diogentes An50-96 (Tables 1-3). This means that our data reveal for HED achondrites the range of anorthite content An50-96. The range of albite content in eucrites Ab4-22, in howardites Ab8-12, and in diogentes Ab4-50. For the whole HED group we have Ab4-50, and orthoclase content is equal to Or0-7, as for diogentes. For eucrites we have Or0-1.8, and for howardites Or0-1.

Table 1 Mean composition of feldspar in eucrites.

Meteorite name	Feldspar	
Petersburg	$Ab_{21.8}An_{78.2}$	Ab22An78
Chervony Kut	$Ab_{11.9}An_{86.3}Or_{1.8}$	Ab12An86Or2
Nuevo Laredo	$Ab_{12.8}An_{86.4}Or_{0.8}$	Ab13An86Or1
HaH 286	$Ab_{12.4}An_{87.6}$	Ab12An88
Stannern	$Ab_{11.4}An_{87.8}Or_{0.8}$	Ab11An88Or1
Petersburg	$Ab_{11.1}An_{88.3}Or_{0.6}$	Ab11An88Or1
Pasamonte	$Ab_{10.6}An_{88.7}Or_{0.7}$	Ab10An89Or1
Y 74450	$Ab_{9.5}An_{89.0}Or_{1.5}$	Ab10An89Or1
Sioux County	$Ab_{9.8}An_{89.8}Or_{0.5}$	Ab10An90
NWA 4039	$Ab_{8.6}An_{91.4}$	Ab9An91
Serra de Mage	$Ab_{4.5}An_{94.5}Or_{0.1}$	Ab5An95
ALH A81001	$Ab_{3.9}An_{95.8}Or_{0.3}$	Ab4An96
Range	$Ab_{3.9\text{-}21.8}An_{78.2\text{-}95.8}Or_{0\text{-}1.8}$	
		Ab4-22An78-96Or0-2
Mean	$Ab_{10.7\pm4.5}An_{88.7\pm4.4}Or_{0.6\pm0.6}$	
	Ab11±5An89±5Or0.6±0.6	

Individual meteorites reveal mean composition of feldspar: i) eucrites: Chervony Kut Ab12An86Or2, Pasamonte Ab10An89Or1, Yamato 74450 Ab10An89Or1, Stannern Ab11An88Or1, Sioux County Ab10An90, Nuevo Laredo Ab13An86Or1, Petersburg Ab11-22An78-88Or0-1, HaH 286 Ab12An88,

NWA 4039 Ab9An91, Serra de Mage Ab5An95, ALH A81001 Ab4An96; ii) howardites: Bununu Ab12An87Or1, Malvern Ab11An88Or1 Kapoeta Ab10.5An89Or0.5, Bholghati Ab10An89Or0.6, Frankfort Ab10An90Or0.5, Yurtuk Ab10An90, Y 7308 Ab10An90Or0.4, Y 82049 Ab8An91Or0.5**;** iii) diogenites: NWA 4965 Ab50An50, Ellemeet Ab31An63Or6, Tatahouine Ab16An83Or1, Shalka Ab20An79Or1, Johnstown Ab4-37An56-96Or0-7, Y 791200 Ab10An90, Y 75032 Ab9An90-91Or0-0.4, NWA 1461 Ab8An92, LAP 91900 Ab6An94.

Table 2 Mean composition of feldspar in howardites.

Meteorite name	Feldspar	
Bununu	$Ab_{11.8}An_{87.4}Or_{0.8}$	Ab12An87Or0.8
Malvern	$Ab_{11.5}An_{87.5}Or_{1.0}$	Ab11An88Or1
Kapoeta	$Ab_{10.5}An_{89.0}Or_{0.5}$	Ab10.5An89Or0.5
Kapoeta	$Ab_{10.4}An_{89.1}Or_{0.5}$	Ab10.5An89Or0.5
Bholghati	$Ab_{10.3}An_{89.1}Or_{0.6}$	Ab10An89Or0.6
Frankfort	$Ab_{9.9}An_{89.6}Or_{0.5}$	Ab10An90Or0.5
Yurtuk	$Ab_{10.0}An_{90.0}$	Ab10An90
Y 7308	$Ab_{9.5}An_{90.1}Or_{0.4}$	Ab10An90Or0.4
Y 82049	$Ab_{8.3}An_{91.2}Or_{0.5}$	Ab8An91Or0.5
Range	$Ab_{8.3\text{-}11.8}An_{87.4\text{-}91.2}Or_{0\text{-}1}$	
	Ab8-12An87-91Or0-1	
Mean	$Ab_{10.2\pm1.0}An_{89.2\pm1.2}Or_{0.5\pm0.3}$	
	Ab10±1An89±1Or0.5±0.3	

Table 3 Mean composition of feldspar in diogenites.

Meteorite name	Feldspar	
NWA 4965	$Ab_{50.5}An_{49.5}$	Ab50An50
Johnstown	$Ab_{36.4}An_{56.3}Or_{7.3}$	Ab37An56Or7
Ellemeet	$Ab_{31.2}An_{62.6}Or_{6.2}$	Ab31An63Or6
Shalka	$Ab_{19.7}An_{79.4}Or_{0.9}$	Ab20An79Or1
Tatahouine	$Ab_{15.9}An_{82.7}Or_{1.4}$	Ab16An83Or1
Y 791200	$Ab_{10.0}An_{90.0}$	Ab10An90
Y 75032	$Ab_{9.2}An_{90.4}Or_{0.4}$	Ab9An90Or0.4
Y 75032	$Ab_{9.4}An_{90.6}$	Ab9An91
NWA 1461	$Ab_{7.9}An_{92.1}$	Ab8An92
Johnstown	$Ab_{7.0}An_{92.6}Or_{0.4}$	Ab7An93Or0.4
LAP 91900	$Ab_{6.3}An_{93.7}$	Ab6An94
Johnstown	$Ab_{4.3}An_{95.7}Or_{0.4}$	Ab4An96Or0.4
Range	$Ab_{4.3\text{-}50.5}An_{49.5\text{-}95.7}Or_{0\text{-}7.3}$	
	Ab4-50An50-96Or0-7	
Mean	$Ab_{10.2\pm1.0}An_{89.2\pm1.2}Or_{0.5\pm0.3}$	
	Ab17±15An81±16Or1.4±2.5	

Table 4 presents the mean composition of Vestan feldspar resulting from various models of Vesta.

Table 4 Mean composition of feldspar in Vesta calculated for mean bulk composition of HED parent body assumed in various models.

Composition data	Feldspar	
RD97 (CM)	$Ab_{11.3}An_{86.2}Or_{2.5}$	Ab11An86Or2.5
Mason 67	$Ab_{13.4}An_{86.6}$	Ab13An87
RD97 (L)	$Ab_{11.7}An_{87.8}Or_{0.5}$	Ab12An88Or0.5
RD97 (CI)	$Ab_{11.3}An_{88.1}Or_{0.6}$	Ab11An88Or0.6
RD97 (EH)	$Ab_{11.2}An_{88.4}Or_{0.4}$	Ab11An88Or0.4
Jones 84	$Ab_{10.6}An_{88.8}Or_{0.6}$	Ab11An89Or0.6
DW80	$Ab_{10.4}An_{89.0}Or_{0.6}$	Ab10An89Or0.6
CD77Met	$Ab_{7.4}An_{92.6}$	Ab7An93
CD77	$Ab_{7.0}An_{93.0}$	Ab7An93
Morgan78	$Ab_{6.4}An_{93.3}Or_{0.3}$	Ab6An93Or0.3
Hertogen77	$Ab_{6.6}An_{93.4}$	Ab7An93
Range	$Ab_{6.4\text{-}13.4}An_{86.2\text{-}93.4}Or_{0\text{-}2.5}$	
	Ab6-13An86-93Or0-3	
Mean	$Ab_{9.8\pm2.4}An_{89.8\pm2.8}Or_{0.5\pm0.7}$	
	Ab10±2An90±3Or0.5±0.7	

Source of data in Table 4: RD97 are Righter and Drake data [3], Jones 84 are Jones data [4], Mason 67 are Mason data [5], DW80 are Dreibus and Wanke data [6,7], CD77 are Consolmagno and Drake data [8], Morgan 78 are Morgan et al. data [9], and Hertogen77 are Hertogen et al. data [10].

Conclusions: The mean composition of feldspar in HED parent body (Ab10An90Or0.5) is close to the eucrite and howardite composition of feldspar. This is expected since plagioclase feldspar is located mainly in eucrites and howardites.

References: [1] Szurgot M. (2013) *76th AMMS*, Abstract #5001. [2] Szurgot M. (2013) *76th AMMS*, Abstract #5264. [3] Righter K and Drake M. *Meteoritics & Planet. Sci., 32*, 929-944. [4] Jones J.H. (1984) *Geochim. Cosmochim. Acta, 48*, 641-648. [5] Mason B. (1967) *American Scientist, 51*, 429-455. [6] Dreibus G. and Wanke H. (1980) *Z. Naturforsch. 35a*, 204-216. [7] Ruzicka A. et al. (1997) *Meteorit. Planet. Sci. 32*, 825-840. [8] Consolmagno G. J. and Drake M. J. (1977) *Geochim. Cosmochim. Acta 41*, 1271-1282. [9] Morgan J.W. et al. (1978) *Geochim. Cosmochim. Acta, 42*, 27-38. [10] Hertogen J. et al. (1977) *Bull. Amer. Astron. Soc. 9*, 458-459.

EARLY DYNAMIC MANTLE MOVEMENTS IN YOUNG, SEMI-CRYSTALLIZED VESTA

B. J. Tkalcec and F. E. Brenker, Goethe University, Altenhöferallee 1, 60438 Frankfurt am Main, Germany. tkalcec@em.uni-frankfurt.

Introduction: Petrologic and geochemical studies of diogenites offer various, partly contradictory, crystallization scenarios [1], [2], [3], [4], [5], [6], [7], [8] on the HED parent body. With their ultramafic composition, diogenites could either represent mantle residue as a result of partial melting and the extraction of more evolved magma or constitute the product of fractional crystallization from molten magma, the latter occurring in magma chambers, multiple magma ponds or a larger scale magma ocean, or they were formed in combinations of these scenarios in multi-step processes. Structural analysis can complement petrologic and geochemical findings by revealing any syn- or post-crystallization deformation undergone by the diogenites, thus offering constraints on dynamic processes occurring and conditions prevailing during cooling of the parent body. Our structural studies of olivine-rich diogenites indicate that the solidification of the HED parent body was not a static progression, but involved large-scale dynamic mantle movements, not unlike those experienced by the early Earth.

Analyses: Comprehensive structural analyses were performed on three olivine-rich diogenites of varying olivine content: NWA 5784 (92% ol.), NWA 5480 (57% ol.) and MIL 07001 (13% ol.). We focused on the olivine crystals in each case, since olivine deforms more readily than orthopyroxene [9], [10], [11], the other abundant mafic mineral in these diogenites. Electron backscatter diffraction (EBSD) was applied to discover any lattice-preferred orientation (LPO) of the olivine crystals as indicator for the respective deformation mechanism. The EBSD analysis includes systematic manual data acquisition across the complete surface of the sample, as well as automatic mapping of selected areas, to measure and record the orientation of the crystallographic axes of each olivine crystal relative to the sample surface. Statistical EBSD data generate orientation, phase and grain-size distribution maps, also rendering a closer look at the grain and phase boundaries. Stereographic plots of the orientations reveal any LPOs, allowing the dominant slip systems activated for the deformation to be identified. Transmission electron spectroscopy (TEM) was applied (in the case of NWA 5480) to visualize more closely the dislocations in the olivine crystal lattice responsible for the discovered deformation. Micro-computer-tomography (Micro-CT) was applied for 3D-visualisation of any internal structures and phase distributions, based upon density measurements. Optical microscopy (OM) was applied to visualize any textural fabrics and grain boundary conditions. The structural analyses were complemented by geochemical analyses using microprobe (EPMA) measurements. In addition, numerical modeling [12] of the asteroidal solidification progression was performed based upon estimated Vestan parameters [12].

Results and discussion: Neither of the three diogenites show any indication of shock-related deformation. However, the results confirm all three diogenites underwent post-crystallization, solid-state plastic deformation under high temperature, anhydrous conditions. For at least two of the three samples, NWA 5480 and NWA 5784, this plastic deformation is clearly distinct from the axial compression [10] or shape-preferred orientation typically occurring in magma chambers or thick lava flows, ruling this deformation mechanism out. NWA 5480 and NWA 5784 were deformed under activation of the slip systems {0kl}[100] and specifically (010)[100], respectively. Furthermore, a direct comparison of the LPOs for NWA 5480 and NWA 5784 confirms a link between these two samples, revealing a progression of increasing deformation temperature [13], or strain [10], also coinciding with increasing olivine content. NWA 5480 displays three different fabrics and hosts at least three populations of olivine crystals with different deformation histories, inferring polystage post-crystallization dynamics.

Numerical models reveal a plausible scenario of a dynamically cooling asteroid with downwellings of dense, cool material with high strength at the base of the solidified lid sinking into warmer softer material, dynamically inducing counter-upwellings of displaced lower-lying mantle. This model accommodates the temperature, strain and hydration constraints as well as the progression correlation inferred by the LPO results of NWA 5480 and 5784. The two slip systems activated for the deformation of these two samples, known as pencil-glide [13] and mantle LPO [14], respectively, are found to be the two most common active slip systems for olivine deformation in the terrestrial mantle [10], [14]. This striking resemblance between the olivine LPOs found in olivine-rich diogenites with those found in olivine mantle rocks from Earth strengthens Vesta's classification as a protoplanet and reaffirms our numerical model of large-scale downwellings in a dynamic mantle as a plausible scenario for the thermal evolution of the young and solidifying Vesta.

References: [1] Sack R. O. et al. (1991) *Geochim. Cosmochim. Acta* 55, 1111–1120. [2] Mittlefehldt D. W. (1994) *Geochim. Cosmochim. Acta* 58, 1537–1552. [3] Stolper E. (1977) *Geochi. Cosmochim. Acta* 41, 587–611. [4] Ruzicka A. et al. (1997) *Meteorit. Planet. Sci.* 32, 825–840. [5] Warren P. H. (1997) *Meteorit. Planet. Sci.* 32, 945–963. [6] Righter K. and Drake M. J. (1997) *Meteorit. Planet. Sci.* 32, 929–944. [7] McSween H. Y. et al. (2011) *Space Sci. Rev*. 163, 141-174. [8] Mandler B. E. and Elkins-Tanton L. T. (2013) *Meteorit. Planet. Sci.* doi: 10.1111/ maps.12135. [9] Christensen N. I. (1984) *JGR* 76, 89–112. [10] Tommasi A. et al. (1999) *Earth Planet. Sci. Lett.* 168, 173-186. [11] Tommasi A. and Mainprice D. (2000) *JGR*, 105, 7893-7908. [12] Tkalcec B. J. et al. (2013) *Nature Geosci.* 6, 93-97. [13] Carter, N. L. and Ave'Lallement, H. G. (1970) *Geol. Soc. Am. Bull*. 81**,** 2181-2202. [14] Frese, K. et al. (2003) *Contrib. Mineral. Petrol.* 145, 75-86.

BULK COMPOSITION OF VESTA AS CONSTRAINED BY THE DAWN MISSION AND THE HED METEORITES. M.J. Toplis[1], H. Mizzon[1], O. Forni[1], M. Monnereau[1], T.H. Prettyman,[2] H.Y. McSween,[3] T.J. McCoy,[4] D.W. Mittlefehldt,[5] M.C. De Sanctis[6], C.A. Raymond,[7] C.T. Russell,[8]. [1]University of Toulouse (mtoplis@irap.omp.eu), [2]Planetary Science Institute, [3]University of Tennessee, [4]Smithsonian Institution, [5]NASA Johnson Space Center, [6]IAPS-INAF, Rome, [7]JPL, Caltech, Pasadena, [8]University of California, Los Angeles.

Introduction: Of the objects in the main asteroid-belt, Vesta is of particular interest as it is large enough to have experienced internal differentiation (520 km diameter), and it is known to have a basaltic surface dominated by FeO-bearing pyroxenes (e.g. [1]). Furthermore, visible-IR spectra of Vesta and associated Vestoids are remarkably similar to laboratory spectra of Howardite-Eucrite-Diogenite (HED) meteorites, leading to the paradigm that the HEDs ultimately came from Vesta (e.g. [2]). Geochemical and petrological studies of the HEDs confirm the differentiated nature of the near-surface region of their parent body, and imply that crust extraction occurred well within the first 10 Ma of solar system history (e.g. [3]).

Vesta is therefore a prime target for studies that aim to constrain the earliest stages of planet building, and it is within this context that the NASA Dawn spacecraft [4] orbited Vesta from July 2011 to September 2012. The results of the Dawn mission so far have significantly reinforced the HED-Vesta connection, confirming a significant degree of internal differentiation [5], a surface mineralogy compatible with that of the HEDs [6], and near-surface ratios of Fe/O and Fe/Si consistent with HED lithologies [7].

The combination of data from the HED meteorites and the Dawn mission thus presents an unprecedented opportunity to use Vesta as a natural laboratory of early differentiation processes in the early solar system. However, the bulk composition of Vesta remains a significant unknown parameter, but one that plays a key role on the physical and chemical properties of the internal and surface reservoirs (core, mantle, crust). Several attempts have been made to constrain the bulk composition of the eucrite parent body, early endeavours relying on petrological or cosmochemical constraints (e.g. [8]). More recently, individual chondrite-class compositions, or mixtures thereof, have been considered, constrained by considerations such as O-isotopes, trace-element ratios and siderophile element concentrations of the eucrites [9-11].

The work presented here builds upon these latter studies, with the primary aims of: i) illustrating the potential diversity of the geochemical and geophysical properties of a fully differentiated Vesta-sized parent body, and ii) assessing which, if any, of the known chondritic bulk compositions are plausible analogues for proto-Vesta.

Methods and general approach: Despite the consensus that the primitive building blocks of the solar system were "chondritic", diverse classes of chondrite exist, from the volatile-rich Ivuna-class (CI), to metal-poor varieties such as the LL ordinary chondrites, to highly reduced types such as enstatite chondrites. While there is no guarantee that Vesta accreted from known chondritic precursors, these compositions provide a convenient reference frame. Twelve chondritic compositions are considered here, comprising 7 carbonaceous groups (CI, CV, CO, CM, CK, CR, CH), the three ordinary chondrite groups (H, L, LL) and the two enstatite chondrite groups (EH, EL). Significant differences in composition exist between these groups, notably in terms of Mg/Si, S and Fe content, volatile content, oxidation state of Fe, and the concentration of incompatible lithophiles such as the REE. The role of these factors on the mineralogy and internal structure of a fully differentiated parent body will be explored.

Because our aim is to quantify the first-order effects of differentiation, we focus on those chemical elements that dominate the mass of the bulk object (Si, Al, Mg, Ca, Ti, Na, Fe, Ni, S, O). Minor and trace elements (e.g. Mn, REE) are considered where they provide complementary constraints. The basis of our analysis consists of distributing each chemical element between one or more of the principal differentiated geochemical reservoirs (core, mantle, crust), assuming a distribution that is consistent with the thermodynamics of element partitioning at magmatic temperature, in particular that for Fe-Mg. An iterative process is applied to find the iron content of the core for a given bulk composition that results in a bulk $Kd^{Mg-Fe}_{mantle-Juvinas}$ that is consistent with relevant olivine-pyroxene mixtures, assuming that the primitive main-group eucrite Juvinas is a first-order proxy of Vesta's crust. Further details of the methods used can be found in [12].

In this way, estimates of the relative masses of the core (Fe-Ni-S), the mantle and the basaltic crust are provided. In detail, the core is divided into a sulphide and a metal component. Relative masses may be converted to absolute masses using the mass of Vesta as determined by the Dawn mission [5]. Masses are converted to volumes using mineral densities (see [12]). The total volume is calculated for each bulk composition and compared with the measured volume of Vesta [5], differences being assigned to porosity.

Constraining bulk composition: *Core size and density.* All bulk compositions tested have a significant core, but the relative proportions of metal and sulphide can be widely different. No satisfactory thermodynamic solution exists for the CI and LL groups. For the other groups, the metal fraction (relative to sulphide) is predicted to be as little as ~20% (in the case of a CM bulk composition), to almost 100% (in the case of a CH bulk composition). Core size (radius) is typically predicted to be in the range 90 to 120 km, although total core size (metal+ sulphide) and average core density nevertheless span significant ranges (Fig. 1).

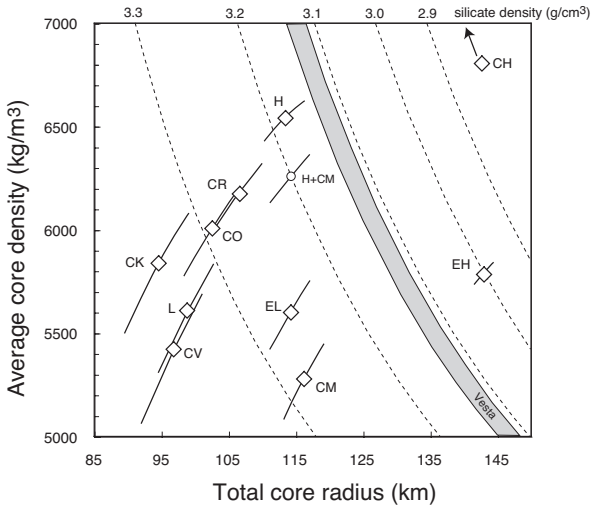

Fig. 1. Optimal values of total core radius and average core density (open symbols), and an indication of the range of possible solutions (solid lines). The range of values constrained by the Dawn mission is shown as a grey band.

The bulk density of Vesta and its J2 gravity coefficient determined by the Dawn mission provide an independent constraint on internal mass concentration. Using simple 2-layer models, it may be shown that for reasonable values of oblateness, the density of the upper silicate layer is in the range 3050- 3140 kg/m^3 [5], constraining core size and density as illustrated in Fig. 1. Interestingly, none of the predicted cores provide a perfect match to the geophysically constrained range of acceptable values, although the closest approach is for H-chondrite composition.

Composition and mineralogy of the crust-mantle system. The geochemistry of HEDs also provides insight into the bulk composition of Vesta. For example, with the estimates of core size and composition above it is possible to calculate the Fe/Mn ratio of the mantle and compare this with geochemical data from the eucrites. This exercise shows that carbonaceous chondrites have predicted Fe/Mn well above observed values, while the H-chondrite and enstatite-chondrite bulk compositions provide satisfactory agreement.

We have also considered if it is possible to generate Juvinas-like liquids at appropriate degree of melting/crystallization using the MELTS thermodynamic calculator, considered the calculated mineralogy of the mantle and the likelihood of generating abundant pyroxene lithologies such as diogenites, as well as calculating crustal thickness. For all criteria, a Na-depleted H-chondrite bulk composition provides the best fit, although oxidation state and O-isotopes are not perfectly reproduced, suggesting that bulk Vesta may contain ~25% of a CM-like component [11].

Identification of an acceptable bulk composition is an important step forward, as it opens the possibility to predict the mineralogy and composition of solid and liquid products over wide ranges of partial melting and crystallization (e.g. the phase diagram shown in Fig. 2), providing a useful and self-consistent reference frame for interpretation of the Dawn data. Furthermore, knowledge of the bulk composition (core and bulk silicate) provides essential constraints for thermal and physical models of Vestan evolution at high temperature that may ultimately lead to a better understanding of the differentiation process on protoplanetary bodies such as Vesta (e.g.[13]).

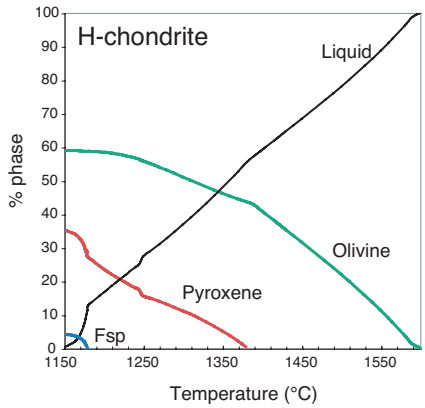

Fig. 2. Preliminary phase diagram for the bulk-silicate fraction of Vesta derived from a Na-depleted H-chondrite source.

References: [1] McCord, T.B., J.B. Adams, T.V. Johnson (1970) *Science*, 168, 1445-1447. [2] Binzel, R.P., S. Xu (1993) *Science* 260, 186-191. [3] Kleine T. et al. (2009) *Geochim. Cosmochim. Acta* 73, 5150-5188. [4] Russell C.T. and Raymond C.A. (2011) *Space Sci. Reviews* 163, 3-23. [5] Russell, C.T. et al. (2012) *Science* 336, 684-686. [6] De Sanctis, M.C. et al. (2012) *Science* 336, 697-700. [7] Prettyman T.H. et al. (2012) *Science* 338, 242-246. [8] Consolmagno G. J., Drake M.J. (1977) *Geochim. Cosmochim. Acta*. 41, 1271-1282. [9] Righter K., and Drake M.J. (1997) *Meteorit. Planet. Sci.* 32, 929-944. [10] Ruzicka, A., Snyder G.A. and Taylor L.A. (1997) *Meteorit. Planet. Sci.* 32, 825-840. [11] Boesenberg J.S. and Delaney J.S. (1997) *Geochim. Cosmochim. Acta*. 61, 3205-3225. [12] Toplis M.J. et al. (2013) *Meteorit. Planet. Sci.* In press. [13] Mandler B. & Elkins-Tanton L.T. (2013) *Meteorit. Planet. Sci.* in press.

GLOBAL RESOLVED TEMPERATURE MAPS OF VESTA. F. Tosi[1], F. Zambon[1], M.T. Capria[1], M.C. De Sanctis[1], F. Capaccioni[1], E. Ammannito[1], T.N. Titus[2], E. Palomba[1], C.T. Russell[3], C.A. Raymond[4], and the Dawn Science Team. [1]INAF-IAPS, Via del Fosso del Cavaliere 100, I-00133 Rome, Italy, federico.tosi@iaps.inaf.it. [2]U.S. Geological Survey, Astrogeology Science Center, Flagstaff, AZ, USA. [3]University of California at Los Angeles, Los Angeles, CA, USA. [4]NASA/Jet Propulsion Laboratory and California Institute of Technology, Pasadena, CA, USA.

Introduction: We present, for the first time, global resolved temperature maps of Vesta as derived by the Visible and Infrared Mapping Spectrometer (VIR) onboard Dawn [1].

On the day side of Vesta, the region of the infrared spectrum beyond ~3.5 μm is dominated by the thermal emission of the asteroid's surface, which can be used to determine surface temperature by means of temperature-retrieval algorithms. To calculate surface temperatures, we applied a Bayesian approach to nonlinear inversion [2] based on the Kirchhoff law $r_\lambda=1-\varepsilon_\lambda$ and the Planck function. Results were compared with those provided by the application of alternative methods (e.g, [3]). In all cases, the minimum retrievable temperature (~180 K) is set by the Noise Equivalent Spectral Radiance (NESR), i.e. the RMS noise of the in-flight measurements expressed in units of spectral radiance. On the other hand, for a given local solar time (LST), the maximum temperature depends on the local incidence angle and surface properties such as thermal inertia, surface roughness, emissivity and Bond albedo.

Results: Such investigation in the case of Vesta has allowed us to derive spatially-resolved thermal images of a significant percentage of the asteroid, with a formal error in the computation which is generally smaller than 1 K for surface temperatures greater than 220 K. Previous results were obtained for local scale features, such as local concentrations of unusual brightness i.e. high-albedo (bright) and low-albedo (dark) material units [4], pitted terrains [5], and spectrally distinct meteorite impact ejecta. The size of Vesta, far larger than that of other asteroids explored by spacecraft, also makes this work the first of its kind for the amount of data and the overall surface area covered.

Temperature maps are divided by mission phase: Approach, Survey, High Altitude Mapping Orbit (HAMO), Low Altitude Mapping Orbit (LAMO), High Altitude Mapping Orbit 2 (HAMO-2), and local solar time intervals. These products can be used to identify regions of Vesta for which temperature measurements carried out in multiple times of the Vestan day are available.

Thermal emission, especially when measured at different points in time, can provide clues to the physical structure of such peculiar sites, which complements the mineralogical investigation based on VIR data collected at shorter wavelengths. A separate project [i.e., 6] is devoted to derive global thermal inertia maps and other thermal properties of Vesta using theoretical models which solve the heat equation for airless bodies and model the distribution of temperatures due to surface roughness variations.

Conclusions and future work: The availability of surface temperature maps for each phase of the Dawn mission at Vesta is a fundamental step for a comprehenive understanding of the surface. In fact, these data are crucial for both the mineralogical analysis and for the determination of thermophysical properties.

It is expected to undertake a similar analysis when Cere data acquired by VIR will be available.

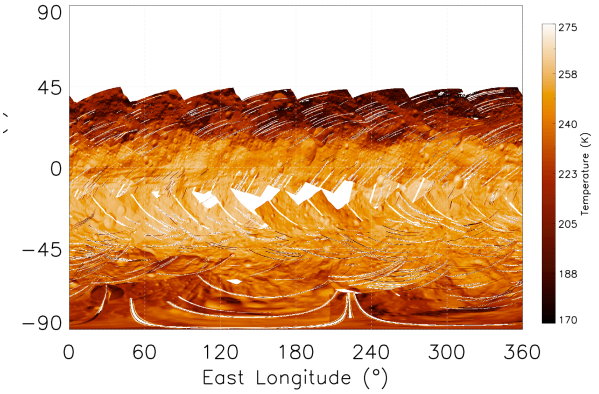

Fig. 1. Map of surface temperature derived by VIR infrared data acquired in the Survey phase. All local solar times are represented here.

Acknowledgements: This work was supported by the Italian Space Agency (ASI), ASI-INAF Contract I/004/12/0. The authors would like to thank the Dawn Science, Operation and Instrument Teams for a successful Dawn at Vesta mission. Several of the authors received support from the NASA Dawn at Vesta Participating Scientist program. The VIR instrument was developed under the leadership of INAF, Italy's National Institute for Astrophysics, Rome. The instrument was built by SELEX-Galileo, Florence, Italy. We warmly thank Robert Gaskell (PSI) for providing a detailed shape model of Vesta that was used in this work. The computational resources used in this research have been supplied by INAF-Institute for Space Astrophysics and Planetology (IAPS) through the DataWell project. Dawn datasets are publicly available at

the Planetary Data System Small Bodies Node (http://pdssbn.astro.umd.edu/).

References:

[1] De Sanctis, M.C., et al. (2011), "The VIR Spectrometer". *Space Science Reviews* 163 (1-4), pp. 329-369. [2] Keihm, S., et al. (2012), "Interpretation of combined infrared, submillimeter, and millimeter thermal flux data obtained during the Rosetta fly-by of Asteroid (21) Lutetia". *Icarus* 221, pp. 395-404. [3] Clark, R.N., et al. (2011), "Thermal removal from near-infrared imaging spectroscopy data of the Moon". *Journal of Geophysical Research* 116, CiteID E00G16. [4] Tosi, F., et al. (2013), "Thermal behavior of dark and bright surface features on Vesta as derived from Dawn/VIR". *Icarus*, submitted. Under review. [5] Denevi, B.W., et al. (2012), "Pitted terrain on Vesta and implications for the presence of volatiles". *Science* 338, pp. 246-249. [6] Capria, M.T., et al. (2013), "Vesta surface thermal properties map". Submited to *Nature Geosciences*.

VESTA IN THE ULTRAVIOLET/BLUE: WHAT WE KNEW BEFORE DAWN'S ARRIVAL, AND HOW DOES IT AUGMENT WHAT WE LEARNED FROM DAWN? F. Vilas[1], A. R. Hendrix[1], J-Y Li[1] and A. L. Cochran[2], Planetary Science Institute, 1700 E. Fort Lowell Rd., Suite 106, Tucson, AZ, 85719, fvilas@psi.edu, McDonald Observatory, University of Texas, Austin, TX 78712.

Earth-based telescopic measurements established that the unique asteroid 4 Vesta was an obvious target for space-based exploration following the discoveries tracing Vesta's spectral reflectance through a string of likely daughter asteroids to the Earth, and tying the asteroid reflectance to the howardite-eucrite-diogenite (HED) meteorite compositions. We review what was known in the ultraviolet/blue spectral regions before Dawn arrived at Vesta, both demonstrating the predictions that Earth-based observations can make about a target asteroid at these wavelengths, and placing the Dawn data in the context of the additional UV/blue Vesta data not covered by Dawn instrumentation. Two areas to be addressed are included here; the broader utility of this spectral region will be discussed.

Surface Mineralogy: From broad-band photometry to high-resolution spectroscopy, variations in Earth-based UV/blue surface reflectance exist across Vesta's surface. Do these variations map to the now-observed higher spatial resolution surface maps of Vesta? Does the detailed Dawn reflectance data of Vesta confirm the results of UV/blue Earth-based reflectance data?

Surface Space Weathering: Current hypotheses predict that the UV/blue wavelength range could constitute a spectral region that provides more advanced indication of the onset and progression of space weathering in S-complex (mafic silicate) asteroids. Were there predictable signs of weathering for the Vesta surface material in the UV/blue data?

SOME PETROLOGICAL CONSTRAINS ON THE VESTA MANTLE FROM THE STUDY OF GRAVITATIONAL POTENTIAL BY THE DAWN MISSION. S. A. Voropaev, GEOKHI RAS, Moscow, Kosygina str. 19, 119991 voropaev@geokhi.ru

Introduction: Space mission Dawn targeted 4 Vesta provides a number of remarkable results concerning as surface coverage as physical parameters of the surviving protoplanet. It was confirmed that Vesta differentiated and Rheasilvia, a giant impact basin at the the south polar region, is the most likely source of howardite-eucrite-diogenite (HED) meteorites [1]. But, degree of Vesta's primary hondritic body melting is not clear till now and depends on the time of its formation at the beginning of the life of the Solar System [2]. So, the core/mantle size and the composition of theirs rocks remains questionable.

Analytical procedure: The Vesta precession rate (due to the gravitational torque from the Sun) and the gravitational potential (modeled by a spherical harmonic expansion) will be determined by unnormalized oblateness J_2 [3]

$C - (A + B) / 2 = J_2 M R^2$,

where $A < B < C$ are principal moments of inertia, M is mass, R is the mean radius (adopt value 265 km) and $J_2 = 0.071060892$.

Most recent and relevant data from Dawn are [4]
major axes, a/b/c - 286.3/278.6/223.2 (km);
mass, M - 2.59076×10^{20} (kg);
bulk density, ρ_b – 3456 (kg/m3);
rotation rate, ω - 1617.333119 (deg/day).

For our purose, the shape of Vesta is reasonably well approximated by a twoaxial oblate ellipsoid, $a_1 = b_1 = 282.4$ (km), $c_1 = 223.2$ (km) with hydrostatic structure at first harmonic degree. An exact analytical treatment provides for homogeneous twoaxial oblate ellipsoid (with an arbitrary bulk density)

$J_2^{(0)} = 1/5\ \varepsilon_1^2$, where eccentricity $\varepsilon_1^2 = 1 - c_1^2/a_1^2$.

So, for homogenous Vesta, $J_2^{(0)} = 0.075$ ($\varepsilon_1 = 0.613$) and $J_2 < J_2^{(0)}$ - indication on the more dense core relative mantle.

In order to explore the implications of the gravity and shape for the interior structure of Vesta, simple two-layer mass-balance model was explored with an assumed core as twoaxial oblate ellipsoid with major axes $a_2 = b_2 > c_2$ and eccentricity $\varepsilon_2^2 = 1 - c_2^2/a_2^2$. In this case,

$M = M_1 + M_2$,

where $M_1 = 4\pi/3\ \rho_1 a_1^2 c_1$, ρ_1 is the mantle's density, $M_2 = 4\pi/3\ (\rho_2 - \rho_1)\ a_2^2 c_2$, ρ_2 is the core's density. So, mass-balance provides

$1 = \rho_1/\rho_b + (\rho_2 - \rho_1)/\rho_b\ (a_2/a_1)^2\ c_2/c_1$

or

$(a_2/a_1)^2 = (\rho_b - \rho_1)/(\rho_2 - \rho_1)\ \sqrt{1 - \varepsilon_1^2}\ /\ \sqrt{1 - \varepsilon_2^2}$ (1)

For two-layer model an exact analytical treatment provides

$J_2^{(1)} = 1/5\ (M_1/M\ \varepsilon_1^2 + M_2/M\ \varepsilon_2^2\ (a_2/a_1)^2)$ (2)

After comparison with (1) we have

$\varepsilon_2^2/\sqrt{1 - \varepsilon_2^2} = (5\ J_2^{(1)} - \rho_1/\rho_b\ \varepsilon_1^2)/\ \sqrt{1 - \varepsilon_1^2}\ (1 - \rho_1/\rho_b)\ (\rho_b - \rho_1)/(\rho_2 - \rho_1) = D1(x,y) > 0$, (3)

$x = \rho_1$, $y = (\rho_2 - \rho_1)$

We assume that the core's eccentricity $\varepsilon_2 < \varepsilon_1$ as for more dense rocks relative mantle. In this case left part of (3) should be less then 0.476. For $J_2^{(1)} = J_2 = 0.071060892$ the right part of the later expression D1(x,y) set limits for the unknown mantle's density x as shown on Fig.1

$3.24 < x = \rho_1 < 3.26$ (g/cm^3)

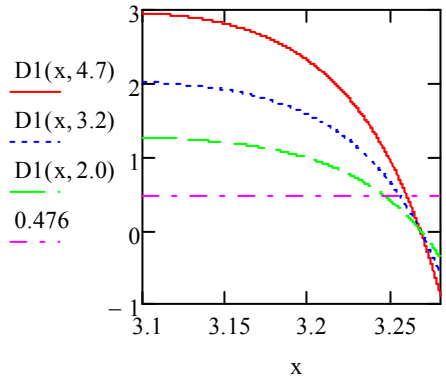

Fig.1

Results and discussion: The above discussed simple core/mantle model provides reasonable value for mean mantle's density. Diogenites are currently believed to originate from deep within the crust of the Vesta and relatively unbrecciated olivine-rich diogenites consist of an equilibrium assemblage of olivine (3.27-3.37 g/cm^3) and magnesian orthopyroxene – harzburgite (2.99-3.2 g/cm^3) [5]. So, we can use this model at analytical treatment for more detailed analyses of the gravitaty of Vesta and implications for internal stresses [6] and hydrostatic equilibrium.

References:

[1] S. Marchi et al. (2012) *Science, 336*, 690-694. [2] A. Coradini et al. (2011) *Space Sci. Rev.*, *163*, 25-40. [3] A.S. Konopliv et al. (2013) *Icarus*, http://dx.doi.org/10.1016/j.icarus.2013.09.005. [4] C. T. Russell et al. (2012) *Science, 336*, 684-686. [5] A.W. Beck, H.Y. McSween (2010) *Meteoritics & Planetary Science, 45*, 850–872. [6] S.A. Voropaev (2013), 44th *LPSC,* Abstract #1135.

STRATEGIES FOR THE GEOLOGIC MAPPING OF SMALL AIRLESS BODIES: THE VESTA EXAMPLE. D. A. Williams[1], R. A. Yingst[2], and W. B. Garry[3] [1]School of Earth & Space Exploration, Arizona State University, Tempe, Arizona 85287 (David.Williams@asu.edu), [2]Planetary Science Institute, Tucson, Arizona, [3]NASA Goddard Spaceflight Center, Greenbelt, Maryland.

Introduction: In July 2011 NASA's Dawn spacecraft entered orbit around the main belt asteroid (4)Vesta, beginning a lengthy orbital study of this unique protoplanet [1,2]. A geologic mapping campaign was developed as part of the Nominal Mission to provide a systematic, cartography-based initial characterization of the global and regional geology of Vesta. In this abstract we highlight major aspects of the geologic mapping campaign for Vesta, including discussion of the goals of the mapping effort, the methodologies used, the challenges that arose in the mapping of a small airless body like Vesta, and a list of lessons learned that future missions should review when designing a mapping program to aid in nominal mission data analyses of small airless bodies.

Purpose & Goals of Mapping: Geologic maps are tools to understand the evolution of the terrestrial planets. The goal of geologic maps is to place observations of surface features into their stratigraphic context to develop a sequence of events for the evolution of planetary surfaces [3,4]. The advantage of geologic mapping over photogeologic analyses alone is that it reduces the complexity of heterogeneous planetary surfaces into comprehensible portions, in which discrete material units are defined and characterized based upon specific physical attributes related to the geologic processes that produced them. The distributions of these units are then mapped, along with structural features, in order to identify the relative roles of various processes in shaping their surfaces.

The Dawn Science Team planned to produce cartographic products of Vesta from the FC images, including global mosaics as well as 15 regional quadrangles [5]. We were chosen to oversee the geologic mapping campaign during the Nominal Mission. We oversaw production of a global geologic map at scale 1:500,000 [6] and production of 15 quadrangle geologic maps at scale 1:250,000, using the cartographic image quadrangles produced by DLR as basemaps. The goal of the Vesta global mapping was to use iterative geologic mapping of increasingly higher spatial resolution FC images obtained during Dawn's orbital phases 1) to support the Geosciences Working Group by providing geologic and stratigraphic context of surface features, and 2) to better support the analysis of data from the Visible and Infrared Spectrometer (VIR) and the Gamma Ray and Neutron Detector (GRaND). The goal of the quadrangle mapping effort was to improve upon the geologic history identified by the global map (made with lower resolution data) using Low Altitude Mapping Orbit (LAMO, FC resolution of 20-25 m/pixel) data, in which identification of the major types of surface features, geologic units, and stratigraphic relations at regional and local scales could be done at greater fidelity. The quadrangle mapping was to be driven by the science questions and hypotheses that arose during the global mapping.

Methodologies: For each quadrangle, mappers assembled the base map mosaics, DTMs, and other materials and imported them into ArcGIS™10 software by ESRI, Inc. to facilitate geologic mapping. Each quadrangle mapper was free to define and characterize subunits and structures derived from the global geologic map [6], with the expectation that units would be updated and modified to take advantage of the higher spatial resolution LAMO data. The quadrangle mappers were encouraged to collaborate with the mappers of neighboring quadrangles, to assure unit contacts matched across quadrangle boundaries, that similar units were used, and that a consistent level of detail in the mapping was maintained.

Challenges: One of the key early findings of the Dawn mission was that Vesta's ratio of surface relief to radius is ~15%, compared to ~1% for the Moon and Mars [7]. This means that extremely steep slopes are common on Vesta compared to other terrestrial planets. These steep slopes cause impact craters to be deformed into an asymmetric shape, or partly buried by subsequent mass movements triggered by later impacts. These crater-related processes often make clearly defined contact boundaries between map units very hard or impossible to identify, except for the youngest (freshest) units. This fact makes delineation and description of units more difficult and identification of the relations between units problematic compared to mapping on other bodies. Thus, Vesta mappers often use approximate, gradational, or inferred contacts when mapping Vesta's large-scale units at high resolution, except where in contact with young crater materials or at steep scarps.

Other challenges encountered with application of geologic mapping to asteroids include: 1) the lack of non-impact processes limits the variety of geological units that can be defined; and 2) many previously studied smaller asteroids are spectrally "bland" with no composition-related color differences. We were pleas-

antly surprised to see strong color and spectral variations on Vesta [8,9].

Lessons Learned: Although not initially driven by specific science goals for each quad, the geologic mapping of the quadrangles provided the team with initial descriptions and interpretations of regional geologic units, building on the work of the global mapping effort [6]. Mappers were able to revise their interpretations in real time to aid the analysis and interpretation of data returned from other science instruments, e.g., identifying the geologic context of mineral or elemental signatures. However, map interpretation did not lend itself well to the compressed mission timeline. The needs of the team for rapidly-produced maps meant that coordination between global and regional efforts was non-trivial, and thus, units were standardized earlier than was ideal. For future missions, we recommend that mappers retain more generic descriptors and planet-centric symbology for as long as possible, until higher-resolution data is obtained and descriptions and interpretations can be refined. Early contact/coordination with the U.S. Geological Survey mapping specialists when beginning the mapping process is essential.

For Vesta the quadrangle mapping began before a first draft global map was completed, where the global map would have enabled recognition of the most interesting regions to which higher resolution mapping was justified. Also, the quad boundaries were defined and mappers assigned prior to Dawn's arrival. The result of this was that, when the mapping process began, it was an impediment to contextual understanding, coordination of mapping effort, and consistency of maps.

The choice to produce 15 quadrangle geologic maps was based on utilization of the FC cartographic products [5]. Although 15 early geological "sketch" maps were useful to display Vesta's unique surface to the scientific community as a series of posters at conferences during the nominal mission, it is now the perspective of the Science Team that attempting to use these same 15 maps as the basis for more detailed geologic mapping studies made the mapping process more difficult. Specifically, key geologic features often crossed quadrangle boundaries, which were rarely crossed during the mapping process, or during the follow-on analysis. Also, differences in expertise with ArcGIS™ software, mapping styles, and experience (mappers ranged from graduate students to mid-career scientists) all were amplified by the large number of mappers (14) to cover 15 quadrangles. Because of these difficulties, we recommend the following for Dawn at Ceres or future missions to small airless bodies:

1) Complete a first draft global geologic map first, identify the regions where more detailed mapping is justified, then assign regions to team members, and match surface features with mappers having the correct expertise, skills and interests to produce quality maps. These regions could use single quadrangles, multiple quadrangles, or parts of quadrangles as defined by the cartographic products. Note that this approach does not preclude work on other topical science studies, including local morphological, compositional, thematic, or geologic mapping. Additionally, it is important that individuals who are assigned quads are experienced mappers, or students with the time and desire to learn how to complete a geologic map.

2) Decrease the number of mappers. The number of mappers assigned for detailed mapping should be based on the size of the regions mapped, the science rationale for mapping, and/or the amount of detail that is observable in the areas.

3) To support coordination of effort, develop mapping templates early in the Nominal Mission, for the ArcGIS™ projects, for conference posters, for the format of mapping publications, and for presenting results.

4) Utilize abstracts and conference presentations as the best way to present preliminary maps that may be based more on cartography than pure geology, which should be separate from future geologic maps for peer-reviewed publications.

5) Rather than requiring each mapper to produce a peer-reviewed paper based on geologic mapping of a cartographic quadrangle, geologic mapping should be based on regional features or process-related science drivers.

6) Geologic mapping is an excellent way for graduate students and younger team members to conduct useful mission-related scientific research and write first-author publications.

7) Ongoing research should be carefully coordinated within the broader science team, to assure that research facilitated by geologic mapping is fully supported, without placing undue pressure on team members to define a potential publication solely by a geologic map where such is not warranted.

References: [1] Russell, C.T. and Raymond, C.A. (2011) *Space Sci. Rev., 163*, 3-23. [2] Russell, C.T., et al. (2012) *Science, 336*, 684-686. [3] Carr, M.H., et al. (1976) *NASA SP-417,* 13-32. [4] Wilhelms, D.E. (1990), in *Planetary Mapping,* Cambridge Un. Press, NY, 208-260. [5] Roatsch, T., et al. (2012) *PSS 73*, 283-286. [6] Yingst, R.A., et al. (2014), *PSS*, in review. [7] Jaumann, R., et al. (2012) *Science, 336*, 687-690. [8] De Sanctis, M.C., et al., (2012) *Science, 336*, 697-700. [9] Reddy, V., et al. (2012) *Science, 336*, 700-704.

GLOBAL VIEW OF THE BRIGHT MATERIAL ON VESTA. F. Zambon[a], M. C. De Sanctis[a], S. Schröder[b], F. Tosi[a], J.-Y. Li[c], A. Longobardo[a], E. Ammannito[a], D. T. Blewett[d], E. Palomba[a], F. Capaccioni[a], A. Frigeri[a], M. T. Capria[a], S. Fonte[a], D. W. Mittlefehldt[e], A. Nathues[f], C. Pieters[g], C. T. Russell[h] and C. A. Raymond[i].

a) INAF-IAPS Istituto di Astrofisica e Planetologia Spaziali, Via del Fosso del Cavaliere, 100, 00133 Rome, Italy; b) Institute of Planetary Research, German Aerospace Center (DLR), Rutherfordstrasse 2, D-12489 Berlin, Germany; c) Planetary Science Institute, 1700 East Fort Lowell, Tucson, AZ, USA; d) The Johns Hopkins University Applied Physics Laboratory, Laurel, MD, USA; e) NASA Johnson Space Center, 2101 NASA Parkway Houston, TX 77058, USA; f) Max Planck Institute for Solar System Research, Max-Planck-Strasse 2, D37191 Katlenburg-Lindau, Germany; g) Brown University 324 Brook Street, Providence, RI USA; h) Institute of Geophysics and Planetary Physics, University of California at Los Angeles, Los Angeles, CA, USA; i) NASA/Jet Propulsion Laboratory and California Institute of Technology, 4800 Oak Grove Drive, Pasadena, CA, USA.

Introduction: At 525 km in mean diameter, Vesta is the second-most massive and one of the brightest asteroids of the main-belt [1, 2, 3]. Here we give a global view of the bright material (BM) units on Vesta. We classified the BMs according to the normal visual albedo [4]. The global albedo map of Vesta [4] allows to be divided the surface into three principal types of terrains: bright regions, dark regions and intermediate regions. The distribution of bright regions is not uniform. The mid-southern latitudes contain the most bright areas, while the northern hemisphere is poor in bright regions [5, 6]. The analysis of the spectral parameters and the normal visual albedo show a dependence between albedo and the strength (depth) of ferrous iron absorption bands (Fig. 1); strong bands correspond with high albedo units. Vesta's average albedo is 0.38, [4, 7] but there are bright material whose albedo can exceed 0.50. Only the E-Type asteroids have albedos comparable to those of the BMs on Vesta. The Dawn mission observed a large fraction of Vesta's surface at high spatial resolution, allowing a detailed study of the morphology and mineralogy of it. In particular, reflectance spectra provided by the Visible and InfraRed spectrometer (VIR) [8], confirmed that Vesta's mineralogy is dominated by pyroxenes. All Vesta spectra show two strong absorption bands at ~0.9 and 1.9 μm, typical of the pyroxenes and associated with the howardite, eucrite and diogenite (HED) meteorites [8-11].

Results: Global analysis of VIR data carried out for the BM units reveals that the mineralogy does not differ from those of other Vesta regions [12]. All these areas have the common characteristic of having deeper pyroxene bands, and has been interpreted as fresh, unweathered material coming from the layers below the surface with a higher concentration of pyroxenes, representative of younger Vesta surface [6] [12] [13].
Notable exceptions are the bright regions in the Northern craters Bellicia and Arruntia, and the bright streak located in the southern crater (lat -65, lon 357) [12]. Unexpectedly, the bright material in Bellicia and Arruntia has been recognized as olivine mixed with pyroxene [14].

The nature of the bright material (the brightest of all the surface) in the southern crater is still under debate, being, at the contrary of all the other BM, the band depth shallower respect with the surrounding.

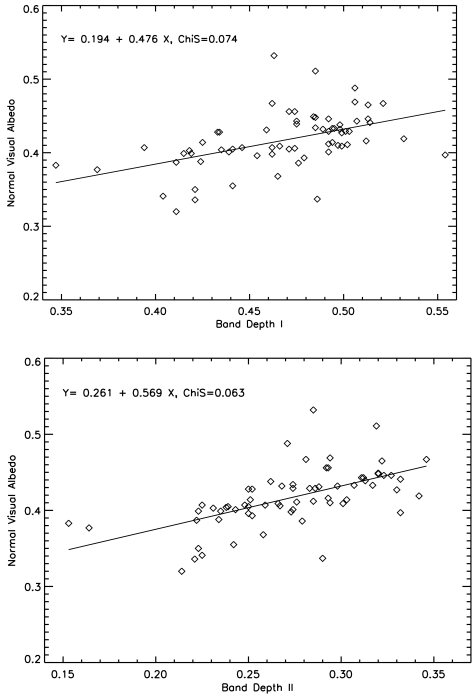

Figure 1: Correlation between band depth of the bright materials on Vesta and their albedo.

Acknowledgements: This work was supported by the Italian Space Agency (ASI), ASI-INAF Contract. The authors would like to thank the Dawn Science, Operation and Instrument teams. The VIR instrument was developed under the leadership of INAF, Italy's National Institute for Astrophysics, Rome, and built by SELEX-Galileo, Florence, Italy.

References: [1] P.C. Thomas et al. 1997, *Science*. [2] M.T. Zuber et al. 2011, *Space Sci. Rev*. [3] C. T. Russell et al., 2012, Science. [4] S. Schröder et al., 2013, *PSS*. [5] Mittlefeldht, D. W., et al., 2012, *LPS XLIII*, Abstract #1680. [6] J-Y. Li et al., 2013, *Icarus*, in review. [7] E.F. Tedesco et al., 1989, *Astron. J.* [8] M.C. De Sanctis et al., 2012, *PSS*. [9] M.C. De Sanctis et al., 2012, *Science*. [10] M.J. Drake, 1979, *Asteroids*. [11] M.A. Feierberg, 1980, *Science*. [12] F. Zambon et al. 2013, *Icarus* in review. [13] C.M. Pieters et al., 2012, *Nature*. [14] Ammannito et al., 2013, *Nature*.